The Nucleus

An Open Access International Scientific Journal

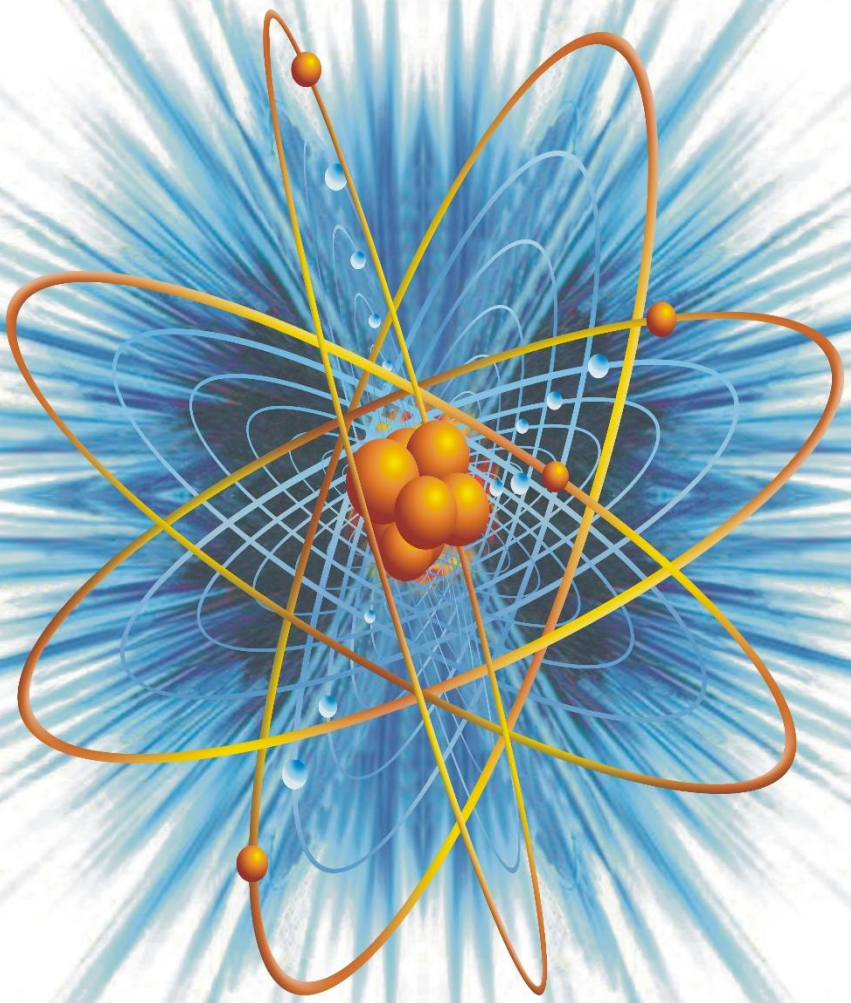

Vol. 60, No. 2, 2023

ISSN 0029-5698 (Print)

eISSN 2306-6539 (Online)

The Nucleus

An international journal devoted to all branches of natural and applied sciences

Website: *www.thenucleuspak.org.pk* **E-mail:** *editorialoffice@thenucleuspak.org.pk*
Phone: +*92-51-9248429* **Fax: +***92-51-9248808*

Editorial Office, The Nucleus

PINSTECH, Nilore, 45650, Islamabad, Pakistan

Printed at

PINSTECH Printing Press

The Nucleus

Aims and Scope: The Nucleus is an open access multidisciplinary peer-reviewed academic journal. It offers a platform for the scientists and engineers to publish their recent research of high scientific values in all areas of natural, applied and management sciences at international level. The journal is being published electronically as well as in paper version. It is easily accessible, free of charge and is being distributed widely.

Abstracting and Indexing: The journal is being abstracted and indexed by Chemical Abstracts, Citefactor, Biological Abstracts, INIS Atom Index, Bibliography of Agriculture (USA), The Institution of Electrical Engineers Publication, Virology Abstracts (England) and Pakistan Science Abstracts. The journal is recognized by the Higher Education Commission of Pakistan (Category Y).

ISSN and eISSN: The international standard serial numbers (ISSN) for The Nucleus are [0029-5698 (Print) and 2306-6539 (Online)].

The Nucleus is published at Pakistan Institute of Nuclear Science & Technology, Islamabad, on behalf of the Pakistan Atomic Energy Commission.

Published since 1964

The Nucleus
ISSN 0029-5698 (Print)
ISSN 2306-6539 (Online)

CONTENTS

The Nucleus ***60***, *No. 2 (2023) 112-119*

www.thenucleuspak.org.pk

The Nucleus
ISSN 0029-5698 (Print)
ISSN 2306-6539 (Online)

Beneficiation of Light Rare Earth Elements from Dubeydib Heavy Mineral Sands Deposits, South Jordan

Osama A. Twaiq[1*], Tariq M. Bhatti[1], Rami Zaza[1], Hezam Al-Awah[2]

[1]*Directorate of Information and Research, Jordan Atomic Energy Commission (JAEC), P.O. Box 70, Amman 11934, Jordan*

[2]*Geology Program, Department of Chemistry and Earth Sciences, College of Arts and Sciences, Qatar University, P.O. Box 2713, Doha, Qatar*

ABSTRACT

This study describes the beneficiation of monazite mineral from heavy mineral sands deposit of Dubaydib, South Jordan. The heavy mineral sand sample contained 1.80% monazite [(Ce,La,Nd,Th)PO_4] based on chemical composition of light rare earth elements such as cerium (Ce), lanthanum (La) and neodymium (Nd). It contained low contents of 0.23% La (0.26% La_2O_3), 0.50% Ce (0.59% Ce_2O_3), 0.21% Nd (0.24% Nd_2O_3), 0.08% Y (0.1% Y_2O_3), 0.13% Th (0.15% ThO_2), 0.015% U (0.018% U_3O_8) and 0.66% P_2O_5. The major elemental composition of 64.4% SiO_2, 6.9% Al_2O_3, 6.0% Fe_2O_3, 6.5% TiO_2 and 3.49% Zr (4.72% ZrO_2) are present in the sample. The monazite sand sample contained quartz, plagioclase, mica, rutile, Ilmenite and zircon as major minerals with monazite as minor mineral. For beneficiation studies, the density separation (hydrocyclone and Wilfley shaking table) and froth flotation techniques were used to produce monazite concentrates from heavy mineral sand. The produced monazite concentrate-1 contained 5.5% La_2O_3, 10.6% Ce_2O_3, 4.8% Nd_2O_3, 0.54% Y_2O_3, 0.97% ThO_2 and 0.11% U_3O_8; whereas the concentrate-2 contained 10.3% La_2O_3, 21.8% Ce_2O_3, 9.2% Nd_2O_3 and 1.33% Y_2O_3.

Keywords: *Heavy Mineral Sand, Monazite, Light Rare Earth Elements (LREE), Hydrocyclone, Wilfley Shaking Table, Froth Flotation*

1. Introduction

Monazite is a reddish-brown crystalline phosphate mineral [(Ce,La,Nd,Th)PO_4] and a major natural source of light rare-earth elements (Ce, La and Nd) and thorium (Th) extraction on commercial scale. Monazite, among 250 known minerals containing rare earth elements is one of the most important minerals as the primary source of Refs [1-4]. The total rare earth oxide contents of monazite exist in the range of 49.60-73.14% REE_2O_3 with average value of 64.31% REE_2O_3. It is a radioactive mineral due to the presence of thorium (Th) and less content of uranium (U). Monazite contains a significant amount of helium (^{2}He) due to alpha (α) decay of Th and U, which can be extracted on heating [5]. It is formed when igneous rocks undergo crystallization and clastic sedimentary rocks undergo metamorphism and occurs as small heavy crystals in granitic and gneissic rocks and their detritus as called monazite sands. Monazite is considered as a group of minerals due to variability in rare earth elements composition. There are five most common species of monazite, depending on the relative amounts of rare earth elements in the mineral; monazite-(Ce), (Ce,La,Nd,Th)PO_4 (the most common member), monazite-(La), (La,Ce,Nd)PO_4, monazite-(Nd), (Nd,La,Ce)PO_4, monazite-(Sm), (Sm,Gd,Ce,Th)PO_4 and monazite-(Pr), (Pr,Ce,Nd,Th)PO_4 [6]. The most common species of the group is monazite-(Ce) which occurs usually in small isolated crystals. Monazite is commonly mined in placer deposits, which are masses of loose sediment mainly consisting of sand. The large deposits of monazite sand occur in Australia, Brazil, China, India, Malaysia, Madagascar, Vietnam and South Africa. Indian beach placers are an important source of monazite [7-11]. It is often mined as a byproduct of heavy mineral deposits.

Monazite and zircon minerals are found in the middle member of Dubaydib Formation (DB2) from the Ordovician age. Dubaydib area is characterized by flat sandy-clayey of alluvial sediments. The sand deposits were transported over a gentle slope from the Arabian-Nubian shield and deposited in the middle member of Dubaydib Formation over a huge area in the south of Jordan [12, 13]. It covers an area of 900 km^2 and is located about 350 km south of Amman city and 100 km north of Aqaba (Fig. 1). The thickness of heavy mineral sand deposit bearing monazite and zircon ranges from 1.5-4.2 meter. The host rock is mainly composed of quartz (SiO_2), plagioclase [$(Na,Ca)Al(Si,Al)Si_2O_8$], biotite [$K(Mg,Fe)_3AlSi_3O_{10}(F,OH)_2$], muscovite [$KAl_2(Si_3Al)O_{10}(OH)_2$] and zircon ($ZrSiO_4$), with small amounts of rutile (TiO_2), monazite [(Ce,La,Nd,Th)PO_4] and tourmaline (a crystalline silicate mineral group in which boron is compounded with Al, Fe, Mg, Li, Na and K) [12]. The Dubeydib heavy mineral sand deposit contained an average concentration of 1% rare earth elements.

In mineral processing sector, beneficiation studies are being used to separate target minerals from gangue minerals by applying differences in their physical properties such as density and magnetic properties. Physical separation techniques can be used to upgrade or to concentrate the ore prior to hydrometallurgical process when the target minerals are present in low concentration. Currently, extensive goal-oriented research work has been conducted to develop beneficiation flowsheet of various REE-bearing deposits [14-20]. In particular, the beneficiation process for placer deposits is well established and includes a combination of gravity, magnetic, electrostatic and flotation beneficiation processes [21-23]. For beneficiation of monazite from heavy mineral sands, shaking table and spiral density separation [24, 25], magnetic [26, 27], electrostatic [28] and froth flotation [29] separation techniques are being used. The quality of monazite is important for the hydrometallurgical process to extract high purity end products of La, Ce, Nd and Y. The present study

*Corresponding author: tosamat@gmail.com

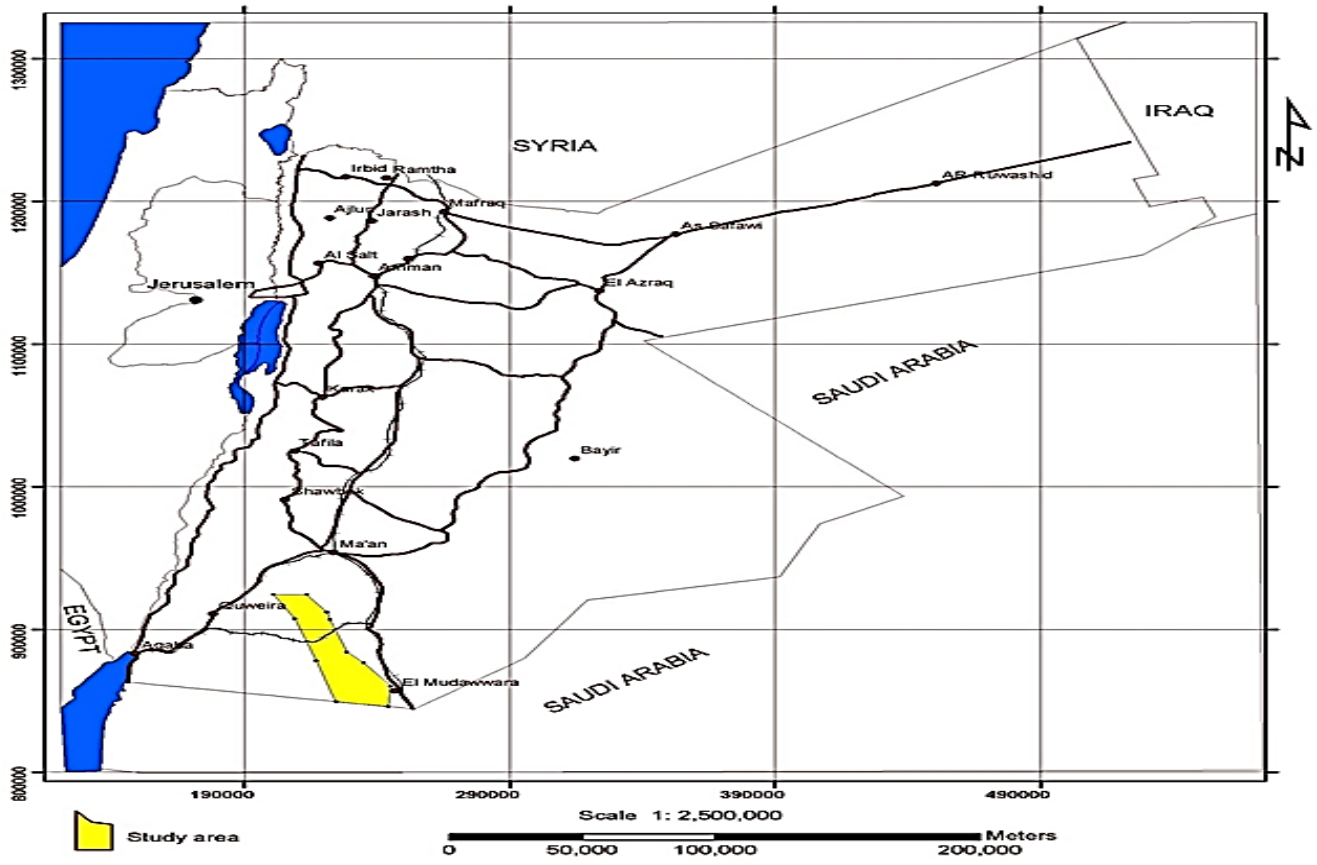

Fig. 1: A simplified Jordan map showing the Dubeydib heavy sand formation (yellow color).

was conducted to produce monazite concentrate from Dubeydib heavy minerals sand by using density separation (hydrocyclone and shaking table) and froth flotation techniques.

2. Materials and Methods

2.1 Heavy mineral sand sample

The heavy mineral sand sample (200-kg) was collected from the Dubeydib deposit site. The sample was crushed, homogenized and the whole sample was pass through 35-mesh size sieve (<500 μm particle size). A representative sub-sample (20 kg) was prepared by thoroughly mixing, coning and quartering technique for chemical and experimental beneficiation studies. Fig. 2 shows the physical appearance of the heavy mineral sand in the field of Dubeydib formation. The mineralogical composition of the heavy mineral sand with mineral formula and specific density is reported in Table 1. X-ray diffraction analysis was carried out to determine the minerals present in the sample.

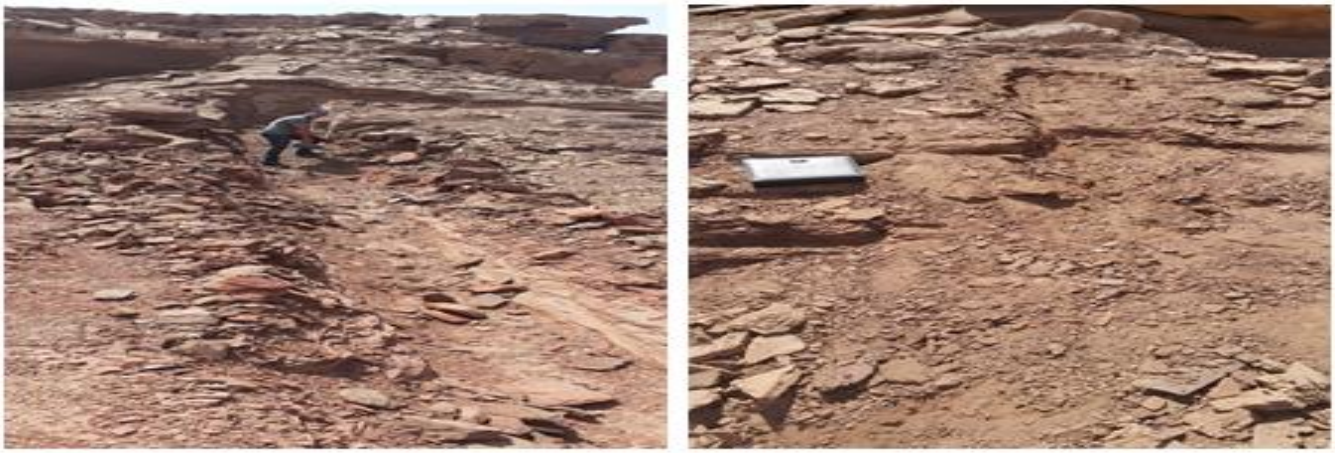

Fig. 2: Dubeydib heavy mineral sands formation – DB2 area

Table 1: Mineralogical characterization of Dubeydib Monazite concentrate

Mineral name	Mineral formula	Specific density (g cm^{-3})
Ce-Monazite	$(Ce,La,Nd,Th,Y)PO_4$	4.98-5.43
Zircon	$ZrSiO_4$	4.60-4.70
Rutile	TiO_2	4.23
Hafnon	$(Hf,Zr)SiO_4$	6.97
Hematite	Fe_2O_3	5.26
Ilmenite	$FeTiO_3$	4.70
Quartz	SiO_2	2.65
Plagioclase	$NaAlSi_3O_8$ - $CaAl_2Si_2O_8$	2.60-2.80

2.2 Beneficiation studies

Hydrocyclone separator was used to separate a stream of particles into fine and coarse size fractions. A water sand slurry (1kg sand in 30-litre water; <500 µm particle size) was pumped at 1 bar pressure to enter at the top of the conical wall of hydrocyclone through a vortex finder which created tangential flow and therefore, a strong vortex in the hydrocyclone. The slurry in the cyclone spined in a high velocity vortex and the fine particles capable of remaining in suspension exit out from the top central pipe (overflow) and the coarse particles spiral down to fall through the underflow at the narrow vortex base. Both the fractions (overflow and underflow) were collected, de-watered, dried and weight fractions calculated and analyzed for chemical composition. Fig. 3 shows the hydrocyclone unit and the process of separation fine size and coarse size fractions.

Holman-Wilfley shaking table (Holman Wilfley Ltd, UK), a gravity separation process was used to recover monazite from heavy mineral sand sample. The batch test was conducted using 2 kg of feed sample at 5º angle of the shaking table, 20 mm shaking amplitude and 2-litre/min water flow rate. Three fractions (light, middling and heavy) were collected, dewatered, dried, weighed and analyzed for rare earth elements. Fig. 4 shows the shaking table unit used for present studies.

Fig. 3: Hydrocyclone classifier (laboratory scale) with overflow and underflow fractions.

For froth flotation studies, 250-g sand sample was taken in 2 litre water in the system, the slurry pH 12.0 was adjusted with dil. NaOH solution, 1.0 g sodium silicate (as conditioner), 1.0 ml oleic acid (as collector) and 2-drops of Aero 619 (as frother) added for experimental studies. The slurry was stirred constantly during the addition of chemicals. The system was operated at 500-rpm with aeration to froth the particles. Two fractions (sink and float) were collected, washed with deionized water thoroughly, de-watered, dried, weighed and analyzed for rare earth elements. Fig. 5 shows the froth flotation unit and the mechanism of operation.

2.3 Chemical analysis

Wavelength-dispersive X-ray fluorescence spectrometer (Bruker S4 Pioneer WD XRF) was used for elemental analysis of the sand sample and sand fractions obtained during beneficiation studies carried out by hydrocyclone, shaking table and froth flotation techniques. The finely ground sample (0.6 g), less than 200-mesh (<73 µm) or finer was mixed with flux (lithium metaborate ($LiBO_2$); 10:1 ratio (0.6 g sample and 6.0 g flux) as the fusion material and glass-forming agent)

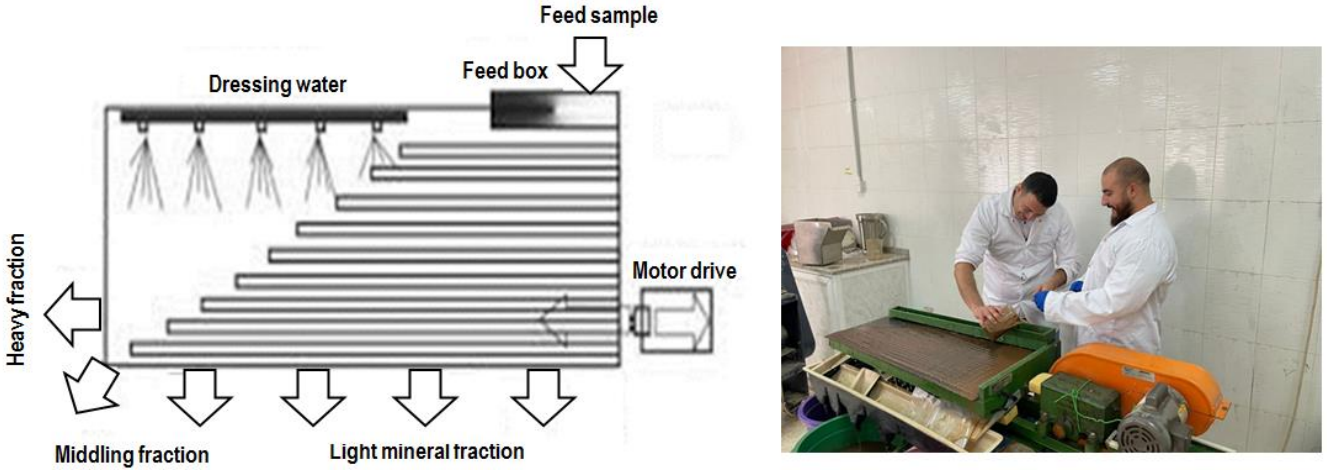

Fig. 4: Wilfley shaking table unit used in the experimental studies and the sketch showing the light, middling and heavy fractions (left) collecting points during beneficiation studies of heavy mineral sand.

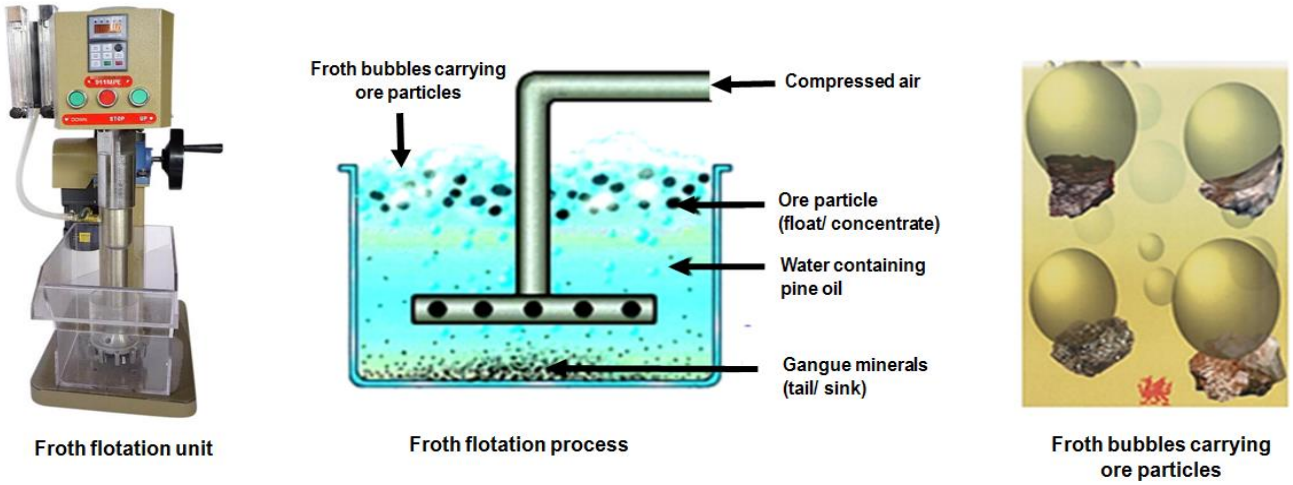

Fig. 5: Froth flotation cell and phenomenon of flotation process for separation of minerals

then placed into a platinum crucible. The crucible was set onto melting position and then the sample was fully automatically oxidized, melted at 1000-1200 ºC, stirred and cast. A high-frequency electromagnetic induction heating and fusing machine (Bead Sampler NT-2000; Nippon Thermonics) was used for glass beads preparation. The platinum crucibles (CS-2 type; 95% Pt – 5% Au) were used for making glass beads from a mixture of powdered rock sample and alkali flux. The cold fusion bead was placed into the XRF for measurement.

3. Results and discussion

3.1 Feed sample analysis

The chemical composition of the heavy mineral sand sample is given in Table 2. It contained 64.4% SiO_2, 6.9% Al_2O_3, 6.5% TiO_2, 6.0% Fe_2O_3, 4.7% ZrO_2 and 2.6% K_2O as major constituents of the sand sample. The sample contained low concentrations of light rare earth elements of 0.22% La (0.26% La_2O_3), 0.50% Ce (0.59% Ce_2O_3) and 0.20% Nd (0.24% Nd_2O_3) with 0.08% Y (0.1% Y_2O_3) as heavy rare earth element.

Table 2: WD-XRF analysis of Dubeydib heavy mineral sand sample

Constituents	Results(%)	Constituents	Results(%)	Constituents	Results(%)
SiO_2	64.40	P_2O_5	0.66	Ba	0.05
Al_2O_3	6.90	SO_3	0.18	Y	0.08
Fe_2O_3	6.01	Mn	0.02	La	0.225
TiO_2	6.50	Zr	3.50	Nd	0.208
K_2O	2.60	Hf	0.12	Ce	0.50
Na_2O	0.43	V	0.04	Mo	0.05
MgO	0.85	Cr	0.03	Th	0.19
CaO	1.18	Sr	0.03	U	0.021

It is indicated from the analytical data that the sample contained total contents of 1.02% REE (1.20% REEO). Cerium (Ce) concentration in the sample is double of the contents of La and Nd (Table 2). It is indicated that the sand sample contained monazite-Ce. Uranium (0.021% U) and thorium (0.19% Th) as radioactive elements.

3.2 Hydrocyclone beneficiation

Hydrocyclone classified fine size particles (overflow fraction) and coarse size particles (underflow fraction) of heavy mineral sand during beneficiation process. The weight fractions and chemical analysis data of rare earth elements (La, Ce, Nd and Y) of overflow and underflow fractions are reported shown in Table 3. The weight of overflow fraction of 118.30 g (11.83% wt) and underflow fraction of 857.50 g (85.75% wt) with weight loss of 24.20 g (2.42% wt) was obtained. The overflow fraction (fine size fraction) contained 688 ppm Ce and 54 ppm Y with contents of La and Nd. The concentrations of P_2O_5 and SiO_2 in the overflow fraction were decreased Al_2O_3, Fe_2O_3 and TiO_2 contents increased as compared to feed sample. The underflow fraction (coarse or heavy fraction) contained higher concentrations of La, Ce, Nd and Y than the feed sand sample. It contained 2309 ppm La, 5496 ppm Ce and 2435 ppm Nd (Table 3). The rare earth elements (La, Ce, Nd and Y) present in the sample are constituents of monazite mineral [(Ce,La,Nd,Th)PO_4] which is a phosphate mineral having high specific density of 4.98-5.43 g/cm^3. The monazite mineral remained in the underflow fraction due to its high density resulted an increase in the concentrations of REE which is indicated from high phosphate content in the underflow fraction (Table 3).

Table 3: Distribution of La, Ce, Nd and Y in overflow and underflow fractions of hydrocyclone beneficiation studies

Description	Fraction weight		Major elements (%)					Rare earth elements (ppm)			
	(g)	(%)	SiO_2	Al_2O_3	Fe_2O_3	P_2O_5	TiO_2	La	Ce	Nd	Y
Feed sample	1,000	100.0	63.4	6.9	6.0	0.66	6.5	2253	5001	2082	798
Overflow	118.3	11.8	29.0	20.6	6.5	0.13	1.5	N.D.	688	N.D.	54
Underflow	857.5	85.5	56.2	27.4	7.7	0.72	11.3	2309	5496	2435	857
Loss	24.2	2.4	-	-	-	-	-	-	-	-	-

The high concentrations of Fe_2O_3 and TiO_2 in the underflow fraction correspond to high density minerals of hematite (5.26 g/cm^3), ilmenite (4.70 g/cm^3) and rutile (4.23 g/cm^3) (Table 1). The hydrocyclone is gravity separation device used in slurry pulps to separate a stream of particles into coarse and fine particles fractions based on mineral particle density. Hydrocyclone separators are used worldwide in mining and mineral processing industries for classification, de-sliming and de-watering applications. Zircon (4.60-4.70 g/cm^3) and hafnon (6.97 g/cm^3) are high density minerals and quartz (2.65 g/cm^3) and plagioclase (2.60-2.80 g/cm^3) are low-density minerals.

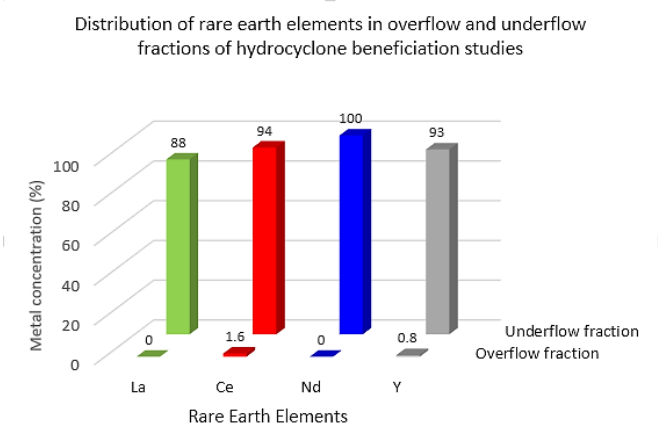

Fig. 6: Distribution of rare earth and radioactive elements in overflow and underflow fractions of Dubeydib heavy mineral sand.

The distribution of La, Ce, Nd and Y in the overflow and underflow fractions of the hydrocyclone beneficiation of Dubeydib heavy mineral sand is shown in Fig. 6. It is indicated that overflow fraction contained negligible amount of rare earth elements. The rare earth elements are mainly ≥88% present in the underflow fraction. It contained 88% La, 94% Ce, 100% Nd and 93% Y distribution of these elements in the underflow fraction. It is indicated that the rare earth elements are concentrated in the overflow fraction (Fig. 6).

3.3. Wilfley shaking table beneficiation

A standard laboratory scale Wilfley shaking table to utilize the gravity concentration process to fractionate both particle density and particle size into light (waste), middling and heavy (monazite concentrate) fractions of Dubaydib heavy mineral sand. During shaking table beneficiation process, five fractions of light, middling-1, middling-2, heavy-1 and heavy-2 were obtained. The weight fractions and chemical analysis of these fractions are reported in Table 4. The weight fractions of 11.1% light, 71.2% middling (middling-1 and middling-2) and 15% heavy (heavy-1 and heavy-2) fractions obtained from heavy mineral sand during Wilfley shaking table beneficiation process. A weight loss of 3.0% wt was also observed.

It is indicated from the analytical data that the light rare earth elements (La, Ce and Nd) are not present in the light fraction of the heavy mineral sand by gravity separation shaking table (Table 4). Only, 125 ppm Y content was observed in the light fraction. The low content of phosphate (0.12% P_2O_5) corresponds to less amount of phosphate mineral (monazite) present in the light fraction. The weight fraction of middling-1 (10.2% wt) exhibited the presence of 1006, 2275, 857 and 408 ppm La, Ce, Nd and Y, respectively. The phosphate content of 0.48% P_2O_5 is also high as compared to light fraction (0.12% P_2O_5). The weight fraction of middling-2 fraction was 61% wt with low contents of rare earth elements as compared to middling-1 fraction. It is indicated from the low phosphate content (0.38% P_2O_5) in this fraction. The concentrations of La, Ce, Nd and Y are higher in the heavy-1 fraction as compared to middling-2 fraction. The rare earth elements concentrated in the heavy-2 fraction which contained 36763 ppm La (3.68% La), 66459 ppm Ce (6.65% Ce), 30192 ppm Nd (3.02% Nd) and 6172 ppm Y (0.62% Y) (Table 4). The monazite-rich heavy-2 fraction contained total rare earth elements of 13.96% ∑REE (16.32% ∑REO) and 8.20% P_2O_5. It is indicated from the beneficiation data that the concentration of REE increased with an increase of phosphate content in the heavy fraction which is mainly attributed to monazite-rich fraction. The shaking table gravity separation process has to be re-tabled to produce monazite-rich concentrate from heavy mineral sand. The gravity separation recovered 76.6% monazite from Senegalese heavy mineral sands deposit [30, 31].

Table 4: Chemical composition of light, middling and heavy fractions of Wilfley shaking table beneficiation studies of Dubeydib heavy mineral sand

Description	Fraction weight		Major elements (%)					Rare earth elements (ppm)			
	(g)	(%)	SiO_2	Al_2O_3	Fe_2O_3	P_2O_5	TiO_2	La	Ce	Nd	Y
Feed sample	2000	100	63.4	6.91	6.01	0.66	6.51	2253	5001	2082	798
Light fraction	222	11.1	31.8	18.13	19.68	0.12	4.20	N.D.	N.D.	N.D.	125
Middling-1	204	10.2	64.7	7.69	5.93	0.48	6.72	1006	2275	857	408
Middling-2	1219	61.0	71.2	5.96	4.58	0.38	6.13	489	1153	474	319
Heavy-1	224	11.2	52.0	3.90	4.47	0.61	13.30	1402	2806	1218	1291
Heavy-2	70	3.5	22.0	1.15	1.87	8.20	7.62	36763	66459	30192	6172
Loss	61	3.1	-	-	-	-	-	-	-	-	-

N.D. = Not detectable (below detection limit)

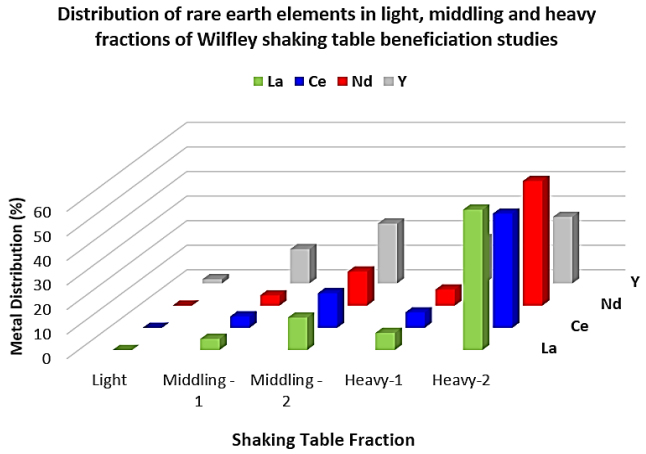

Fig. 7: Distribution of La, Ce, Nd and Y in various fractions of Wilfley shaking table beneficiation studies of Dubeydib heavy mineral sand.

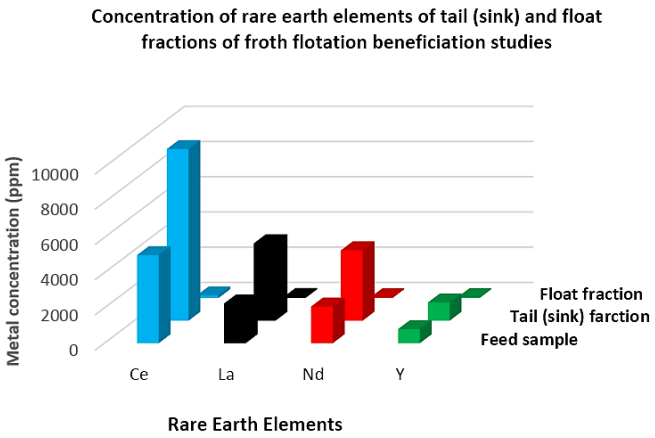

Fig. 8: Concentration of Ce, La, Nd and Y in heavy mineral sand (feed sample), tail (sink) and float fractions of froth flotation beneficiation studies.

The distribution (%) of rare earth elements (La, Ce, Nd and Y) in the various fractions obtained from heavy mineral sand during shaking table beneficiation process is shown in Fig. 7. It is indicated that monazite-rich concentrate fraction (heavy-2) contained the highest contents of 57% La, 47% Ce, 51% Nd and 27% Y. The light fraction (waste) contained 1.7% Y with no contents of La, Ce and Nd. The middling-2 fraction having 61% weight fraction contained 13-27% rare earth elements. This fraction and middling-2 and heavy-1 fractions required re-tabled process to separate REE to produce monazite-rich concentrate. The monazite rich fraction cannot be concentrated to a salable grade by single step or solely separation technique. Hence, monazite fraction has to be re-tabled to separate high recovery from the treated sand. The shaking tabletop strip part is treated for monazite recovery.

3.4. Froth flotation beneficiation

Rare earth elements are floatable using cationic collectors such as oleic acid and sodium oleate in the pH range of 7-11 [32]. Zirconium minerals are depressed at ~~a~~ pH greater than 10 by using sodium silicate and oleic acid for flotation of monazite ore sample to concentrate Zr. The conditioning time for flotation was 6 min and 2 drop of aero float (Aero 619) was added into sample water slurry. The tail (sink) fraction of 48 g and float fraction of 201 g were recovered. The tail fraction has the $1/5^{th}$ weight of the float fraction. The rare earth elements (monazite mineral) were separated and recovered in the tail fraction which contained 737 ppm Ce (0.97% Ce), 4389 ppm La (0.44% La), 3992 Nd (0.4% Nd) and 1092 ppm Y (0.11% Y) (Fig. 8). The float fraction (major fraction by weight) has negligible amounts of REE. It is indicated that the REE containing monazite mineral is separated and recovered in the tail (sink) fraction in froth flotation beneficiation studies.

A monazite-rich concentrate (concentrate-1) was produced by combining hydrocyclone and shaking table density separation techniques (Table 5). In the first step, heavy mineral sand was separated into overflow and underflow fractions using hydrocyclone and then underflow fraction was used as feed material for Wilfley shaking table. The shaking tabletop strip part was used for the separation and recovery of heavy fraction to produce of monazite-rich concentrate. The chemical analysis of the concentarte-1 are reported in Table 5. It contained 5.48% La_2O_3, 10.54% Ce_2O_3, 4.78% Nd_2O_3 and 0.55% Y_2O_3. The total rare earth elements in the monazite concentrate were 21.40% ∑REEO. The high phosphate content of 10.80% P_2O_5 indicated the monazite-rich mineralization in the concentrate sample. It is indicated that the hybrid gravity separation process (hydrocyclone + shaking table) produced concentrate containing high content of 21.40% ∑REO as compared to monazite-rich fraction (heavy-2) solely produced by shaking table experiment which contained 16.32% ∑REO (section 3.3). The existence of 1.05% Al_2O_3, 3.9% TiO_2 and 1.53% Fe_2O_3 in the concentrate indicated the presence of minerals containing Al, Ti, and Fe as impurities.

Table 5: Chemical composition of produced monazite concentrates from Dubeydib heavy mineral sand

Description	Beneficiation process	Metal concentration (%)				
		La_2O_3	Ce_2O_3	Nd_2O_3	Y_2O_3	∑REEO
Feed sample	-	0.26	0.59	0.24	0.10	1.20
Concentrate-1	Hydrocyclone + Wilfley shaking table	5.48	10.54	4.78	0.55	21.40
Concentrate-2	Hydrocyclone +Wilfley shaking table + Froth flotation	10.3	21.82	9.15	1.33	53.60

Similarly, a monazite-rich concentrate (concentrate-2) was produced from the Dubeydib heavy mineral sand by the combination of two gravity separation techniques (hydrocyclone+shaking table) and froth flotation beneficiation process. The overall schematic presentation of the combined beneficiation studies is shown in Fig. 9. The monazite-rich heavy fraction of sand sample produced by

hydrocyclone and shaking table was used as feed material for the separation and recovery of monazite concentrate by froth flotation. The monazite-rich concentrate was separated and recovered in the sink (tail) fraction, de-watered, washed with ethanol to remove adhering organic compound(s) from the surface of the particle, dried and analyzed by WD XRF. The chemical analysis of the produced monazite-rich concentrate is reported in Table 5. The analysis data showed the presence of 8.76% La (10.3% La_2O_3), 18.63% Ce (21.82% Ce_2O_3), 7.84% Nd (9.15% Nd_2O_3) and 1.05 % Y (1.33% Y_2O_3). The total rare earth contents present in the concentrate are 45.7% ∑REE (53.6% ∑REO). It is indicated that the concentrate-2 produced by the combination of three beneficiation techniques (hydrocyclone+ shaking table + froth flotation) exhibited high contents of rare earth elements as compared to concentarte-1 produced by combined gravity separation techniques (hydrocyclone + shaking table).

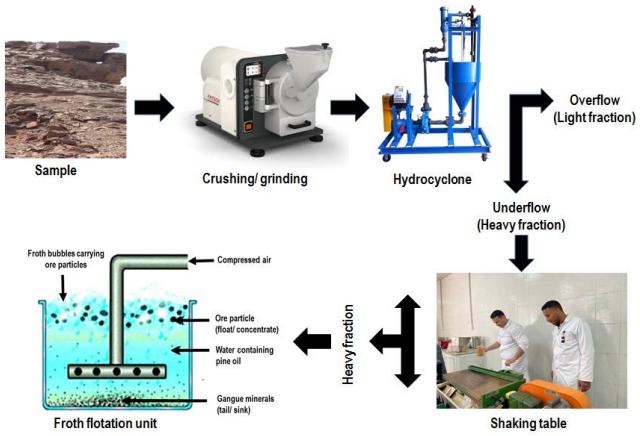

Fig. 9: Schematic presentation of the overall beneficiation process for production of monazite concentrate-2 from Dubeydib heavy mineral sand

From the beneficiation studies, it is observed that the separation and recovery of REE from Dubeydib heavy mineral sand in the concentrates produced by solely hydrocyclone, shaking table, combined hydrocyclone + shaking table and combined hydrocyclone + shaking table + froth flotation techniques contained rare earth contents of 1.30%, 16.32%, 21.40% and 53.6% ∑REO, respectively. It is indicated that the monazite-rich concentrate cannot be produced to a salable grade by single step or solely separation technique. Generally, monazite contains about 70% ∑REO, with REE fraction constituted by 20 to 30% Ce_2O_3, 10 to 40% La_2O_3 and significant amounts of Nd, Pr and Sm [33].

4. Conclusions

Dubaydib heavy mineral sand contains monazite-Ce mineral as source of light rare earth elements (La, Ce and Nd) and yttrium (Y). A number of experimental beneficiation studies were carried out to produce monazite-rich concentrate from heavy mineral sand by using hydrocyclone, shaking table and froth flotation. The results showed that the separation and recovery of monazite from Dubaydib Formation by shaking table is much higher than hydrocyclone gravity separation technique under present experimental conditions. The best combination of two gravity separation techniques (hydrocyclone+shaking table) produced monazite-rich concentrate containing 21.4% ∑REO) and the combined three techniques (hydrocyclone+shaking table + froth flotation) gave high values of monazite mineral which contained 53.6% ∑REO. The results obtained proved that the increase of phosphate content, the concentrations of La, Ce, Nd and Y increased in the recovered concentrate.

Acknowledgments

The authors would like to thank Jordan Atomic Energy Commission (JAEC) and the technical staff for their assistance and cooperation during experimental studies and analytical support.

References

[1] Y. Kanazawa and M. Kamitani, "Rare earth minerals and resources in the world," Journal of Alloys and Compounds, Vol. 408-412, pp. 1339-1343, 2006.

[2] G.J. Simandl, "Geology and market-dependent significance of rare earth element resources," Mineralium Deposita, vol. 49, pp. 889-904, 2014.

[3] A. Golev, M. Scott, P.D. Erskine, S.H. Ali and G.R. Ballantyne, Rare earths supply chains: Current status, constraints and opportunities, Resource Policy, vol. 41, pp. 52-59, 2014.

[4] K. Zglinicki, K. Szamałek and G. Kono, "Monazite-bearing post processing wastes and their potential economic significance," Gospodarka Surowcami Mineralnymi – Mineral Resources Management, vol. 36, issue 1, pp. 37-58, 2020.

[5] H. Chaudhuri, B. Sinha and D. Chandrasekharam, "Helium from geothermal sources," Proceedings World Geothermal Congress 2015, Melbourne, Australia, 19-25 April 2015.

[6] A.R. Chakhmouradian and R.H. Mitchell, "Lueshite, pyrochlore and monazite-(Ce) from apatite-dolomite carbonatite, Lesnaya Varaka complex, Kola Peninsula, Russia," Mineralogical Magazine, vol. 62, pp. 769-782, 1998.

[7] S.K. Haldar, "Mineral exploration principles and applications," Elsevier: Waltham, USA, pp. 55-57, 2013.

[8] D.M. Hoatson, S. Jaireth and Y. Miezitis, "The major rare-earth-element deposits of Australia: geological setting, exploration and resources," Geoscience Australia, p. 204, 2011.

[9] K. Szamałek, G. Konopka, K. Zglinicki and B. Marciniak-Maliszewska, "New potential source of rare earth elements," Gospodarka Surowcami Mineralnymi – Mineral Resources Management, vol. 29(4), pp. 59-76, 2013.

[10] B.S.V. Gosen, D.L. Fey, A.K. Salah, P.L. Verplank and T.M. Hoefen, "Deposit model for heavy-mineral sands in coastal environments," Scientific Investigations Report 2010-5070-L. U.S. Geological Survey, Reston, VA, p. 51, 2014.

[11] W. Chen, H. Honghui, T. Bai and S. Jiang, "Geochemistry of monazite within carbonate related REE deposits," Resources, vol. 6, 51, 2017.

[12] A. Al Malabeh, Z. Al-Smadi and J. Alali, "Mineralogy, geochemistry and economic potential of zircon and associated minerals in Dubaydib sandstone formation, Jordan," Iraqi Geological Journal, vol. 50, No. 1, pp. 1-11, 2017.

[13] B. Friedrich, "Geology of the Arabian Peninsula Jordan," United States Government Printing office, Washington, 1975.

[14] H. Cui and C.G. Anderson, "Alternative flowsheet for rare earth beneficiation of Bear Lodge ore," Minerals Engineering, vol. 110, pp. 166-178, 2017.

[15] A. Jordens, R.S. Sheridan, N.A. Rowson and K.E. Waters, "Processing a rare earth mineral deposit using gravity and magnetic separation," Minerals Engineering, vol. 62, pp. 9-18, 2014.

[16] A. Jordens, C. Marion, R. Langlois, T. Grammatikopoulos, N.A. Rowson and K.E. Waters, "Beneficiation of the Nechalacho rare earth deposit. Part 1: Gravity and magnetic separation," Minerals Engineering, vol. 99, 111-122, 2016.

[17] A. Jordens, C. Marion, R. Langlois, T. Grammatikopoulos, R.S. Sheridan, C. Teng, H. Demers, R. Gauvin, N.A. Rowson and K.E. Waters, "Beneficiation of the Nechalacho rare earth deposit. Part 2: Characterisation of products from gravity and magnetic separation," Minerals Engineering, vol. 99, 96-110, 2016.

[18] L.Z. Li and X. Yang, "China's rare earth ore deposits and beneficiation techniques," In: Proceedings of the European Rare Earth Resource Conference, September 4-7, 2014, Milos Island, Greece.

[19] R. Panda, A. Kumari, M.K. Jha, J. Hait, V. Kumar, J.R. Kumar and J.Y. Lee, "Leaching of rare earth metals (REMs) from Korean monazite concentrate," Journal of Industrial and Engineering Chemistry, vol. 20, 2035-2042, 2014.

[20] X. Yang, J.V. Satur, K. Sanematsu, J. Laukkanen and T. Saastamoinen, "Beneficiation studies of a complex REE ore," Minerals Engineering, vol. 71, pp. 55-64, 2015.

[21] M.I. Moustafa and N.A. Abdelfattah, "Physical and chemical beneficiation of the Egyptian beach monazite," Resource Geology, vol. 60, pp. 288-299, 2010.

[22] G.R. Rajan and M. Sundararajan, "Combined magnetic, electrostatic and gravity separation techniques for recovering strategic heavy minerals from beach sands," Marine Georesources & Geotechnology, vol. 36, pp. 959-965, 2018.

[23] W.L. Xiong, J. Deng, B.Y. Chen, S.Z. Deng and D.Z. Wei, "Flotation-magnetic separation for the beneficiation of rare earth ores," Minerals Engineering, vol. 119, 49-56, 2018.

[24] M.I. Moustafa and N.A. Abdelfattah, "Physical and chemical beneficiation of the Egyptian beach monazite," Resource Geology, vol. 60, issue 3, pp. 288-299, 2010.

[25] S. Routray and R.B. Rao, "Beneficiation and characterization of detrital zircons from beach sand and red sediments in India," Journal of Minerals and Materials Characterization and Engineering, vol. 15, issue 11, pp. 1409-1428, 2011.

[26] K. Kim and S. Jeong, "Separation of monazite from placer deposit by magnetic separation," Minerals, vol. 9, 149, 2019.

[27] X. Yang, N. Heino and L. Pakkanen, "Beneficiation studies of a rare earth ore from the Olserum deposit," Natural Resources, vol. 10, pp. 346-357, 2019.

[28] C.C. Gonçalves and P.F.A. Braga, "In-depth characterization and preliminary beneficiation studies of heavy minerals from beach sands in Brazil," The Tenth International Heavy Minerals Conference, 16-17 August, 2016, Sun City, Southern African Institute of Mining and Metallurgy, pp. 289-302.

[29] A. Jordens, Y.P. Cheng and K.E. Waters, "A review of the beneficiation of rare earth element bearing minerals," Minerals Engineering, vol. 41, pp. 97-114, 2013.

[30] M. Dieye, M.M. Thiam, A. Geneyton and M. Gueye, "Monazite recovery by magnetic and gravity separation of medium grade zircon concentrate from Senegalese heavy mineral sands deposit," Journal of Minerals and Materials Characterization and Engineering, vol. 9, pp. 590-608, 2021.

[31] I. Park, Y. Kanazawa, N. Sato, P. Galtchandmani, M.K. Jha, C.B. Tabelin, S. Jeon, M. Ito and N. Hiroyoshi, "Beneficiation of low-grade rare earth ore from Khalzan Buregtei Deposit (Mongolia) by magnetic separation," Minerals, vol. 11, 1432, Dec., 2021.

[32] A. Jordens, Y.P. Cheng and K.E. Waters, "A review of the beneficiation of rare earth element bearing minerals," Minerals Engineering, vol. 41, pp. 97-114, 2013.

[33] C.K. Gupta and N. Krishnamurthy, "Extractive Metallurgy of Rare Earths, CRC Press, Florida, 2005. Print ISBN: 978-0-415-33340-5. eBook ISBN: 978-0-203-41302-9.

The Nucleus ***60***, *No. 2 (2023) 120-125*

www.thenucleuspak.org.pk

The Nucleus
ISSN 0029-5698 (Print)
ISSN 2306-6539 (Online)

Physico-chemical Properties of Various Types of Wastewaters Used as Source of Irrigation

Amna Javed[1*], Samreen Shehzadi[2], Tanveer Ahmad[2], Syed Azam Shah[2]

[1]*Pakistan Institute of Engineering and Applied Sciences (PIEAS), Islamabad, Pakistan*

[2]*Pakistan Nuclear Society (PNS), Islamabad, Pakistan*

ABSTRACT

Wastewater is widely used for irrigation of agricultural lands due to scarcity of freshwater, its reliable supply and high nutrients value. However, untreated wastewater is mostly contaminated with organic pollutants and toxic heavy metals including: cadmium (Cd), chromium (Cr), mercury (Hg), lead (Pb), copper (Cu), nickel (Ni), zinc(Zn), cobalt (Co), Iron (Fe), molybdenum (Mo) and boron (B). Therefore, chemical analyses of wastewater is of great concern for safe agricultural irrigation. A study was conducted at Central Analytical Facility Division (CAFD) of Pakistan Institute of Nuclear Science and Technology (PINSTECH), Islamabad with the objective to collect various types of wastewater and analyze for their nutrient composition (macro & micronutrients), heavy metals content (As, Hg, Cr, Cd, Pb, Ni) and other physicochemical characteristics including: pH, electrical conductivity (EC), total dissolved solids(TDS), total suspended solids(TSS), chemical oxygen demand (COD) and biological oxygen demand (BOD). Three categories of wastewater including sewage water, industrial wastewater and domestic wastewater being used as irrigation source were collected from various places and were analyzed using atomic absorption spectrometry (AAS) and inductively coupled plasma- optical emission spectrometry (ICP-OES). The obtained results revealed that domestic wastewater (Shah Town, Islamabad) and industrial wastewater (Hayatabad, Peshawar) were found environmentally safe. It was found that sewage water collected from Tarlai farms, Islamabad had no toxic heavy metals except mercury (2.67 ng mL^{-1}) which was slightly above than FAO safe limits. However, sewage water collected from Sohan village, Islamabad is not recommended for irrigation due to its high mercury content (342.14 ng mL^{-1}).

Keywords: *Industrial Wastewater, Domestic Wastewater, Sewage Water, Heavy Metals*

1. Introduction

Wastewater is widely used for irrigation of agricultural lands in developed countries as well as in underdeveloped countries like Pakistan [1]. Almost 20 million hectares of agricultural land is irrigated by wastewater around the globe which is almost 10% of irrigated agrarian land [2]. Droughts, climate change and urban development have put a substantial pressure on freshwater supplies [3]. It is assessed that during next 50 years, more than 40% of the world's population will face water scarcity problem [4]. Pakistan is also facing water scarcity problem as freshwater supply is decreasing gradually. Water scarcity will have significant impacts on agriculture by reducing crop productivity [5] and it will pose serious challenges to food security [6].

Wastewater is produced by different sources such as domestic discharges, industrial effluents, water received from commercial areas, hospitals and urban runoff [7]. Annually 962,335 million gallons of wastewater is generated in Pakistan where 288,326 million gallons receive from industrial discharge and 674,009 million gallons of water from municipal use [8].

Due to shortage of freshwater and high nutrients in waste water has increased its utilization for irrigation purposes [9]. Reusing wastewater for irrigation reduces the need for artificial fertilizers, increases crop yields and helps conserve natural water resources [10]. The nutrient content in the wastewater may exceed the desired level which may damage the crop [11]. Several contaminants such as pathogens, organic pollutants and non-biodegradable toxic heavy metals including Cd, Cr, Hg, Pb, Cu, Ni, Zn, Co, Fe and Mo, are present in untreated wastewater [12]. Hence, consistent use of untreated wastewater for irrigation may cause heavy metal accumulation in agricultural soil [13]. These harmful pollutants can be absorbed by plants, which can then enter in the food chain, posing a serious health risk [14]. Consumption of contaminated food may result in serious health problems in humans such as growth retardation, gastro intestinal cancer and kidney and liver malfunctions [15]. Therefore, assessing chemical quality of wastewater is of great concern for safe agricultural irrigation [16]. The, wastewater must be analyzed for its toxicity and other physico-chemical characteristics prior using for irrigation purposes.

2. Materials

The study was conducted during 2018 to 2019 at the Central Analytical Facility Division (CAFD), PINSTECH, Nilore, Islamabad. The study was carried out with the objective to analyze physicochemical characteristics of different categories of wastewater used as source of irrigation.

2.1 Wastewater collection

Composite samples of wastewater (sewage water, industrial wastewater, domestic wastewater) used for irrigation of agricultural fields and vegetable farms were collected from four different sites as shown in Table 1.

Industrial wastewater samples were collected from two different sites in Hayatabad Industrial Estate (HIE), Peshawar. The estate discharges effluents into Kabul River which is main irrigating canal of Peshawar. Match factories, paint factories and pharmaceutical industries discharge their effluents in these sites. Site 2 was located 10 meters away from the main drain while Site 7 was 100 meters away.

*Corresponding author: amnajaved12@yahoo.com

Table 1: Wastewaters samples collected from various sites.

Type of wastewater	Collection Date	Collection Site
Industrial waste water Site 2 & Site 7	March 20, 2019	Hayatabad Industrial Estate (HIE), Peshawar
Domestic Waste Water	Jun 12, 2019	Shah Town, Sohan Islamabad
Sewage water	Jun 12, 2019	Sohan Village, Islamabad
Sewage Water	Jun 12, 2019	Tarlai Farms, Islamabad

Sewage water samples were collected from Sohan, Islamabad (33°39'44.7"N 73°06'06.7"E) and P&V Farms, Tarlai, Islamabad (33°38'40.4"N 73°08'15.0"E) whereas domestic wastewater was collected from Shah town, Sohan, Islamabad. The wastewater samples were collected below 10 cm of water surface to avoid floating particles and were preserved in pre cleaned plastic bottles. Non-powdered gloves and face mask were worn during samples collection. After proper labeling, the samples were safely transported to the Atomic Absorption lab at CAFD, PINSTECH Nilore, Islamabad. The samples were kept in the refrigerator to inhibit any microbial activity in the samples.

2.2 Chemical analysis

The waste water samples were analyzed using Inductively Coupled Plasma Optical Emission Spectrometry for macro and micro nutrients determination while Atomic Absorption Spectrophotometer (AAS) for heavy metals analysis. The analytical procedures and respective instruments used for physico-chemical analysis of organic wastes are described in Table 2.

Table 2: List of parameters and instruments used for physico-chemical analysis of wastewater.

Parameters	Instruments/Model
Heavy Metals	
(Pb, Cd	GFAAS, Hitachi Z-8000
As, Hg, Se, Sb)	HGAAS, GBC-932plus
Macro-nutrients	
(Na, Ca, Mg, P, K)	ICP-OES, Thermo, iCAP-6500
Micro-nutrients	
(Cu, Mn, Zn, Cu, Fe)	ICP-OES, Thermo, iCAP-6500
Physico-chemical Parameters	
pH	pH meter, Oakton pH 2100 series
Conductivity, TDS	Conductivity meter, InoLab
TSS, Ammonia	Photometer, MultidirectLovibond
Sulphide, Fluoride, Nitrate Chloride, COD	Photometer, Spectrodirect RS-232
BOD	DO meter

2.3 Heavy metal analysis

Heavy metal analysis of wastewater samples was performed using atomic absorption spectrometry. Graphite Furnace AAS (Hitachi Z-8000) was used for Pb and Cd analysis while Hydride Generation Spectrophotometer (GBC-932plus) was used for determination of As, Se, Sb and Hg in samples. Some macronutrient (N, P, K, Mg, Na, Ca) and micronutrients (Fe, Cu, Zn) were determined by using (ICP-OES), Thermo, iCAP-6500.

3. Results and Discussion

According to an estimate, up to one-tenth of the population of the world consumes food produced by using wastewater as irrigation source [12]. Farmers use wastewater for irrigation because of its nutrient content and reliable supply. In Pakistan, various types of wastewater are being used as a source of irrigation. In this study, three types of wastewater i.e., sewage water, industrial wastewater and domestic wastewater were analyzed for various physico-chemical parameters and elemental profile.

3.1 Sewage water

Sewage water is being used for irrigating the vegetables, as it contains several macro-nutrients and micro-nutrients. In this study, sewage water was collected from Tarlai Farms, Islamabad and Sohan, Islamabad and analyzed for its physico-chemical chemical characterization.

The quality of sewage water was evaluated with respect to its nutrient composition, heavy metals and for its various other physico-chemical parameters. The results are given in Table 3 and Table 4.

3.1.1 Tarlai farms

The results showed that sewage water had pH 7.6 and electrical conductivity of 1.12 dS m^{-1}. Total dissolved solids (TDS) is an important parameter which indicates the presence of inorganic salts in the form of cations and anions [17]. The results showed that TDS value was 614 mg L^{-1} which is below the safe limit. The results further revealed that ammonia (0.12 mg L^{-1}), fluoride (0.60 mg L^{-1}), chloride (16.26 mg L^{-1}), alkalinity (516 mg L^{-1}) and sulphate (31.75 mg L^{-1}) in sewage water were in the permissible limit as described by WHO, 2006 [18].

Table 3: Physicochemical properties of the sewage water (Tarlai Farms and Sohan, Islamabad) with safe limits [18]

Parameters	Units	*Tarlai Farms*	*Sohan Village*	Safe Limits
pH	-	7.6	7.3	6.5-8.4
Conductivity	dS m^{-1}	1.12	0.65	0.25-3.00
TDS	mg L^{-1}	614	355	<2000
TSS	mg L^{-1}	24	7	50-100
Ammonia	mg L^{-1}	0.12	4.13	5
Alkalinity	mg L^{-1}	516	209	<610
Sulfide	mg L^{-1}	ND	ND	
Fluoride	mg L^{-1}	0.60	0.45	1.0
Chloride	mg L^{-1}	16.26	15.79	<350
Sulphate	mg L^{-1}	31.75 ± 0.17	39.77 ± 0.15	500
Nitrate	mg L^{-1}	ND	ND	
COD	mg L^{-1}	23	520	250
BOD	mg L^{-1}	36	42	

However, sulphide was not detected in the sample. Another important parameter i.e., COD (Chemical Oxygen Demand) is useful which indirectly measures the number of organic compounds in water The COD value was found to be

23 mg L^{-1} which is within permissible limits proposed by WHO.

The analyses of sewage water performed using ICP-OES showed that sewage water contains macronutrients including calcium (69.43 µg mL^{-1}), potassium (16.37 µg mL^{-1}), magnesium (28.24 µg mL^{-1}), phosphorus (1.63 µg mL^{-1}) and sodium (84.77 µg mL^{-1}) as shown in Table 3.2. Potassium content is higher than 2 µg mL^{-1} which is the value recommended by FAO [19]. Among micronutrients, only Zn (10 ng mL^{-1}) was detected in the water sample while other micronutrients such as Cu, Fe, Mn were not detected in the sample.

Toxic metals concentration analysis showed that Pb, Cd, Sb, Hg, Se, Cr, Ni were not detected in the sewage water. Although As (5.64 ng mL^{-1}) was found in the sample but it was well below the safe limits proposed by WHO 2006 [18]. However, Hg (2.67 µg mL^{-1}) was a little (0.67 ng mL^{-1}) higher than the safe limit.

Table 4: Elemental profile of sewage water (Tarlai Farms and Sohan, Islamabad) with safe limits.

Elements	Unit	*Tarlai Farms*	*Sohan*	Safe Limits
Ca	µg mL^{-1}	69.43 ± 1.38	73.88 ± 1.19	230
K	µg mL^{-1}	16.37 ± 0.11	9.14 ± 0.03	<2.0
Mg	µg mL^{-1}	28.24 ± 0.38	14.69 ± 0.18	< 61
P	µg mL^{-1}	1.63 ± 0.02	1.55 ± 0.01	
Na	µg mL^{-1}	84.77 ± 1.6	32.78 ± 0.5	230
Fe	µg mL^{-1}	ND	0.02 ± 0.00	0.1-1.5
Mn	µg mL^{-1}	ND	ND	0.1-1.5
Cu	µg mL^{-1}	ND	ND	200
Zn	ng mL^{-1}	10	10	2000
Ni	µg mL^{-1}	ND	ND	0.20
Cr	µg mL^{-1}	ND	ND	100
As	ng mL^{-1}	5.64 ± 0.33	ND	100
Cd	ng mL^{-1}	ND	ND	10
Pb	ng mL^{-1}	ND	ND	5000
Se	ng mL^{-1}	ND	ND	20
Sb	ng mL^{-1}	ND	ND	
Hg	ng mL^{-1}	2.67 ± 0.02	342.14 ± 0.62	2

Sewage water from Tarlai Farm, Islamabad was also analyzed by M. Zeeshan et al. [20]. The reported results are close to results of this study including ammonia (0.03-0.46 mg L^{-1}), fluoride (0.5-0.95 mg L^{-1}) and chloride (4.7- 24.1 mg L^{-1}).

However, elemental profile of the two studies is quite different such as Hg was not detected by Zeeshan et al [20] while in our study Hg is above the safe limit (2.67 mL^{-1}), As, Ca and K reported by Zeeshan were 2.17 ng mL^{-1} , 34.38 µg mL^{-1} and 6.32 µg mL^{-1} respectively which are different from the results of this study.

3.1.2 Sohan village Islamabad

The physicochemical properties of sewage water samples collected from Sohan village, Islamabad are given in Table 4.

The results showed that sewage water had a pH of 7.3 and an electrical conductivity of 0.65 dS m^{-1} which falls in safe limit. The results showed that TDS value was 355 mg L^{-1} which is below the safe limit. The results further revealed that sulfide, fluoride, chloride, alkalinity ammonia and sulphate in sewage water (Sohan Village) were in the permissible limit as described by WHO, 2006[18]. COD parameter indirectly measures the number of organic compounds in water. The analyses showed that COD (520 mg L^{-1}) was higher than the safe limit which indicates that a high quantity of organic contaminants is present in the sewage water samples [21]. However, BOD was below the safe limit.

The macro-nutrients for Ca, K, Mg, P and Na were found 73.88 µg mL^{-1}, 9.14 µg mL^{-1}, 14.69 µg mL^{-1},1.55 µgmL^{-1} and 32.78 µg mL^{-1} respectively as shown in Table 4. Among micronutrients Fe (0.02 µg mL^{-1}) and Zn (10 ng mL^{-1}) were detected in the water sample while other micronutrients such as Cu and Mn were absent in the samples.

The toxic heavy metal profile of sewage water samples showed that Pb, Cd, As, Cr, Ni, Se, Sb were not detected in the sewage water. However, Hg (342.14 ng mL^{-1}) was much higher (171 times) than the safe limit proposed by WHO [18]. The higher level of Hg in water sample can be attributed to the disposal of hospital wastes in the water. Hospital wastes contained many mercury sources like thermometer, teeth fillers etc. Due to presence of higher Hg content and its ability to bio accumulate this water is not suitable for agricultural use to avoid contamination of food chain. Since Hg is highly toxic and can accumulate in human body causing severe neurological disorders and effects fetal development if mother is exposed to mercury [22].

3.2 Industrial wastewater

In developing countries, effluents from industrial areas have been used as source of irrigation because these effluents are considered as nutrient-rich irrigation source [23]. Industrial wastewater was obtained from Site 2 and Site 7 in Hayatabad Industrial Estate (HIE), Peshawar which is being used as a source of irrigation of crops and vegetable farm. The effluents from match factories, pharmaceutical industries and paint industries were discharged at these sites. Site 7 was 10 meters away from the main drainage while Site 2 was 100 meters away.

3.2.1 Site 2, Peshawar

The quality of industrial wastewater was evaluated with respect to heavy metals content, macronutrients and for its various other physicochemical properties and the results are shown in Table 5 and 6.

Table 5: Physico-Chemical parameters of industrial wastewater (Site 2 and Site 7 Hayatabad, Peshawar)

Parameters	Units	*Site 2*	*Site 7*	Safe Limits
pH		7.8	8.2	6.5-8.4
Conductivity	dS m^{-1}	0.82	0.93	0.25-3.00
TDS	mg L^{-1}	449	511	<2000
TSS	mg L^{-1}	57	6	50-100
Ammonia	mg L^{-1}	8.6	0.23	5
Alkalinity	mg L^{-1}	-	216	<610
Sulphide	mg L^{-1}	ND	ND	
Fluoride	mg L^{-1}	0.78	0.62	1.0
Chloride	mg L^{-1}	5.08	51.58	<350
Sulphate	mg L^{-1}	110.46 ± 1.35	238.73 ± 0.53	500
Nitrate	mg L^{-1}	11.25	9.62	
COD	mg L^{-1}	40	400	250

The results showed that wastewater had pH 7.8 and electrical conductivity of 0.82 dS m^{-1}. Electrical conductivity value showed that water contained ionic species. The results showed that TDS and TSS value in wastewater were 449 mg L^{-1} and 57 mg L^{-1} (Table 5). TSS value was above the safe limits which indicate the presence of solid pollutants.

The results further revealed that COD, sulfide, fluoride, chloride and sulphate in sewage water were in the permissible limit as described by WHO, 2006 [18] as shown in Table 5. The COD value of wastewater was 40 mg L^{-1} which is below the safe limit proposed by WHO [18].

The analyses of wastewater performed using ICP-OES showed that wastewater contained macronutrients including P (2.11 µg mL^{-1}), Na (51.77 µg mL^{-1}), Ca (55.96 µg mL^{-1}), K (3.58 µg mL^{-1}) and Mg (31.15 µg mL^{-1}) as shown in Table 6. Except for K, all macro-nutrients were within the permissible limits. Among micronutrients, results showed that water contained Fe (0.03 µg mL^{-1}) and Zn (1.16 µg mL^{-1}) while Cu and Mn were not detected in the sample.

Heavy metal analysis of wastewater showed that Hg, Pb, Cd, As, Cr, Ni and Se were not detected in the industrial wastewater. As and Sb were found (4.39 ng mL^{-1}) and (2.07 ng mL^{-1}) respectively but these were below the safe limits proposed by WHO [18].

3.2.2 Site 7, Peshawar

The elemental profile and results of various other physico-chemical parameters are shown in Table 5 and Table 6. The physicochemical properties of industrial water samples are given in Table 5. The results showed that sewage water had pH in alkaline range (8.2) and electrical conductivity of 0.93 dS m^{-1}. The results showed that TDS (511 mg L^{-1}), TSS (6 mg L^{-1}) and alkalinity (216 mg L^{-1}) in wastewater were below the safe limit. The results further revealed that sulfide, fluoride, chloride and sulphate in sewage water were in the permissible limit as described by WHO, 2006 [18]. COD value 0f 400 mg L^{-1} is indicating organic load.

The macro-nutrients analysis of wastewater showed that all macronutrients (Ca, Mg, Na, P, K, Na) were within permissible limits except Potassium as shown in Table 6. The upper limit for K proposed by WHO is 2µg mL-1 measured value for K was 4.28 µg mL-1. Plants need P for development of ATP, nucleic acids and sugars. Plants suffering from P deficiency appear weak and maturity is delayed. Hence, this source of water used as a source of irrigation will affect plant growth. The results showed that none of the micro-nutrients was present in the sample which would affect plant growth parameters.

Table 6: Elemental Profile of industrial wastewater (Site 2 and Site 7 Hayatabad, Peshawar.

Elements	Unit	Site 2	Site 7	Safe Limits
Ca	µg mL^{-1}	55.96 ± 3.15	111.11 ± 3.3	230
K	µg mL^{-1}	3.58 ± 0.13	4.28 ± 0.11	<2.0
Mg	µg mL^{-1}	31.15 ± 0.70	29.94 ± 0.06	< 61
P	µg mL^{-1}	2.11 ± 0.06	0.09 ± 0.00	
Na	µg mL^{-1}	51.77 ± 2.69	34.89 ± 0.90	230
Fe	µg mL^{-1}	0.03 ± 0.00	ND	0.1-1.5
Mn	µg mL^{-1}	0.03 ± 0.00	ND	0.1-1.5
Cu	µg mL^{-1}	ND	ND	200
Zn	µg mL^{-1}	± 0.05	ND	2
Ni	µg mL^{-1}	ND	ND	0.20
Cr	µg mL^{-1}	ND	ND	100
As	ng mL^{-1}	4.39 ± 0.12	ND	100
Cd	ng mL^{-1}	ND	ND	10
Pb	ng mL^{-1}	ND	ND	5000
Se	ng mL^{-1}	ND	1.57 ± 0.03	20
Sb	ng mL^{-1}	2.07 ± 0.03	2.59 ± 0.07	
Hg	ng mL^{-1}	ND	ND	2

Among toxic heavy metals Pb, Cd, As, Hg, Ni and Cr were not detected in the wastewater. Although Sb (2.59 ng mL^{-1}) and Se (1.57 ng mL^{-1}) were detected in the sample but they were well below the safe limits proposed by WHO 2006 [18].

3.3. Domestic wastewater

Domestic wastewater was collected from a residential colony located in Sohan, Islamabad. The quality of domestic wastewater used as a source of irrigation to vegetables was analyzed for macro and micro-nutrients, heavy metals content and other parameters.

3.3.1 Shah town, Islamabad

Analysis of domestic wastewater was performed at laboratories at CAFD, PINSTECH. The results are mentioned in Table 7 and 8.

The domestic wastewater had a pH of 7.3 and an EC of 1.05 dS m^{-1}. The results showed that TDS (581 mg L^{-1}), TSS (27 mg L^{-1}) and alkalinity (240 mg L^{-1}) in wastewater were below the safe limit. The results further revealed that COD, sulfide, fluoride, chloride and sulphate in sewage water were in the permissible limit as described by FAO, 1985 [16].

Table 7: Physico-chemical characteristics of domestic wastewater (Shah Town, Islamabad).

Parameters	Units	Value	Safe Limits
pH	-	7.3	6.5-8.4
Conductivity	dS m^{-1}	0.11	0.25-3.00
TDS	mg L^{-1}	581	<2000
TSS	mg L^{-1}	27	≤50
Ammonia	mg L^{-1}	2.3	5
Alkalinity	mg L^{-1}	240	<610
Sulfide	mg L^{-1}	ND	
Fluoride	mg L^{-1}	0.79	1.0
Chloride	mg L^{-1}	42.72	<350
Sulphate	mg L^{-1}	45.32 ± 0.29	500
Nitrate	mg L^{-1}	ND	
COD	mg L^{-1}	220	250

The analyses of domestic wastewater performed on ICP-OES showed that it contained macronutrients including P(4.10 µg mL^{-1}), Na (60.01 µg mL^{-1}), Ca (81.52 µg mL^{-1}), K (21.29 µg mL^{-1}) and Mg (21.46 µg mL^{-1}) as shown in Table 8. K content is much higher than the recommended value of 2 µg mL^{-1} among micronutrients results showed that water contains Fe (0.03 µg mL^{-1}), Mn (0.12 µg mL^{-1}) and Zn (0.03 µg mL^{-1}) while Cu was not detected in the sample.

The elemental profile of domestic wastewater samples showed that none of the toxic heavy metals such as Hg, As, Pb, Cd, As, Ni, Cr, Sb and Se were detected in the domestic wastewater.

Table 8: Elemental profile of domestic wastewater used for irrigation at Shah Town, Islamabad.

Elements	Unit	Concentration	Safe Limits
Ca	µg mL^{-1}	81.52 ± 3.5	230
K	µg mL^{-1}	21.29 ± 0.56	<2.0
Mg	µg mL^{-1}	21.46 ± 0.45	< 61
P	µg mL^{-1}	4.10 ± 0.08	
Na	µg mL^{-1}	60.01 ± 2.59	230
Fe	µg mL^{-1}	0.03 ± 0.00	0.1-1.5
Mn	µg mL^{-1}	0.12 ± 0.01	0.1-1.5
Cu	µg mL^{-1}	ND	200
Zn	µg mL^{-1}	0.03 ± 0.00	2
Ni	µg mL^{-1}	ND	0.20
Cr	µg mL^{-1}	ND	100
As	ng mL^{-1}	ND	100
Cd	ng mL^{-1}	ND	10
Pb	ng mL^{-1}	ND	5000
Se	ng mL^{-1}	ND	20
Sb	ng mL^{-1}	ND	
Hg	ng mL^{-1}	ND	2

4. Conclusion

Among wastewater as irrigation source, domestic wastewater (Shah Town, Islamabad) is safe for irrigation as it contains no toxic heavy metals as presented in Fig. 1. Industrial wastewater Hayatabad, Peshawar was also found environmentally safe according to WHO limits. It was found that sewage water (Sohan Village, Islamabad) is highly harmful for irrigation due to very high Hg content (342.14 ng mL^{-1}). It is recommended that proper wastewater treatment system shall be introduced for removing toxic heavy metals content prior using for irrigation purposes.

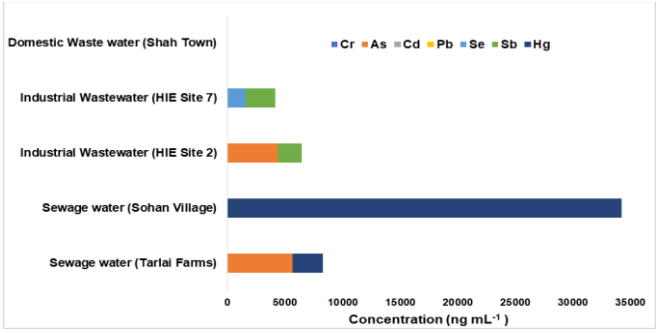

Fig. 1. Heavy Metal Profile of Wastewater Samples.

Acknowledgements

The authors acknowledge the effort of all the colleagues who supported in this research work especially Dr. Masroor Ahmad (PIEAS) and Dr. Kashif Naeem (CAFD).

References

[1] S.A. Khan, X. Liu, B. R. Shah, W. Fan, H. Li, S.B.Khan and Z. Ahmad, "Metals uptake by wastewater irrigated vegetables and their daily dietary intake in Peshawar, Pakistan," Ecol. Chem. Eng. Sci., vol. 22, no. 1, pp. 125–139, 2015, doi: 10.1515/eces-2015-0008.

[2] W. Han-Jie, J. Wang and X. YU,"Wastewater irrigation and crop yield: a meta-analysis," J. Integ. Agric.,vol. 21, no. 4, pp 1215-1224, 2022

[3] B.M. Gawlik, "Minimum quality requirements for water reuse in agricultural irrigation and aquifer recharge towards a water reuse regulatory instrument at EU level," 2017, doi: 10.2760/804116.

[4] W.H.O,"Guidelines for the safe use of wastewater, excreta and greywater", vol. 1, World Health Oragnization, 2006.

[5] W.A. Kasi, S. Panezai, and S.E. Saqib, "Wastewater irrigation and associated health and environmental factors in Pakistan : A scoping review," Resour. Environ., vol. 12, no. 3, pp. 76–87, 2022, doi: 10.5923/j.re.20221203.02.

[6] M.K. Masoud Khanpaea, Ezatollah Karamia, Hamideh Maleksaeidi, "Farmers' attitude towards using treated wastewater for irrigation: The question of sustainability," J. Clean. Prod., vol. 243, 2020.

[7] S. Bijikar, H.D. Padariya, V.K. Yadav, A. Gacem, M. Hassan, N.S. Awwad, K.K. Yadav, S. Islam, S. Park and B. Jean, "The state of the art and emerging trends in the wastewatertreatment in developing nations", Water, vol. 14, no. 16, 2022, doi:10.3390/w14162537.

[8] H. Raheed, F. Naz, F. Altaf, S. Imran and M. Ashraf,"Wastewater assessment and treatment need analysis of district Jhelum", Pakistan Council of Research in Water Resources (PCRWR), pp. 52, 2020.

[9] D.P. X.Garcia, "Reusing wastewater to cope with water scarcity: Economic, social and environmental considerations for decision-making," Resour. Conserv. Recycl., vol. 101, pp. 154–166, 2015.

[10] M.L. Dotaniya, V.D. Meena, J.K Saha, C.K. Dotany, A. Mahmoud, B.L. Meena, M.D. Meena, R.C. Sanwal, R.S. Meena, R.K. Dotaniya, P. Solanki, M. Lata and P.K. Rai, "Reuse of poor-quality water for sustainable crop production in the changing scenario of climate," Environ. Dev. Sustain., 2022, doi: 10.1007/s10668-022-02365-9 .

[11] S. Rezapour, A. Nouri, H. Jalil, S.A Hawkings and S.B. Lukeset, "Influence of treated wastewater irrigation on soil nutritional-chemical attributes using soil quality imdex," Sustainability, vol. 13, no. 4(1952) 2021, doi: 10.3390/su13041952.

[12] M.A. Agoro, A.O. Adeniji, M.A. Adefisoye, and O.O. Okoh, "Heavy metals in wastewater and sewage sludge from selected municipal treatment plants in Eastern Cape Province, South Africa," Water, vol. 12, no. 10, pp. 2746, 2020, doi: 10.3390/w12102746.

[13] H. Raza, M. Maqsood, M.M. Nazir, I. Tariq, K. Ahmed, Q.Ain, A. Raza, H. Bilal, M. B. Shoukat, A. Rehman, A. Rasheed and M. Z.Gulzar, "Wastewater irrigation possess a risk on food chain, health, and its treatment with constructed wetlands," J. Innov Sci., vol. 7, no. 2, pp. 206–317, 2021.

[14] A. Alengebawy, S.D Abdelkhalek, S.R. Qureshi and M. Wang, "Heavy metals and pesticides toxicity in agricultural soil and plants: Ecological risks and human health implications," Toxics, vol. 9, no. 3(42), 2021, doi: 10.3390/toxics9030042.

[15] F. Ali, H. Ullah, and I. Khan, "Heavy metals accumulation in vegetables irrigated with industrial influents and possible impact of such vegetables on human health," Sarhad J. Agric., vol. 33, no. 3, pp. 489–500, 2017, doi:10.17582/journal.sja/2017/33.3.489.500.

[16] M. Helmecke, E. Fries, and C. Schulte, "Regulating water reuse for agricultural irrigation: risks related to organic micro-contaminants," Environ. Sci. Eur., vol. 32, no. 4, 2020, doi: 10.1186/s12302-019-0283-0.

[17] T. Sarwar H. Shakoor, J. Khan, A. Shah, S. Amin, A. Sajjad, Ziaullah and J. Iqbal,"Analysis of water quality using physico-chemical properties in different cities of Pakistan", Int. J. Chem., vol. 14, no. 2, pp 28-44, 2022, doi:10.5539/ijc.v14n2p28.

[18] W.H.O, "Safe use of wastewater , excreta and greywater guidelines: Wastewater use in agriculture,"vol. 2,World Health Organization, 2006, doi: 10.1007/s13398-014-0173-7.2.

[19] R.S. Ayers and D.W. Westcot, "Water quality for agriculture," Food and Agriculture Organization, United Nations ,Rome,Italy, 1985.

[20] M. Zeeshan and S. Shehzadi, "Impact of sewage water Irrigation on soil and radish (Raphanus sativus L.) with respect to heavy metals in Tarlai , Islamabad," Nucl., vol. 56, no. 2, pp. 63–69, 2019.

[21] K. Doke, E. Khan, J. Rapolu, and A. Shaikh, "Physico-chemical analysis of sugar industry effluent and its effect on seed germination of Vigna angularis, Vigna cylindrical and Sorghum cernum," Ann. Environ. Sci., vol. 5, no. 1, pp. 7–11, 2011.

[22] R. Li, H. Wu, J. DIng, W. Fu, L. Gan, and Y. Li, "Mercury pollution in vegetables, grains and soils from areas surrounding coal-fired power plants," Sci. Reports-Nature Portf., vol. 7, no. May, pp. 1–9, 2017, doi: 10.1038/srep46545.

[23] N. Amin, M. Ayaz, S. Alam, and S. Gul, "Heavy metals contamination through industrial effluent to irrigation water in Gadoon Amazai (Swabi) and Hayatabad (Peshawar) Pakistan," J. Sci. Res., vol. 6, no. 1, pp. 111–124, 2013, doi: 10.3329/jsr.v6i1.16336.

The Nucleus ***60***, *No. 2 (2023) 126-130*

www.thenucleuspak.org.pk

The Nucleus
ISSN 0029-5698 (Print)
ISSN 2306-6539 (Online)

Environmental Footprints and Occupational Hazards of Clay Mining – A Case Study from Patel Nagar, Birbhum, West Bengal, India

Bikas Saha

Department of Geology, Durgapur Government College, J.N. Avenue, Durgapur, West Bengal, India

ABSTRACT

Mining is one of the main economic activities of any developing country. Pressure among mining and conservation is anticipated to escalate with the growing human population and technological advancement. However, mining has both negative and positive impacts on the environment as well as on society. During mine establishment and exploitation, habitat destruction is a part of all mining activities. Clay mining has major effects on the health of local people and causes the environment to break down. Both economically and ecologically, the china clay mines of Patel Nagar in Birbhum district hold a governing position. Both geomorphological processes and environments are affected due to china clay mining. Patel Nagar and the places around have a lot of good farmlands, which suffer the adverse effects of clay mining. Hydrological cycles are getting polluted along with the degradation of landforms, soot in the air, water and noise contamination, soil corrosion, and effects on natural drainage systems in the studied area. The majority of the local poor tribal people who work in mines also have certain health-related issues as an integral part of their occupational hazards.

Keywords: *Clay Mining, Environmental Degradation, Defaced Landform, Agriculture Land Reduction, Occupational Hazards.*

1. Introduction

Since the 16th century, clay has drawn scientists and technicians from a variety of fields. Clay is defined differently by scientists to suit their individual needs. The term "clay" was once used by sedimentologists to refer to particles less than 1/256 mm. Some sheet silicate minerals were first referred to as "clay" by mineral scientists. A dusty substance with some inherent mechanical strength is what clay is to an engineer (please correct this sentence). Therefore, it was necessary to provide a constant and widely accepted definition for clay and related materials in order to clear up this enigma and doubt. Thus, in 1995, the Clay Minerals Society (CMS) and the International Association for the Study of Clays (AIPEA) established the Joint Nomenclature Committee, which provided a consistent and generally accepted definition of clay.

The name "clay" refers to a naturally occurring substance predominantly made up of fine-grained minerals. At the proper water content, clay is typically flexible but will harden when dried or burnt [1, 2]. Kaolin/China clay, bentonite, bleaching earth, common clay, ball clay, fire clay, and refractory clay are the materials which are fulfilling all the conditions stated in the above definition. China clay, also known as kaolin, is made up of about 85% kaolinite [$Al_2Si_2O_5(OH)_4$]. It forms due to the weathering and thermal alteration of the mother rock, the precursor of clay, under favorable conditions. And mother rocks, in this case, are feldspars, muscovite, and other Al-rich silicates of acid igneous rocks like granite, rhyolite, quartz, diorite, etc. China clay also typically contains small amounts of mica, feldspar, illite, and quartz. Because of its favorable physical, mineralogical, and chemical characteristics, Kaolin is significantly used in manufacturing ceramics, cement, paints, refractory bricks, tiles, papers, drugs, toothpaste, fabrics, rubbers, and plastics [3]. They are also universally used as raw materials for building and construction because kaolin-made bricks are cheap, easy to produce, and have good geotechnical properties [4, 5].

Along the long path of civilization, humans stopped hunting for food as soon as they learned to use clay. Since the Stone Age, clays and clay minerals have been mined. Clays and clay minerals are one of the most important minerals used in manufacturing and the environmental field. So after the Stone Age, the clay age started. They used clay for home building, home decorations, and home utensils [6]. It has been confirmed from the archaeological excavation that man had used bricks to build houses from clay. During Harappa and Mohenjo-Daro civilizations from the Indus River Valley, human-used clay for different purposes [7]. With the expansion of civilization, increased use of clays in the industrial sector and their substitution for metals become infallible. Deposits of china clay are found in several locations around the Mohammad Bazar block. These resources are both sizable and profitable commercially. In this region, the qualities and grades of these clays vary from location to location as shown in Fig. 1. Kaolinite from various locations was evaluated by the Central Glass and Ceramic Institute (CGCRI), along with the research region, i.e., Patel Nagar, and was found to be advantageous for the ceramics industry. We will now focus our research on the Patel Nagar neighborhood in the Mohammad Bazar block of the Birbhum district.

Major economic activity which contributes significantly to the economy of India is the mining industry. It provides significant numbers of job opportunities. But environmental problems are created due to the mining. And, kaolin mining is no exception. Chemical and physical, these two types of environmental degradations are created due to kaolin mining and its beneficiation. Industrial applications of clay and its by-products are numerous and diverse. The acceptability of clay in a particular manufacturing unit depends on the properties of the clay. For the production of high-end porcelain, kaolinite-rich clay is majorly used. It is also used in the rubber industry because of its high surface affinity and very fine grain size. For the filling and coating of paper, clay is also used in the paper industry. It improves the appearance of the paper.

*Corresponding author: sahabikas@gmail.com

Fig. 1: Various types of clays in the study area. Red-colored, ferruginous clay is marked by the black arrow.

Clay minerals can also be used as filters and absorbents because of their cation property of some clay minerals. For this reason, bentonite clays are used as lubricating agents in drilling fluids. Therefore, clay can be used as an adsorbent, de-coloration agent, ion exchange, and molecular sieve catalyst [8].

Water and different types of chemicals are used during the beneficiation of kaolin, as a result, the water becomes contaminated and is discharged after the beneficiation. If we discharged these contaminated waters to the fields, then it will affect the crops. Water discharged from mines also creates problems for crops. Moreover, for human consumption, this contaminated water is hazardous (Fig. 2).

Fig. 2: Water infiltrated the china clay quarry at Patel Nagar, especially during rainy sessions and discharged water after the beneficiation of clay.

2 Geology of the Area

2.1 Regional Geology

The Archean rocks, consisting of granites, granite gneiss, biotite-schists, and calc-granulites are exposed in the South-West and North-West side of the Birbhum district and forms the basement of the Rajmahal Basin. Among these rocks, gneiss is predominant and intruded in the pre-existing schists. The Rajmahal Basin hosts undifferentiated Lower Gondwana sediments followed by Upper Triassic Dubrajpur and Middle Jurassic to Lower Cretaceous Rajmahal Formation [9]. In the southeastern part of the Basin, the Dubrajpur Formation unconformably overlies the Archean rocks. The lithology of the Dubrajpur Formation is gritty and ferruginous sandstone and shaly clay. Well-preserved fossil plant impressions indicate the Upper Gondwana age. Rajmahal Formation is the uppermost unit of the Gondwana Supergroup and comprises mostly of fine to coarse-grained basalts consisting of pyroxenes and plagioclase feldspars with ophitic textures. Basaltic lava was emplaced either on the Upper Triassic Dubrajpur Formation or on the Lower Gondwana sediments. Rajmahal trap achieves a thickness of about 330 m. Towards the south, near the eastern part of Raniganj Coalfield, the thickness of Rajmahal traps was reduced to about 100 m. The intertrappean sediments show variation in thickness from 1 to 26 m [10].

Cenozoic sediments overlie the Gondwana sediments patchily and are exposed near Patel Nagar Mokdamnagar-Mohammad Bazar area, Chaknurai, and Chaubatta areas. This Tertiary succession is comprised mainly of clays and sandstones, overlying the Rajmahal traps on the Northern side as in Chaubatta [11]. In the South near Adda, the basement rock of the Archean age gets exposed. The study area is mainly underlain by the Archean basement rocks and Rajmahal traps. A generalized succession of the region is given in Table 1 [12].

Table 1. Generalized Stratigraphic Sequence of Birbhum District [12]

Age	Formation	Lithology
Recent	Alluvium	Loose soil, silt & clay
Quaternary / Tertiary	Undifferentiated Surficial deposits	Laterites, lateritic soil, lateritic gravel with petrified wood & china clay
	Unconformity	
Middle Jurassic to Lower Cretaceous	Rajmahal Traps and Intertrappeans	Flows of basalt and intertrapeans Sediments (Sandstone, shale, etc.).
	Unconformity	
Lower Jurassic (Upper Triassic)	Dubrajpur	Conglomerates, coarse to medium-grained sandstone, grey siltstone, mottled shale & thin coal bands.
	Unconformity	
Lower Permian	Barakar	Coarse to medium-grained sandstone, carbonaceous sandstone with grey shale, fire clay, carbonaceous shale, and coal seam.
Upper carboniferous to Lower Permian (Permocaboniferous)	Talchir	Greenish sandstone, siltstone, tillite, olive green shale
	Unconformity	
Precambrian	Metamorphics	Granites and granitoid, gneiss, pegmatite, quartz veins, and metabaic dykes

2.2 *Local Geology*

Sediments deposited in the western part of Birbhum district are mostly alluvium in disseminated hillocks. The subsurface geological succession found in these areas is given below Table 2.

Table 2. Local Geological Succession of the Study Area

Recent	Alluvium
	Laterites and lateritic gravels with fossil wood
Tertiary	Clay beds
	Ferruginous and telepathic sandstones end clay beds
Middle Jurassic	Traps (Rajmahal)
Lower Jurassic (Upper Gondwana)	Flaggy Shales, clays, and compact sandstones (Dubrajpur Beds)
Unconformity	
Archaean	Granitegneisses, biotite-schists, cale-granulites with quartz and pegmatite veins.

Sedimentary rocks of the Dubrajpur formation unconformably overlie the Archean basements, towards the southeastern part of the studied area. Following Rajmahal traps are of Middle Jurassic in age. The unconformably overlying Tertiary succession of this area consists of mainly sandstone and clay along with some loose and friable sand and grit. These Tertiary clay beds occurred as thick beds forming the economic deposits of the district. The minimum thickness of these clay beds is about 30 m [13]. Though the Tertiary sediments mainly overlie the Rajmahal Traps, locally they overlie even the Archean basement also, especially towards the west and south of Makhdumnagar [13].

Vesicular-type laterites occur as a cap rock over the basalt and Tertiary sediments all over the study area. But the platy laterite varieties are found as a patchy deposit. Lateritic gravel of detrital nature occurs extensively. Few loose fragments of silicified wood fossils were found in these clay beds as well as in the Tertiary sediments.

3. Results and Discussion

Various types of reactions are occurring in the environment. Some of these reactions contribute to environmental pollution. These are energizing processes, whereas some reactions are generating resistance to environmental pollution. These are reactions that neutralize environmental pollution. Regardless of the surface conditions of the planet, clay remains stable. Therefore, they are not stimulating any reactions. Rather can assist us by eliminating contaminants and pollutants from the solution. As it is extracted, commonly with the open-cast mining process, the basic environmental balance in and around the mining area gets disturbed. The environmental impacts depend on mining policy, hydrology of the area, climatic conditions, rock types of the area, size of operation, landscape, and many other reciprocal factors [14].

To get a diversified idea about the negative impacts of china clay on the environment, we have to understand the following two ideas separately:

a) During mining activities, the environment may be degrading. Beneficiation activities of the china clay also affect the environment.

b) China clay may present with other economic materials in the host rock, country rock, or even the overburdened material of those economic deposits. So during the mining activity of those economic deposits, the environment may degrade due to clay. Even the clays of dumping yards, building sites, or manufacturing sites have negative impacts on the environment.

Open-cast mining has different stages. First of all, before starting mining, miners have to excavate and remove the vegetation, soil, and overburden from the mining area. During excavation, they also have to dispose of the waste materials in a proper place so that these waste disposals cannot create any further environmental degradation. During the beneficiation of china clay, impurities are removed to give the clay the desired form.

Each stage of these mining processes has different negative impacts on the environment. Due to the stripping of overburden, the top of the mine area has to remove along with a large amount of vegetation. Surrounding environments are affected by the removal of vegetation. Part of the aquifer may also be affected while extracting clay from the mining area, especially during deeper mining. Due to the evaporation of water from the exposed aquifer, there will be a loss of groundwater. It will affect groundwater circulation. As the aquifer is exposed, so it also increases the chances of groundwater pollution [15]. Even shallow mines also can stop the runoff and interflow. As a result, water wastage is increasing and scarcity of water is also expanding within the surface water bodies of the area [16]. It will destroy more vegetation and topsoil in an area when we dump the mine waste in that area. Moreover, harmful chemicals containing dump waste will release pollutants into water, especially during rainy seasons (Fig. 3). This leached-out water will pollute the sub-surface water and surface water bodies of the surrounding areas.

With no exception in Patel Nagar, Birbhum, kaolin mining activity is also creating problems for the environment. During the beneficiation of kaolin, a huge amount of water is discharged from the clay plant. This water is mostly contaminated. Hence, it will pollute the whole area wherever it is released. Land degradation is another problem due to the opening of kaolin mining in the study area. Besides this, extracted materials have to store or dump in an area. For this, land area is also used, and due to contact with the clay, the area may degrade. For achieving china clay, sometimes the topsoil has to be removed from the proposed mine area. This removed soil is again dumped in another place and thus land of the area is degraded. The abandoned mine site is another problem. Thus, it must be filled with some other materials like sand and soil. Due to solid waste disposal, the environment is also degrading in the study area as shown in Fig. 2. Moreover,

deforestation will account for the drastic change in atmospheric conditions. Deforestation accounts for 27% of the total added global warming potential in India. To establish mine, especially in the forest, requires deforestation. Apart from this, there will be no plants or cultivation in the mine area as long as the mining will continue.

Fig. 3: Mined Clay locally stored in the dump yard, immediately after the mining and later on transported the raw clay to the factory for further processes.

Open cast mining is done by using different types of equipment like draglines, power shovels, front-end loaders, backhoes, scraper-loaders, and shale planers [17]. Operations of this equipment will create noise. The unwanted noise will affect the health of mine workers.

Dust is produced during carrying out the mining operations. Most of the China clay mines are open-cast in Patel Nagar. Though the dust produced by mining activity itself is of low amount, a huge amount of dust is being produced due to the transportation of clay and overburdened materials. Subsequently, the environment is affected due to this dust.

Kaolin occurs widely in ambient air as it is a natural component of soil [14]. Due to the mining and refining of kaolin, the locals are considerably exposed to kaolin. They are also significantly exposed to kaolin during paper, rubber, and plastic production, as kaolin is one of the raw materials for these industries.

As a part of occupational hazards, laborers of kaolin mines often develop radiologically diagnosed pneumoconiosis as they expose to kaolin for a longer time [18, 19]. With the help of prominent radiological investigation, declining lung function and deterioration of respiratory function, and allied symptoms are identified. Quartz is one of the composition of kaolin. That is why miners are often affected by silicosis and lung cancer [19, 20, 21]. It has been reported that, due to exposure to quartz, there are significant increases in the incidence of or mortality from chronic bronchitis and pulmonary emphysema among the miners of Patel Nagar. IARC (International Agency for Cancer Research) [22] categorizes inhaled crystalline silica, such as quartz or cristobalite, as a Group-1 carcinogen. Silicosis is the most important effect for hazard identification and exposure–response evaluation (Fig. 4). Again it may lead to mild pneumoconiosis, known as kaolinosis due to long-term exposure to kaolin [19, 23-25].

In Patel Nagar, china clay of a white hue is extracted via open-pit mining. Therefore, when sunlight strikes mined china clay, it reflects the light and creates a scintillating effect on the eye. As a consequence of this ophthalmic issue, the mine worker's vision is impaired [26].

Fig. 4: Deploying indigenous labor for the clay slurry beneficiation process.

4. Conclusion

Similar to many other human activities, clay mining has a substantial impact on the environment. The effects of clay mining include soil erosion, air and water contamination, geo-environmental catastrophes, biodiversity loss, and economic loss. A similar trend has been observed in and around the Patel Nagar clay extraction sites. The local people suffer from different orders of ailments arising from their exposure to kaolin. The effect on the groundwater circulation system and agriculture is also detrimental. Proper mitigative measures should be taken to nullify such hazards. Rapid population growth, urbanization, and associated industrial development are the causes of unchecked mining, the emergence of new industries, and countless construction projects in various regions of the globe. Each of these generates massive amounts of waste, as well as toxins and contaminants. These pollutants are the greatest threat to the earth's surface. Researchers from all across the world are attempting to identify cost-effective methods for preventing waste-related environmental pollution and contamination. Due to the unique characteristics of clay, it can be used to address waste-related environmental issues. Therefore, concurrent investigation into the origin and nature of the clay is also required.

Acknowledgments

The author expresses gratitude to Durgapur Govt. College for infrastructural facilities. Special thanks to my brother, Mr. Manas Debangshi, who helped me during my fieldwork in Patel Nagar. I am also thankful to the editors and reviewers for reviewing my manuscript carefully.

References

[1] S. Guggenheim and R.T. Martin, "Definition of clay and clay mineral. Joint report of the AIPEA nomenclature and CMS nomenclature committees," Clays and Clay Minerals, vol. 43, no. 2, pp. 255–256, 1995.

[2] S. Guggenheim and R.T. Martin, "Reply to the comment by D.M. Moore on "Definition of clay and clay mineral: Joint report of the AIPEA nomenclature and CMS nomenclature committees," Clays and Clay Minerals, vol. 44, no. 5, pp. 713–715, 1996.

[3] S. Turhan, "Radiological impacts of the usability of clay and kaolin as raw material in manufacturing of structural building materials in Turkey," Journal of Radiological Protection, vol. 29, no. 1, pp. 75–83, 2009. doi:10.1088/0952-4746/29/1/005.

[4] Dailytrust, "How Nigeria can exploit untapped kaolin deposits," 2018. Available at https://www.dailytrust.com.ng/how-nigeria-can-exploit-untapped-kaolin-deposits-265327.html

[5] Leadership, "Kaolin as Nigeria's untapped goldmine," 2018. Available at https://leadership.ng/2018/08/15/kaolin-as-nigerias-untapped-goldmine/

[6] S. Ranaveera, "History of Art", Wasana Publication, Dankotuwa, 2004.

[7] F. Jesse, "Early ceramics in the Sahara and the Nile Valley. In Krzyzaniak, L., Kroeper, K. & Kobusiewicz, M. (Eds.), Cultural markers in the later prehistory of Northeastern Africa and Recent Research (Studies in African archaeology 8), pp. 35–50, 2003. Poznań: Poznań Archaeological Museum.

[8] H.H. Murray, "Overview of clay mineral applications", Appl. Clay Sci. vol. 5, pp. 379-395, 1991.

[9] A. Tripathi and A. Ray, "Palynostratigraphy of the Dubrajpur Formation (Early Triassic to Early Cretaceous) of the Rajmahal Basin, India', Palynology, vol. 30, pp. 133–149, 2006.

[10] B. Prasad and B.S. Pundir, "Gondwana biostratigraphy and geology of West Bengal Basin, and its correlation with adjoining Gondwana basins of India and western Bangladesh", J. Earth Syst. Sci., vol. 129, no. 22, 2022. https://doi.org/10.1007/s12040-019-1287-2

[11] S.S.K. Pillai, M.C. Manoj, R.P. Mathews, S. Murthy, M. Sahoo, A. Saxena, A. Sharma, S. Pradhan and S. Kumar, "Lower Permian Gondwana sequence of Rajhara (Daltonganj Coalfield), Damodar Basin, India: floristic and geochemical records and their implications on marine ingressions and depositional environment", 2023. DOI: 10.1007/s10653-023-01517-8

[12] C. Karunakaran, M.G. Rao and S. Sinharoy, Rec. Geol. Surv. India, vol. 98, 1969.

[13] DSR, District Survey Report of Birbhum District, West Bengal, 2019.

[14] S. Mukherjee, "The Science of Clays–Applications in Industry, Engineering and Environment", Capital Publishing, vol. 351 pp, 2013.

[15] P.L. Younger, "Impacts of mining on physical hydrogeology. *In:* 2nd Image Train Advanced Study Course. 2003," Pecs, Hungary, 2003.

[16] L. Mukhopadhyay and B. Ghosh, "Mining induced desiccation and consequent impact on traditional economic livelihood – An analytical framework. *In:* XIII Annual Bioecon Conference at IHEID, Geneva, Switzerland," 2011. Available in: www.bioecon-network.org/pages/13th_2011/Mukhopadhay.pdf

[17] S.G. Ampian, "Clays In: Mineral facts and problems. Washington, DC, US Bureau of Mines, pp 1–13, Bulletin 675 Pretoria, South Africa and University of Zimbabwe, Geology Department: Harare, Zimbabwe, 1985.

[18] P.D. Oldham, "Pneumoconiosis in Cornish China Clay Workers", vol. 40, no. 2, pp. 131-137, May, 1983. https://www.jstor.org/stable/27723692

[19] Z. Adamis, J. Fodor, R.B. Williams, "Bentonite, Kaolin, and Selected Clay Minerals", Environmental Health Criteria, WHO, 2005. ISBN 9241572310, ISSN 0250-863X

[20] M. Wiemann, A. Vennemann and W. Wohlleben, "Lung Toxicity Analysis of Nano-Sized Kaolin and Bentonite: Missing Indications for a Common Grouping", Nanomaterials, vol. 10, 2020. doi:10.3390/nano10020204

[21] A.G. Heppleston, "Pulmonary Toxicology of Silica, Coal and Asbestos", Environmental Health Perspectives, vol. 55, pp. 111 – 127, Apr., 1984. https://doi.org/10.2307/3429696

[22] IARC, "Silica. In: Silica, some silicates, coal dust and para-aramid fibrils. Lyon, International Agency for Research on Cancer," IARC Monographs on the Evaluation of Carcinogenic Risks to Humans, vol. 68, pp. 41 – 242, 1997.

[23] L.W. Hale, J. Gough, E.J. King and G. Nagelschmidt, "Pneumoconiosis of Kaolin Workers", British Journal of Industrial Medicine, Vol. 13, No. 4, pp. 251–259, 1956.

[24] J.R. Burt, S.A. Burt, N. Paladugu and G.J. Aquino, "Kaolin Pneumoconiosis", The American Journal of Medicine, vol. 134, no. 3, pp. E203–E204, 2021.

[25] E.B. Altekruse, B.A. Chaudhary, M.G. Pearson and W.K. Morgan, "Kaolin dust concentrations and pneumoconiosis at a kaolin mine", Thorax, vol. 39, pp. 436–441, 1984.

[26] D.A.C. Manning, "Introduction to Industrial Minerals", Springer, 287 p, 1995.

The Nucleus ***60****, No. 2 (2023) 131-135*

www.thenucleuspak.org.pk

The Nucleus
ISSN 0029-5698 (Print)
ISSN 2306-6539 (Online)

Absorption and Fluorescence Mechanisms of Red Mega 480 Laser Dye Coupled with Silver Nanoparticles

S.T. Dadami[1], V.B. Tangod[2*]

[1]*Department of Physics, Nrupatunga University, N.T Road, Bengaluru-560001, Karnataka, India*

[2]*Department of Physics, Government First Grade College for Women, Opposite to R N Shetty Stadium Office Dharwad-580008, Karnataka, India*

ABSTRACT

Herein, we used the chemical reduction method to synthesize silver nanoparticles. The characterization of synthesized particles is done using UV-Vis, SEM, and TEM techniques, which reveal sizes in the range of 4–12 nm. In this particular instance, the optical absorption spectra of synthesized silver nanoparticles produced a maximal spike in the 400–410 nm region. This spike is attributed to surface plasmon resonance. The spectra of emission and absorption intensities of the exceptionally brilliant laser Red Mega 480 dye in alcohol solvents with the addition of silver nanoparticles indicate quenching. This is related to the size, shape, and transfer of energy between silver nanoparticles and dye. The quenching of fluorescence intensity in the presence of nanoparticles with Red Mega 480 dye leads to advancements in biomolecular labeling, printing technology, 3D graphics, glossy painting, fluorescence patterning, and cancer treatment.

Keywords: *Nanoparticle, Fluorescence, Absorption, Silver, Red Mega 480*

1. Introduction

In the most recent technical discipline, nanoscience and nanotechnology are leading civilization into new realms of efficient technology. Every interdisciplinary subject, such as physics, chemistry, biology, or applied science: such as medicine or engineering, is bursting with incredible new nanoscale discoveries. Between isolated atoms and aggregates large enough to be referred to as bulk material, nanoparticles are particles with diameters ranging from 1 to 100 nm. Since nanoparticles are bigger than individual atoms but smaller than bulk solids, materials in the nanoscale size range behave in a way that is halfway between that of macroscopic solids and an atomic or molecular system. These discrepancies can be explained by three primary reasons [1–5]:

1. Large ratio of surface to volume.
2. The effect of being bigger than an atom and smaller than a macroparticle
3. Maxwellian interactions.

Metal nanoparticles, specifically silver nanoparticles, are currently attracting a lot of interest due to their many fascinating features [6], plus several applications in medicine and technology. The optical properties of various nanomaterials have sparked a lot of interest. The radius-to-wavelength proportion becomes critical when silver is broken into increasingly tiny fragments and when the particle is smaller than the wavelength, the Rayleigh approximation (i.e., no retardation) holds and the mathematics becomes easy to understand. Mie's theory [7] established that plasmonic stimulation takes place when the radius is greater than the wavelengths of light and the plasmon retarding effect must be included to produce accurate results.

Silver particles (AgNPs) exhibit a yellow tint when they are tiny enough, owing to their substantial ability to absorb the green wavelength at 408nm that matches the frequency at which a plasmon resonance phenomenon happens when interacting with silver [8]. When the conductor's measurements are reduced, borders and contact with surfaces become more apparent. As a result, the collectively oscillating motion of conduction electrons dominates the optical characteristics [9] of tiny metal nanoparticles. Surface plasmon resonance (SPR) occurs when the incoming photon frequency is resonant with the collective oscillation of conduction band electrons. When laser dye comes into touch with a nanoparticle, the surface Plasmon resonance peaks are quenched, which inspires us to do research that will have more sophisticated industrial and medical applications.

Quenching of optical fluorescence and absorbance of Red Mega 480 [1-(5-carboxypentyl)-6-2-[7-(diethylamino)-2-oxo-2H-chromen-3-yl] ethenyl pyridinium-3-sulfonate] is reported in this communication [10,11].

The effect of AgNPs on the compound Red Mega 480 in laser dye has essential industrial applications such as security printing, lithographic printing plates and many more printing applications. Despite various industrial applications, no systematic investigation on the impact of the optical absorption and fluorescence of Red Mega 480 on various solvents in an environment of silver nanoparticles has been undertaken to date. In terms of optical absorption and fluorescence quenching with AgNPs, this study explains the novel and different spectroscopic characteristics of Red Mega 480 fluorescent dye [10, 11].

2. Experimentation

2.1 Chemicals and Dye

Sigma Aldrich's AR-grade methanol, propanol, ethanol, nanonol, decanol, and laser dye RedMega480 are used in this work. The chemical structure of Red Mega 480 is given in Fig. 1.

*Corresponding author:vadirajtangod@gmail.com

Chemical composition of Red Mega 480 Laser dye: $C_{26}H_{30}N_2O_7S$

Nomeniclature:1-(5-carboxypentyl)-6-2-[7(diethylamino) -2-oxo2-chromen-3-yl] ethenylpyridiniumm -3-sulfonate

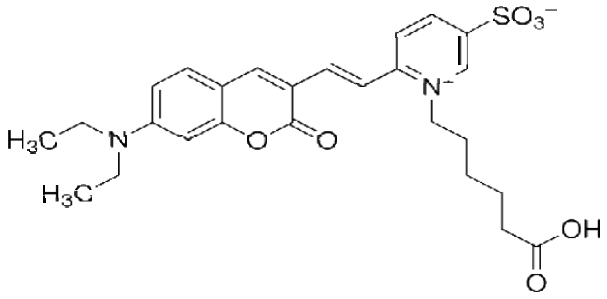

Fig. 1: Red Mega 480's molecular structure and IUPAC name

2.2 Synthesis of silver nanoparticles (AgNPs)

Silver nanoparticles can be synthesized by chemically reducing silver ions in an aqueous solution with sodium borohydride. The chemical reduction approach is used to create silver nanoparticles [12, 13]. Silver nitrate drops to 1.0 mM in 20 milliliters of substantially hydrogenated water. The colloidal yellow color solution was created after adding 0.1 ml of trisodium citrate to $AgNO_3$ solution drop by drop with continued and constant agitation and additional admixing of 0.6 milliliters of 0.1 mM sodium borohydrate dropwise, indicating the synthesis of silver nanoparticles. There was no direct incident light during the preparation process. Absorption spectroscopy of the yellow solution revealed the production of silver nanoparticles. The chemical equations are presented below [4]:

$$4Ag + C_6H_5O_7Na_3 + 2\,H_2O \longrightarrow 4Ag + C_6H_5O_7H_3 + 3\,Na^+ + H^+ + O^2\uparrow$$

$$AgNO_3 + NaBH_4 \longrightarrow Ag + \tfrac{1}{2}H_2 + \tfrac{1}{2}B_2H_6 + NaNO_3$$

2.3Experimental Arrangements

Spectra suite HR4000 highly resolving powered spectrometer was used to measure optical absorption and fluorescence measurements.

3. Theory

Mie's scattering theory has been extensively used to examine the spectroscopic characteristics of silver nanoparticles, specifically the size of the particle, dependency on surroundings, and impact on targeted dye molecules in the presence of alcoholic solvents. Specifically, Mie's theory [14–16] is a quantum mechanical explanation for the scattering of electromagnetic radiation by spherically shaped nanoparticles that are in the surrounding medium. Mie's mathematical scattering equations start with the electric field vector E and the magnetic field vector H:

$$\nabla \cdot E = 0 \quad (1)$$

$$\nabla \cdot H = 0 \quad (2)$$

$$\nabla \times E = \iota\omega\mu H \quad (3)$$

$$\nabla \times H = -\iota\omega\varepsilon E \quad (4)$$

The Helmholtz relation [17, 18] explains the arrangement of an occurrence electromagnetic field with two parts.

$$\nabla^2 E + K^2 E = 0 \quad (5)$$

$$\nabla^2 H + K^2 H = 0 \quad (6)$$

Here, the wavenumber is k, which is assigned to

$$k^2 = \omega^2\varepsilon\mu \quad (7)$$

Depending on the particle size range, the influence of particulate size resonance peak wavelength is induced by two distinct processes. In the limit of $2R << \lambda$ (R is the average radius of particles and λ is the wavelength of the light in the medium), mainly the dipole electrical components contribute considerably [5, 7, 15, 19] to the extinction cross-section (σ_{ext})

$$\sigma_{ext} = 9\,\frac{\omega}{c}\varepsilon_m^{3/2}V\,\frac{\varepsilon_2(\omega)}{[\varepsilon_1(\omega)+2\varepsilon_m]^2+[\varepsilon_2(\omega)]} \quad (8)$$

Here, $V = (4/3)\,R^3$ represents the volume of a spherical particulate, c represents exciting light's angular frequency, m, ε_m, and $\varepsilon(\omega)$ represent dielectric frictions of the enveloping medium and its material, where $[\varepsilon(\omega) = \varepsilon_1(\omega) + i\varepsilon_2(\omega)]$. The condition for resonance is $\varepsilon_1(\omega) = -2\varepsilon_m$ is called SPR.

4. Discussion and Results

The optical absorption spectrum of Red Mega 480 laser dye in alcohol solvents with AgNPs is shown in Fig. 3 which shows a wide band in the wavelength range of 470–510 nm. Fig. 4 depicts a fluorescence spectrum with a wide band in the range 590–650 nm.

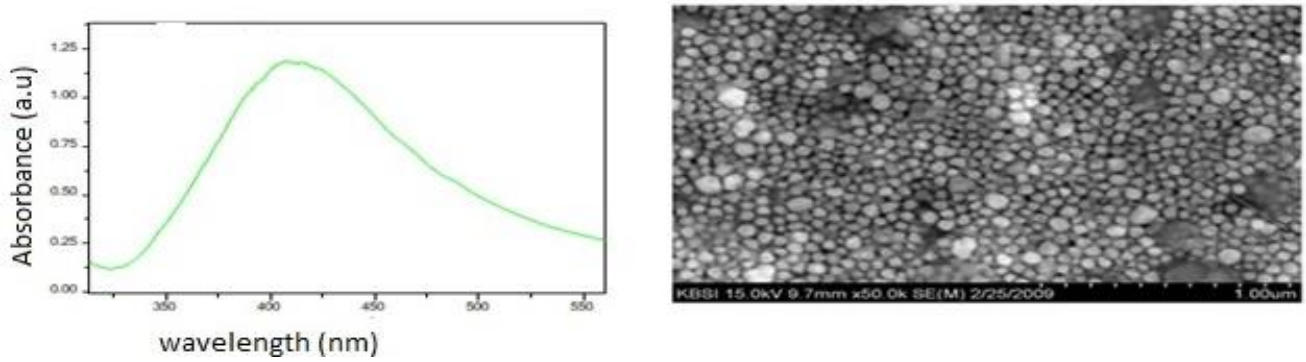

Fig. 2. (a): Surface plasmon resonance of AgNP; (b) SEM image

When AgNP's are injected into Red Mega 480 laser dye, the absorption spectrum peak swings to the longer wavelength side (redshift), peaking at 498nm (methanol), 501nm (ethanol), 502nm (propanol), 497nm (nonanol), 503nm (butanol) and 491nm (decanol), along with absorbance intensity values quenching. Similarly, fluorescence band shifts in the higher region peaked at 637 nm (methanol), 629nm (ethanol), 620nm (propanol), 623nm (butanol), 606nm (nonanol) and 603 nm (decanol) and fluorescence intensity quenched (Figure 3 shows absorbance quenching and Figure 4 shows fluorescence quenching) specifically when molecules complexed with the AgNPs, the band was quenched and widened. The quenching of the Ag peak demonstrates the binding of the AgNPs to the Red Mega 480 laser dye via alcoholic, ester, and thiol groups, which changes the density of electrons in the AgNPs; as a result, the surface-bound Red Mega 480 laser dye absorption is immediately affected in addition to the SPR silver nanoparticles are closely bonding with the negative group element like sulphonyl and alcoholic group as a result sudden intensity in the absorption or fluoresce will fall down (Fig. 5.)

When AgNPs were added to the probe molecule of Red Mega 480 laser dye, the vibrational features of the probe molecule were well determined and the intensity had been quenched because AgNP's were adsorbed on the OH^- group, SO^- group, ester group, and formed hydrogen bonds with the Red Mega 480 molecule as shown in Fig. 5.

In this scenario, suppression of absorption and fluorescence for Red Mega 480 dye molecules in alcohols connected with AgNPs via hydrogen bonding was possible. Three factors influence the rate of the transfer of energy between the dye and the nanoparticles [15, 21, 22].

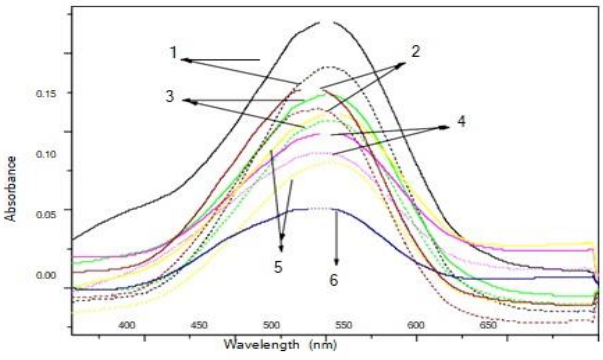

Fig. 3: Laser dye molecule Red Mega 480 in various solvent absorption spectra with and without silver nanoparticles (1-Methanol, 2-decanol, 3-ethanol, 4-Propanol, 5-butanol, 6-nonanol) (Line-Without, dashed line-with silver nanoparticles).

1. The integral of Coloumbic overlap.
2. Location(SPR)
3. Broadening of the band (inverse SPR lifetime) of the absorption spectrum of silver nanoparticles with dye.

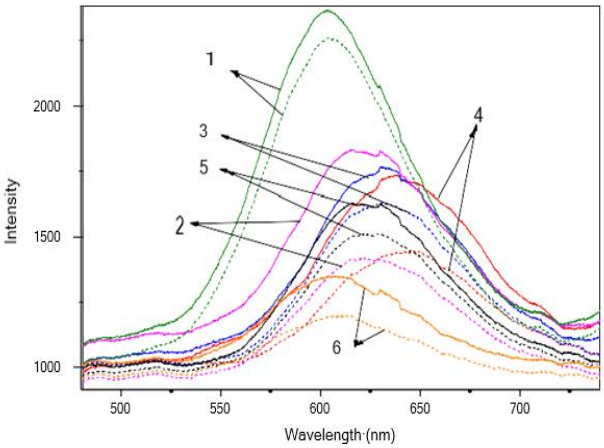

Fig. 4: Laser dye molecule Red Mega 480 in various solvent fluorescence spectra with and without silver nanoparticles (1-Methanol, 2-decanol, 3-ethanol, 4-Propanol, 5-butanol and 6-nonanol) (Line-Without, dashed line-with silver nanoparticles)

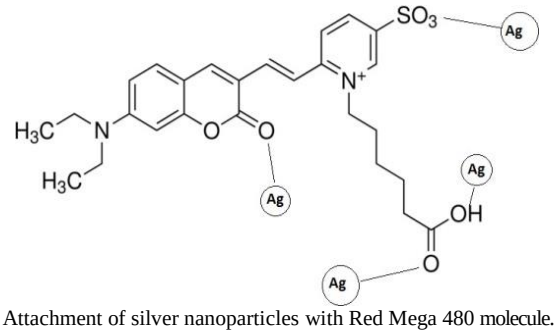

Fig.5: Attachment of silver nanoparticles with Red Mega 480 molecule.

The effect of Coulombic interactions on energy transmission has been investigated using two components.

1. The interaction of dye and AgNPs is determined by their relative densities of charge.
2. Dipole approximation during interaction

The electron concentrations on a probe molecule, dye dipole moments, and Ag-NPs account for the way in which energy transfers dye to silver nanoparticles, which induces a quench in optical absorption. Ultraviolet-visible spectra show a band range of 470-510nm which is assigned to π-π^* transitions.

Based on the dye's chemistry, the attachment of AgNPs to dye's molecules causes a heavy quenching of fluorescence [21, 23, 24]. The modifications in chemical and structural bindings and the complex fluorescence of AgNP's in close proximity to a metal are explained by the broadening of a plasmon and the fluorescence rate of the molecules is a function of the distance between the probe molecule and the AgNPs. The fluorescence of a molecule is completely quenched when it comes into direct contact with the nanometal [22, 23, 25, 26]. In our situation, the interaction of AgNPs with dye molecules is slightly larger. The impact of

silver nanoparticle on the sulphonyl and alcoholic group makes the quenching of absorbance and fluoresce intensity [27, 28] on the location of the surface plasmon region of alcohol series functional nanoparticles of silver was investigated through the application of the dye molecule for evaluating UV-Vis absorbance spectra in the range 450-800nm. Because particular interactions with the -OH group, the ester group of the Red Mega 480 dye chain, might have a substantial influence on the optical properties of AgNPs, alcohols were chosen as the solvent.

Energy may be confined to tiny spatial regions by surface plasmon resonance stimulation when the size of nanoparticles grows shorter compared to the wavelength of the stimulating light ($2R<<\lambda$) [Reference??]. The optical characteristics of metal nanoparticles are greatly impacted by their size, shape, and surroundings, as well as resonant energy transmission between closely spaced metal nanoparticles and the surrounding molecule [2].

A non-radiative decay-based resonance energy transfer model [21, 29] provides a theoretical explanation for these quenching fluorescence findings. The spectral characteristics of molecules adsorbed on or encapsulated in metallic and dielectric particles have been explored experimentally and theoretically in recent years. When an excited particle oscillates in an incoming electromagnetic field, the excited system could possess a changing electrical dipole moment, resulting in radiation. The light radiation from the dipole moment provides an outlet for radiative decay [22]. These fields' joule heating and plasmon absorption, on the other hand, open non-radiative decay paths. The competition for radiant and nonradiative decaying energies affects the fluorescence emissions of molecules around particles. Fluorescence quenching occurs when nonradiative degradation takes over [32]. The observed yield of quantum particles always diminishes with a modest separation from a metallic nanoparticle because the radiative and nonradiative rates function differently at various distances.

The reported quenching of fluorescence is caused by the transfer of resonance energy between Red Mega 480 and AgNPs. This non-radiative decay may be studied using the Forster transfer of resonance energy (FRET) hypothesis [21, 30]. Due to physical adsorption, whenever AgNPs in the colloidal form are injected into a solution with Red Mega 480 dye molecules in various alcohol solvents, molecules preferentially cluster around silver particles. More molecules adsorb on the silver particles as the concentration of Red Mega 480 rises. The quantum yield of nanoparticles of silver is quite high.

$$Q = \frac{\Gamma^{R}}{\Gamma^{R}+\Gamma^{NR}} \quad (9)$$

Γ^{R} decay due to radiation rate; Γ^{NR} rate of non-radiative degradation.

The adsorption of AgNPs containing dye causes an increase in the non-radiative decay rate [21, 31], resulting in a loss in quantum efficiency or fluorescence quenching. Static quenching may also be attributed to dye interaction among AgNPs via nanometal complexes with the -OH alcoholic group or ester group [21, 32, 33, 34].

Conclusion

In Conclusion, silver nanoparticles are synthesized by the chemical reduction method. SEM and TEM analysis displayed the averaged particle size in the range of 4-12 nm. Further, absorbance and fluorescence quenching intensities with Red Mega 480 laser dyes using different alcohols, with and without the attachment of silver nanoparticles are seen. It is all because of size, energy transfer, and bonding with the probe molecule. This quenching of fluorescence with Red Mega 480 laser dye leads to innumerable usages, specifically in advancements in bimolecular labeling, printing technology, 3D graphics, glossy painting, and fluorescence patterning.

References

[1] J.D. Jackson, “Classical Electrodynamics”, Wiley, New York, 1975.

[2] G. Schmid, “Clusters and colloids–from theory to applications”, VCH, Weinheim, Germany, 1994.

[3] C.F. Bohren, D.R. Huffman, “Absorption and Scattering of Light by Small Particles”, Wiley Interscience: New York, 1983.

[4] T. Pradeep, “NANO: The Essentials: Understanding Nanoscience and Nanotechnology”, Tata McGraw-Hill Publishing Company Limited New Delhi, 2007.

[5] S.K. Ghosh, Tarasankar, “Interparticle coupling effect on the surface plasmon resonance of gold nanoparticles: from theory to applications”, Chem.Rev. vol. 107, no. 11, pp. 4797–4862, 2007.

[6] S. Eustis, A.Mostafa El-Sayed, “Why gold nanoparticles are more precious than pretty gold: Noble metal surface plasmon resonance and its enhancement of the radiative and nonradiative properties of nanocrystals of different shapes”, Chem. Soc. Rev. vol. 35, pp. 209-217, 2006.

[7] J. Perez-Juste, P. Mulvaney, L.M. Liz-Marzan, “Shape control in gold nanoparticle synthesis”, Int. J. Nanotechnol, vol. 4, no. 3, pp. 215, 2007.

[8] A. Akbarzadeh, D. Zare, A. Farhangi, M.R. Mehrabi, D. Norouzian, S. Tangestaninejad, M. Moghadam and N. Bararpour, “Synthesis and Characterization of Gold Nanoparticles by Tryptophane”, American Journal of Applied Sciences, vol. 6, no. 4, pp. 691-695, 2009.

[9] M.S. Yavuz, G.C. Jensen, D.P. Penaloza, T.A.P. Seery, S.A. Pendergraph, J.F. Rusling, G.A. Sotzing, “Gold nanoparticles with externally controlled, reversible shifts of local surface plasmon resonance bands”, Langmuir, vol. 25, no. 22, pp. 13120-13124, 2006.

[10] V.B. Tangod, P.U. Raikar, B.M. Mastiholi, and U.S. Raikar, “Solvent polarity studies of highly fluorescent laser dye ADS740WS and its fluorescence quenching with silver nanoparticles”, Canadian Journal of Physics, vol. 92, no. 2, pp. 116-12, 2014.

[11] V.B Tangod, B.M. Mastiholi, P. Raikar, S.G. Kulkarni, U.S. Raikar, “Studies of the photophysics of highly fluorescent Red Mega 480 laser dye in solutions: Steady state spectroscopy”, Spectrochimica Acta Part A: Molecular and Biomolecular Spectroscopy, vol. 148, pp.105-113, 2015.

[12] N. Usen, S.A. Dahoumane, M. Diop, X. Banquy, D.C. Boffito, “Sonochemical synthesis of porous gold nano- and microparticles in a Rosette cell,” Ultrasonics Sonochemistry, vol. 79, pp. 105744, 2021.

[13] N.R. Jana, L. Gearheart, C.J. Murphy, “Evidence for Seed-Mediated Nucleation in the Chemical Reduction of Gold Salts to Gold Nanoparticles”, Chem. Mater, vol.13, no. 7, pp. 2313–2322, 2001.

[14] J. Turkevich, P.C. Stevenson, J. Hiller. “A study of the nucleation and growth processes in the synthesis of colloidal gold”, Discuss. Faraday Soc. vol. 11, no. 55, 1951.

[15] J. Gersten, A. Nitzan, “Spectroscopic properties of molecules interacting with small dielectric particles”, J. Chem. Phys, vol. 75, pp. 1139–1152, 1981.

[16] M. Umadevi, N.A. Sridevi, A.S. Sharmila, B.M. Rajkumar, M.Briget Mary, P. Vanelle, T. Terme, O. Khoumeri, "Characterization of Ag Nanocrystals for use in Solar Cell Applications", J. Fluorese, vol.20, pp.153, 2010.

[17] C.E. Rayford, G. Schatz, K. Shuford, "Optical Properties of Gold Nanospheres Optical Properties of Gold Nanospheres", Nanoscape, vol.27, no. 1, 2005.

[18] L. Novotny, B. Hecht, "Principlesofnano-optics", Cambridge, UK, 2006.

[19] S.A. Maier, "Plasmonics, Fundamentals and applications", Spinger, Berlin, 2007

[20] K.G. Thomas, BinilIttyIpe, P.K. Sudeep, "Photochemistry of chromophore-functionalized gold nanoparticles", Pure Appl. Chem. vol.74, no.9, pp.1731, 2002.

[21] M.A. Bratescu, N. Saito, H. Mori, O. Takai, "Localized surface plasmon resonance of silicon compounds adsorbed on silver nanoparticles", Surf. Sci. vol. 601, pp. 3886, 2007.

[22] C.A. Sabatini, R.V. Pereira, M.H. Gehlen, "Fluorescence modulation of acridine and coumarin dyes by silver nanoparticles" J.Fluoresc. vol. 17 no. 4, pp. 377-382, 2007.

[23] G.F. Schneider, V. Subr, K. Ulbrich and G. Decher. "Multifunctional Cytotoxic Stealth Nanoparticles. A Model Approach with Potential for Cancer Therapy", Nano Letters, vol. 9, no. 2, pp. 636-422, 2009.

[24] D. Ancukiewicz, "Enhanced Light Emission Using Plasmonic Gold Nanoparticles", Applied Physics, Columbia University, Optics and Opto-Electronics", pp. 100-101, 2008.

[25] K.G. Thomas, P.V. Kamat," Making Gold Nanoparticles Glow: Enhanced Emission from a Surface-Bound Fluoroprobe", J. Am. Chem. Soc. vol. 122, no. 11, pp. 2655-2656 2000.

[26] K. Pradhan, R.B. Konda, H. Mustafa, R. Mundle, O. Bamiduro, U.N. Roy, Y.C.A. Urger, "Surface plasmon resonance in CdSe semiconductor coated with gold nanoparticles", vol.16, no.9, pp. 6202, 2008.

[27] H. R. Stuart, D.G. Hall, "Enhanced Dipole-Dipole Interaction between Elementary Radiators Near a Surface", Phys. Rev.Lett. vol. 80, pp. 5663. 1998.

[28] T. Soller, M. Ringler, M. Wunderlich, T.A. Klar, J. Feldmann, H.P. Josel, J. Koci, Y. Markert, A. Nichtl, K. Kürzinger," Streptavidin reduces oxygen quenching of biotinylated ruthenium(II) and palladium(II) complexes" J. Phys Chem B, vol. 112, no. 40, pp. 12824. 2008.

[29] J. Lee, O. Azamat, A.O. Govorov, N.A. Kotov, "Solvent Effect in Dynamic Superstructures from Au Nanoparticles and CdTe Nanowires: Experimental Observation and Theoretical Description," J. Phys. Chem. C, vol. 114, no.3, pp.1404-1410, 2010.

[30] P.P.H. Cheng, D. Silvester, G. Wang, G. Kalyuzhny, A. Douglas, R.W. Murray, "Dynamic and static quenching of fluorescence by 1-4 nm diameter gold monolayer-protected clusters" J. Phys. Chem B. vol.110, pp. 4637, 2006.

[31] E. Dulkeith, M. Ringler, T.A. Klar, "Gold nanoparticles quench fluorescence by phase induced radiative rate suppression", J. Feldmann, Nano Lett. vol. 5, no.4, pp.585, 2005.

[32] V.B Tangod, "Quenching of Fluorescent ADS680HO molecule with Eco-Friendly Synthesized Silver Nanoparticles", The Nucleus, vol. 60, no.1, pp.56-59, 2023.

[33] T. Foster, "Zwischenmolekulare Energiewanderung und Fluoreszenz," Annalen der Physik Ann.Phys.vol.2, pp. 55-75, 1948.

[34] M. Ringler, A. Schwemer, M. Wunderlich, A. Nichtl, K. Kürzinger, T. A. Klar, and J. Feldmann, "Emission Spectra of Fluorescent Molecules with Single Plasmonic Nano resonators", Phys. Rev. Lett., vol.100, pp. 203002, 22 May 2008.

[35] B.M. Mastiholi, P.U. Raikar, V.B. Tangod, S.G. Kulkarni and U.S. Raikar, "Fluorescence Enhancement of C 314 Laser Dye Based on ICT between C 314 Laser Dye and Green Synthesized Gold Nanoparticles", IOSR Journal of Applied Physics (IOSR-JAP), vol. 6, no.6(III), pp. 43, 2014.

The Nucleus ***60***, *No. 2 (2023) 136-144*

www.thenucleuspak.org.pk

The Nucleus
ISSN 0029-5698 (Print)
ISSN 2306-6539 (Online)

Effect of Sutural Pattern on Shell Shape: A Case Study Including Two Ammonite Subfamilies from the Western India

Pinaki Roy

Department of Geology, Durgapur Government College, Durgapur, India.

ABSTRACT

Shell morphology of ammonites and its connotation with ecological constraints has long been a matter of debate. The present study involves comparison of shell morphology with sutural complexity between Eucycloceratin and Reineckein ammonites of Kutch and Jaisalmer from India. Statistically significant differences between fractal-dimensions (D_f), whorl expansion rate of evolute and involute shells are interpreted. There is also a correlation between the flank's shape and complexity of suture. The planulate shells show highest D_f value and the lowest ones are found in whorl cross section with convex flanks. It may also be stated that sutural complexity is not the primary function to resist shell implosion and is thereby related to bathymetry.

Keywords: *Ammonite, Suture, Shell-geometry, Eucycloceratinae, Reineckeinae, Western India.*

1. Introduction

The present study has attempted to find out the relationship between the complexly frilled ammonoid suture patterns and their shell geometry. The complexity of ammonoid sutures is such that Euclidean geometry is unable to describe them properly [1]. The fractal dimension (D_f) of the suture was measured in a more favorable manner using fractal analysis, which may serve as a morphometric descriptor of the complexity. Its value lies between 1 and 2 since a straight line has a Euclidean dimension of one and a curve's sinuosity can closely fill a plain, which provides an effective or fractal dimension approximately equivalent to two [1]. Thus, sutures with greater complexity have a D_f value that is closer to two. In the ammonite morpho-space, D_f values are mainly determined by structural (shell architecture) and ornamental factors (sculpture strength rather than density of ornamentation). Previous studies [2] have found little evidence to suggest that the complexity of sutures in Late Jurassic ammonites is largely determined by the bathymetry of epicontinental and epioceanic environments, with the highest values of D_f found in planulate shells and the lowest in whorl cross sections with convex flanks. The enigmatic complexity of ammonoid sutures has confounded researchers [3] for many years. Two primary queries are yet to be answered: Why did the sutures form such diverse patterns which were not correlated to the shell morphology, and why did these sutural patterns evolve so quickly compared to the limited range of shell shapes? Despite considerable effort, these questions remain largely unresolved. Different explanations have been proposed for the complexity of septal geometry in ammonites: according to functional morphological aspect, the frilled sutures increased buttressing, which strengthened the shell against implosion. This is allowed for respiration and transport of cameral liquid. The frills were a result of body attachment and muscle attachment, mantle tie-points, and interactive vaulting. The physical properties of this included viscous fingering in fluid interfaces during morphogenesis, as well as compression and decompression of a bladder due to the movability of a fleshy membrane [4]. This can be related to accommodation space within the body chamber of ammonite–compressed shell needs more accommodation space, so complex sutures. Shell with convex flanks already has enough space for accommodating a bladder, so a simpler suture serves the purpose in this case.

Fig. 1: *Reineckeia tyrraniformis* from the subfamily Reineckeinae (Scale bar = 1 cm)

To testify the above hypothesis, two ammonite subfamilies have been chosen viz. Reineckeinae belonging to the family Reineckeidae (Fig. 1) and Eucycloceratinae belonging to the family Sphaeroceratidae (Fig. 2) from the Middle Jurassic of western India. Samples mainly have been collected from Kuldhara River section (Latitude =26°48′74″ N and Longitude = 70°48′1″E) in the Kuldhara Member of the Jaisalmer Formation, 16 km southwest of Jaisalmer, Rajasthan and near Bhakri village (Latitude = 23°22′34″ N and Longitude = 69°36′29″E), which lies to the northwestern part

*Corresponding author: pinakieroy@gmail.com

of the district town Bhuj, in Kutch, Gujarat. Both the ammonite subfamilies were widespread in their distribution in those two separate basins. Samples from two palaeobiogeographic distribution were taken to understand if there is any variability in ammonite morpho-space. Samples of three species from the subfamily Reineckeinae viz., *Reineckeia* (*Reineckeia*) *tyranniformis*, *Reineckeia* (*Loczyceras*) *turgida* and *Reineckeia* (*Loczyceras*) *reissi* and three species from the subfamily of Eucycloceratinae viz., *Idiocycloceras dubium*, *Idiocycloceras perisphinctoides* and *Nothocepahlites paradoxus* have been considered within this present study. Those two groups of species show variability in their degree of whorl inflation (rate of increment of whorl width relative to whorl height) as well as degree of involution (degree of tightness of coiling of ammonite shell).

Fig. 2: *Nothocephalites paradoxus* from the subfamily Eucycloceratinae (Scale bar = 1 cm.)

2. Geological Setting of the study area

The basins of Jaisalmer and Kutch originated in response to the reactivation of ancient fracture zones, which was a part of the overall rifting history of the Gondwana super plate. The initiation of the rifting in the region was at the start of Permian and in general proceeded from north to south. The Bikaner-Nagaur and Jaisalmer areas of Western Rajasthan and Axial Belt, Kirthar-Sulaiman and Kohat-Potwar areas of Pakistan formed the already emerged Indian shield's north-western slopes which were bounded on the three sides by the basement ridges of the Aravalli-Delhi fold belt (NW-SE Aravallis in the southeast, Delhi-Sargodha ridge in the northeast and Delhi ridge in the south).

2.1 Kutch Basin

Due to recurrent transgression and regression processes, sedimentation began shortly after the Kutch Basin opened as an early rifting of Gondwana in the Middle Jurassic [5]. Bathonian to Middle Tithonian Jurassic rocks can be encountered in the Kutch Basin. Biswas [6] established a litho-stratigraphic classification based on extensive mapping and lithofacies studies of the intra-rift sub-basins. The Kutch Mainland, the Pachham, and the Eastern Kutch litho-stratigraphic areas were distinguished. The Rann, a large salt flat, separated these settlements (see Fig. 3). The regional structure consists of three parallel anticlines that run northwest to southeast. North of the basin, in the middle anticline, the most developed Jurassic rocks can be found [7, 8]. As seen at the famous Callovian sequence locations of Jara, Jumara, Keera, and Jhura, these anticlines have undergone superimposition of folding, resulting in the characteristic interference pattern cropping up as topographical domes. The northern flanks of these domal formations are terminated by an east-west trending fault that was triggered by the intrusion of later Deccan Trap Volcanics. The Kutch Basin is divided into several distinct lithostratigraphic units, the most important of which are the Patcham, Chari, Katrol, and Bhuj Formations [9, 10]. Inliers of the younger Katrol Formation border the older Patcham and Chari Formations.

There are currently a number of important papers [11, 12] on the sedimentology and facies study of the region. The Chari Formation is comprising of shale, limestone, and sandstone heterolithic facies association that was deposited in a mid-shelf setting. Lower Callovian rocks in this Formation are dominated by shale-limestone (packstone/wackestone) alternations, whereas Middle Callovian rocks are made up of siliciclastics at their base. The present study relies on fossils acquired from the Bhakri sections of the Chari Formation.

2.2 Jaisalmer Basin

The Jaisalmer Basin is a pericratonic basin and represents mainly the westerly dipping eastern flank of the Indus Shelf. The existence of faults with strike-slip regime with its complimentary structural styles governing sedimentation history has been noticed in the basin [13]. The Jaisalmer Basin experienced its first sedimentation on igneous/metamorphic basement during Late Palaeozoic time which continued up till recently and sediments of huge thickness of the order of 10,000 m or so were deposited. Lithostratigraphically, the Jurassic sediments of the basin have been grouped into Lathi, Jaisalmer, Baisakhi and Bhadasar Formations in ascending order (Fig. 4) [14-18]. The thickness of individual formation ranges from 70 to 1000 m [14, 19]. Among these, the Jaisalmer Formation Ranges from Late Bajocian to Oxfordian age i.e., the Jurassic time. Lithostratigraphically, the Jaisalmer Formation has been divided, in ascending order, into the Hamira, Joyan, Fort, Badabag, Kuldhara and Jajiya Members [14, 20]. The Callovian-Oxfordian sediments of the Jaisalmer Formation, grouped into Kuldhara and Jajiya Members, are predominantly Carbonates deposited in the shoreface zone to off-shore transition zone above storm wave-base [21]. These are the best outcrops of the Callovian and Oxfordian sediments in the Jaisalmer Basin. The specimens of the present study have been collected from the Kuldhara Member of Jaisalmer Formation.

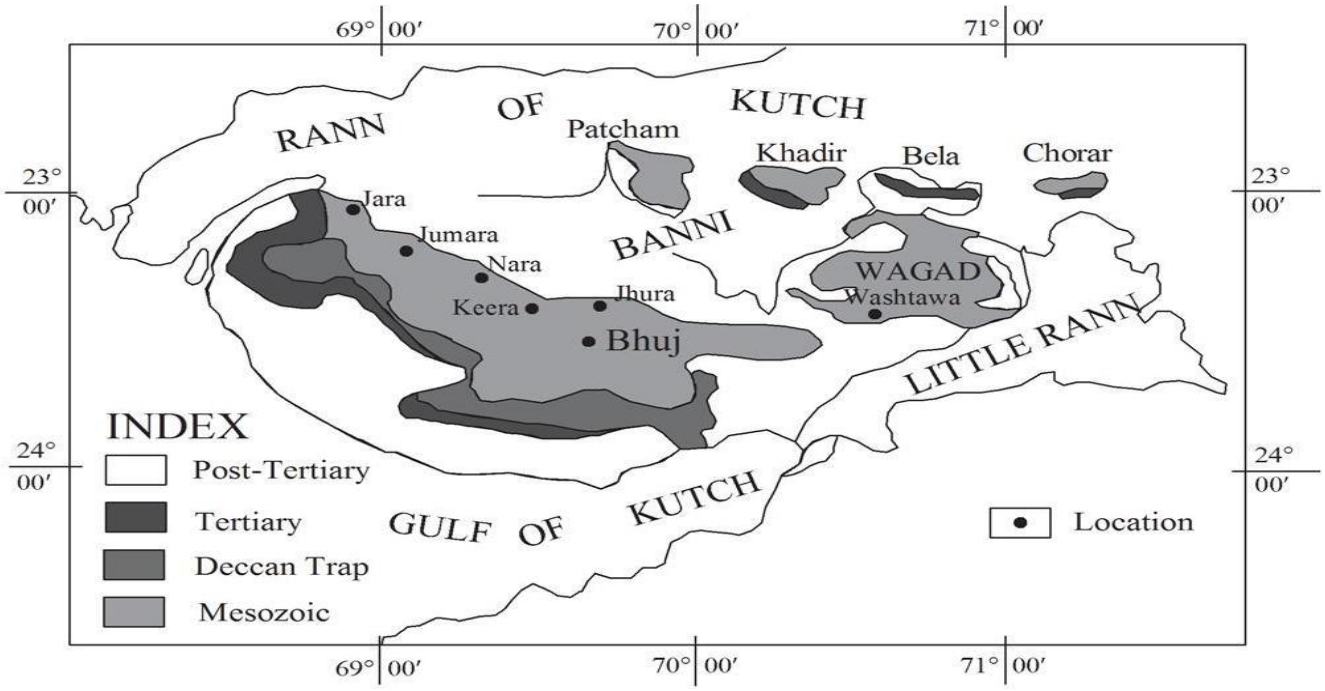

Fig. 3: Geological map of Kutch western India with the geographical locations of the study area.

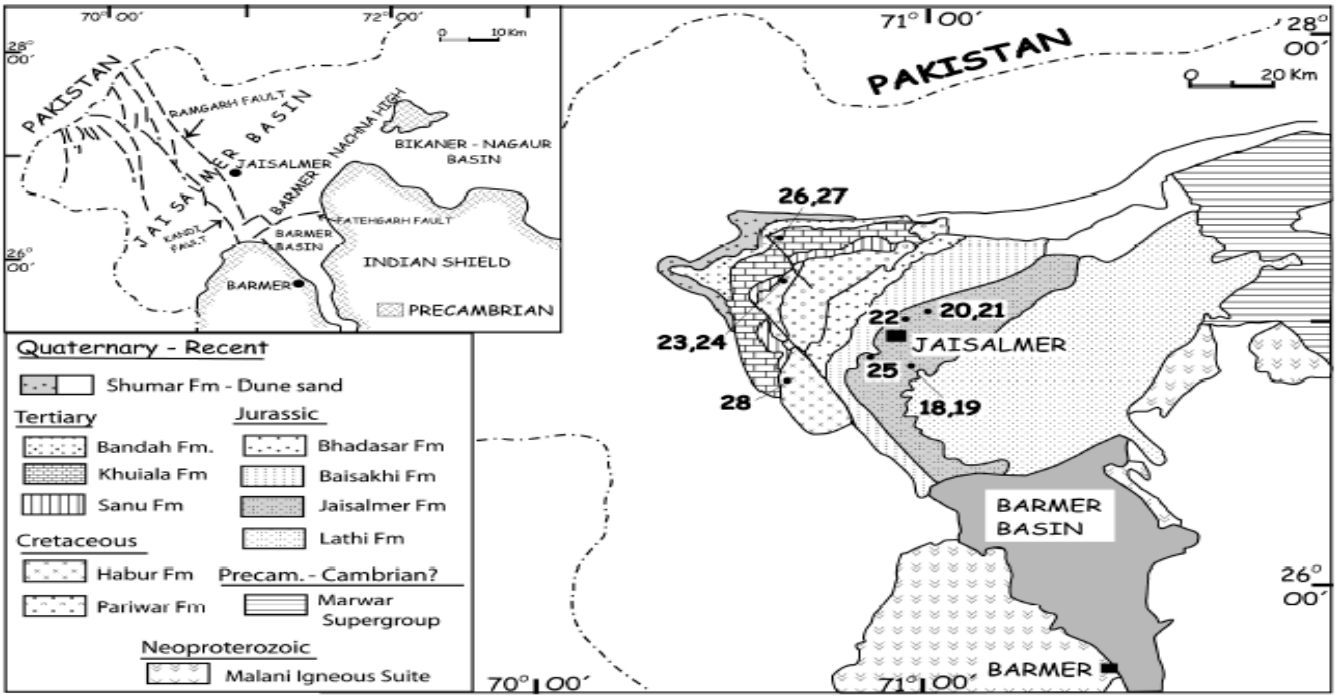

Fig. 4: Geological setting and location of the Jaisalmer basin.

3. Materials and Methods

The analyzed sutures were traced out from scaled photographs of actual specimens collected from the field. The dataset comprises 14 specimens and in each 3 sutures were analyzed, based on ontogeny. The specimens belong to 3 genera and 6 species.

The complexity of the sutures of these ammonites was analyzed based on their fractal dimension values. Two of the most commonly used methods to determine the fractal dimension of ammonite sutures are the Richardson step-line division method [22, 23] and the box method. The Richardson analysis [2, 24, 25] determines how the length of a curve is correlated to the stride length of a divider, or the length of the ruler, used to measure it. As the length of the ruler or step size decreases, the lengths of the fractal curves increase, and a log-log graph of the length measurement vs. the corresponding strides will yield a straight line if the curve exhibits a truly

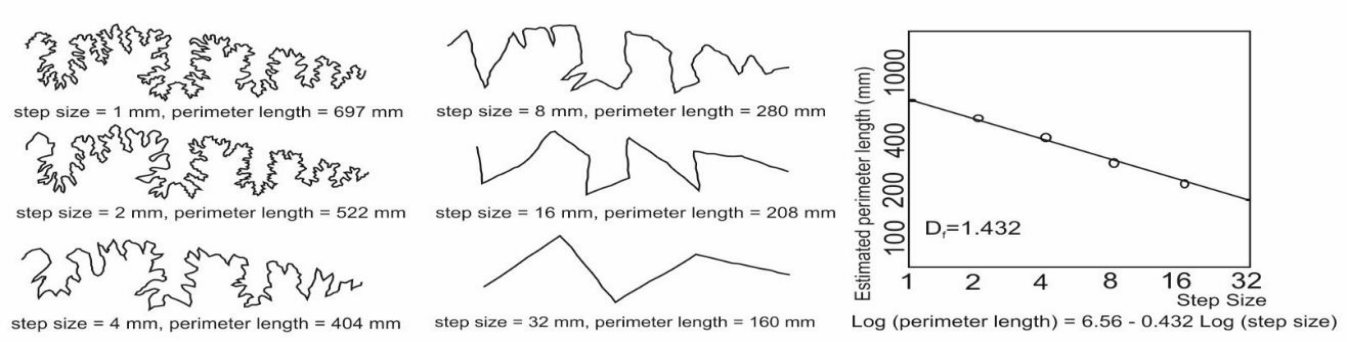

Fig. 5: Perimeter length measurement and estimation of the fractal-dimension (of) value of an ammonitic suture using the step-line method. The bi-variate graph shows how the perimeter estimated for the curve is inversely related to the length of the ruler.

fractal nature (Fig. 5). The fractal dimension value of the curve can be obtained from the following equation, which is adjusted by least-squares regression:

Log (perimeter length) =Log(k) + (l-D_f) Log (step size)

where ***k*** is the Y-intercept or length measurement for unit ruler length (step-size= 1).

The number of squared boxes of a given size required to cover a curve is used in the box analysis [26-28] or grid-cell procedure to determine the curve's length. A gauge of the length of the line can be made by duplicating the quantity of involved squares by the size of the square. The resolution at which the length of the line is measured is actually determined by the size of the grid that has been placed over the line. The D_f value can be measured with ease from this method by the following formula:

$$\text{Log } N = \alpha + \beta \log (1/s)$$

Where '**s**' is the dimension of the grid cells and **'**N' is the number of cells counted. As it is evident from the formula that it appears to bear the equation of a straight line where **α** and β are constants and the slope of the straight line, respectively. The product of 'N' and 's' gives the estimate of the perimeter length. The fractal dimension (D_f) for the grid-cell procedure is given by the addition of the slope of the regression of log {N X s} on log (1/s) by 1.

As the box size decreases, the length of the fractal curves also increases exponentially. In this study, the D_f values of the suture lines were measured using this method.

According to [25], the step-line process and the box approach yield different coefficients of determination (r2) values for the least-squares regression of length measurements vs. step-size or box size. As a result, this value is typically larger when the first method is applied; since box data tend to scatter more about the regression line, making it more difficult to determine the fractal dimension of relatively simple ammonite sutures. Due to Checa and Garcia-Ruiz's [26] demonstration that small upsides of the estimating unit provide information about the range of scale showing Euclidean way of behaving, the incline of this portion of the relapse line relating bend length to box size is consequently somewhat diminished, while for large box-measures the number of filled boxes will generally sway occasionally, some caution is also necessary when assessing the right D_f upsides of a bend using the case strategy.

According to Lutz and Boyajian [25], the suture sinuosity index is essentially a type of fractal index with measurements at only two length scales: the ratio of the external suture length to the whorl circumference (i.e., the suture perimeter of the digitized suture/Euclidean distance between the endpoints of the suture). For truly fractal bends, such as the majority of complicated ammonoid sutures, the resolution powers of the sinuosity measure and the fractal dimension are identical at greater complexities. However, the fractal dimension has better resolution at lower complexity since it measures length at several scales. The Whorl Expansion Rate is measured by the following formula:

Whorl Expansion Rate (WER) = Whorl Diameter (W)/Whorl Diameter (W)-Apertural Height (AH). The whorl expansion rate gives an insight into the shell geometry (Fig. 6) to know about the degree of involution of a shell. Sutures of specimens analyzed in the present work were digitized by tracing them

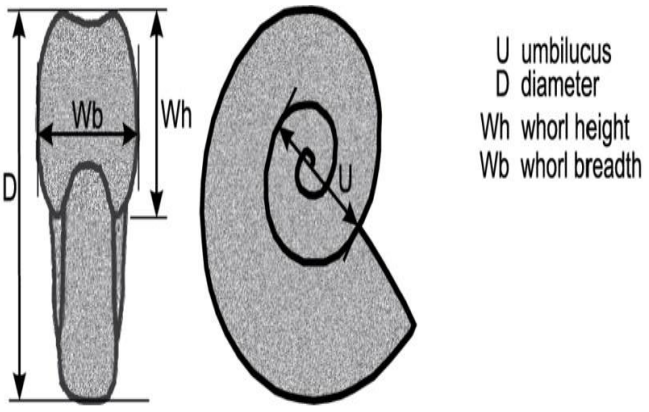

Fig. 6: Ammonite shell geometry with dimension parameters.

out from their images, with proper scale. Grids measuring 1 sq. mm, 4 sq. mm, 16 sq. mm and 36 sq. mm were placed respectively on the traced-out curves and the number of boxes were counted. The D_f values were obtained from the data

Table 1: Table showing the Raupian Parameters for three specimens, two of *Reineckeia tyranniformis* and one of *Nothocephalites paradoxus*.

Specimen No. and species name	Whorl Diameter W	Apertural height AH	W-AH	W/(W-AH)	WER
DGC/2013/J/65 *R. tyranniformis*	18.548	5.1422	13.4058	1.3835802	1.914294
DGC/2013/J/142 *R. tyranniformis*	18.25	5.8437	12.4063	1.4710268	2.16392
DGC/2013/J/148 *N. paradoxus*	10.07	3.7	6.37	1.5808477	2.49908

acquired by plotting the curve of Log(**NXs**) over Log(**1/s**). The D_f is calculated by the addition of 1 to the value of the slope of the regression line obtained.

4. Data Analysis

Mainly 14 specimens, belonging to three broad genera, have been studied. The mean D_f value obtained was of the order of 1.444 with the maximum and minimum counts of 1.607 and 1.283 respectively.

4.1 Structural Features

4.1.1 Coiling

Most of the specimens studied, featured evolute coiling of shell only 1 specimen showed an intermediate coiling. The intermediately coiled specimen comprised a value of D_f = 1.478 which is less than the D_f values obtained for the evolute shells (1.570), suggesting that the latter required strengthening (Table 2,4; Figs. 8-10). According to Oloriz et. al. [1] the D_f values are related to the surface-to-volume ratio (S:V), i.e., the sutural complexity depends on the surface-to-volume ratio of the camera of an ammonite shell. This has also been proved by the calculation of Whorl Expansion Rate (WER) (Table 1), suggesting that shells that are relatively involute have higher WER (2.49908) than shells with evolute coiling (1.914294).

4.1.2 Whorl section

In the present study, it has been observed that the ammonite genera which have compressed high oval whorl cross sections have greater D_f (1.607 for Eucycloceratins) values than those which have oval or sub circular whorl cross sections (1.522 for Reineckeins). This is also an indication regarding the surface-to-volume ratio of camera, which is lowest for sub-circular whorl cross sections and highest for more compressed high oval whorl cross sections [1].

4.2 Ornamental Features

Evidence from the present study suggests that ammonites with medium-sized ribs have higher D_f values than ammonites with large sized ribs. Again, shells with no or medium-sized tubercles have higher D_f values than shells having larger-sized ribs or tubercles. Since the strength of ribs and tubercles changes with ontogeny; the Reineckeins species exhibit changes in D_f value accordingly (Table 2; Figs. 7-8). The Genus *Idiocycloceras* has medium sized ribs and no tubercles, corresponding to a higher D_f value (1.607) than the specimens belonging to Genus *Reineckeia* (D_f = 1.483), which have larger ribs and coarse tubercles (Table 2; Figs. 9). Similar changes can be observed in *Nothocephalites paradoxus* during its ontogeny (Table 3; Fig. 10).

5. Bathymetry

The D_f values for specimens living on epicontinental shelves and swell regions of epioceanic fringes are similar. This indicates that there are no significant differences in the habitat depth of epicontinental and epioceanic ammonites, and that correlations between sutural complexity and bathymetry are implausible. [2].

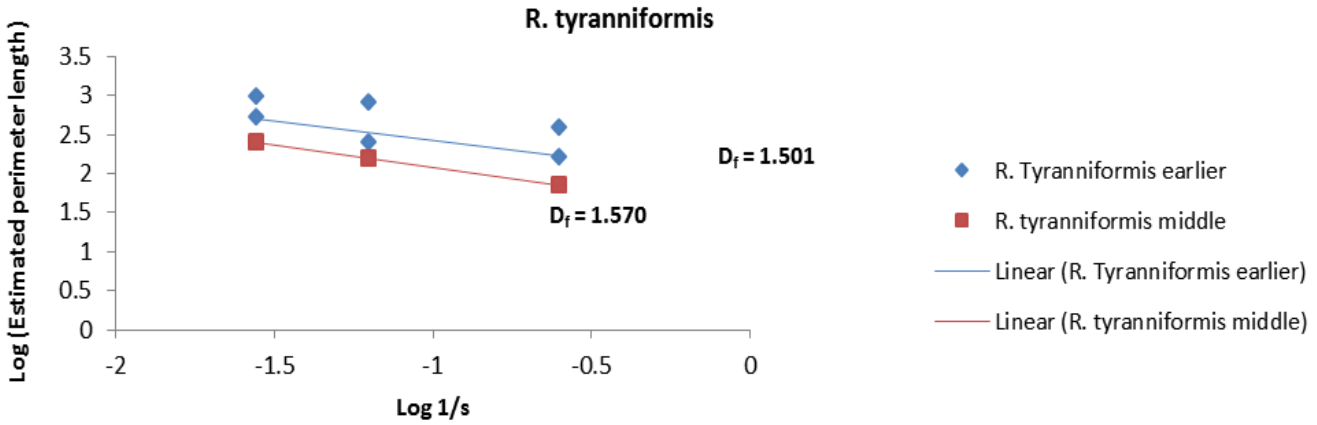

Fig. 7: Graph showing the ontogenetic variation of D_f values in *Reineckeia tyranniformis* (based on data from Table 2).

Table 2: Table showing the number of boxes counted, according to ontogeny, covering the digitized forms of suture lines, their estimated perimeter lengths, and logarithmic values for the genus *Reineckeia*. [s= Number of grid cells, N= Late growth stage, N1= Early Growth stage and N2= Middle Growth stage].

Specimen No. and species name	s	N	Ns	1/s	log (1/s)	log N	log Ns	N1	N2	N1s	N2s	log (N1s)	log(N2s)
DGC/2013/J/2	36	27	972	0.027778	-1.5563	1.431364	2.987666						
R. tyranniformis	16	51	816	0.0625	-1.20412	1.70757	2.91169						
	4	100	400	0.25	-0.60206	2	2.60206						
	1	197	197	1		2.294466	2.294466						
DGC/2013/J/65	36	15	540	0.027778	-1.5563	1.176091	2.732394						
R. tyranniformis	16	16	256	0.0625	-1.20412	1.20412	2.40824						
	4	41	164	0.25	-0.60206	1.612784	2.214844						
	1	73	73	1		1.863323	1.863323						
DGC/2013/J/142	36	7	252	0.027778	-1.5563	0.845098	2.401401	16		576		2.760422	
R. tyranniformis	16	10	160	0.0625	-1.20412	1	2.20412	25		400		2.60206	
	4	18	72	0.25	-0.60206	1.255273	1.857332	45		180		2.255273	
	1	40	40	1		1.60206	1.60206	83		83		1.919078	
DGC/2013/J/122	36	9	324	0.027778	-1.5563	0.954243	2.510545						
R. turgida	16	15	240	0.0625	-1.20412	1.176091	2.380211						
	4	43	172	0.25	-0.60206	1.633468	2.235528						
	1	89	89	1		1.94939	1.94939						
DGC/2013/J/105	36	18	648	0.027778	-1.5563	1.255273	2.811575						
R. reissi	16	32	512	0.0625	-1.20412	1.50515	2.70927						
	4	69	276	0.25	-0.60206	1.838849	2.440909						
	1	146	146	1		2.164353	2.164353						
DGC/2013/J/131	36	13	468	0.027778	-1.5563	1.113943	2.670246	5		180		2.255273	
R. reissi	16	22	352	0.0625	-1.20412	1.342423	2.546543	5		80		1.90309	
	4	41	164	0.25	-0.60206	1.612784	2.214844	16		64		1.80618	
	1	85	85	1		1.929419	1.929419	33		33		1.518514	
DGC/BHK/11	36	6	216	0.027778	-1.5563	0.778151	2.334454	4	3	144	108	2.158362	2.033424
R. reissi	16	10	160	0.0625	-1.20412	1	2.20412	6	4	96	64	1.982271	1.80618
	4	23	92	0.25	-0.60206	1.361728	1.963788	9	10	36	40	1.556303	1.60206
	1	48	48	1		1.681241	1.681241	18	24	18	24	1.255273	1.380211
DGC/BHK/8	36	11	396	0.027778	-1.5563	1.041393	2.597695	3	4	108	144	2.033424	2.158362
R. reissi	16	17	272	0.0625	-1.20412	1.230449	2.434569	4	4	64	64	1.80618	1.80618
	4	38	152	0.25	-0.60206	1.579784	2.181844	9	13	36	52	1.556303	1.716003
	1	70	70	1		1.845098	1.845098	15	25	15	25	1.176091	1.39794
DGC/2013/J/116	36	2	72	0.027778	-1.5563	0.30103	1.857332						
R.reissi	16	10	160	0.0625	-1.20412	1	2.20412						
	4	21	84	0.25	-0.60206	1.322219	1.924279						
	1	44	44	1		1.643453	1.643453						

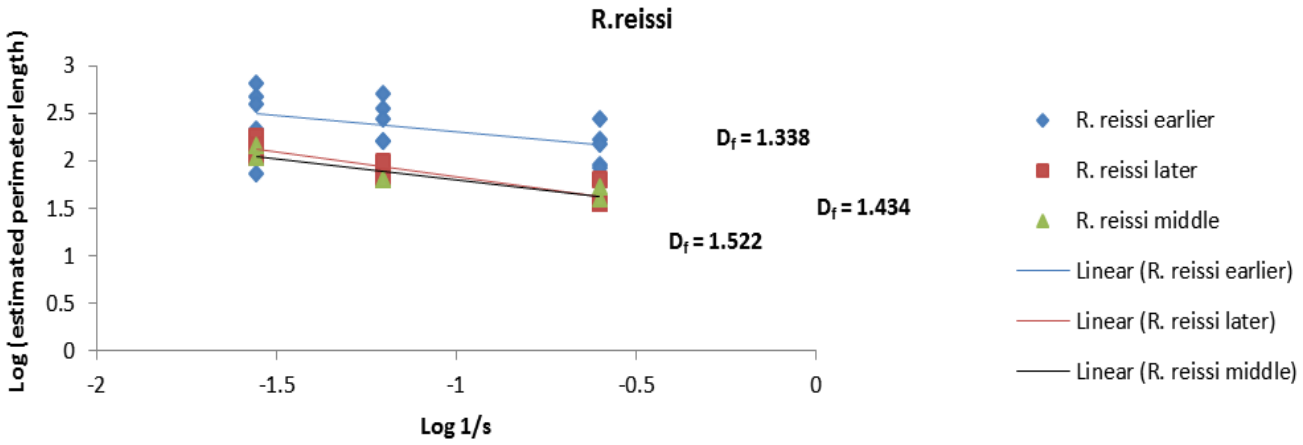

Fig. 8: Graph showing ontogenetic variation of D_f values in *Reineckeia reissi* (based on data from Table 2).

Table 3: Table showing the number of boxes counted, covering the digitized forms of suture lines, their estimated perimeter lengths, and logarithmic values for the genus *Idiocycloceras.* [s= Number of grid cells, N= Late growth stage].

Specimen No. and species name	s	N	Ns	1/s	log (1/s)	log N	log Ns
DGC/2013/137	36	17	612	0.027778	-1.5563	1.230449	2.786751
I. dubium	16	19	304	0.0625	-1.20412	1.278754	2.482874
	4	35	140	0.25	-0.60206	1.544068	2.146128
	1	68	68	1		1.832509	1.832509
DGC/2013/J/78	36	10	360	0.027778	-1.5563	1	2.556303
I. dubium	16	14	224	0.0625	-1.20412	1.146128	2.350248
	4	25	100	0.25	-0.60206	1.39794	2
	1	50	50	1		1.69897	1.69897
DGC/2013/J/132	36	13	468	0.027778	-1.5563	1.113943	2.670246
I. dubium	16	16	256	0.0625	-1.20412	1.20412	2.40824
	4	32	128	0.25	-0.60206	1.50515	2.10721
	1	65	65	1		1.812913	1.812913
DGC/2013/J/134	36	5	180	0.027778	-1.5563	0.69897	2.255273
I. perisphinctoides	16	9	144	0.0625	-1.20412	0.954243	2.158362
	4	16	64	0.25	-0.60206	1.20412	1.80618
	1	36	36	1		1.556303	1.556303

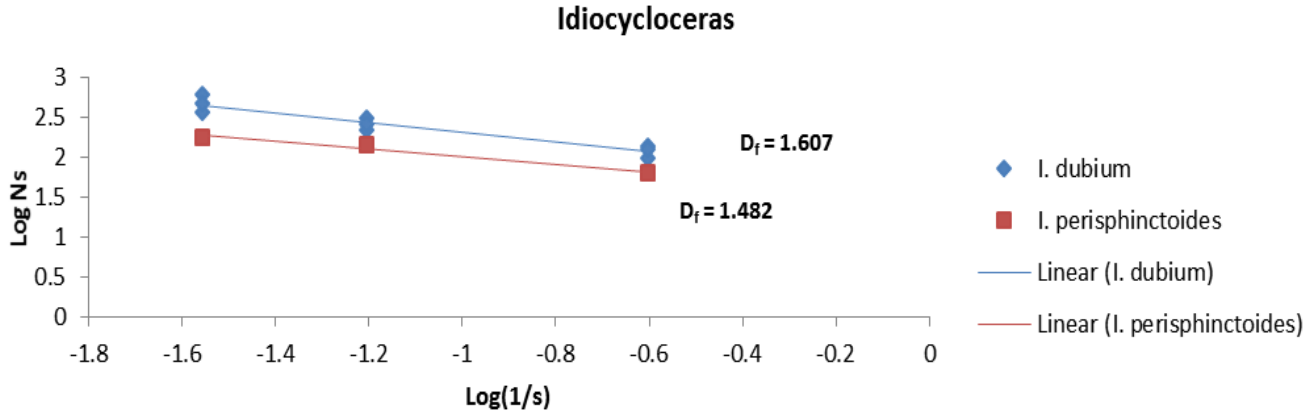

Fig. 9: Graph showing the variation in D_f values among *Idiocycloceras dubium* and *Idiocycloceras perisphinctoides* (Based on the data from Table 3).

Table 4: Table showing the number of boxes counted, according to ontogeny, covering the digitized forms of suture lines, their estimated perimeter lengths, and logarithmic values for *Nothocephalites paradoxus*. [s= Number of grid cells, N= Late growth stage, N1= Early Growth stage and N2= Middle Growth stage].

Specimen No. and species name	s	N	Ns	1/s	log (1/s)	log N	log Ns	N1	N2	N1Xs	N2Xs	log (N1s)	log (N2s)
DGC/2013/J/148	36	16	576	0.02778	-1.5563	1.20412	2.760422	2	3	72	108	1.857332	2.033424
N. paradoxus	16	30	480	0.0625	-1.20412	1.477121	2.681241	2	4	32	64	1.50515	1.80618
	4	52	208	0.25	-0.60206	1.716003	2.318063	7	7	28	28	1.447158	1.447158
	1	97	97	1		1.986772	1.986772	9	17	9	17	0.954243	1.230449

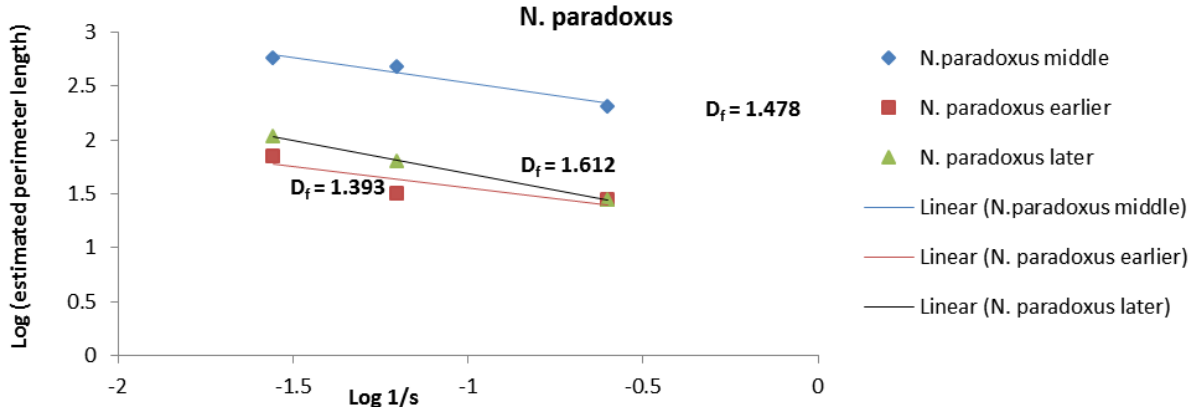

Fig. 10: Graph showing ontogenetic variation of D_f values in *Nothocephalites paradoxus* (Based on the data from Table 4).

6. Conclusion

Based on shell geometry, sculpture, and anticipated palaeoenvironments, fractal analysis of suture lines in Middle Jurassic ammonite groups reveals that sutural complexity was highly tied to shell traits and less so to fundamental ecology

According to some authors [29, 30], the sutural complexity is closely related to phragmocone's whorl height and degree of shell involution. In lieu of these observations presented by Pérez-Claros et al. [30], in the present study it has been observed that ammonite shells whose degree of involution is higher, has a greater D_f value than the ammonite shells with a lower degree of involution.

The present study also confirms that the complexity of suture lines is dependent on the shape of the whorl cross section i.e. highest values of D_f are seen in shells having a high oval to acute whorl cross section and the lowest values are attributed to shells with sub-circular whorl cross section. It has also been observed that shape of flanks is highly correlated with sutural complexity. Shells that are planulate have more complex sutures, hence higher D_f value, probably to accommodate a fleshy membranous bladder to become efficient in controlling the buoyancy. Moreover, the present study also unable to find any relationship between sutural complexity and bathymetry to combat shell implosion.

Acknowledgment

The author is thankful to the Principal, Durgapur Government College for providing infrastructural and laboratory support for the research work. The author also acknowledges financial support was provided by the DST-SERB project (CRG/2018/003717).

References

[1] F. Olóriz, P. Palmqvist and J.A. Pérez-Claros, "Shell features, main colonized environments, and fractal analysis of sutures in Late Jurassic ammonites," Lethaia, vol. 30, no. 3, pp. 191-204, 1997.

[2] F. Olóriz and P. Palmqvist, "Sutural complexity and bathymetry in ammonites: fact or artifact", Lethaia, vol. 28, no. 2, pp. 167-170-204, 1995.

[3] W.B. Saunders, "The ammonoid suture problem: relationships between shell and septum thickness and suture complexity in Paleozoic ammonoids", Palaeobiology, vol. 21, no. 3, pp. 343-355, 1995.

[4] P.D. Ward, "Function of cameral water in Nautilus", Paleobiology, vol.6, no. 2, pp. 168–172, 1980.

[5] S.K. Biswas, "Mesozoic Stratigraphy of Kutch, Gujarat", Quarterly Journal of Geology Mining Metallurgical Society of India, vol. 49, no. 3, pp. 1-52, 1977.

[6] S.K. Biswas, "Stratigraphy and sedimentary evolution of the Mesozoic Basin of Kutch, Western India", In: S.K. Tandon, Charu C. Pant and S.M. Casshyap (Eds.), Sedimentary Basins of India, Tectonic Context. Gyanodaya Prakashan, Nainital, pp.74-103, 1991.

[7] A.B. Wynne, "Memoir on the Geology of Kutch to accompany the map compiled by A.B. Wynne and F. Fedden during the sessions 1867-68 & 1868-69", Memoires of Geological Survey of India, vol. 9, no. 289, 1872.

[8] Rajnath, "A contribution to the statigraphy of Kutch", Quarterly Journal of Geology Mining Metallurgical Society of India, vol. 4, no. 4, pp. 161-174, 1932.

[9] K.C. Mitra, S. Bardhan and D.N. Bhattacharya, "A study of Mesozoic stratigraphy of Kutch, Gujarat with special reference to rock-stratigraphy and biostratigraphy of Keera dome", Bulletin of Indian Geological Association, vol. 12, no. 2, pp. 129-143, 1979.

[10] J. Krishna, "Current Status of Jurassic stratigraphy of Kachchh, Western India", In: International Symposium of Jurassic Stratigraphy (Eds. O. Michelsen and A. Zeiss), vol. 3, pp. 730-741, 1984.

[11] F.T. Fursich and W. Oschmann, "Shell beds as tools in basin analysis: The Jurassic of Kachchh, Western India", Journal of Geological Society of London, vol. 150, pp. 169-185, 1993.

[12] F.T. Fürsich, D.K. Pandey, W. Oschmann, A.K. Jaitly and I.B. Singh, "Ecology and adaptive strategies of corals in unfavourable environments: Examples from the Middle Jurassic of the Kachchh Basin, Western India", Neues Jahrbuch für Geologie und Paläontologie – Abhandlungen, vol. 194, no. 2-3, pp. 269-303, 1994.

[13] N.P. Singh, "Mesozoic Lithostratigraphy of the Jaisalmer Basin, Rajasthan", Journal of Palaeontological Society of India, vol. 51, no. 2, pp. 1-25, 2006.

[14] S.K. Das Gupta, "A revision of the Mesozoic-Tertiary stratigraphy of the Jaisalmer basin, Rajasthan", Indian Journal of Earth Sciences, vol. 2, no. 1, pp. 77-94, 1975.

[15] D.K. Pandey, D. Kashyap and S. Choudhary, "Microfacies and depositional environment of the Gharoi River section (upper Jaisalmer Formation), west of Baisakhi Village, Jaisalmer Basin, Rajasthan", Proceedings of the National Seminar on Oil, Gas & Lignite Scenario with Special Reference to Rajasthan, pp. 117-130, 2005.

[16] D.K. Pandey, J. Sha and S. Choudhary, "Depositional history of the early part of the Jurassic succession on the Rajasthan Shelf, western India", Progress in Natural Science (Special Issue of IGCP 506 on the Jurassic Boundary Events), vol. 16, pp. 176-185, 2006.

[17] D.K. Pandey, F.T. Fürsich, and M. Alberti, "Stratigraphy and palaeoenvironments of the Jurassic Rocks of the Jaisalmer Basin Field Guide", Beringeria, Special Issue, vol. 9, pp. 1-111, 2014.

[18] D.K. Pandey, F.T. Fürsich and J. Sha, "Interbasinal marker intervals – A case study from the Jurassic basins of Kachchh and Jaisalmer, western India", Science China, Series D Earth Sciences, vol. 52, pp. 1924-1931, 2009.

[19] H.S. Pareek, "Pre-Quaternary geology and mineral resources of northwestern Rajasthan", Geological Survey of India, Memoirs, vol. 115, pp. 1-99, 1984.

[20] R.P. Kachhara and R.L. Jodhawat, "On the age of Jaisalmer Formation, Rajasthan, India", Proceedings of IX Indian Colloquium on Micropalaeontology and Stratigraphy, pp. 235-247, 1981.

[21] D.K. Pandey, J. Sha, and S. Choudhary, "Sedimentary cycles in the Callovian–Oxfordian of the Jaisalmer Basin, Rajasthan, western India", Volumina Jurassica, vol. 8, pp. 131-162, 2010.

[22] B.B. Mandelbrot, "The fractal geometry of nature", W. H. Freeman, New York, 1983.

[23] G. Sugihara and R.M. May, "Nonlinear forecasting as a way of distinguishing chaos from measurement error in time series", Nature, vol. 344, no. 6268, pp. 734-741. doi: 10.1038/344734a0

[24] G.E. Boyajian and T. Lutz, "Evolution of biological complexity and its relation to taxonomic longevity in the Ammonoidea", Geology, vol. 20, pp. 983–986, 1992.

[25] T.M. Lutz, and G. E. Boyajian, "Fractal geometry of ammonoid sutures: Paleobiology", vol. 21, no. 3, pp. 329–342, 1995.

[26] A.G. Checa and J. M. Garcia-Ruiz, "Morphogenesis of the septum in ammonoids,", In: Ammonoid paleobiology (Eds. N. H. Landman, K. Tanabe and R. A. Davis), pp. 253–296, New York: Prenum, 1996.

[27] J.M. García-Ruíz, A. Checa and P. Rivas, "On the origin of ammonoid sutures", Paleobiology, vol. 16, no. 3, pp. 349–354, 1990.

[28] J.M. García-Ruiz and A.G. Checa, "A model for the morphogenesis of ammonoid septal sutures", Geobios, vol. 26, no. 1, pp. 157-162, 1993.

[29] W.B. Saunders and D.M. Work, "Shell morphology and suture complexity in Upper Carboniferous ammonoids", Paleobiology, vol. 22, no. 2, pp. 189–218, 1996.

[30] J.A. Pérez-Claros, F. Olóriz and P. Palmqvist, "Sutural complexity in Late Jurassic ammonites and its relationship with phragmocone size and shape: a multidimensional approach using fractal analysis", Lethaia, vol. 40, no. 3, pp. 253-272, 2007.

The Nucleus ***60****, No. 2 (2023) 145-152*

www.thenucleuspak.org.pk

The Nucleus
ISSN 0029-5698 (Print)
ISSN 2306-6539 (Online)

A Comparison of Address Matching Techniques to Improve Geocoding: A Case Study of Islamabad, Pakistan

Abdul Basit Bashir, Muhammad Farooq Iqbal*

Applied Geo-Informatics Research Lab, Department of Meteorology, COMSATS University Islamabad (CUI), Park Road, Chak Shahzad, Islamabad 45550, Pakistan

ABSTRACT

Geocoding is the process of converting addresses into spatial coordinates. It has become a need for the modern world in many fields such as strategy making, disaster management, location-based analysis, and planning of infrastructure, etc. Address matching is of critical importance in geocoding and is dependent on the language, address format, and components of the addresses. Different algorithms, tools, and applications have been designed for improving address matching. The goal of the research was to standardize geocode addresses using different Natural Language Processing (NPL) models. To standardize and geocode distinct types of addresses, Islamabad was chosen as the study area because it incorporates standard and unusual addresses. Address datasets were obtained from telecommunication industries operating in the study area. In this research, two NLP models including DeepParse (DP) and SpaCy's Named Entity Recognition (NER) were utilized and trained for address standardization. Each of the models operates using different techniques for parsing the addresses. The SpaCy model performed well with an accuracy of over 80% in all types of addresses. The DP model only outperformed the SpaCy model in urban areas with an accuracy of 95%, the others were less than 80%. This study focused on what types of addresses must be used to improve geocoding. Methods discussed in this study would be helpful in achieving a higher success rate for improving address matching percentage in the geocoding process. This research will help in choosing the best technique to improve address matching of addresses in Pakistan.

Keywords: *Geocoding, Address standardization, Address matching, Natural Language Processing, DeepParse, SpaCy, Named Entity Recognition*

1. Introduction

In this era of digitalization, development, and extensive applications of Geographic Information System (GIS), geocoding plays a significant role in filling the gap between non-spatial and spatial data [1]. Geocoding is the process of converting addresses into spatial coordinates. It has become a need for the modern world in many fields such as strategy making, disaster management, location-based analysis, and planning of infrastructure, etc., to be mentioned [2]. Address matching is of critical importance in geocoding, because of which geocoding is quite difficult in many rural or poorly mapped areas. Different algorithms, tools, and applications have been designed for improving address-matching percentages. Address matching is dependent on the language, address format, and the components of the address [3].

An address contains information about a specific place on a map. This information includes name, street, city, and province. Despite having address components, there is still a lack in positional accuracy of addresses. To improve this accuracy, geocoding comes in where addresses are assigned geographical coordinates i.e., latitude and longitude values [1]. Researchers use geocoding in various fields such as environmental variables leading to diseases [4], error corrections for InSAR point cloud [5], crime mapping [6], public safety, route directions [7], the relationship between household environment and health consequences [8], environmental epidemiology [9], locating traffic crashes [10] and the need of predictive policing [11]. Researchers used census data to geocode households and individual's addresses [12]. The addresses are collected on a daily, monthly and annual basis by many organizations such as educational institutions, health departments, police stations, courts etc. Many applications have been developed to geocode addresses, and much literature has been written on how to improve the match rates, and which technique should be used for improved accuracy at the local or national level [2].

Multiple models and algorithms have been designed for reducing spelling errors and improving the accuracy of geocoding of the street-level addresses. Levensthein et al introduced a method efficient enough to correct, delete, insert, and reverse each string to convert one string to another [13]. Perez-Diez et al used SpaCy's NER in the identification of medical texts written in Spanish from radiology reports and achieved a precision score of 99.87%, recall score of 99.28%, and F1 score of 99.58% [14]. In another study, the same model was used to identify names of the places from historical masses [15]. Another method introduced by Western Airlines in 1977 was a match rating computer approach focused on comparing and indexing homonymous words [16]. Repeat and near repeat analyses help in learning the sensitivity of repetition to geocoding [17]. Zandbergen et al [18] compared three data models including street network, parcel boundaries and address/point and it was suggested that address point data model is more effective for positional accuracy and reaching maximum match rate. Spatial point pattern test developed by Andersen can help to find similarities and differences in one or more spatial point patterns [19]. Geocoding was also used to solve classification difficulties, for this LGGeoCoder; a deep learning neural network was developed [3]. A study conducted by Abid et al [20] trained the deep learning model using optical character recognition (OCR) that takes input in an image form and returned the classified address, BLSTM layer was also used to improve the results. Study assessed the model on addresses of the United States of America, where

*Corresponding author:farooqbuzdar@gmail.com

usually addresses are not complex and 90.44% accuracy was achieved.

A lot of work on improving geocoding address matching has been done. In India, due to invalid address formats, learning algorithms were designed to understand and solve errors in addresses [21]. To deal with many unstructured address data, a deep learning-based address matching method was introduced which helped to identify semantic similarities between address records [22]. China faces the same issue regarding addresses, the major issue is the language barrier. Since the Chinese language has no delimiters among words, an optimized Chinese address-matching method was built to improve geocoding, address standardization, address modeling, and matching [2]. Dilek et.al. [23] designed a processing system through which communication with the device was made easier. To improve geocoding accuracy and address matching in Turkey, Matchi et al. [24] used two NLP techniques, i.e., Levenshtein distance algorithm (LDA) and match rating approach to standardize non-standard Turkish addresses, and concluded that geocoding can be used to track crime, monitoring of epidemics. Another method to update older tree inventories with coordinates by means of street-level panorama images and a global optimization framework for tree occurrence matching, geolocations of tree inventories were obtained using street addresses and a global positioning system (GPS) [25]. A study was conducted on spatial mobility patterns of victims and child abuse offenders under the crime mobility triangle methodology which is useful for criminal investigation in France [26].

Pakistan is the country where addresses are written in Roman Urdu and it is the first and foremost problem in address matching, as computers can neither read nor write Roman alphabet. Other problems include spelling mistakes, missing address components, and abbreviations. Addresses vary from simple to complex, there are developed cities that have standard addresses and cities with incomplete addresses. These issues lead to inaccurate geocoding and less match ratio. Thus, to improve the match ratio, addresses need to be standardized.

The core objective of this study is to improve geocoding by standardizing addresses using Natural Language Processing (NLP) techniques. The second objective is to develop an address parsing model that helps communicate with the computer in natural language. Lastly, to compare geocoded addresses using the address parsing models.

2. Data and Methodology

2.1 Study Area

Islamabad, the capital of Pakistan lies at 33.68°N and 73.04°E, at an elevation of 1475 meters with moderate climate [27]. The total area of the capital city is 906 km² and is divided into five zones including commercial, residential, and diplomatic areas. Out of these five zones, only zone-I and zone-II were developed following the master plan. Zone-I and zone-II are assigned for urban areas whereas the rest of the zones are assigned for rural areas. Urban zones are further divided into sectors and each sector comprises 2 km² with a central shopping mall [28]. Fig. 1 shows the study area map with zones and elevation.

2.2 Datasets

Address data used in this study was obtained from Pakistan telecommunication company limited (PTCL) because it operates both in rural and urban areas. PTCL provided data in comma-delimited format (.csv). After making sure that file contained only addresses of the study area, the address data was then divided into six categories including residential, urban, commercial, banks, rural, and schools. To train machine learning (ML) models specifically, DeepParse (DP) and SpaCy, another dataset was extracted via Google scrapping methods containing a total number of 349,637. Distinct types of addresses were then parsed through these trained models. To assess the accuracy of the trained models, ground data was collected using GPS by doing a ground survey of the addresses collected from PTCL. Random GPS points of the 100 addresses were taken to validate the results obtained from the models.

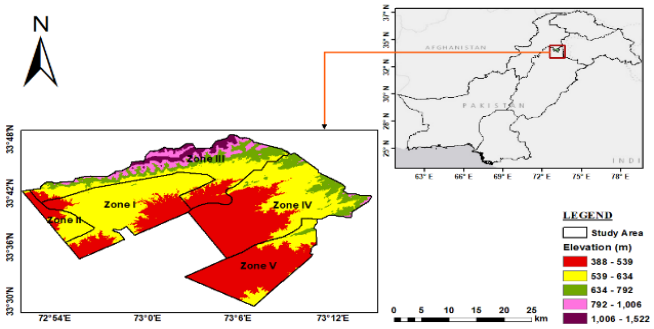

Fig. 1: Study area map of Islamabad showing zones along with the elevation in meters.

2.3 Methodology

2.3.1 Data Preparation

The ML models are typically predictive in nature and thus require preprocessed data to perform proficiently. The acquired dataset contains a lot of ambiguous data which decreases the model's accuracy and does not allow it to train the model. Therefore, data must be passed through the cleaning phase, where white spaces, illegal characters, duplicates, and repetitions of words in addresses, commas, and periods were all removed. After cleaning the data, it was prepared to make the model's prediction better. In this process, labels were assigned to each component of the address to make the model's prediction accurate.

2.3.2 Address Standardization Using Natural Language Processing Techniques

The NLP removes the communication barrier between computer and human language using artificial intelligence (AI) techniques [24]. The NLP-based techniques identified spelling errors and multiple spellings of any word in any component of an address. A dictionary was created in which all the possible spellings and the correct spelling of words were listed and programmed in such a way that it displayed

the correct addresses database and generator. Parser read dictionaries and broke the address into different bits. Analyzer read all the bits of the addresses, checked, and corrected errors using named entity recognition (NER) and DP model. These models checked for names, street numbers, and city names to produce accurate spellings for each address fragment. Output of an address, major components of NLP were the dictionary, parser, and semantic analyzer. Fig 2 demonstrates the methodology for the research.

2.3.2.1 SpaCy's Named Entity Recognition Model

The NER is one of the NLP methods to extract information from a text. The NER model for this study was trained using SpaCy which is an open-source NLP library that uses neural network or deep learning formulas to employ NLP models for embedding, encoding, attending, and predicting components in tasks such as parts of speech tagging, NER, and parsing etc. For this study, the model was trained in four steps (i) embedding, (ii) encoding, (iii) attention, and (iv) prediction.

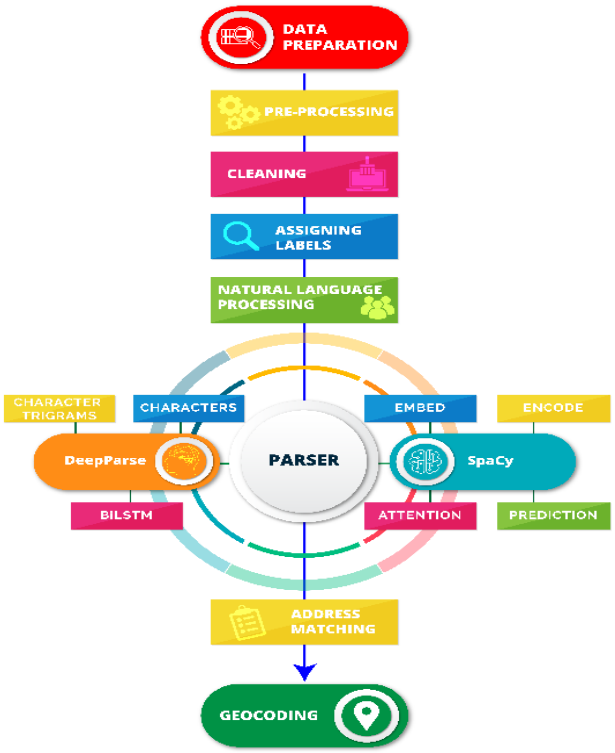

Fig. 2: Methodology of how the addresses were first standardized using NLP method.

The embedding stage of SpaCy uses prefixes, suffixes, shapes, and upper/lower case words to extract hashed values that reflect the similarity of words. In the encoding stage, hashed values passed through a convolutional neural network (CNN) so that values get fused with their framework. The result of the encoding stage to represent information is in the form of a matrix of vectors. Before the prediction of a tag, the matrix must pass through the attention layer of the CNN, this sums up the input and passes it onto the prediction stage. At the prediction stage, an entity ruler (ER) function was used to predict the tag for the available entity. The ER function has a variety of rules or patterns to allow the SpaCy model to predict and place each entity in the correct location. Since, ER function reads patterns of the words, and in the current study, addresses have unique patterns which the model can't predict or read. For the model to predict a tag for any entity in the given address, a new rule was designed to define the pattern of sectors, cities, and countries. This is how ER function was pre-trained before it could predict the location of any entity.

Table: 1 Multiple spelling of the same word to help the model read the patterns.

Tag	Check 1	Check 2	Check 3	Check 4
Islamabad	Isl	Isb	Isld	Islamabad
Pakistan	Pk	Pak	Pakistan	-
Sector	I8/1	G9/2	E8/3	F6/4

Table 1 shows every possible spelling of the city, country, and sector's patterns. Multiple spellings of the same word were first identified in the data, which was fed to ER to predict the right tag for every component of the address. Every sector and its sub-sectors were identified and passed to the ruler. This is how the model was trained.

For the model's evaluation precision, recall, and F_1 scores were calculated using Eq. (1) to (3).

$$P = \frac{C}{M} \tag{1}$$

$$R = \frac{C}{N} \tag{2}$$

$$F_1 = \frac{2PR}{P+R} \tag{3}$$

Where P is the precision, R is recall, C is the number of corrected entities, M is the number of matched entities with the reference data and N is the total number of predicted entities.

2.3.2.2 DeepParse Model

The DP model is a trainable postal address parser to parse global street addresses based on Recurrent Neural Network (RNN) architecture that uses Long-Short Term Memory (LSTM) Bi-directional Long-Short Term Memory (BLSTM) to parse non-standardized addresses [20]. Since postal addresses are memory dependent and cope with sequential issues.

Hochreiter et al [29] introduced LSTMs to cater to information that must be remembered throughout the model training process. The DP model works in three steps including (i) characters, (ii) character trigrams, and (iii) words. It takes the address as input and divides each word into a list of words. After making a list of words, each word was then divided into an alphabet/character and then trigrams were made. These trigrams were then embedded to convert into vectors to make these words pass through RNN layers that put and classify the words to their respective attribute.

Fig. 3 shows the workflow of the DP model. The DP model takes input in three formats including words, characters, and character trigrams. These inputs were used to generate vector representation and pass through the

embedding stage. After getting the vectors of each word, these were then passed on to BLST layer individually and studied their picture. The dropout layer of BLSTM was then applied to each word and it ignores irrelevant information, thus producing only valuable information. The projection layer of BLSTM makes the output data appropriate according to the dimensions, by taking the output of BLSTM and the dropout layer, linking them, and making the data ready for another layer i.e., the learning layer. The learning layer concatenates the projected layer's output and embedded words. It works on the classification by studying the features at the word level making the model learn patterns effectively and classifies it accordingly [22]. To train the model fasttext (FT) library of words for text learning and classification was used. The FT helps in processing the words before any parsing model starts working. The FT is a quick and efficient method that learns and represents words in vector form and classifies it [30]. The FT instead of learning the representation of words, it focuses on the core structure of words. This is important in the interpretation of different morphological forms of words separately [31].

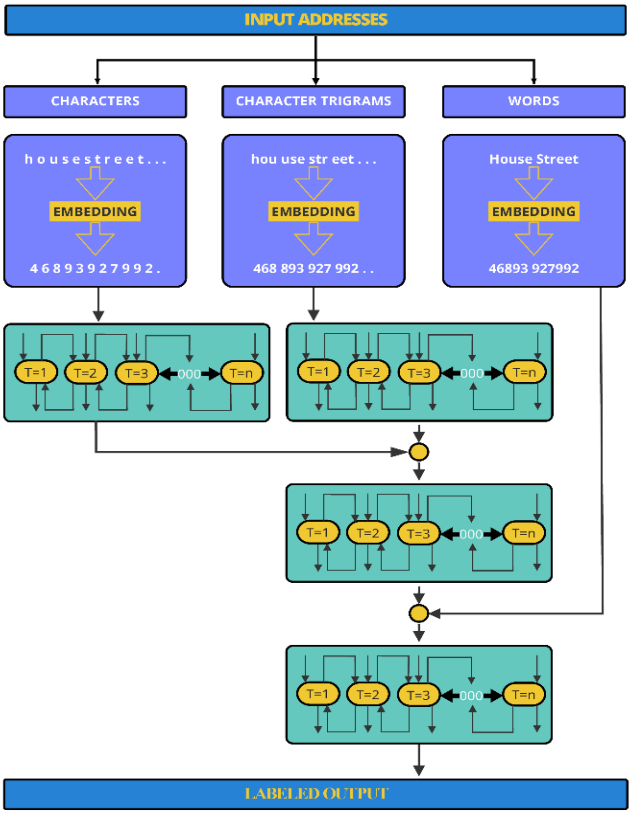

Fig. 3: The workflow of the DP model including the embedding of characters, characters trigrams, and words-for-word predictions.

This model was trained on 26,000 textual addresses of Islamabad. These addresses were divided into two parts, 80% of the addresses were used to train the model whereas the remaining 20% was used for testing the model. After completing all the pre-processing steps, the model training started by setting epoch to 5, batch size to 8, and learning rate to 0.01. A learning rate scheduler was also implemented to reduce the learning rate per epoch, this prevented the model from overtraining or overfitting. After training DP model, its FT function was again retrained for the model's fine-tuning and another addition of an attention layer that pays close attention to every single address before delivering the output. This is how the model was trained.

Lastly, to predict the model's results, a CSV file in which preprocessed, cleaned, and labeled addresses of urban, rural, residential, and commercial, banks and schools were imported. Moreover, pandas, urlopen, and json libraries were imported. A loop from 0 to the end of the column was defined, where each address in the files was passed to the model and returned the formatted or parsed address.

The matched and unmatched addresses were checked by passing both original and parsed addresses using Google API. This was done by comparing the latitude of the original address with the latitude of the parsed address, and their match score was achieved. These parsed addresses were then passed on to the Google API that returned the latitude and longitude of the addresses and were geocoded.

2.3.3 Statistical Analysis

2.3.3.1 Spatial Point Pattern Test

A spatial point pattern test developed by [32] was used to identify the similarities and differences among points. The test's initial use involved a comparison of the spatial patterns of various crime types. Their values ranged between 0 and 1. Where 0 represents no similarity and 1 represents ideal similarity. This test was applied in numerous situations. The test was also applied to the following research topics: altering international trade patterns [33] and crime's spatial seasonality [34].

Using the results of the above-mentioned statistical tests, a similarity index between the results of the three datasets was computed. The similarity index, S was used to assess how similar the two datasets are to one another. The value ranged between 0 and 1, where 0 represents no similarity, while 1 is the perfect similarity. Since the values were too small to find the similarities and differences, tolerance was also set to 0.003m. A similarity index was calculated using Eq. (4).

$$S = \frac{\sum_{i=1}^{n} Si}{n} \quad (4)$$

Where, S is the similarity index and S_i is 1, if the point pattern of two datasets is the same and n is the number of points taken.

2.3.3.2 Mean Absolute Error and Root Mean Square Error Metrics

The mean absolute error (MAE) and root mean square error (RMSE) statistical metrics are employed frequently in model evaluation studies. To calculate RMSE, the distance between the points i.e., from ground points to SpaCy's and from ground points to DP were calculated using Eq. (5). Once distance was computed, it was used to calculate MAE and RMSE of both the datasets i.e., SpaCy and DP, considering

ground data to be accurate. Eq. (6) and (7) were used to calculate MAE and RMSE respectively.

$$\boldsymbol{d}\,(\boldsymbol{g},\boldsymbol{m}) = \sqrt{\sum_{i=1}^{n}(\boldsymbol{g_i} - \boldsymbol{m_i})^2} \quad (5)$$

Where *d* is the distance, *g*, and *m* are the points, g_i, and m_i are Euclidean vectors in space, and *n* is space.

$$\boldsymbol{MAE} = \sum_{n=1}^{i}|\boldsymbol{g} - \boldsymbol{m}| \quad (6)$$

$$\boldsymbol{RMSE} = \sqrt{\frac{1}{n}\sum_{n=1}^{n}(\boldsymbol{g} - \boldsymbol{m})^2} \quad (7)$$

Where *n* is the total number of observations *g* is the ground data and *m* is the data obtained from models.

3. Results

3.1 Address Standardization Using NLP

3.1.1 DeepParse Model

Fig. 4a shows the geocoding results of the addresses parsed by DP model. The DP model performed well in urban areas of Islamabad with a 95% accuracy rate. A total of 80 addresses were parsed and geocoded out of which only 4 were not matched, the remaining 76 were perfectly matched and geocoded. Rural areas of Islamabad in Zone-III have complex addresses with missing components and addresses were written in Roman which couldn't be parsed well. Out of 95 addresses for rural 48 were parsed and matched whereas 47 addresses remained unmatched. This mismatch affected geocoding accuracy which dropped to 50.53%. Because of address components such as flat/apartment number, floor number, and house names instead of house numbers in the address data for residential areas, such addresses couldn't be parsed correctly and didn't find any matching address in the Google geocoding API.

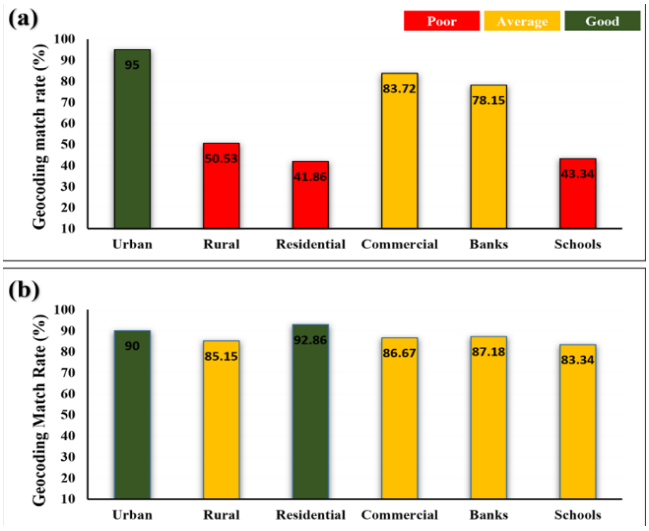

Fig. 4 (a) Number of geocoded addresses in percentage with Google API by using standardized addresses of DeepParse model and (b) displays number of geocoded addresses in percentage Google API by using standardized addresses of SpaCy model.

A total of 43 residential addresses were parsed by DP model where 18 addresses were matched, and 25 addresses were unmatched with an accuracy of 41.86% geocoding. Commercial areas usually have simple addresses and are easy to match and geocode, but this accuracy drops in some cases where addresses include shop number, floor number, or a building/plaza number. Such information couldn't be parsed and geocoded well. However, geocoding results for the commercial areas of Islamabad were 83.72%. For commercial addresses out of 43 addresses, 36 were matched and 7 were unmatched.

Banks are located in both urban and rural areas. Addresses are easy to parse in urban areas but in some cases plots, shops, or building numbers have affected the results whereas, in rural areas, khasra numbers in the addresses were hard to parse by the model. A total of 41 bank addresses were parsed, out of which 32 addresses matched and 9 addresses were unmatched. The total geocoding accuracy for the banks was 78.15%. For schools, a total of 30 addresses were parsed out of which only 13 were matched and 17 were unmatched, making geocoding accuracy of 43.34%. This is because schools don't have proper addresses, they are usually searched by their name, and one school may have multiple branches and all branches can't have the same latitude and longitude values, hence reducing geocoding results. Fig. 5a shows the comparison for matched and unmatched addresses of all types of addresses using DP model.

3.1.2 SpaCy's Named Entity Recognition Model

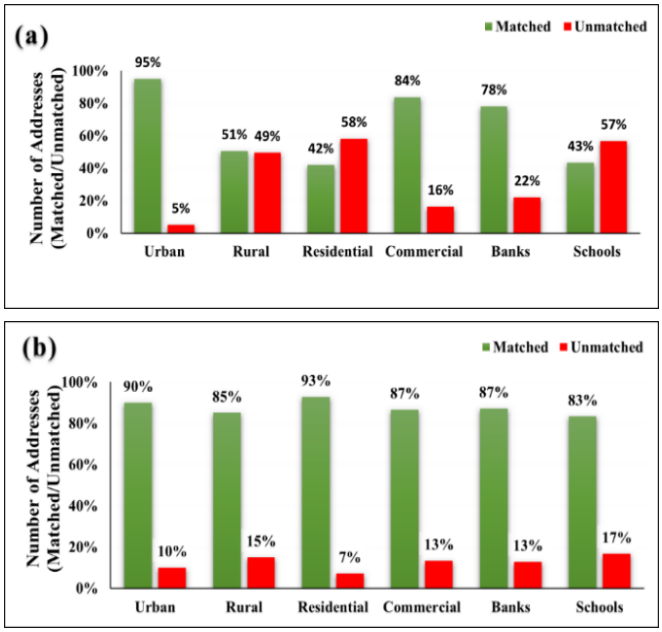

Fig. 5 (a) Comparison of matched and unmatched addresses with Google Geocoding API using DeepParse model and (b) Comparison of matched and unmatched addresses with Google Geocoding API using SpaCy model.

Fig. 4b shows the geocoding results for SpaCy's NER model that were performed in all types of addresses including urban, rural, residential, commercial, banks and schools. A total of 80 urban addresses were parsed out of which 72 were correctly parsed and matched whereas the remaining 8 addresses didn't parse and remained unmatched with an accuracy of 90% geocoded addresses. Out of 87 addresses of

rural areas of Islamabad, 74 addresses were parsed and matched with an accuracy of 85.15% geocoded, while 13 didn't parse and remained unmatched. A total of 42 addresses for residential areas were parsed, of which 39 were parsed and matched, whereas 3 didn't parse and matched, thus making geocoding accuracy of 92.86%. Geocoding accuracy for commercial addresses was 86.67% where 39 addresses out of 45 were perfectly matched. Around 87.18% and 83.34% of addresses were parsed, matched, and geocoded for banks and schools, respectively. Fig. 5b shows the comparison of matched and unmatched addresses of urban, rural, residential, commercial, banks, and schools using the SpaCy model.

3.2 Statistical Analysis

3.2.1 Spatial Point Pattern Test

The comparison of both the DP and SpaCy models showed that the SpaCy model performed better in all types of addresses with an accuracy of more than 80%, while DP model showed variations depending on the region or type of addresses. Fig. 6 shows the statistical comparison of both models. In urban areas, the DP model gave an accuracy of 95% while the SpaCy model had an accuracy of 90%. In rural areas, SpaCy model outperformed DP model with an accuracy of 85.15%, whereas DP model could only achieve 50.53%. In residential areas, an accuracy of 41.86% and 92.86% were achieved by DP and SpaCy models respectively. Both models performed well in commercial areas with a difference of 2.95%. The DP model observed 83.72% accuracy whereas the SpaCy model observed 86.67% accuracy. Around 78.14% and 87.18% accuracies were achieved by DP and SpaCy models respectively for the addresses of banks. The SpaCy model hit an accuracy of 83.34% for school addresses, whereas the DP model resulted in an accuracy of 43.34%.

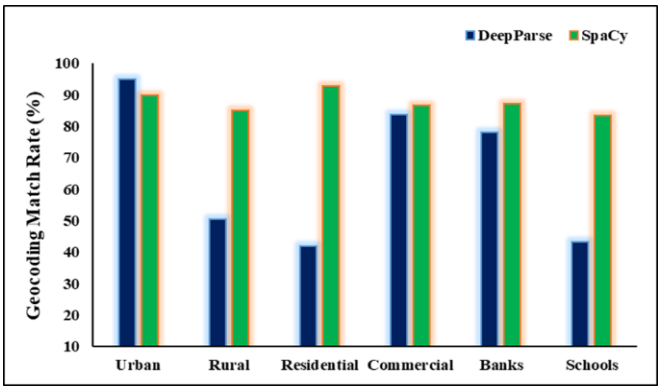

Fig. 6: Comparison of geocoded results achieved by using DeepParse and SpaCy models.

3.2.2 MAE and RMSE Metrices

The MAE of the SpaCy model was 0.10 m whereas 0.12 m was observed for the DP model. The RMSE for the SpaCy model was 0.26 m whereas for DP model it was 0.32 m. The MAE and RMSE of both the models show that the SpaCy model turned out to be more accurate as it had less MAE and RMSE, when addresses were compared with the ground data. Table 2 shows the distance between the GPS ground points and the points obtained from DP and SpaCy models. Fig. 7a illustrates the classified distance between the DP model's geocoded points and GPS points while 7b illustrates the classified distance between the SpaCy model's geocoded points and GPS points.

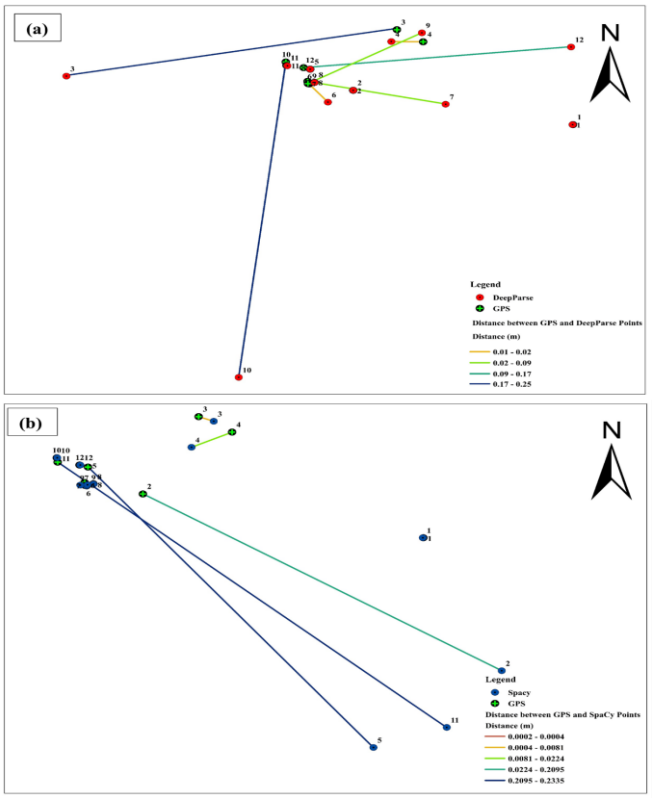

Fig. 7: (a) Classifications of distance (m) between GPS and DP model points, and (b) classifications of distance (m) between GPS and SpaCy model points.

4. Discussions

Two address parsers including DP and SpaCy models were trained to read, parse, and geocode addresses. In the current study, DP model was trained using the FT function of BLSTM on different types of addresses in Islamabad with addresses from simple to complex. The overall accuracy calculated was 65.43%. This is mainly due to the complex nature of addresses, as these are written in Roman, and in some areas, these don't have complete address components, thus making it difficult to be parsed by the parser. The model is best performed in urban areas with 95% accuracy rate as these follow a standard address pattern.

The second model used in this research was SpaCy's NER, and it turned out to be a good parser because of its ability to understand and learn the patterns. This was trained on 26,000 Islamabad addresses to calculate the precision, recall, and F1 score. Results obtained by NER were totally dependent on the training data, it can't check the sequence of the words like DP, and it depends on the patterns provided for the training. NER techniques were applied to our dataset and a precision score of 93.90%, recall score of 92.86%, and F1 score of 93% was achieved.

The results obtained from the models helped in standardizing the address to be geocoded more accurately.

These results can help the courier services to find the address efficiently and fast, it can also help the food delivery services to reach the exact location instead of asking customers for the exact location.

Future researchers can use these techniques to study the addresses and geocode them in their own areas of interest. Geocoding can be performed to study the crime rate in any area or to control traffic accidents at any spot. Every city has different checks in their addresses, we could only address some of the checks in Islamabad, and these models can be trained by using addresses throughout Pakistan.

5. Conclusions

In this study, two address parsing models were utilized and trained to improve geocoding results in the capital city of Islamabad. The DP and SpaCy's NER models were used to parse addresses, their accuracy was accessed, and their results were compared. The DP model which is an international address parser could only perform well in urban areas with 95% accuracy rate. Whereas, SpaCy model outperformed in all types of addresses with an overall accuracy of 80% from assessing simple to complex addresses. The address data is written in both English and Roman, so it is quite difficult for the computer to read and parse the addresses.

For accurate address matching and geocoding, all the addresses were standardized using NLP techniques. The NLP methods identified and removed duplicate words, spelling errors, abbreviations, and ambiguous data. The techniques used in this study also removed the communication barrier between human and computer language, thus making address standardization easy. Two NLP models including DP and SpaCy's NER were picked and trained for address geocoding. Each of the models operates using different techniques for parsing the addresses. The DP model uses ML approaches that include bidirectional long short-term memory. This method memorizes the training data and presents results based on the training data provided. Whereas SpaCy model reads the patterns of the words, embeds, encodes and passes these addresses through the attention layer of the convolution neural network layer and then predicts the output. The results of both models were then compared. Both models performed well in urban areas with an accuracy of over 90% each. This was achieved because urban areas in the capital city are planned and follow standard address patterns. The SpaCy model outperformed DP model in rural, residential, commercial, bank and school address data. Because of its ability to read the patterns, it could easily read and predict the address word by word. It was trained in patterns, this is why it could easily read house, street, sector, and city information, even if these addresses were abbreviated.

In conclusion, SpaCy can be an efficient and effective solution for addressing standardization because of its ability to read patterns using NLP techniques. SpaCy's model efficiency and performance have been demonstrated in this study, thus making it a valued model to manage large datasets.

Acknowledgment

The authors would like to express their sincere gratitude to Pakistan Telecommunication Company Limited for giving the address data. Their cooperation in sharing this dataset has greatly helped the success of the study, and genuinely appreciate their support.

Table 2: The distance between the ground points acquired using GPS and the points obtained from DP and SpaCy models.

SpaCy			GPS		DeepParse		
Latitude	Longitude	Dist (m)	Latitude	Longitude	Latitude	Longitude	Dist (m)
33.657	73.157	0.0002	33.111	73.157	33.652	73.157	0.0184
33.570	73.196	0.0004	33.679	73.016	33.679	73.016	0.0203
33.722	73.052	0.0081	33.725	73.044	33.689	72.832	0.2146
33.714	73.040	0.0225	33.716	73.061	33.716	73.040	0.1721
33.525	73.132	0.2095	33.695	72.988	33.695	72.988	0.0904
33.683	72.988	0.2224	33.683	72.988	33.669	73.000	0.0830
33.684	72.985	0.2345	33.685	72.987	33.668	73.075	0.2461
MAE	0.10					0.12	
RMSE	0.26					0.32	

References

[1] F. Melo and B. Martins, "Automated geocoding of textual documents: A survey of current approaches," Transactions in GIS, vol. 27, no. 2, pp. 3-38, 2017.

[2] Q. Tian, F. Ren, T. Hu, J. Liu, R. Li, and Q. Du, "Using an optimized Chinese address matching method to develop a geocoding service: A case study of Shenzhen, China," ISPRS International Journal of Geo-Information, vol. 5, no. 11, pp. 650-667, 2016.

[3] Z. Yan, C. Yang, L. Hu, J. Zhao, L. Jiang, and J. Gong, "The integration of linguistic and geospatial features using global context embedding for automated text geocoding," International Journal of Geo-Information, vol. 10, no. 9, pp. 572, 2021.

[4] S. E. K. M. Rompa et al., "An approach to the asthma-protective farm effect by geocoding: good farms and better farms," Pediatric Allergy Immunol, vol. 29, no. 3, pp. 275-282, 2018.

[5] S. Montazeri, F. R. Gonzalez, and X. X. Zhu, "Geocoding error correction for InSAR point clouds," Remote Sensing, vol. 10, no. 10, pp. 1523, 2018.

[6] C. White and D. Weisburd, "A co-responder model for policing mental health problems at crime hot spots: Findings from a pilot project," Policing: A Journal of Policy and Practice, vol. 12, no. 2, pp. 194-209, 2018.

[7] K. J. Sydow, S. Stobernack, and S. Wienecke, "Accuracy of address geocoding with GIS: A data analysis of households in a German City," Transactions in GIS, vol. 12, no. 3, pp. 333-354, 2008.

[8] B. Wilson, N. Wilson, and S. Martin, "Using GIS to advance social economics research: geocoding, aggregation, and spatial thinking," Forum for Social Economics, vol. 50, no. 4, pp. 480-504, 2021.

[9] E. J. Kinnee, S. Tripathy, L. Schinasi, J. L. C. Shmool, P. E. Sheffield, F. Hpuguin, and J. E. Clougherty, "Geocoding error, implications for exposure assessment and environmental epidemiology," International Journal of Environmental Research and Public Health, vol. 17, no. 16, pp. 5845, 2020.

[10] X. Qin, S. Parker, Y. Liu, J. A. Graettinger, and S. Forde, "Intelligent geocoding system to locate traffic crashes," Accident Analysis and Prevention, vol. 50, pp. 1034-1041, 2012.

[11] J. M. Caplan, L. W. Kennedy, E. L. Piza, and J. D. Barnum, "Using vulnerability and exposure to improve robbery prediction and target area selection," Applied Spatial Analysis and Policy, vol. 12, no. 1, pp. 113-136, 2019.

[12] N.S. Walford, "Bringing historical British population census records into the 21st century: A method for geocoding households and individuals at their early-20th century addresses," Population Space and Place, doi: 10.1002/psp.2227.

[13] V. I. Levenshtein, "Binary codes capable of correcting deletions, insertions, and reversals," Soviet Physics – Doklady, vol. 10, pp. 707–710, 1965.

[14] D. Perez-Diez, D. Rodriguez, V. Blanco-Valero, A. Caceres, and G. Castellanos-Dominguez, "Identification of medical texts written in Spanish from radiology report using SpaCy'NER," Journal of Biomedical Informatics, vol. 113, pp. 103647, 2021.

[15] J. Won, J. Seo, J. Lee, and Y. Choi, "Named entity recognition of historical places in Korean Buddhist scriptures," Digital Scholarship in the Humanities, vol. 33, no. 2, pp. 401-412.

[16] G. B. Moore, "Accessing individual records from personal data files using nonunique identifiers. Final report. Computer science & technology series," 1977.

[17] C.P. Haberman, D. Hatten, J.G. Carter, and E.L. Pizza, "The sensitivity of repeat and near repeat analysis to geocoding algorithms," Journal of Criminal Justice, vol. 71, pp. 101721, 2021.

[18] P.A. Zandbergen, "A comparison of address point, parcel and street geocoding techniques," Computers, Environment and Urban Systems, vol. 32, pp. 214-232, 2007.

[19] M. Andresen, T. W. Jørgensen, and P. J. Diggle, "Spatial point pattern analysis of crime incidents: An overview and some open research problems," Statistical Science, vol. 35, no. 2, pp. 283-298, 2020.

[20] N. Abid, A. Hasan, and F. Shafait, "DeepParse: A trainable postal address parser," in Digital Image Computing: Techniques and Applications, pp. 1–8, 2018.

[21] V. Srivastava, P. Tejaswin, L. Dhakad, M. Kumar, and A. Dani, "A geocoding framework powered by delivery data," in Proceedings of the 28th ACM SIGSPATIAL International Conference on Advances in Geographic Information Systems, 2020, pp. 1-4, doi: 10.1145/3397536.3422254.

[22] Y. Lin, M. Kang, Y. Wu, Q. Du, and T. Liu, "A deep learning architecture for semantic address matching," International Journal of Geographical Information Science, vol. 34, no. 3, pp. 559-576, 2020.

[23] A. E. Dilek, C. Yan, H. Jin and M. Bektasoglu, "An optimized Chinese address matching method based on address standardization, modeling and matching," Journal of Cleaner Production, vol. 171, pp. 1213–1223, 2018.

[24] D.K. Matchi and U. Avdan "Address standardization using the natural language process for improving geocoding results" Computers, Environment and Urban Systems vol.70, pp. 1–8, 2018.

[25] D. Laumer, N. Lang, N. Van Doorn, O. M. Aodha, P. Perona, and J. D. Wegner, "Geocoding of trees from street addresses and street level images," ISPRS Journal of Photogrammetry and Remote Sensing, vol. 162, pp. 125-136, 2020.

[26] J. Chopin and S. Caneppele, "Geocoding child sexual abuse: An explorative analysis on journey to crime and to victimization from French police data," Child Abuse and Neglect, vol. 91, pp. 116-130, 2019.

[27] A. Aslam, I. A. Rana, and S. S. Bhatti, "The spatiotemporal dynamics of urbanisation and local climate: A case study of Islamabad, Pakistan," Environmental Impact Assessment Review, vol. 91, pp. 1-10, 2021.

[28] M.J. Butt, A. Waqas, M.F. Iqbal, G. Muhammad and M.A.K. Lodhi "Assessment of Urban Sprawl of Islamabad Metropolitan Area Using Multi-Sensor and Multi-Temporal Satellite Data" Arabian Journal for Science and Engineering, vol. 37:pp. 101–114, 2012.

[29] S. Hochreiter and J. Schmidhuber, "Long Short-Term Memory," Neural Computation, vol. 9, no. 8, pp. 1735–1780, Nov. 1997.

[30] I. Santos, N. Nedjah, and L. M. Mourelle, "Sentiment analysis using convolutional neural network with fastText embeddings," in IEEE Latin American Conference on Computational Intelligence, 2017, doi: 10.1109/LA-CCI.2017.8285683.

[31] P. Bojanowski, E. Grave, A. Joulin, and T. Mikolov, "Enriching word vectors with subword information," Transactions of the Association for Computational Linguistics, vol. 5, pp. 135-146, 2017.

[32] M.A. Andresen, "Testing for spatial dependence in the distribution of property crime using point pattern analysis and GIS," Journal of Quantitative Criminology, vol. 25, no. 3, pp. 339-366, 2009.

[33] M. A. Andresen, "Canada-United States interregional trade: quasi-points and spatial change," The Canadian Geographer, vol. 54, no. 2, pp. 139-157, 2010.

[34] M.A. Andresen and N. Malleson, "Spatial heterogeneity in crime analysis," in Crime Modeling and Mapping Using Geospatial Technologies, M. Leitner, Ed. New York, NY: Springer, pp. 3-23, 2013.

The Nucleus ***60***, *No. 2 (2023) 153-157*

www.thenucleuspak.org.pk

The Nucleus

ISSN 0029-5698 (Print)
ISSN 2306-6539 (Online)

Water Productivity of Garlic (Allium sativum L.) under the Responsive Drip Irrigation (RDI) System Compared to the Drip and Furrow Irrigation Systems in Silty Loam Soil

Ghani Akbar*, Zafar Islam, Bashir Ahmad

Climate, Energy and Water Research Institute (CEWRI), National Agricultural Research Centre (NARC), Islamabad, Pakistan.

ABSTRACT

Rapid population growth and climate change-induced water scarcity are challenging food security. Therefore, growing more food with less water and energy is urgently needed. The innovative responsive drip irrigation (RDI) system recently introduced in Pakistan responds to plant demand for water and nutrients and may be helpful in achieving this goal. Therefore, the yield, irrigation input and water productivity of garlic (Allium sativum L.) were evaluated under the RDI in comparison with the drip irrigation (DI) and furrow irrigation (FI) system (control) under silty loam soil at Islamabad, Pakistan. The treatments were three times replicated in a randomized block design. The average results show a significant (94%, 48%) water saving for the RDI and DI respectively than the FI (443 mm). The average dry garlic yield was also higher (3%, 11%) for the RDI and DI treatments respectively than the FI (13.491 tons/ha). Consequently, reducing irrigation water input and increasing crop yield resulted in a significant (94%, 46%) increase in the water productivity of garlic for the RDI and DI systems respectively than the FI (1.536 kg/m^3). Thus, the newly introduced RDI system in Pakistan has indicated the prospects of increasing the yield and water productivity of garlic at the household level. Hence, promoting the concept and principles of the RDI system may be helpful in enhancing climate change resilience in water-scarce areas and vegetable production at household levels in urban areas, which may enhance local food and nutrition security in the country.

Keywords: *Garlic Yield, Responsive Drip Irrigation, Furrow Irrigation, Water Productivity, Silty Loam*

1. Introduction

Pakistan is facing severe food security issues due to rapid population growth, climate change, and mismanagement of resources. The total cultivated area of the country is around 22 million ha comprising 23% rainfed and 67% irrigated. The majority (90%) of crop production comes from irrigated agriculture, where excessive use of the canal and groundwater is the norm [1]. Moreover, the irrigated production system is mainly focused on cereal crops whose yields are also far below the demonstrated achievable potential. Consequently, the water productivity of irrigated agriculture is below global average values [2]. On the other hand, the production from rainfed areas is negligible due to a lack of water conservation and mismanagement issues. We need to implement special water conservation strategies to tape the full potential of the varying rainfall patterns across the spatial and temporal boundaries of the country. The rainfall across the country's geographical area varies from 125 mm to 1500 mm and around 70% of the country receives less than 250 mm of rainfall, while 67% of the rainfall occurs during three monsoon months [3]. Areas suitable for cereal crops and vegetables need to be prioritized to fulfill the rising food demand. Vegetable production is extremely essential for local food and nutrient security. However, vegetables are grown in limited areas in Pakistan due to larger input costs, water scarcity and awareness issues. Vegetable productivity is generally very sensitive to water stress, diseases and pests. Moreover, Pakistan is facing climate change at the forefront. Consequently, climate change-induced frequent water scarcity, increased pests, diseases and heat or cold waves negatively impact vegetable productivity leading to reduced farmer interest and less productivity. Furthermore, vegetable production at the household level is negligible due to a lack of skills and awareness regarding new technologies.

Garlic (*Allium sativum L.*) is an important vegetable due to its medicinal value, as the Allicin of garlic has anti-bacterial properties [4] and higher nutritive value (rich in phosphorus, calcium, and carbohydrates) than the other bulb crops [5]. Generally, garlic is used in sauces, soups, vinegar, and for seasoning foods. In Pakistan, garlic is marketed fresh in raw form as a fresh bulb, green garlic, or garlic scape, while the marketing of processed products like spreads and chopped garlic is negligible. The local garlic production in Pakistan is around 125000 tons [6], which is sufficient to meet 67% of the domestic needs, thus precious foreign exchange (US$ 69 to 102 million) is spent on garlic import to fulfill the local requirement. Although the garlic yield in Pakistan is higher than the major rice-exporting countries including India (the world's third largest garlic exporter) [7, 8] and Bangladesh (the world's second largest garlic exporter) [9] but still the total garlic production is relatively less in Pakistan. Lack of resources and awareness of new technologies and improved management practices are considered the main reasons for low garlic productivity in Pakistan.

The responsive drip irrigation (RDI) system is a novel irrigation method that allows plants to self-regulate their own water delivery. When crops and plants need water and nutrients, they emit root exudates that allow them to uptake what they need from the surrounding soil. The RDI system responds and interacts with these root exudates, allowing water and nutrients to be released out of the billions of "smart micropores" in the polymer tubing. It provides a slow-release delivery of water flow that matches the roots' absorption capacity. The RDI resembles in properties the Moistube which is an innovative irrigation method comprised of a flexible semi-permeable nano-porous membrane with around 100,000 nanopores per square centimetre and of 10 to 900 nm pore size [10] that facilitates moisture movement by soil water

*Corresponding author:ghani_akbar@hotmail.com

potential difference [11] and system pressure [12]. The soil water matric potential alone drives the flow in case of the absence of the system pressure [11] but both drive the flow, if the water head is available [12]. The Moistube irrigation system is highly efficient, low pressure, less power consuming, low maintenance cost, and ensures long steady plant-responsive irrigation [13]. It did not require technical skills in irrigation scheduling for the different crops and soil types, because it self-regulates the irrigation application. The farmers need to keep the water available in the feeding reservoir alone. This technique has been successfully used in the middle east, Africa, and water-stressed areas of China and Pakistan [14], thus may be very beneficial for revolutionizing farming in water-scarce areas in general and vegetable production at the household level in particular. The RDI system has been recently introduced by the Climate, Energy, and Water Research Institute (CEWRI) of the National Agricultural Research Centre (NARC) in Pakistan. The research and demonstration sites have been established at Islamabad, district Lasbella in Baluchistan, Umerkot in Sindh, Peshawar, and Lakki Marwat in Khyber Pakhtunkhwa provinces. However, the current main limitations of RDI are the high cost and convenient availability of its parts in remote areas, while its resistance to rodents and soil disturbance during mid-season operation, pressure drop in RDI lines and clogging are not yet known under the local conditions. The RDI technology may have wide scope for the rainfed and desert areas of Pakistan. Therefore, the main objective of this study is to evaluate the effectiveness of the innovative RDI system in comparison to the conventional drip and furrow irrigation systems for the garlic vegetable under silty loam soil of the NARC, Islamabad, Pakistan.

2. Materials and Methods

2.1 Site description

The study was conducted during the October 2021 to May 2022 period, at the field station of CEWRI, NARC located at 498 m above mean sea level and l33° 40’ 31” N, 73º 08’ 15” E, Chak Shahzad, Islamabad, Pakistan. The soil properties at the experimental site are given in Table 1. The weather data in Table 2 is from October 2021 to May 2022 and recorded during the garlic season.

2.2 Experimental treatments

The experimental treatments were comprised of three irrigation methods: (1) RDI, (2) (DI), and (3) (FI) Systems (control). The treatments were thrice replicated in a split-plot complete block design. The nine experimental blocks were laid in three columns and three rows. Each column and row were separated by 75 cm (2.5ft) compacted earthen ridge of 30 cm (1 ft) height as a buffer area to avoid mutual interference of treatments. The land preparation, furrow bed sizes, seed rate (spacing), and all inputs, except irrigation applications, were the same for all the treatments. The irrigation was managed through a pipe delivery network using digital flow meters for

Table 1: Key soil hydraulic, chemical, and physical properties of the experimental site

Parameter Description	Value
Soil Bulk density	1.42 ± 0.13*
Soil Type	Silty Loam
pH	7.84 ± 0.11
EC (dS m^{-1})	0.44 ± 0.05
N (mg kg^{-1})	1.23 ± 0.79
P (mg kg^{-1})	4.78 ± 1.34
K (mg kg^{-1})	78.75 ± 13.78
WP (%)	12.40
FC (%)	27.70
SAT (%)	46.70
AW (mm m^{-1})	150.00

**SD - standard deviation; WP - wilting point; FC - field capacity; SAT-saturation; AW - available water = FC – WP; Ksat - saturated hydraulic conductivity.*

Table 2: Key weather parameters recorded at the field site of CEWRI-NARC Islamabad during 2021 and 2022 seasons

Month	*T min (°C)	T max (°C)	Humidity (%)	Wind (km/day)	Rainfall (mm)
Oct 21	15.00	29.13	75.39	36.01	166
Nov 21	7.30	24.63	67.90	18.04	0
Dec 21	3.47	19.43	76.70	33.10	10
Jan 22	5.35	15.84	89.26	43.62	165
Feb 22	6.36	19.43	78.50	54.84	22
Mar 22	13.00	28.74	72.32	35.15	54
Apr 22	16.33	35.30	52.40	35.01	5
May 22	20.13	36.58	62.90	49.64	14

**T_{min} = Monthly average minimum temperature, T_{max} = Monthly average maximum temperature*

flow measurements in m^3 by maintaining 15 psi pressure for the DI, 2 m constant head for the RDI system, and free gravity flow for the FI system. Irrigation scheduling for the FI and DI was based on the local farmer practice. The Humayun Garlic 1 (HG1) variety developed by NARC was planted on October 5, 2021, and harvested on May 16, 2022.

2.3 Data Collection and Analysis

The data collection was comprised of recording daily weather data, agronomic activities, fertilizers, and irrigation applications. The harvest samples were collected from the whole block by weighing the total green weight and the total dry weight of each block. Daily water use for the RDI treatment was recorded at 9:00 AM daily for consistency. However, the irrigation data of drip and furrow irrigation was recorded at the time of irrigation applications, while the local irrigation schedule was followed depending on the appearance and feel of the DI and FI systems. The Microsoft Excel spreadsheet 2007 was used for statistical analysis and mutual comparisons. All the data sets were checked for compliance with the ANOVA assumption. The Tukey’s (HSD) test at $p \leq 0.05$ was used to identify significant differences [15] among treatments. The standard deviation

was used to show data variations from the mean. The root zone soil water balance and transpiration were

assessed using the AquaCrop model of the Food and Agricultural Organization (FAO) according to guidelines given by [16]. The AquaCrop model simulates the soil-plant-atmosphere system by considering water and nutrients in the soil, growth, development, and yield in the plant and thermal regime, rainfall, evaporation, and carbon dioxide concentration in the atmosphere. The AquaCrop model has been widely used for simulating the water balance in the soil and atmosphere and the yield of vegetables [17, 18].

3. Results

3.1 Irrigation Applications

The analysis of irrigation applications is presented in Fig. 1. The results show 48% and 94% reduced irrigation applications to DI and RDI systems respectively than the FI system (443 mm). The average irrigation application per event were 1, 18 and 37 mm for the RDI, DI and FI systems respectively during the garlic season. The total irrigations event in excess of 1 mm per event were 21, 13 and 12 for the RDI, DI and FI treatments respectively.

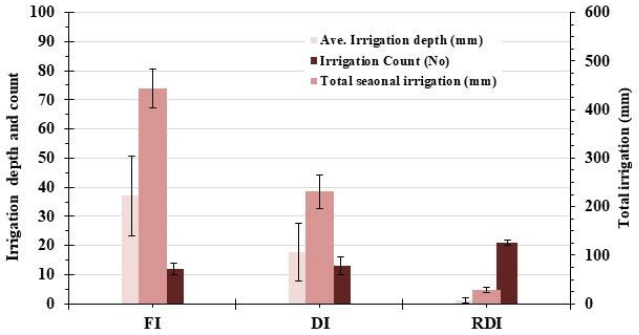

Fig. 1: Effect of FI, DI and RDI systems on average irrigation depth, irrigation count and total seasonal irrigation depth applications to garlic vegetable at NARC under silty loam soil *(vertical bars show standard deviations)*

3.2 Crop Yield

The crop yield results of garlic under the three irrigation methods are summarised in Fig. 2. The results show 1 and 3% higher dry garlic yield for the DI and RDI systems respectively than the FI (13.491 ton/ha) system.

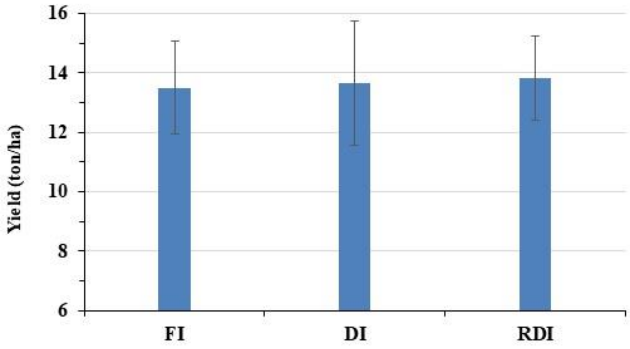

Fig. 2: Effect of DI and RDI systems compared to FI on yield of garlic (*vertical bars show standard deviations*)

3.3 Water Productivity of garlic

The water productivity of garlic under three irrigation methods is summarised in Fig. 3. The results show 34% and 88% higher water productivity for DI and RDI respectively than the FI (1.536 kg/m^3) system. The larger, water productivity of RDI than the FI is due to the relatively larger yield and significantly reduced irrigation applications to the RDI than the FI system.

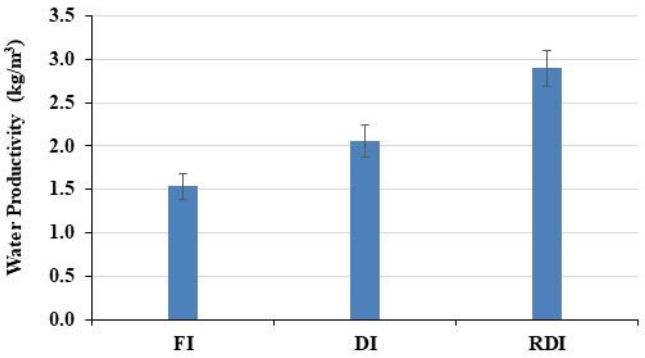

Fig. 3: Effect of FI, DI and RDI systems on the water productivity of garlic at NARC (*vertical bars show standard deviations*)

3.4 Rootzone Water Balance Analysis

The root zone profile (80 cm) moisture content variations for the three irrigation methods and rainfall events during the garlic season is presented in Fig. 4. The total rainfall of 435 mm was received in 31 rainfall events, with two major rainfall events including 96 mm on Oct 17, 2021 (early season) and 72 mm on January 7, 2022 (mid-season). The rainfall distribution and relatively less temperature during the season helped in keeping the rootzone above field capacity level, thus the water release from the RDI system was negligible to fulfil the soil moisture deficit in the rootzone during the crop season. However, irrigation in excess of demand was applied to FI and DI system. Consequently, the seasonal average profile moisture content in 80 cm rootzone profile was less (2%, 10%) for the DI and RDI systems respectively than the FI system (366 mm) system. The RDI system has shown a decreasing trend due to drainage and evapotranspiration in absence of rainfall, as the profile soil moisture content remained in excess of field capacity, except in the late season. However, the two daily rainfall in excess of 70 mm helped in equalizing the soil moisture content of all the irrigation treatments. The rootzone profile moisture content under the RDI system demonstrated larger rainwater conservation than the FI and DI systems, as the relatively dry rootzone profile of RDI allowed more rainfall runoff to store in the rootzone.

The water balance including details of all the water inputs and water outputs from the rootzone profile (80 cm) under the three irrigation methods using AquaCrop model is given in Fig. 5. The data shows maximum total infiltration, irrigation drainage and evapotranspiration for the FI system and minimum for the RDI system. Results shows 24 and 47% reduced infiltration, 28 and 55% reduced drainage, 29 and 35% reduced evaporation, 2% larger and 6% reduced

transpiration and 9 and 17% reduced evapotranspiration for the DI and RDI systems respectively than the FI system.

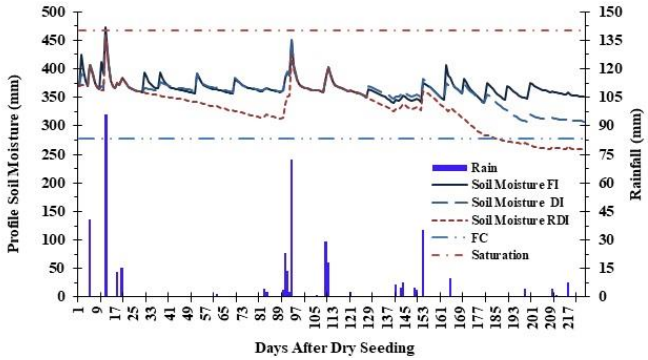

Fig. 4: Rainfall and rootzone profile moisture content variation relative to saturation and field capacity during the garlic season (Oct 5, 2021 to May 16, 2022) for the FI, DI and RDI systems

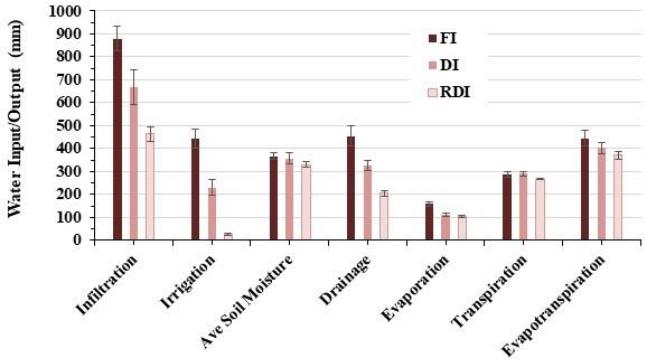

Fig. 5: Seasonal water input and output analysis in the rootzone profile (0-80 cm) for the FI, DI and RDI systems

4. Discussion

Vegetable production is important for the food security and healthy diet in Pakistan [19, 20]. However, despite being a short duration crop and generally grown on limited areas of farms [21], the demand for vegetables is rapidly increasing due to population growth, climate change induced water scarcity, diseases and pest infestation. Other reasons of less vegetable production and low quality are the less shelf life, market access issues, use of low quality water [22] and price variations due to supply and demand fluctuation. The unreliable water availability and less informed irrigation scheduling is further negatively impacting the vegetable productivity and quality [23]. Therefore, the use of innovative RDI technology used in the current study has elevated importance in using less water for growing more and healthy garlic. The 94% water saving indicates negligible irrigation application by the RDI than the FI system, which also helped in effectively using the available rainfall in the study area and fulfilling the water need without causing any water stress. These results also closely agree with the findings of RDI studies conducted at UAE showing water saving of 50% for date palm, 23% for cabbage and 33% for tomato than the DI system (personal communication). Therefore, the RDI system can be instrumental in enhancing crop yield and expanding vegetable grown areas in the water scarce regions. Moreover, vegetable production at household level or kitchen gardening can also be promoted in urban areas because the RDI system is less laborious, demands no frequent opening or closing of the valves and can irrigate vegetable using the available domestic water tanks and can ensure no vegetable damage in case the residents are away from home for several days. Although DI system also caused significant 48% saving in irrigation applications but still the water release was not according to the crop water requirement and is dependent on human decision of keeping the valve on or off, thus resulted over irrigation at the cost of more water, energy and labor.

The 1and 3% larger garlic fresh yield for the DI and RDI systems indicates that the garlic vegetable yield cannot be improved by increasing irrigation application but rather over irrigation make it more susceptible to weaker crop health, diseases and pest infestation due to increased humidity and submergence [24]. In contrast, other studies on RDI for tomato in Pothohar has shown up to 78% increase in yield and 41.5% overall benefit to the farmer than the conventional flood irrigation system [25]. Therefore, beside saving in irrigation water, the crop yield can also be increased by using the RDI system [14]. Hence, increasing crop yield and decreasing irrigation applications, the RDI and DI system showed 88 and 34% increase in water productivity of garlic crop respectively than the FI system [26], which can be helpful in producing more garlic with less water, especially in water scarce and urban areas of the country.

5. Conclusions

Growing garlic through RDI system can significantly decrease (94%) irrigation application and increase yield (3%), thus may lead to significant increase (88%) in water productivity than the furrow irrigation (FI) system. The use of DI system can also significantly increase water saving (48%) at no yield tradeoff, thus may lead to significant increase (34%) in water productivity of garlic than the conventional FI system. Producing more garlic yield with less water, less pumping energy, less labor and no technical knowledge regarding irrigation scheduling along with more rainwater conservation has indicated the prospects of larger vegetable production by adapting the RDI system in the water-scarce and urban areas of Pakistan. The concept of RDI system can be helpful in improving the climate change resilience and food security of vulnerable communities in the climate change-prone water-scarce areas of the country.

Acknowledgement

The authors gratefully acknowledge the material support by the Eva Ana Farm company for providing the RDI system and the staff of CEWRI field station for the physical support in conducting the research study. The authors also gratefully acknowledge the vegetable program of NARC for providing the HG1 garlic seed for the experiment.

References

[1] G. Akbar, S. Raine, A. D. McHugh, G. Hamilton, and Q. Hussain, "Strategies to improve the irrigation efficiency of raised beds on small farms," Sarhad Journal of Agriculture, vol. 33, no. 4, pp. 615-623, 2017.

[2] G. Akbar, S. Hameed, and Z. Islam, "Assessing water productivity and energy use for irrigating rice in Pakistan," Irrigation and Drainage, vol. 72, no. 2, pp. 478-486, 2023.

[3] A. Rashid, J. Ryan, and M. A. Chaudhry, "Challenges and strategies for dryland agriculture in Pakistan," Challenges and Strategies of Dryland Agriculture, vol. 32, pp. 359-371, 2004.

[4] S. J. Sterling and D. R. Eagling, "Agronomics and allicin yield of Australian grown garlic (Allium sativum)," Acta Horticulturae, vol. 6, no. 1, pp. 63-73, 2001, doi: https://doi.org/10.17660/ActaHortic.2001.555.6.

[5] S. Al-Otayk, M. Motawei, and M. El-Shinawy, "Variation in productive characteristics and diversity assessment of garlic cultivars and lines using DNA markers," Journal of Meteorology, Environment and Arid land Agriculture Sciences, vol. 20, no. 1, pp. 63-77, 2009.

[6] PBS, Agricultural Statistics of Pakistan, Agricultural Statistical Division, Ministry of Finance and Special Initiative, 2022.

[7] S. Srivastava, U. Sharma, B. Singh, and H. Yadava, "A profile of garlic production in India: facts, trends and opportunities," International Journal of Agriculture, Environment and Biotechnology, vol. 5, no. 4, pp. 477-482, 2012.

[8] T. Seth, Y. Lyngdoh, A. Chattopadhyay, A. B. Sharangi, and G. Mishra, "Export of onion, garlic and Chilli: three essential spices in daily kitchen," Indian Spices: The Legacy, Production and Processing of India's Treasured Export, pp. 359-378, 2018.

[9] M. J. Rana, S. Islam, and M. Kamruzzaman, "Growth and instability in area, production and productivity of major spices in Bangladesh," Journal of Agriculture and Food Research, vol. 6, pp. 1-8, 2021, doi: https://doi.org/10.1016/j.jafr.2021.100216.

[10] E. K. Kanda, "Soil water dynamics and response of cowpea to water availability under moisture irrigation," PhD, School of Engineering, University of KwaZulu-Natal, Pietermaritzburg, 2019.

[11] W. Yang, L. Tian, D. R. DU T, and Q. Yang, "Research prospect of the water-saving irrigation by semi-permeable film," J. Water Resour. Water Eng, vol. 19, no. 6, pp. 60-63, 2008.

[12] W. Niu, J. Zhang, L. Zhang, W. Xue, and L. Zhang, "Effects of buried depth and pressure head on water movement of wetted soil during moistube-irrigation," Nongye Jixie Xuebao= Transactions of the Chinese Society for Agricultural Machinery, vol. 44, no. 12, pp. 128-134, 2013.

[13] T. Dirwai, T. Mabhaudhi, E. Kanda, and A. Senzanje, "Moistube irrigation technology development, adoption and future prospects: A systematic scoping review," Heliyon, vol. 7, no. 2, pp. 1-12, 2021.

[14] G. Akbar, Z. Islam, S. Hameed, and B. Ahmad, "Yield and water productivity of rice as influenced by responsive drip irrigation, alternate wetting and drying versus conventional flooding under silty loam soil texture," Water Resources and Irrigation Management-WRIM, vol. 12, no. 1-3, pp. 1-13, 2023.

[15] R. G. d Steel and J. H. Torrie, Principles and procedures of statistics: a biometrical approach. McGraw-Hill New York, NY, USA, 1986.

[16] P. Steduto, T. C. Hsiao, D. Raes, and E. Fereres, "AquaCrop-The FAO crop model to simulate yield response to water: I. Concepts and underlying principles," Agronomy Journal, vol. 101, no. 3, pp. 426-437, 2009, doi: https://doi.org/10.2134/agronj2008.0139s.

[17] D. Raes, P. Steduto, T. Hsiao, and E. Fereres, "AquaCrop-The FAO crop model for predicting yield response to water: II. Main algorithms and software description," Agronomy Journal, vol. 101, no. 3, pp. 438-447, 2009, doi: https://doi.org/10.2134/agronj2008.0140s.

[18] E. Vanuytrecht et al., "AquaCrop: FAO's crop water productivity and yield response model," Environmental Modelling & Software, vol. 62, pp. 351-360, 2014, doi: https://doi.org/10.1016/j.envsoft.2014.08.005.

[19] M. Ahmad and U. Farooq, "The state of food security in Pakistan: Future challenges and coping strategies," The Pakistan Development Review, pp. 903-923, 2010.

[20] M. A. ur Rehman et al., "Unveiling of genetic variability in garlic (Allium sativum L.) genotypes grown in Pakistan," Journal of Pure and Applied Agriculture, vol. 5, no. 3, pp. 53-64, 2020.

[21] H. Khan, M. Hussain, G. Jellani, S. Tariq, T. Naseeb, and S. Mahmood, "Evaluation of garlic genotypes for yield and yield components in Islamabad, Pakistan environment," The Nucleus, vol. 55, no. 1, pp. 22-26, 2018.

[22] J. H. Ensink, T. Mahmood, W. Van der Hoek, L. Raschid-Sally, and F. P. Amerasinghe, "A nationwide assessment of wastewater use in Pakistan: an obscure activity or a vitally important one?," Water policy, vol. 6, no. 3, pp. 197-206, 2004.

[23] A. H. Tefera, S. G. Kebede, and G. T. Mola, "Optimal irrigation scheduling for garlic (Allium sativum L.) in the central highland vertisols areas of Ethiopia," International Journal of Food Science and Agriculture, vol. 5, pp. 308-316, 2021.

[24] M. Ayyachamy, K. Khelawan, D. Pillay, K. Permaul, and S. Singh, "Production of inulinase by Xanthomonas campestris pv phaseoli using onion (Allium cepa) and garlic (Allium sativum) peels in solid state cultivation," Letters in applied microbiology, vol. 45, no. 4, pp. 439-444, 2007.

[25] Q. Arshad et al., "Conserving water: cost and productivity analysis of responsive drip and conventional irrigation," Environmental Engineering and Management Journal, vol. 22, no. 4, pp. 639-649, 2023.

[26] N. Heydari, "Water productivity in agriculture: challenges in concepts, terms and values," Irrigation and drainage, vol. 63, no. 1, pp. 22-28, 2014.

The Nucleus ***60***, *No. 2 (2023) 158-167*

www.thenucleuspak.org.pk

The Nucleus
ISSN 0029-5698 (Print)
ISSN 2306-6539 (Online)

Geotourism Prospect in and around Dubrajpur, Birbhum, West Bengal, India

Bikas Saha

Durgapur Government College, J.N. Avenue, Durgapur, West Bengal, India

ABSTRACT

In this era, it is not a luxury to see new places but a natural urge of the people, making tourism a huge industry. Tourists used to travel and tour for religious, cultural, educational, employment, business, health and adventure purposes. Geomorphologically, the Indian subcontinent is a land of great diversity. It is famous for its grand scenery. Almost all the geomorphic landscapes of the earth are present in this subcontinent. The Himalaya came up with blessings for India and India's grand scenery in the subcontinent. Geotourism is a new form of tourism that is based on geomorphology, geology and also on different geological environments. Geotourism offers a new form of sustainable tourism that is more holistic than previous niche forms of tourism. There are some incredible rocks/rock formations across the Indian Sub-continent which can be the foundation of a geotourism site. The balancing rock forms a startling type, where one or more rocks are balancing on each other. Some of the finest examples are the 'Balancing rock' of Jabalpur, the balancing rock of Mahabalipuram, Tamil Nadu which is distinguished as 'Krishna's Butter Ball', and the balancing rocks of 'Mama-Bhagne Pahar' in Dubrajpur. Among these three amazing spots, the first two is already well known to tourists, however, Mama-Bhagne pahar also offers a famous geomorphosite that has potential from geotourism perspective. However, there are some problems related to anthropogenic interventions that have to overcome to make it a famous geotourism site. Therefore, in the present study, an attempt has been made to formulate geoconservation and geotourism development strategies for the concerned geomorphosite that will protect the site from human activities and promote local tourism in a sustainable way. Moreover, Dubrajpur is located in the approachable vicinity of some popular and famous tourist spots of Birbhum district like Tarapith, Nalhati, Pathar Chapuri, Siuri, Amkhoi, Bolpur, Santiniketan and the very famous Bakreswar.

Keywords*: Geomorphosite, Geodiversity, Geotourism, Mama-Bhagne pahar, Anthropogenic Interventions, Bakreswar, Amkhoi*

1. Introduction

There is immense contrast in geology, structure, tectonism, climate, and elevation along with the long coastal zone in India. This huge diversity in landforms is known as geodiversity. Abiotic richness is also indicated by the geodiversity. During the early 90s', the concept of geodiversity emerged. Sharples (1993) [1] defined geodiversity as "the diversity of Earth features and systems". Some elaboration was given to Sharples's definition. And the definition emerged as "the diversity of Earth's features and systems" [1]. Later, the definition was elaborated and it included ''the range or diversity of geological (bedrock), geomorphological (landform) and soil features, assemblages, systems and processes" [2, 3, 4]. Later Gary (2004) [5] define geodiversity as "the natural range (diversity) of geological (rocks, minerals, fossils), geomorphological (landform, processes) and soil features including their assemblages, relationships, properties, interpretations and systems". Researchers and developers are trying to define "Geotourism" in different possible ways for the past few years. The term "Geotourism" was first coined by Tourtellot and Sally [6]. It is a new and fast-growing special tourism [7] where high values of geological and geographical landscapes act as the center of attraction. Geotourism nurtures abiotic elements of nature [8] and focuses on the interpretation and preservation of these earthly features by increasing their touristic value. But that is not the case in ecotourism. Ecotourism focuses on the biotic elements i.e., on flora and fauna. And in the year 1995, Thomas Alfred Hose defined it as "The provision of interpretative and service facilities for geosites and geomorphosites and their encompassing topography, together with their associated in-situ and ex-situ artifacts, to constituency-build for their conservation by generating appreciation, learning, and research by and for current and future generations" [9, 10].

The Indian subcontinent is a land of great diversity in terms of geomorphology and is famous for its grand scenery. Almost each and every geomorphic landscape are there in this subcontinent which are comparable to any other such continental landscapes of the world. Starting from the striking glacier valley of Siachen, the frozen ice peaks of Kangchenjunga to the mangrove forest of Sundarbans, the coral chains of Andaman, rocky-sandy desert of Jaisalmer and Thar, dense forest of Bandhabgarh, brakish water lakes of Kerala, flat top mountains of Decan Trap are a few among others are there to give the witness of geodiversity of India. Towering Himalaya formed, out of the Tethys Sea and the adjacent foreland basin, due to the northward drifting of India and collision with Eurasia. The formation of the Himalaya is a blessing for the development of the grand scenery in the Indian subcontinent. Some of the oldest rocks present on the planet Earth is there in the geomorphologically diversified India. Rocks ranging from Archean age to Quaternary age are also there in India. As a result, the Indian landmass gets enough time for landscape evolution due to this long timescale [11].

There are some incredible rocks/rock formations in India. Because of the amazing shape and size of these natural rocks, they have ranked in the list of the World's most amazing rock formations [11]. Some of these rocks/rock formations are turtle-shaped 'Toad Rock' near Nakki Lake of Arbuda Mountain; 'Bugle Rock' is a massive rock in Bangalore; black basalt rock of 'Gilbert Hill' of Andheri, Maharashtra; 'Yana Rocks', located in the Sahyadri mountain range of the Western Ghats; 'Marble Rocks' of Jabalpur; pillar-shaped

*Corresponding author: sahabikas@gmail.com

'Pillar Rocks' of Kodaikanal, Tamil Nadu; 'Phantom Rock' of Wayanad, Kerala; 'Hampi's Boulders' or 'Running Rocks' of Hampi; 'Nijagal Betta' near Bangalore; 'Natural Arch' of Tirumala hills of Andhra Pradesh [11]. The Rock art of Bhimbetka and huge rock-cut images of Unakoti hills are a few amazements of India. Because of all these varieties of landforms and landscapes, India become one of the most fascinating places on the planet Earth.

Apart from these above features, there are a few amazing landforms are there in India where one or more rocks are balancing with each other. But they are stable for hundreds of years. These are called 'Balancing Rocks' of India. This types of three famous landforms are there in India. These are the 'Balancing rock' of Jabalpur (Fig. 1), 'Krishna's Butter Ball' – balancing rock at Mahabalipuram, Tamil Nadu (Fig. 2), and the balancing rocks of 'Mama-Bhagne Pahar' in Dubrajpur (Fig. 3). First two are very renowned and very popular to the tourist. Contextually, 'Krishna's Butter Ball' – the balancing rock of Mahabalipuram, Tamil Nadu is a UNESCO World Heritage Site. Jabalpur is also very famous among the tourists. In comparison, '*Mama-Bhagne Pahar'* is not well introduced to the people may be due to lack of publicity and negligence of the authority to some extent.

Fig. 1: Balancing Rocks of Jabalpur, Madhya Pradesh, India.

This stunning rock formation is the extension of the Chota Nagpur Plateau in Dubrajpur, Birbhum. Here, two rocks balanced over each other naturally and are regarded as a tourist spot as many people come to see the very existence of the balancing rock formation. Because of the astonishing balance and bonding of the two rocks, they are known as Mama and Bhagne, and the hill is known as 'Mama-Bhagne Pahar'. The shape of these two rocks is globular. Field investigation indicates the pair of these rocks are of granite rock. Microscopic study of thin sections of these rocks under plain polarized and crossed polarized light corroborates the granitic interpretation (Fig. 4). Apart from these two main balancing rocks, there are numerous fractured boulders in and around them. The rocks here are composed of grey granite with a mineral composition of plagioclase feldspar,

Fig. 2: Balancing rock at Mahabalipuram, Tamil Nadu, distinguished as 'Krishna's Butter Ball'.

Fig. 3: Mama-Bhagne Pahar of Dubrajpur.

K-feldspar, biotite, and apatite (Fig. 4). The famous Shiva Temple or 'Pahareswar' temple is situated at the base of the hill. According to the geologists, volcanic eruption created this rock formation along with the balancing rock during the formation of the Chota Nagpur Plateau [12].

The visitors will have a strange affection with magnificent stretches of rural fields in the entire area. Most of the rocks here in Dubrajpur 'Mama-Bhagne' pahar are spherical in shape. Though the rocks are of different shapes and sizes, they are a creation of nature.

If you look at the size of these three balancing rocks, the size of Mama-Bhagne pahar is much bigger. Even complexity-wise, Mama-Bhagne pahar is more complex compared to the balancing rocks of Mahabalipuram and Jabalpur. But, both Mahabalipuram and Jabalpur are well-established tourist spots due to the policy by the authorities. Moreover, these three areas have been formed due to some

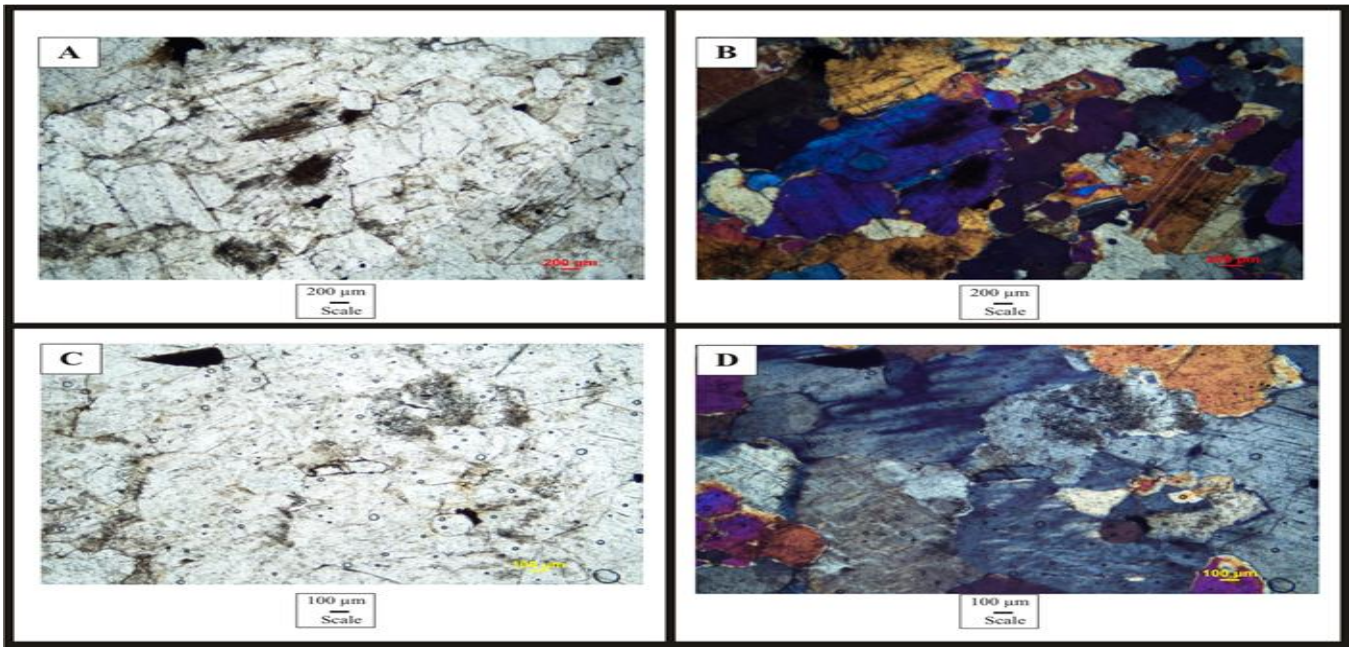

Fig. 4: Photomicrographs of Rock of Mama-Bhagne pahar (A & C: under Plain Polarized Light & B & D: under Crossed Polarized Light)

geological events. Like Mama-Bhagne pahar formed due to volcanic eruption along with Chota Nagpur Plateau. So, due to both geological and geomorphological evolution, Mama-Bhagne pahar has evolved. Thus, tourist spots like Mama-Bhagne pahar can be famous for geotourism if we opt for a sustainable tourism process here in Dubrajpur.

Geosites are part of the geosphere with a specific significance to understand the history of the earth and different human-recognized geological geomorphological features with a scientific, cultural/historical, aesthetic, and/or social/economic value [11]. Lithological sites, stratotypes, geosystems, geological or geomorphological landscapes, caves and grottos, mineral sites, historical mine sites, fossil sites, meteorite impacts, and the geological environment that supports an ecosystem all are part of geosites (Fig. 5).

2. Geology of the Study Area:

The Rajmahal basin is situated to the northeast of the Damodar basin, in Peninsular India (Fig. 6). Trend of the basin is in the north–south oriented. Exposed Gondwana sediments in this area are bounded by the Ganga River in the north, by Rajmahal Traps in the east, metamorphic rocks in the west and laterite and alluvium in the south (Table – 1). At the Western flanks of the Rajmahal Basin, a number of detached outcrops of the Gondwana sediments are exposed laterally [13].

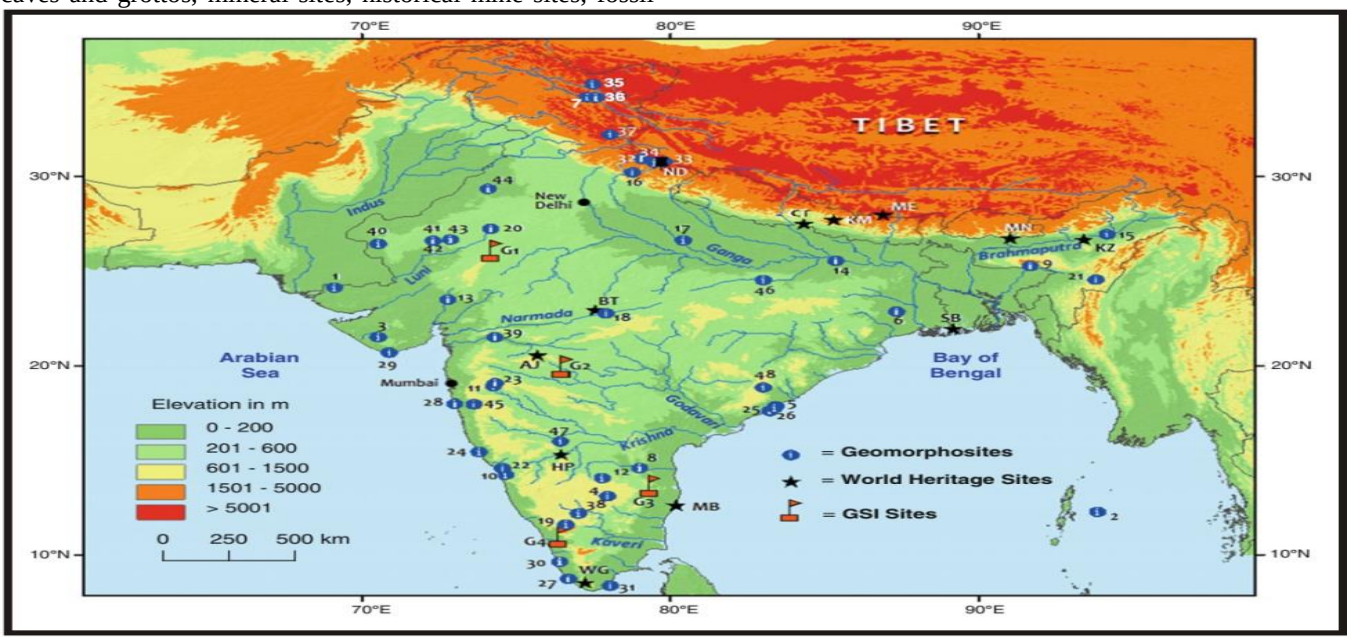

Fig. 5: The potential geomorphosites in India [11]

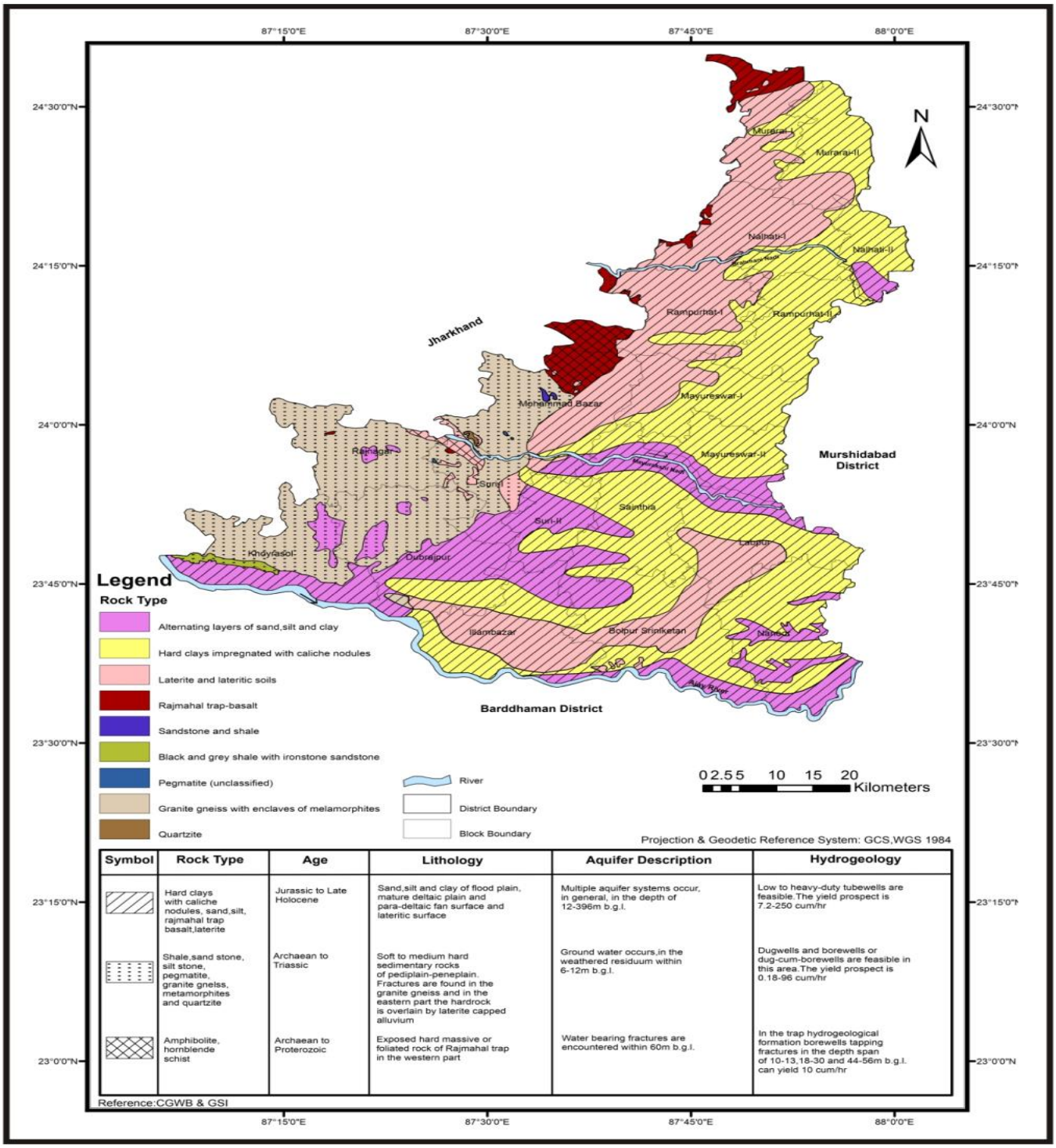

Symbol	Rock Type	Age	Lithology	Aquifer Description	Hydrogeology
	Hard clays with caliche nodules, sand,silt, rajmahal trap basalt,laterite	Jurassic to Late Holocene	Sand,silt and clay of flood plain, mature deltaic plain and para-deltaic fan surface and lateritic surface	Multiple aquifer systems occur, in general, in the depth of 12-396m b.g.l.	Low to heavy-duty tubewells are feasible.The yield prospect is 7.2-250 cum/hr
	Shale,sand stone, silt stone, pegmatite, granite gneiss, metamorphites and quartzite	Archaean to Triassic	Soft to medium hard sedimentary rocks of pediplain-peneplain. Fractures are found in the granite gneiss and in the eastern part the hardrock is overlain by laterite capped alluvium	Ground water occurs,in the weathered residuum within 6-12m b.g.l.	Dugwells and borewells or dug-cum-borewells are feasible in this area.The yield prospect is 0.18-96 cum/hr
	Amphibolite, hornblende schist	Archaean to Proterozoic	Exposed hard massive or foliated rock of Rajmahal trap in the western part	Water bearing fractures are encountered within 60m b.g.l.	In the trap hydrogeological formation borewells tapping fractures in the depth span of 10-13,18-30 and 44-56m b.g.l. can yield 10 cum/hr

Fig. 6: Generalized Stratigraphic Map of Birbhum District.

Table-1 shows the Gondowana succession as it has developed in the Rajmahal basin [14-16]. Gondwana succession is again divided into Lower Gondwana succession and Upper Gondwana succession. The Lower Gondwana Group consists of the Early Permian Talchir Formation (Asselian–Sakmarian) and the Early Permian Barakar Formation (Artinskian–Kungurian) [17]. Whereas, Dubrajpur and Rajmahal formations together form the Upper Gondwana Group [13]. The Dubrajpur Formation unconformably overlies the Barakar Formation, showing that erosion was active between the two periods of deposition [16].

The centers of tourist appeal across the world are the spectacular scenic beauty or cultural heritage or other forms of the touristic charm of a lot of places. Due to the lack of responsible and conservative nature of travel, many promising tourist places are ruined especially because of environmental

Table – 1: Generalized Stratigraphical Succession of the Rajmahal Basin [14, 15, 16]

Series	Lithostratigraphic Unit	Lithology
Recent	Alluvium	Loose soil, silt, and clay
Upper Tertiary	Alluvium	Coarse- to medium-grained sandstone, gravel, pebble beds
----------Unconformity----------		
Lower Cretaceous	Rajmahal Formation (traps and intertrappean)	Flows of basalt, pitchstone, and intertrappean beds (sandstone, shale, ash)
Lower Triassic to Lower Cretaceous	Dubrajpur Formation	Pebbly and coarse- to medium-grained sandstone, siltstone, clay, grey to pink shale
----------Unconformity----------		
Upper Permian		Coal, shale, sandstone
Lower Permian	Barakar Formation	Coarse- to medium-grained and pebbly sandstone, grey shale, clay and coal
	Talchir Formation	Tillite, fine- to medium-grained sandstone, olive-green shale
----------Unconformity----------		
Precambrian		Basement rocks, amphibolite, quartzite, gneiss and granite

problems [18]. As a result, the tourist place was unable to achieve the sustainable goal of tourism. Again, some areas are vulnerable in spite of their tourism potential. Therefore, prudent drafting and evaluation are required to sustain the immaculate standard of mother earth. If we want to bring cerebral peacefulness and pleasure in humanity, then tranquility and a pristine class of nature will help more than that of a decomposed natural scenery [19]. Fortunately, there are still many pockets in India which are unexplored and own huge tourism potential.

3. Discussion

It is a very futuristic idea to identify the tourism potential of any area. Tourism gives rise to income for the local people, eases the poverty situations, and guides sustainable development as well as socio-economic development for the tourist spots and adjoining areas. The centers of tourist appeal across the world are the spectacular scenic beauty or cultural heritage or other forms of the touristic charm of a lot of places. Many promising tourist places are ruined especially because of environmental problems [18]. As a result, the tourist place was unable to achieve the sustainable goal of tourism. Again, some areas are vulnerable in spite of their tourism potential. Thus, to sustain the immaculate standard of mother earth, prudent drafting and evaluation are required [19]. If we want to bring cerebral peacefulness and pleasure in humanity, then tranquility and a pristine class of nature will help more than that of a decomposed natural scenery [19] [Repetition, change it]. Fortunately, there are still many pockets in India that are unexplored and own huge tourism potential.

Mama-Bhagne pahar is located at Dubrajpur of the district of Birbhum, West Bengal, India (Fig. 7) [20, 21]. It is a hill-like rock formation. From the scientific viewpoint, it is not a hill but an excellent example of tors which are formed by several huge granite rocks (Fig. 8). Among these granite rocks, the famous Mama-Bhagne pahar is balancing one on top of the others (Fig. 3) and thus creating the one of the biggest balancing rock of India and a good geomorphosites. The grey-coloured granites present here in Mama-Bhagne pahar are made up of glassy quartz, plagioclase feldspar, K-feldspar and black biotite (Fig. 4) [22]. Mama-Bhagne pahar is the far-reaching part of Chotanagpur Granite Gneiss Complex (CGGC) [22]. By using Linton's two-stage model, we can explain the formation of Mama-Bhagne pahar [23]. Due to volcanic eruption during the Archean period, intrusion of granite took place in this area. Later, due to warm, humid climates, chemical weathering took place during the Tertiary period resulting in thick regolith with core rock. Finally, the core rock has an upstanding tor result because thick regolith has been removed by erosion.

For the reconstruction of local paleo-geomorphic processes and paleoclimate, Mama-Bhagne pahar has great importance. That is why it has significant scientific value in terms of geology and geomorphology. The area is not more than 1 sq. km and is referred to as "Pahareswar" or "God of the rock" by the local people (Fig. 9). According to the belief of the Santhal tribes, the place belongs to "Bongaburu", God of the tribal people. So, Mama-Bhagne pahar also has cultural or religious value. That is why local people made a temple of Lord Shiva or "Pahareswar" at the base of the 'pahar', known as "Paharreswar Mandir" (Fig. 10). Height of Mama-Bhagne pahar is about 122 m. Balancing rocks on the hill attracts thousands of tourists every year because of its aesthetic view. Mama-Bhagne pahar has a circumference of about 1252.49 m and an area of about 73,665 sq. m. [21]. Hence, such a typical landform can be undoubtedly termed as geomorphosite because of its scientific, cultural, aesthetic, and socio-economic values. Geomorphisite covering $\geq$ 1 sq. km area but $<$ 10 sq. km are considered medium-scale geomorphosites as per Brocx and Semeniuk [24].

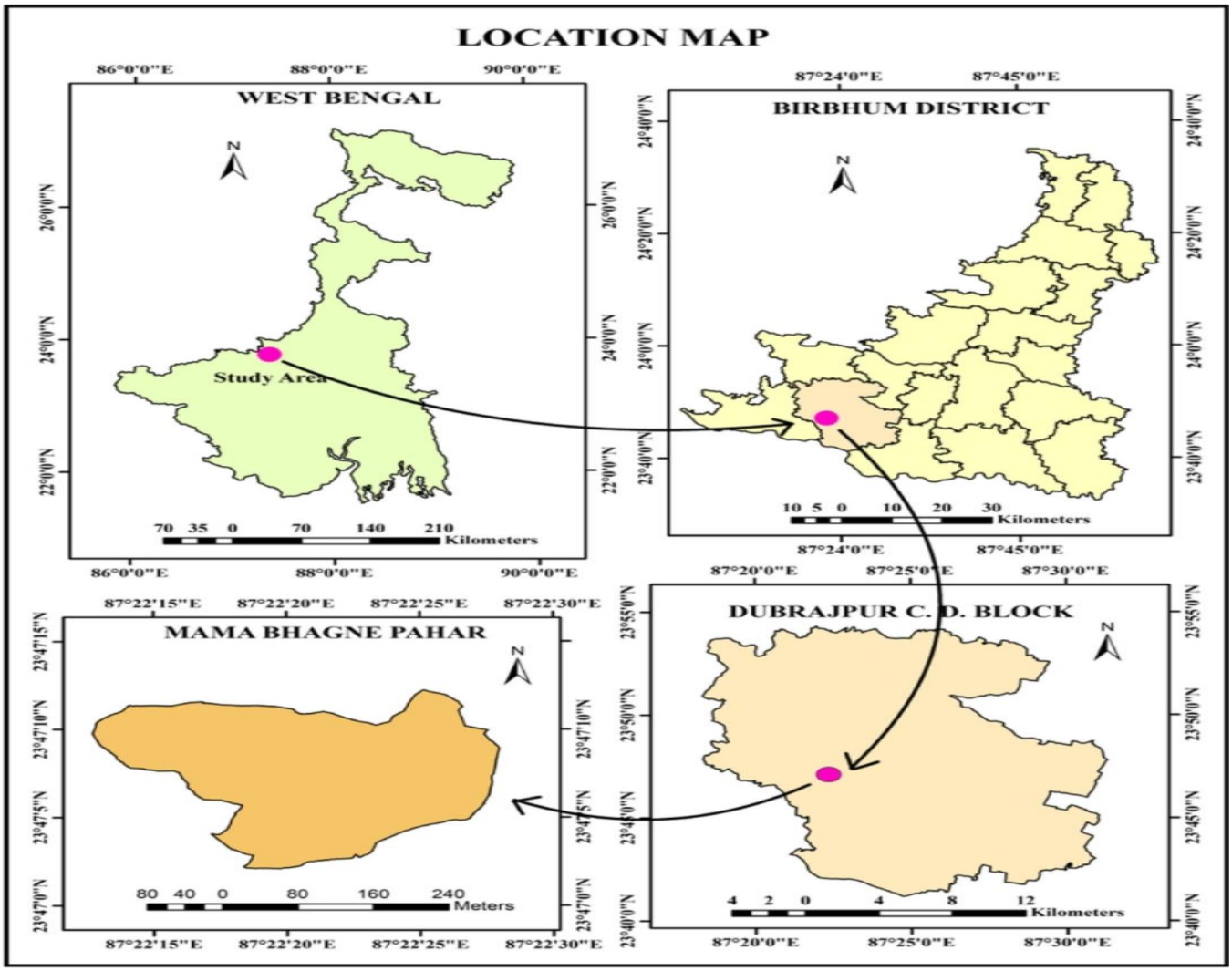

Fig. 7: Location map of the Mama-Bhagne Pahar [20].

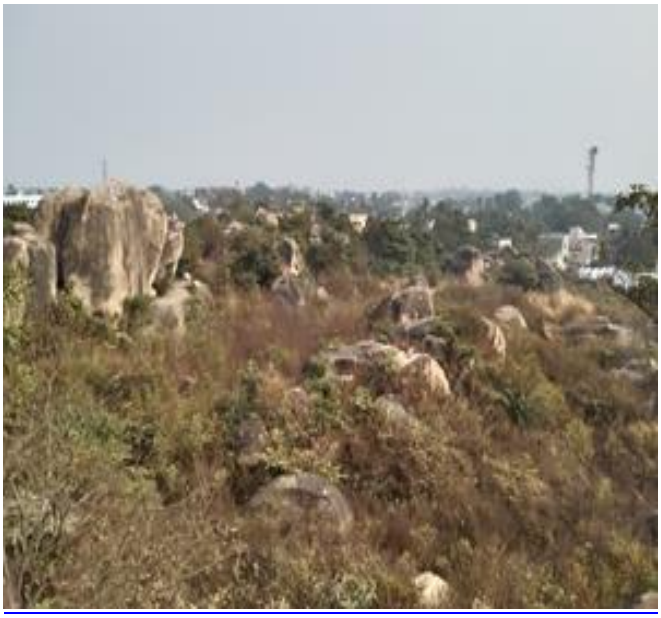

Fig. 8: Mama Bhagne Pahar and its nearby area.

Fig. 9: Lord Shiva inside the Shiva temple

Fig. 10: Lord Shiva temple or "Pahareswr Mandir" at the base of the Mama-Bhagne Pahar.

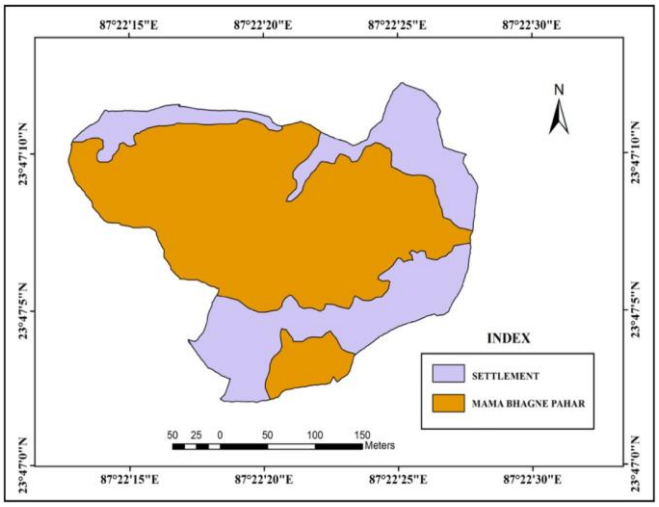

Fig. 11: Human settlements encroached within the area of Mama Bhagne Pahar which is highly vulnerable ([22]).

From the above discussion, we can designate Dubrajpur Mama-Bhagne pahar as an important geomorphosites. But presently the site is heavily decaying due to various anthropogenic interventions. Among these various stressors, the most common is human encroachment and habitation within the periphery of the geomorphosites. People are building their houses within the area of the geomorphosite with the help of immoral politics of the local political leaders (Fig. 11) [22]. Due to a lack of geoeducation and because of their poverty, humanity uses the rocks as an advertising board for various types of commercial statements as well as various rubbish posters on the surface of the rocks (Fig. 12). These advertisements create visual pollution for the tourists. Here and there, tourists are discarding waste all around the geomorphosites and thus polluting the area (Fig. 13). Moreover, the rocks of the Mama-Bhagne pahar are suffering from weathering, a natural phenomenon. While visiting the study area, we witnessed all three types of weathering, namely physical, chemical, and biological weathering. Due to storms and rain, the rocks are coming in contact with different types of chemical agents. As a result, cracks develop in the rocks and after some time, they are broken down (Fig. 14). As the Tropic of Cancer line passes through Panagarh of West Bengal, which is very near Dubrajpur, the temperature fluctuation in summer and winter is very high. Apart from this, the temperature is normally high in Dubrajpur. Thus, physical weathering is very active in Dubrajpur. And Mama-Bhagne is also suffering from these climatic conditions. Moreover, due to lack of care, a huge number of plants grew in and around the geomorphosite. As a consequence, cracks have developed due to the roots of plants in the rocks of the geomorphosite. Hence, both mechanical, chemical and biological wear and tear take place among the rocks of Mama-Bhagne pahar and if one is not cautious, all the large-sized rocks will be converted to smaller rock particles (Fig. 14).

Fig. 12: Advertisement on the rocks of Mama-Bhagne Pahar

Fig. 13: Discarded waste by the tourists.

Fig. 14: Cracks developed within the rocks and they are widening day by day due to weathering, both physical, chemical and biological weathering.

The people of this part of West Bengal are very poor. Cultivation is not good enough in the Dubrajpur block area. Most of the people of this area go outside this area for their income due to unemployment and poverty. To protect the geomorphosites i.e., Mama-Bhagne pahar from human interventions and to promote local tourism sustainably, humanity, along with local bodies, should try to work out geoconservation and geotourism development strategies. Special attention should be given to geoeducation, tourism promotion, socio-economic development of the local people, and legal protection of the site while formulating the strategy of geoconservation as well as geotourism.

These days' the major issue of any tourism hotspots is to achieve sustainability in various developing countries. India is also not an exception since such areas have been interfacing with many categories of environmental problems due to the advent of huge numbers of tourists. As soon as the concept of geotourism emerged in the arena of tourism, it provides favourable openings for sustainable development by achieving quality management of natural settings and ensuring responsible tourism activities.

Dubrajpur is well connected via rail, road or even air. Because Andal airport is only 33 km away from Dubrajpur. Tourists who will visit Dubrajpur Mama-Bhagne pahar can also visit many famous tourist spots like Tarapith, the famous Kali Temple for Hindu pilgrims. It is also famous for the Sadhak Bamahepa and Tarapith is only 70 km. Among the 51 Sati Pitha, one is here in Nalhati of Birbhum which is 85 km away from Dubrajpur. Traditionally, it is believed that the throat or 'Nala' fell here. Subsequently, from this 'Nala', the name of the place is Nalhati. And Maa Nalateswari has a resemblance with Kamakhya, Assam and Kalighat, Kolkata pithas. Santiniketan and Viswa Bharti of Bolpur is 45 km away from Dubrajpur. Tourists who have come to visit Dubrajpur can also visit Bolpur and Santiniketan of Birbhum district. In between Dubrajpur to Bolpur roads, there is a famous Wood Fossil park. The name of the place is Amkhoi and the name of the park is Amkhoi Wood Fossil Park [25]. Tourists can also visit Amkhoi while visiting Dubrajpur and Bolpur. Bakreswar is famous for its hot springs [26]. There are seven 'Kunda' or Hot Springs in Bakreswar which is very near Dubrajpur. It is only 10 km from Dubrajpur Mama-Bhagne pahar to Bakreswar. While moving from Dubrajpur to the district headquarters, Siuri, there is a pilgrimage place called Pathar Chapuri. It is a 'Darga', where both Hindu and Muslim people used to go. So, geotourists who come to visit Mama-Bhagne pahar can visit numerous tourist places which are nearby Dubrajpur (Fig. 15).

4. Conclusion

To judge the Geotourism potential of Mama-Bhagne pahar, Dubrajpur, an attempt has been made in this paper. The findings show what a great moment it was for the area to become a Geotourist destination. But the different level's authorities have to work together focusing on the natural resource management and economic development of the study area. From the earlier discussion, we can conclude that Mama-Bhagne Pahar of Dubrajpur, Birbhum, West Bengal, is an important geomorphosite because of its lofty scientific, aesthetic, cultural and economic values with respect to human perception. But the site is perpetually decaying due to various anthropogenic interventions. Unemployment and poverty of the local people are the catalysts of this continuous deterioration of the geomorphosite. But, if we consider the possibilities of tourism in the concerned site, huge scopes are there. The best way to protect the site from human intervention is geoconservation. To promote tourism in Dubrajpur and to protect the geodiversity of Dubrajpur, we have to cultivate the geotourism most sustainably. The promotion of tourism and the economic advancement of the local people should be the first priority during the formation of the strategy. Encouragement of geoeducations among the local people as well as tourists is the next important step to promote tourism in a sustainable way in Dubrajpur. Among all the geoconservation sites across the world, legal protection is one of the most important strategies. So, we have to take legal protection to protect the geodiversity of Dubrajpur.

It has been observed during field surveys that various anthropogenic interventions are the crucial environmental warnings to Mama Bhagne Pahar The maximum burden in the decaying of the study area is human occupancy. The volume of human occupancy is about one-third of the study area [22]. It is a very subtle issue and the adaptive capabilities of these human-occupied areas are very low compared to the rest of the area. If the government, local bodies as well as local people do not rigidly prohibit such activities, then we shall no longer have our beloved geomorphosite in the near future.

To fruitfully apply all the above-mentioned measures, to conserve the site, we have to extend constructive apprehension about the site among the tourists, local people, and business houses. Then, only we can save a stunning geomorphosite like Dubrajpur Mama-Bhagne pahar.

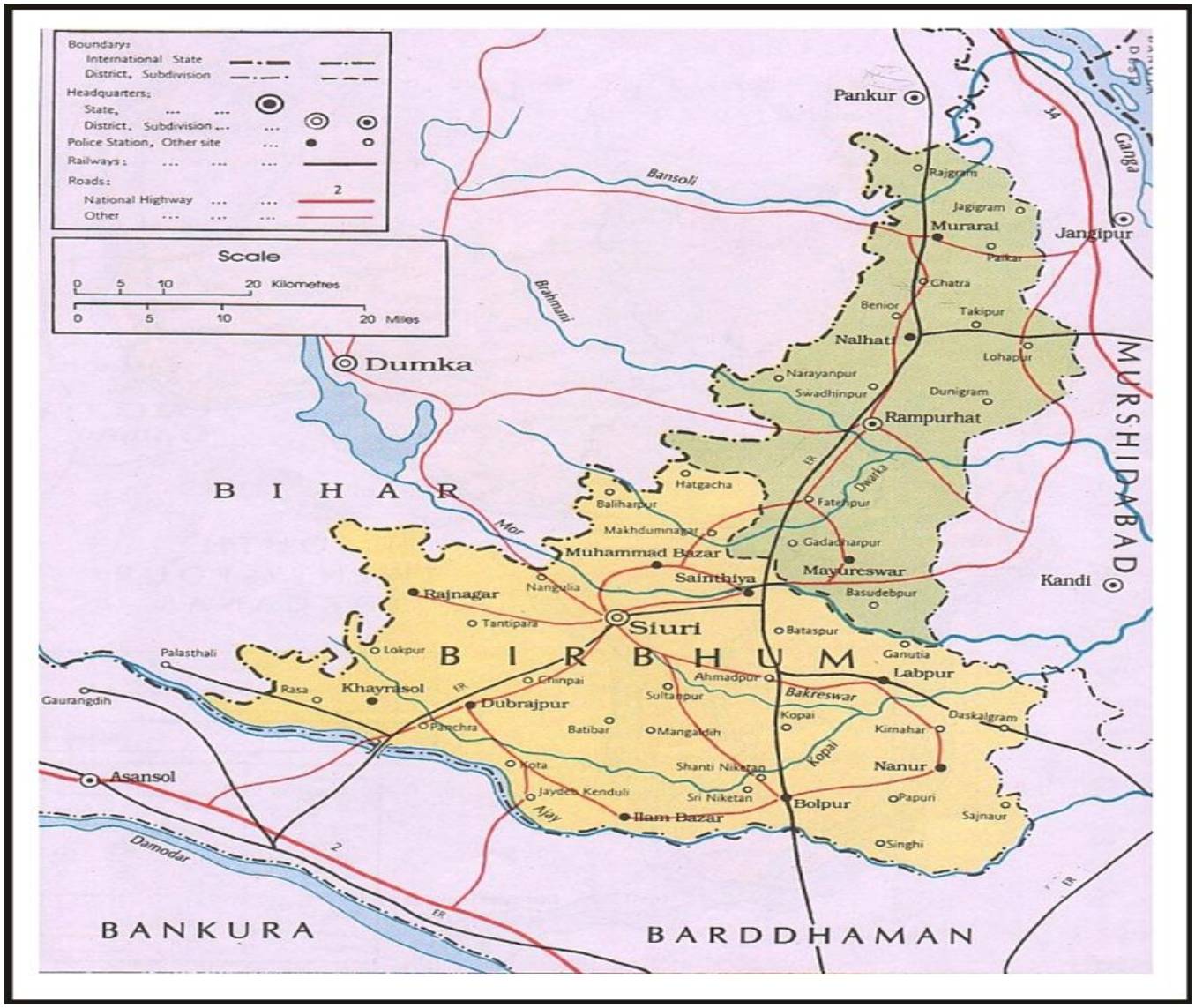

Fig. 15: Various tourist spots near Dubrajpur

Declaration of Competing Interest:

The authors declare that they have no known competing financial interests or personal relationships that could have appeared to influence the work reported in this paper.

Acknowledgements:

The author expresses gratitude to Durgapur Govt. College for infrastructural facilities. This research did not receive any kind of grant from any funding agencies.

References:

[1] C. Sharples, "A methodology for the identification of significant landforms and geological sites for geoconservation purposes," Report to Forestry Commission, Tasmania, 1993.

[2] C. Sharples, "Geoconservation in forest management – principles and procedures," Tasforests, Forestry Tasmania, Hobart, vol. 7, pp. 37 – 50, Dec. 1995.

[3] G. Dixon, "Geoconservation: An International Review and Strategy for Tasmania; A Report to the Australian Heritage Commission, Occasional Paper no. 35, Parks & Wildlife Service, Tasmania, 1996.

[4] AHC, "Australian Natural Heritage Charter for the Conservation of Places of Natural Heritage Significance; Australian Heritage Commission in association with Australian Committee for IUCN," Sydney (2nd Edition; first edition 1996).

[5] M. Gray, "Geodiversity: valuing and conserving abiotic nature," Wiley, Chichester, pp. 434, 2004.

[6] T.A. Hose, S. Markovic, B. Komac and M. Zorn, "Geotourism: A short introduction," Acta Geographica Slovenica, vol. 51, no. 2, pp. 339 – 341, 2011. https://doi.org/10.3986/AGS51301

[7] R.K. Dowling, "Geotourism's global growth. Geoheritage," vol. 3, pp. 1 – 13, 2011. https://doi.org/10.1007/s12371-010-0024-7

[8] T.A. Hose and D. Vasiljevic, "Defining the Nature and Purpose of Modern Geotourism with Particular Reference to the United Kingdom and South-East Europe," Geoheritage, vol. 4, no. 25, pp. 25 – 43, 2012. https://doi.org/10.1007/s12371-011-0050-0

[9] T.A. Hose, "3G's for modern geotourism," Geoheritage, vol. 4, no. 1–2, pp. 7 – 24, 2012. https://doi.org/10.1007/s12371-011-0052-y

[10] A. Ghosh and B. Bera, "Landform classification and geomorphological mapping of the Chota Nagpur Plateau, India", Quaternary Science Advances, vol. 10, 2023. https://doi.org/10.1016/j.qsa.2023.100082

[11] V.S. Kale (Geomorphosites and Geoheritage Sites in India, In: V. S. Kale (ed.), Landscapes and Landforms of India, World

Geomorphological Landscapes, Springer, 2014. DOI: 10.1007/978-94-017-8029-2_27.

[12] E. Reynard, "Geosites–In: A.S. Goudie (ed.): Encyclopedia of Geomorphology," Routledge, pp. 440, 2004.

[13] C.S. Raja Rao, "Coal resources of Bihar (excluding Dhanbad District)," Bulletin Geological Survey India Series, vol. 45, no. IV, pp. 300 – 332, 1987.

[14] R.S. Tiwari and A. Tripathi, "Palynological assemblages and absolute age relationship of Intertrappean beds in the Rajmahal Basin, India," Cretaceous Research, vol. 16, pp. 53 – 72, 1995.

[15] A. Tripathi, "Palynochronology of Lower Cretaceous volcano-sedimentary succession of the Rajmahal formation in the Rajmahal Basin, India," Cretaceous Research, vol. 29, pp. 913 – 924, 2008.

[16] V. Ball, "Geology of the Rajmahal Hills," Memoir Geological Survey India, vol. 13, pp. 155 – 248, 1877.

[17] A. Saxena, M.M. Khan, N. Raychowdhury and K.J. Singh, "Early Permian macroCoral diversity in Indian Gondwana: Evidence from Talchir Formation of Singrauli coalfield, Son–Mahanadi valley basin, central India," J. Earth Syst. Sci., vol. 131, 2022. https://doi.org/10.1007/s12040-021-01805-w

[18] J.W. Lee and T. Brahmasrene, "Tourism effects on the environment and economic sustainability of sub-Saharan Africa," International Journal of Sustainable Development & World Ecology, vol. 23, no. 3, pp. 221 – 232, 2015. https://doi.org/10.1080/13504509.2015.1114976

[19] H. Hui-Chuan and K.M. Hua, "A Study on Tourist Satisfaction in Sanyi," International Journal of Innovation, Management and Technology, vol. 5, no. 4, pp. 244 – 248, 2014. DOI: 10.7763/IJIMT.2014.V5.521

[20] K. Datta, "Application of SWOT-TOWS Matrix and Analytical Hierarchy Process (AHP) in the Formulation of Geoconservation and Geotourism Development Strategies for Mama Bhagne Pahar: An Important Geomorphosite in West Bengal, India," Geoheritage, vol. 12, no. 45, 2020. https://doi.org/10.1007/s12371-020-00467-2

[21] L.L.S. O'Malley, "Bengal District Gazetteers: Birbhum," Calcutta: The Bengal Secretariat Book Depot, 1910.

[22] K. Datta and S. Sarkar, "Calculation of area, mapping and vulnerability assessment of a geomorphosite from GPS survey and high resolution Google Earth satellite image: a study in Mama Bhagne Pahar, Dubrajpur C. D. block, Birbhum district, West Bengal," Spat Inf Res, vol. 27, pp. 521 – 528, 2019. https://doi.org/10.1007/s41324-019-00249-1

[23] D.L. Linton, "The problem of tors," The Geogr J, vol. 121, pp. 470 – 487, 1955. https://www.jstor.org/stable/1791756

[24] M. Brocx and V. Semeniuk, "Geoheritage and geoconservation: History, definition, scope and scale," Journal of the Royal Society of Western Australia, vol. 90, pp. 53 – 87, 2007.

[25] B. Saha, "Amkhoi Geopark: Geotourism and Socio-economic Development of the Rural Areas of Chaupahari Forest and Adjoining Area, Birbhum, West Bengal, India," The Nucleus, vol.60, no. 1, pp. 71 – 77, 2023.

[26] B. Saha, "Geotourism in and Around the Hot Springs of Bakreswar, West Bengal, India," International Journal of Research and Analytical Reviews, vol. 6, no. 2, pp. 812 – 822, 2019.

The Nucleus ***60***, *No. 2 (2023) 168-173*

www.thenucleuspak.org.pk

The Nucleus

ISSN 0029-5698 (Print)
ISSN 2306-6539 (Online)

Hydrothermal Synthesis and Structural Characterization of $BaTiO_3$ Powder

Muhammad Farhan Mehmood[1,2*], Amir Habib[1,3]

[1]*Department of Materials Engineering, School of Chemical and Materials Engineering (SCME), National University of Sciences and Technology (NUST), Islamabad, Pakistan*

[2]*Department for Nanostructured Materials, Jožef Stefan Institute, Jamova cesta 39, SI-1000 Ljubljana, Slovenia*

[3]*Physics Department, University of Hafar al Batin, Hafar al Batin-39524, Saudi Arabia*

ABSTRACT

The main purpose of the present study was to synthesize and characterize the structural morphology of barium titanate ($BaTiO_3$) powder. The synthesis of $BaTiO_3$ powder was carried out by hydrothermal process using barium hydroxide ($Ba(OH)_2$) and titanium dioxide (TiO_2) as precursors in a high-pressure stirred reactor autoclave for a 7-hour reaction time at various temperatures (100, 150 and 180 °C). The physical appearance of the synthesized $BaTiO_3$ powder was white crystalline. X-ray diffraction (XRD), Raman spectroscopy, and scanning electron microscopy (SEM) were used to characterize the $BaTiO_3$ powder. Raman spectroscopy and XRD techniques confirm the formation of cubic-phase $BaTiO_3$. Raman peaks at 305 and 516 cm^{-1} confirmed the formation of $BaTiO_3$. SEM micrographs showed different shapes and a highly dispersed size distribution of particles. The crystal structure of $BaTiO_3$ powder changed as the reaction temperature changed during the synthesis process. The morphological properties of the $BaTiO_3$ powder prepared at 100 °C clearly indicated spherical, irregular, and cubic rod-like structures. The particle size of $BaTiO_3$ powder was very fine at higher reaction temperatures of 150 and 180 °C. Cubic-phase $BaTiO_3$ was obtained in all the synthesized samples. Barium carbonate ($BaCO_3$) and residual unreacted TiO_2 phases as impurities were detected in the $BaTiO_3$ powder. The purity of $BaTiO_3$ powder was high at 180 °C under these synthesis conditions.

Keywords: *Cubic Phase, Powder, Hydrothermal Synthesis, X-ray Diffraction, Raman Spectroscopy, Scanning Electron Microscopy*

1. Introduction

Barium titanate ($BaTiO_3$) is the most widely used perovskite structure ceramic material due to its excellent dielectric, piezoelectric, pyroelectric, and ferroelectric properties. It has commercial applications in piezoelectric and optoelectronic devices, pyroelectric sensors, lasers, nonlinear optical devices, image processing, pattern recognition, dielectric amplifiers, and manufacturing of multilayer ceramic capacitors (MLCs) due to the high dielectric constant and low dielectric loss [1-3]. $BaTiO_3$ nanoparticles showed antibacterial activity [4] and therapeutic applications such as cancer therapy and drug delivery due to their biocompatibility [5-9]. The demand of non-conducting dielectric ceramic materials is increasing continuously and attempts are being made to reduce the size of communication devices as much as possible. Barium titanate ($BaTiO_3$) has become more and more important in ceramic materials due to its high dielectric constant and photocatalytic characteristics.

For the synthesis of high-purity $BaTiO_3$ powder, various chemical methods were used, such as barium tetanyl oxalate [10, 11] hydrolysis of barium titanium alkoxide [12, 13], co-precipitation [14-16], one-step sol-gel [17-19], molten salt [20] and hydrothermal process [21-26]. Hydrothermal synthesis process proceeds in a strong alkaline solution to prepare high-purity homogeneous and ultrafine $BaTiO_3$ powder at low-temperature (60-180 °C) chemical reactions. This process involves the chemical reaction of barium hydroxide ($Ba(OH)_2$) or barium chloride ($BaCl_2{\cdot}2H_2O$), or barium acetate ($C_4H_6BaO_4$) as barium (Ba) source and titanium dioxide (TiO_2), titanium tetrachloride ($TiCl_4$) or titanium alkoxide ($C_{12}H_{28}O_4Ti$) as titanium (Ti) source at 85-250 °C during a couple of hours reaction time. The reaction temperature has a pronounced effect on the synthesis of $BaTiO_3$ [27-30]. The formation of $BaTiO_3$ at room temperature was not experimentally observed even after 12 12-hour reaction time due to slow kinetics. $BaTiO_3$ (pseudo-cubic phase) was produced at 60 ºC and above with a small amount of $BaCO_3$ as the secondary phase [31]. This method has been widely used for the synthesis of $BaTiO_3$ powders, nanotabulars, and nanowires. The formation of cubic or tetragonal phase $BaTiO_3$ depends on temperature, the presence of counter-anions, and the characteristics of powders (size of crystallites and presence of defects) [32]. The present study is focused on synthesizing nanosized $BaTiO_3$ powder using a hydrothermal process in a stirred reactor autoclave at various reaction temperatures.

2. Experimental

Titanium dioxide powder (TiO_2; >99.90%, Merck) and barium hydroxide octahydrate ($Ba(OH)_2{\cdot}8H_2O$; 98%; Sigma-Aldrich) were used for the synthesis of $BaTiO_3$ nanopowder. Formic acid (HCOOH; 85%; Merck) was used to wash the synthesized $BaTiO_3$ powder. All the chemicals were reagent-grade and used without further purification.

For hydrothermal synthesis of $BaTiO_3$ powder, a weight of 19.0 g $Ba(OH)_2{\cdot}8H_2O$ and 3.40 g TiO_2 powder were mixed in a 250-mL Teflon reaction vessel containing 60 mL deionized water. The Teflon reaction vessel was kept in a laboratory high-pressure stirred autoclave (Model limbo li, Büchi AG, Switzerland) to operate at 100, 150 and 180 °C for 7 hours with a stirring speed of 60 rpm. After the hydrothermal reaction, the contents of the Teflon vessel were cooled to room temperature and the soluble impurities and adsorbed ions were removed with a dilute (0.25 M) formic acid solution (9.50 mL of 85% formic acid in 250 ml deionized water). The contents of the

*Corresponding author: mehmood.mfarhan@gmail.com

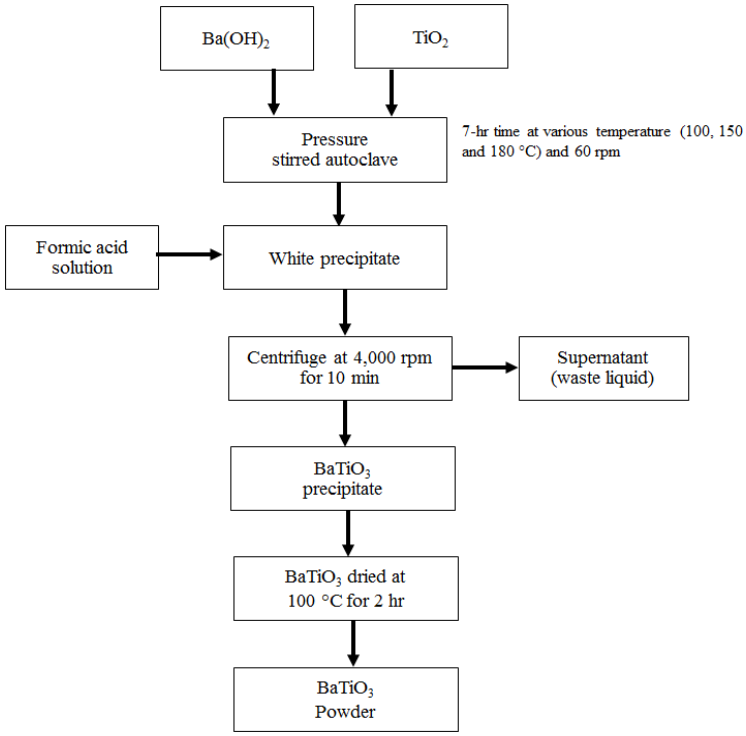

Fig. 1: Flow chart of the step-wise procedure for the synthesis of BaTiO3 powder by hydrothermal process

Teflon reaction vessel were transferred into centrifuge bottles to separate the $BaTiO_3$ precipitate. After centrifugation at 4,000 rpm for 10 min, the supernatant was decanted and the yellowish-white precipitate was washed initially with a dilute formic acid solution and then with deionized water. Finally, the washed precipitate and residue were dried in an oven at 100 °C for 2 hours.

The structural properties of the $BaTiO_3$ powder samples were characterized by X-ray diffraction (Bruker D8 Advance X-ray Diffractometer, Germany). A scanning electron microscope (Model JEOL JSM-6490A, Japan) was used to characterize the microstructure and particle morphology of $BaTiO_3$ powders. The powder samples were mounted on Cu stubs and sputter-coated with Au for 90 s using JFC-1500 ion sputtering device operated at an accelerating voltage of 20 kV. The Raman spectra of $BaTiO_3$ powders were recorded using a Micro Raman Spectrophotometer (Dongwoo Optron Co., Ltd. Korea) with a laser (532 nm) power of 150 mW equipped with a CCD detector and monochromator M320. The flow chart of the hydrothermal process of $BaTiO_3$ powder is shown in Fig. 1.

3. Results and Discussion

3.1 Synthesis of $BaTiO_3$ powders

Barium titanate ($BaTiO_3$) powders were prepared using a stirred-reactor autoclave using 19.0 g $Ba(OH)_2 \cdot 8H_2O$ and 3.40 g TiO_2 powder as precursors in 250-ml Teflon reaction vessel containing 60-ml deionized water at 100, 150, and 180 °C for 7-hour reaction time by the hydrothermal method according to the following chemical reactions:

$$Ba(OH)_2 \leftrightarrows Ba^{2+} + 2OH^- \quad (1)$$

$$TiO_2 \cdot nH_2O + 2OH^- \leftrightarrows Ti(OH)_6^{2-} + (n-2)H_2O \quad (2)$$

$$Ba^{2+} + Ti(OH)_6^{2-} \leftrightarrows BaTiO_3 + 3H_2O \quad (3)$$

According to the above chemical reaction equilibrium, an increase in OH^- and Ba^{2+} ion concentration resulted in the formation of $BaTiO_3$ products (equations 2 and 3). An increase in the Ba-to-Ti ratio as precursors during the synthesis process resulted in the formation of $BaTiO_3$. So, the overall net chemical reaction for $BaTiO_3$ synthesis is described below:

$$Ba(OH)_2 + TiO_2 \rightarrow BaTiO_3\,(\text{crystallite}) + H_2O \quad (4)$$

The formation of $BaTiO_3$ (equation 4) is controlled by the solubility of $Ba(OH)_2$. If the limit of solubility of $Ba(OH)_2$ is reached before completion, the reaction stops and the yield is stabilized [33]. The hydrothermal process involves a simple chemical reaction between $Ba(OH)_2$ and TiO_2 in an aqueous solution in a stirred autoclave to produce $BaTiO_3$ precipitate and water. The kinetics of $BaTiO_3$ formation from $Ba(OH)_2$ and TiO_2 were studied by Hertl [30], reporting that Ba^{2+} or $Ba(OH)^+$ ions react chemically with titanium precursors to form $BaTiO_3$ by heterogeneous nucleation on its surface. The hydroxide ions (OH^{-1}) play a vital role in the nucleation of $BaTiO_3$ crystals and act as a catalyst by promoting the growth of $BaTiO_3$ under hydrothermal conditions [34]. The dynamic nature of the interaction between TiO_2, $Ba^{2+,}$ and OH^{-1} leads to a crystallization mechanism involving nucleation, growth, and crystal dissolution. The role of OH^{-1} could be to facilitate the hydrolysis of Ti-O-Ti bonds [35].

3.2 *Characterization of $BaTiO_3$ powder*

The typical XRD patterns of the $BaTiO_3$ powders synthesized at 100, 150, and 180 °C are shown in Fig. 2. The XRD patterns of $BaTiO_3$ powders exhibited that X-ray diffraction peak intensities at 2Θ = 22.00° (100), 31.35° (110), 38.65° (111), 44.95° (200) and 55.80° (211) increased with an increase in reaction temperature during synthesis process (Fig. 2).

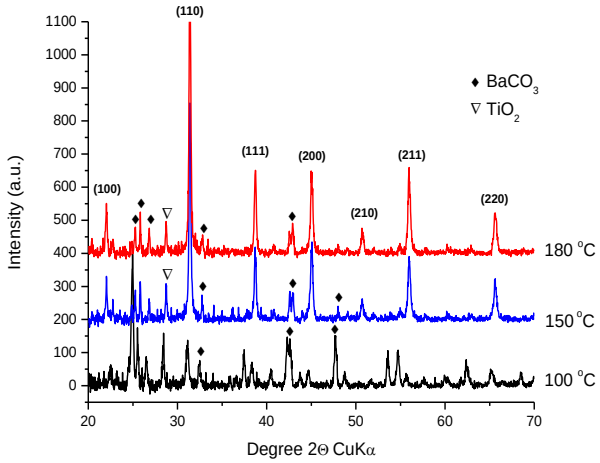

Fig. 2: XRD patterns of $BaTiO_3$ powder synthesized at 100, 150 and 180 °C by the hydrothermal process.

The unit cell parameter for the crystalline $BaTiO_3$ was determined to be a=3.994 Å and c=4.035 Å, which fit well with the peak positions of standard cubic-phase $BaTiO_3$ [JCPDS no. 01-089-1428]. It is clear that the X-ray diffraction peak (110) becomes sharper and stronger with an increase in reaction temperature. When the reaction temperature increased from 100 °C to 150 °C and then 180 °C, the XRD patterns became sharp-edged, which represents the crystallinity of $BaTiO_3$ powders. The temperatures higher than about 130 °C (Curie temperature), $BaTiO_3$ exists in the cubic perovskite structure. In this crystal structure, the Ba^{+2} ions occupy the corners of the elementary cell, the Ti^{+4} ions are in the volume center and the O^{-2} ions are in the surface center. Below the Curie point, the crystal structure transforms from the cubic phase to the distorted tetragonal structure with a displacement of the center of positive and negative charges within the sub-lattice [35]. The crystallinity of $BaTiO_3$ (cubic) was estimated by measuring the XRD intensities of cubic $BaTiO_3$ (100) peak at 2Θ = 22.160 ° with few by-products of $BaCO_3$ [36]. The XRD patterns of $BaTiO_3$ powders synthesized at 100, 150, and 180 °C clearly showed shifting of reflections around 2Θ = 45° (200) (Fig. 3). XRD patterns exhibited an appreciable increase in peak intensities and small shifting of peak positions at 150 and 180 °C that presumably due to small particle size, which confirmed the cubic structure of $BaTiO_3$ powder. The single peak reflection around 2Θ = 45° (200) region matched well with the typical XRD peaks of cubic $BaTiO_3$ [37].

The presence of $BaCO_3$ and unreacted TiO_2 phases was also identified in the products as impurities (Fig. 2). The concentration of $BaCO_3$ in the product decreased with the increase in reaction temperature (Fig. 4). Newalkar et al. [32] reported the formation of barium carbonate ($BaCO_3$) as a

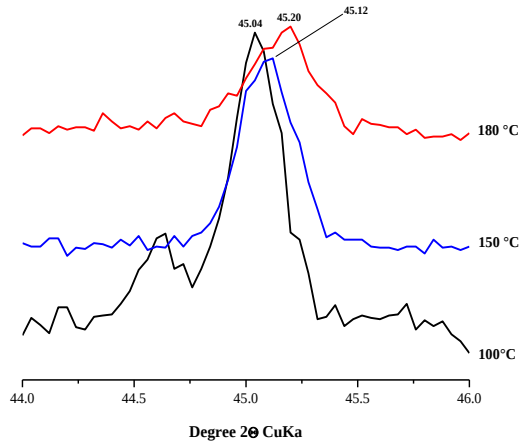

Fig. 3: XRD pattern of $BaTiO_3$ powders synthesized at 100, 150, and 180 °C showing clear reflections (200) of the cubic phase $BaTiO_3$

minor impurity in $BaTiO_3$ powder synthesized in the temperature range of 60-160 °C during the microwave hydrothermal process. Guo et al. [21] observed that the grain size of $BaTiO_3$ powder increased due to the agglomeration of fine particles with the increase in reaction time during the microwave hydrothermal process. $BaTiO_3$ crystallizes in the perovskite structure as a cubic lattice with barium ions occupying the corners of the unit cell, oxide ions occupying the face centers, and titanium ions occupying the centers of the unit cells. $BaTiO_3$ has a cubic structure above 120 °C.

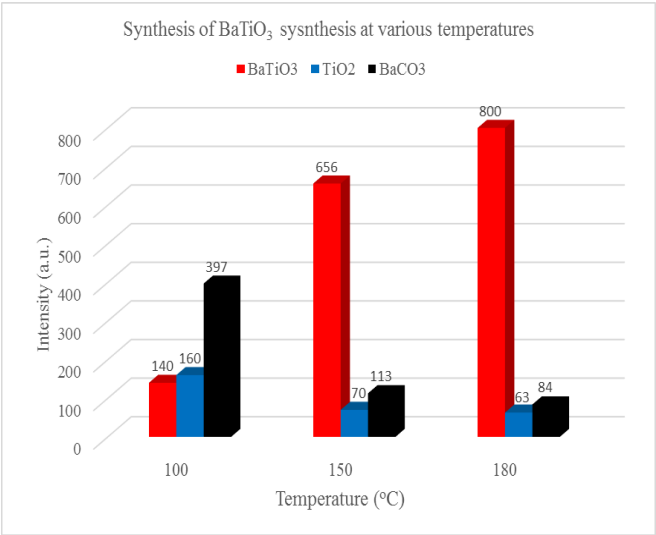

Fig. 4: XRD peak intensities show concentrations of $BaTiO_3$, $BaCO_3$, and unreacted TiO_2 in $BaTiO_3$ powders synthesized at 100, 150 and 180 °C by hydrothermal processes.

Barium carbonate ($BaCO_3$) might be decomposed to barium oxide (BaO) and carbon dioxide (CO_2) at a higher reaction temperature during the hydrothermal process and its reaction with TiO_2 could produce $BaTiO_3$, as stated by the following chemical reactions:

$$BaCO_3 \rightarrow BaO + CO_2 \quad (5)$$

$$BaO + TiO_2 \rightarrow BaTiO_3 \quad (6)$$

The decomposition reaction of $BaCO_{3\,(solid)} = BaO_{\,(solid)} + CO_{2\,(gas)}$ was investigated by thermogravimetric analysis (TGA) and differential thermal analysis (DTA) methods [38]. Nanocrystalline $BaTiO_3$ was prepared by solid-state reaction of TiO_2 with $BaCO_3$ of different particle sizes (650, 140, and 50 nm) [39].

The Raman scattering spectra of the $BaTiO_3$ powders synthesized at 100, 150, and 180 °C are shown in Fig. 5. The frequency range covered is from 100-1000 cm^{-1}. Raman spectra clearly showed sharp bands at 145, 160, 197, 397, 516, and 637 cm^{-1}, a sharp small band at 980 $cm^{-1,}$ and two small broad bands at 305 and 797 cm^{-1} in all the products (Fig. 5). Two broad shoulder bands at 792 and 984 cm^{-1} are also appeared in the sample obtained at 7-hour reaction time. It is clear from the Raman spectra of both samples that they contained bands of predominantly cubic-phase $BaTiO_3$ identified by the bands around 166, 196, 394, 512, and 636 cm^{-1}. It was observed that the peak intensities decreased with an increase in the reaction temperature of the synthesis process. The frequencies near 190 and 516 cm^{-1} modes come from the *F*1u cubic phase modes, the 303 cm^{-1} mode comes from the breaking of the cubic silent *F*2u mode [33]. Ávila et al. [34] suggested that the peaks at 639, 396, and 144 cm^{-1} correspond to the anatase shape of TiO_2.

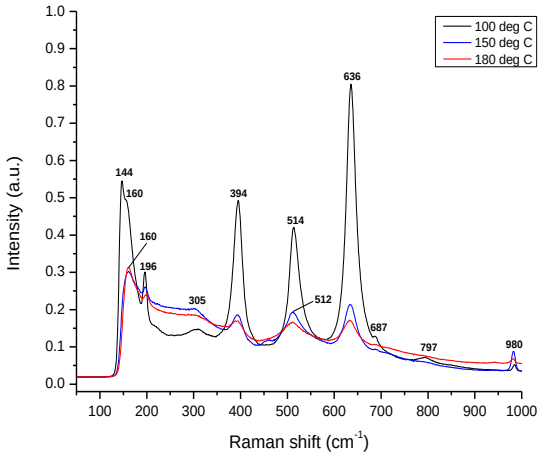

Fig. 5: Raman spectrum of $BaTiO_3$ powder prepared at 100, 150, and 180 °C by hydrothermal process. ∗ = denotes Raman peaks at 305 and 516 cm^{-1}, which correspond to $BaTiO_3$.

The experimental data shows that the chemical reaction between $Ba(OH)_2$ and TiO_2 was incomplete after 7-hour reaction time. The presence of unreacted TiO_2 coexisted in all the synthesized $BaTiO_3$ powders (Fig. 4). The concentration of unreacted TiO_2 corresponding to peak intensities decreased with an increase in reaction temperature during the synthesis process. Frey and Payne [37] suggested that the spectral peak at 193-195 cm^{-1} represents the existence of an orthorhombic $BaTiO_3$ phase. In this study, the Raman spectra showed a sharp band around 195-198 cm^{-1} in $BaTiO_3$ powders. The Raman spectra clearly showed the cubic distortion of $BaTiO_3$ structure coexisting with unreacted TiO_2 at 394 and 635 cm^{-1}. Raman bands near 630 cm^{-1} correspond to $BaCO_3$ phase, anatase TiO_2, or hexagonal $BaTiO_3$, which is stabilized at room temperature by high surface energy [40-42]. Cubic phase $BaTiO_3$ showed Raman spectrum at 166, 196, 394, 512, and 636 cm^{-1} [43]. It is clear from the Raman spectra that the synthesized powders contained bands of predominantly cubic phase $BaTiO_3$ at 166, 196, 394, 512, and 636 cm^{-1}. The intense Raman spectra near 144, 394, 514, and 636 cm^{-1} correspond to unreacted anatase TiO_2 phase in the $BaTiO_3$ powders as an impurity which is attributed to the increase of peak intensities near 394, 514, and 636 cm^{-1} due to coexistence with cubic phase $BaTiO_3$ spectral lines (Fig. 5).

SEM micrographs of $BaTiO_3$ powders are shown in Fig. 6. The $BaTiO_3$ particles showed irregular, sphere-like, cube-like particles and cube-rod structures. The average particle sizes of $BaTiO_3$ powders are 38-92, 45-63, and 28-52 nm at 100, 150, and 180 °C, respectively. The shape and particle size distribution in $BaTiO_3$ powder showed agglomeration due to nano-sized particles. $BaTiO_3$ powders synthesized at 100 °C appeared heterogeneous morphology (cube, hexagonal and rod-shaped) (Fig. 6A), whereas powder synthesized at 150 °C appeared to be very uniform spherical morphology (Fig. 6B) and cube-shaped (Fig. 6C).

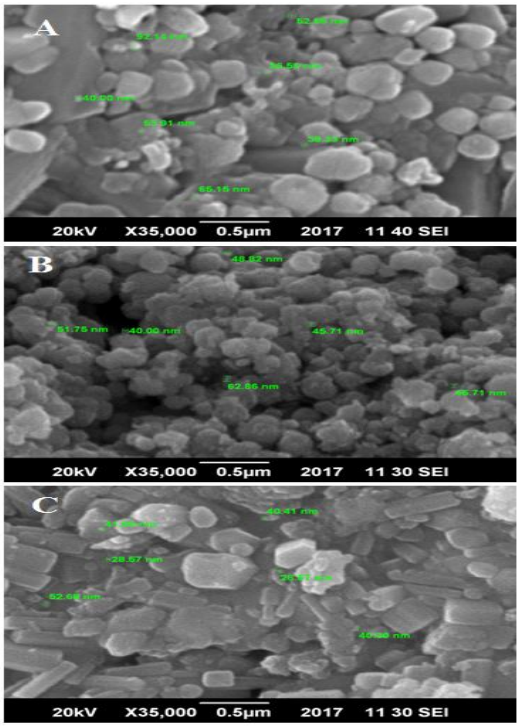

Fig. 6: SEM micrographs of $BaTiO_3$ powders synthesized at 100 °C (A), 150 °C (B), and 180 °C (C) by hydrothermal process

4. Conclusions

Hydrothermal method is the most promising route to synthesize ceramic oxide powders with controlled morphology, and high crystallinity in a one-step process. XRD and Raman spectroscopy data revealed that cubic-phase $BaTiO_3$ powders were successfully synthesized by hydrothermal processes. It is clear that cubic-phase $BaTiO_3$ nanocrystalline powder was directly crystallized by using $Ba(OH)_2{\cdot}8H_2O$ to TiO_2 at a ratio of (4:1) as a starting material in a stirred reactor autoclave by hydrothermal process. The hydrothermal synthesis process offers a promising approach to producing high-purity crystalline $BaTiO_3$ powder.

Acknowledgments

The authors are very grateful to the Department of Materials Engineering, School of Chemical and Materials Engineering (SCME), NUST, Islamabad, for assistance of scanning electron microscopy and NILOP for Raman Spectroscopy.

References

[1] Q. Feng, M. Hirasawa, K. Yanagisawa, "Synthesis of crystal-axis-oriented $BaTiO_3$ and anatase platelike particles by a hydrothermal soft chemical process," Chemistry of Materials, vol. 13, pp. 290-296, 2001.

[2] W.L. Suchanek, R.E. Rimen, "Hydrothermal synthesis of advanced ceramic powders," Advances in Science & Technology, vol. 45, pp. 184-193, 2006.

[3] M.M. Vijatović, J.D. Bobić, B.D. Stojanović, "History and challenges of barium titanate: Part II," Science of Sintering, vol. 40, pp. 235-244, 2008.

[4] A.A. Shah, A. Khan, S. Dwivedi, J. Musarrat, and A. Azam, "Antibacterial and antibiofilm activity of barium titanate nanoparticles," Materials Letters, vol. 229, pp. 30-133, 2018.

[5] M. Ahamed, M.J. Akhtar, M.A.M. Khan, H.A. Alhadlaq, and A. Alshamsan, "Barium titanate ($BaTiO_3$) nanoparticles exert cytotoxicity through oxidative stress in human lung carcinoma (A549) cells," Nanomaterials, vol. 10, Article No. 2309, 2020.

[6] T.M. Alfareed, Y. Slimani, M.A. Almessiere, M. Nawaz, F.A. Khan, A. Baykal, E.A. Al-Suhaimi, "Biocompatibility and colorectal anti-cancer activity study of nanosized $BaTiO_3$ coated spinel ferrites," Scientific Reports, vol. 12, Article No. 14127, 2022.

[7] M. Fakhar-e-Alam, S. Saddique, N. Hossain, A. Shahzad, Inaam Ullah, A. Sohail, M.J.I. Khan, and M. Saadullah, "Synthesis, characterization and application of $BaTiO_3$ nanoparticles for anti-cancer activity," Journal of Cluster Science, vol. 34, pp. 1745-1755, 2023.

[8] Y.N. Yoon, D.S. Lee, H.J. Park, and J-S. Kim, "Barium titanate nanoparticles sensitise treatment-resistant breast cancer cells to the antitumor action of tumour-treating fields," Scientific Reports, vol. 10, Article No. 2560, 2020.

[9] G.G. Genchi, A. Marino, A. Rocca, V. Mattoli, and G. Ciofani, "Barium titanate nanoparticles: promising multitasking vectors in nanomedicine," Nanotechnology, vol. 27, 232001, 2016.

[10] K. Hur, J. Lee, "Method for preparing $BaTiO_3$ powder by oxalate synthesis," United State Patent US6, 692, 721, B2, 2004.

[11] N.B. Mahmood, and E.K. Al-Shakarchi, "Three techniques used to produce $BaTiO_3$ fine powder," Journal of Modern Physics, vol. 2, pp. 1420-1428, 2011.

[12] M. Zeng, N. Uekawa, T. Kojima, and K. Kakegawa, "Formation process of $BaTiO_3$ particles by reaction between barium hydroxide aqueous solution and titania obtained by hydrolysis of titanium alkoxide," Journal of Materials Research, vol. 22, issue 8, pp. 2631-2638.

[13] T.M. Stawski, S.A. Veldhuis, R. Besselink, H.L. Castricum, G. Portale, D.H.A. Blank, and J.E. ten Elshof, "Nanostructure development in alkoxide-carboxylate-derived precursor films of barium titanate," The Journal of Physical Chemistry C, vol. 116, pp. 425-434, 2012.

[14] J.M. Hwu, W.H. Yu, W.C. Yang, Y.W. Chen, and Y.Y. Chou, "Characterization of dielectric barium titanate powders prepared by homogeneous precipitations chemical reaction for embedded capacitor applications," Materials Research Bulletin, vol. 40,issue. 10, pp. 1662-1679, 2005.

[15] M.Z.-C. Hu, G.A. Miller, E.A. Payzant, and C.J. Rawn, "Homogeneous (co)precipitation of inorganic salts for synthesis of monodispersed barium titanate particles," Journal of Materials Science, vol. 35, pp. 2927-2936.

[16] C.-J. Huang, K.-L. Chen, P.-H. Chiu, P.-W. Sze, and Y.-H. Wang, "The novel formation of barium titanate nanodendrites," Journal of Nanomaterials, vol. 2014, Article ID 718918, 6 pages, 2014.

[17] K.-M. Hung, W.-D. Yang, and C.-C. Huang, "Preparation of nanometer-sized barium titanate powders by a sol-precipitation process with surfactants," Journal of the European Society, vol. 23, issue 11, pp. 1901-1910, 2003.

[18] G. Pfaff, "Sol-gel synthesis of barium titanate powders of various compositions," Journal of Materials Chemistry, vol. 2, issue 6, pp. 591-594, 1992.

[19] A. Kareiva, S. Tautkus, and R. Rapalaviciute, "Sol-gel synthesis and characterization of barium titanate powders," Journal of Materials Science, vol. 34, pp. 4853-4857, 1999.

[20] S Ahda, S Misfadhila, P Parikin, and T.Y.S. P Putra, "Molten salt synthesis and structural characterization of $BaTiO_3$ nanocrystal ceramics," IOP Conference Series: Materials Science and Engineering, vol. 176, Article No. 012048, 2017.

[21] L. Guo, H. Luo, J. Gao, L. Guo, and J. Yang, "Microwave hydrothermal synthesis of barium titanate powders," Materials Letters, vol. 60, issue 24, pp. 3011-3014, 2006.

[22] İ.C. Kaya, V. Kalem, H. Akyildiz, "Hydrothermal synthesis of pseudocubic $BaTiO_3$ nanoparticles using TiO_2 nanofibers: Study on photocatalytic and dielectric properties," Applied Ceramic Technology, vol. 16, issue 4, pp. 1557-569, 2019.

[23] H. Chen, J. Wang, X. Yin, C. Xing, J. Li, H. Qiao, and F. Shi, "Hydrothermal synthesis of $BaTiO_3$ nanoparticles and role of PVA concentration in preparation, "Materials Research Express, vol. 6, No. 5, 055028, 2019.

[24] J. Moon, E. Suvaci, A. Morrone, S.A. Costantino, and J.H. Adair, "Formation mechanisms and morphological changes during the hydrothermal synthesis of $BaTiO_3$ particles from a chemically modified, amorphous titanium (hydrous) oxide precursor," Journal of the European Society, vol. 28, issue 12, pp. 2153-2161.

[25] S.W. Lu, B.I. Lee, Z.L. Wang, and W.D. Samuels, "Hydrothermal synthesis and structural characterization of $BaTiO_3$ nanocrystals," Journal of Crystal Growth, vol. 219, issue 3, pp. 269-276, 2000.

[26] X. Zhua, J. Zhua, S. Zhoua, Z. Liua, N. Minga, and D. Hesseb, "$BaTiO_3$ nanocrystals: Hydrothermal synthesis and structural characterization,: Journal of Crystal Growth, vol. 283, issues 3-4, pp. 553-562, 2005.

[27] S. Zhigang, Z. Weiwei, C. Jianfeng, and J. Yun, "Low temperature one step synthesis of barium titanate: Particle formation mechanism and large-scale synthesis," Chinese Journal of Chemical Engineering, vol. 14, issue 5, pp. 642-648, 2006.

[28] R. Asiaie, W. Zhu, S.A. Akbar, and P.K. Dutta, "Characterization of submicron particles of tetragonal $BaTiO_3$," Chemistry of Materials, vol. 8, issue 1, pp. 226-234, 1996.

[29] P. Pinceloup, C. Courtois, A. Leriche, and B. Thierry, "Hydrothermal synthesis of nanometer-sized barium titanate powders: Control of barium/titanium ratio, sintering, and dielectric properties," Journal of American Ceramic Society, vol. 82, issue 11, pp. 3049-3056, 1999.

[30] W. Hertl, "Kinetics of barium titanate synthesis," Journal of the American Ceramic Society, vol. 71, pp. 879-883, 1988.

[31] M.M. Lencka, and E. Riman, "Thermodynamic modeling of hydrothermal synthesis of ceramic powders," Chemistry of Materials, vol. 5, issue 1, pp. 61-70, 1993.

[32] B.L. Newalkar, S. Komarneni, and H. Katsuki, "Microwave-hydrothermal synthesis and characterization of barium titanate

powders," Materials Research Bulletin, vol. 36, issue 13-14, pp. 2347-2355, 2001.

[33] Z. Lazarević, N. Romćević, M. Vijatvić, N. Paunović, M. Romćević, B. Stojanović, and Z. Dohćević-Mitrović, "Characterization of barium titanate ceramic powders by Raman spectroscopy," Acta Physica Polonica A, vol. 115, pp. 808-810, 2009.

[34] H.A. Ávila, L.A. Ramajo, M.M. Rebreed, M.S. Castro, and R. Parra, "Hydrothermal synthesis of $BaTiO_3$ from different Ti-precursors and microstructural and electrical properties of sintered samples with submicrometric grain size," Ceramics International, vol. 37, pp. 2383-2390, 2011.

[35] R. Vijayalakshmi, and V. Rajendran, "synthesis and characterization of cubic $BaTiO_3$ nanorods via facile hydrothermal method and their optical properties," Digest Journal of Nanomaterials and Biostructures, vol. 5, issue 2, pp. 511-517, 2010.

[36] P. Nanni, M. Leoni, V. Buscagalia and G. Aliprandi, Low-temperature aqueous preparation of barium metatitanate powders," Journal of the European Ceramic Society, vol. 14, issue 1, pp. 85-90, 1994.

[37] M.H. Frey, and D.A. Payne, "Grain size effect on structure and phase transformations for barium titanate," Physical Review B, vol. 54, pp. 3158-3168, 1996.

[38] I. Arvanitidis, D. Sichen, and S. Seetharaman, "A study of the thermal decomposition of $BaCO_3$," Metallurgical and Materials Transactions B, vol. 27, pp. 409-416, 1996.

[39] M.T. Buscaglia, M. Bassoli, and V. Buscaglia, "Solid-state synthesis of ultrafine $BaTiO_3$ powders from nanocrystalline $BaCO_3$ and TiO_2," Journal of American Ceramic Society, vol. 88, issue 9, pp. 2374-2379, 2005.

[40] J. Yu, and J. Chu, "Encyclopedia of Nanoscience and Nanotechnology," vol. 6, pp. 389-416, 2004.

[41] Y. Shiratori, C. Pithan, J. Dornseiffer, R. Waser, "Raman scattering studies on nanocrystalline $BaTiO_3$," part I- isolated particles and aggregates," Journal of Raman Spectroscopy, vol. 38, pp. 1288-1299, 2007.

[42] Y.X. Gan, A.H. Jayatissa, Z. Yu, X. Chen, and M. Li, "Hydrothermal synthesis of nanomaterials, "Journal of Nanomaterials,' vol. 2020, Article ID 8917013, pp. 1-3, 2020.

[43] J.L. Parson, and L.Rimai, "Raman spectrum of $BaTiO_3$," Solid State Communications, vol. 5, pp. 423-427, 1967.

The Nucleus ***60***, *No. 2 (2023) 174-184*

www.thenucleuspak.org.pk

The Nucleus
ISSN 0029-5698 (Print)
ISSN 2306-6539 (Online)

Communication in Multi-Agent Reinforcement Learning: A Survey

Rimsha Khan*, Nageen Khan, Tauqir Ahmad

Department of Computer Science, University of Engineering and Technology, Lahore, Pakistan

ABSTRACT

Agents can use communication to coordinate their actions and achieve their goals. The agents in multi-agent reinforcement learning (MARL) have the ability to enhance their overall learning performance by acquiring communication skills. They can transmit various types of messages to either all agents or particular groups, utilizing diverse communication channels. Their study on MARL with communication (Comm-MARL) is expanding. Nonetheless, currently, there is no methodical approach to differentiate and categorize present Comm-MARL (Communication Multi-agent reinforcement learning) systems. This article surveys recent research in the Comm-MARL domain, scrutinizing diverse communication aspects that could be incorporated into MARL systems. Several dimensions are suggested to examine, establish, and contrast Comm-MARL systems. This paper presents a comprehensive review of the nine dimensions influencing communication in multi-agent collaboration. The dimensions explored include communication type, communication policy, communicated messages, message combination, inner integration, communication constraints, communication learning, training schemes, and controlled goals. By examining these dimensions, the study aims to shed light on the intricate dynamics of agent interaction in complex environments. This review emphasizes the significance of effective communication strategies in achieving common objectives among agents and highlights the importance of factors such as context awareness, adaptability, and learning from past experiences. The insights provided in this paper offer valuable guidance for enhancing collaboration and communication strategies across various multi-agent systems and applications.

Keywords: *Reinforcement Learning, Multiagent, Centralized, Decentralized, Concatenation, Observable Environment.*

1. Introduction

Multi-agent collaboration refers to the process of multiple agents working together to achieve a common goal or set of goals. Collaboration among agents involves communication, coordination, and cooperation, where agents exchange information and coordinate their actions to achieve a common goal [1]. The field of multi-agent systems has gained significance because of its numerous applications in recent years, in various domains such as robotics, self-directed vehicles, and communication networks. Multi-agent collaboration is a field of research that studies how multiple agents can work together to acquire a common objective. Agents can be anything from physical robots to software programs and they can be either cooperative or competitive. The term "collective intelligence" refers to the ability of a group of people to solve problems more effectively than any individual could. This is because when people collaborate, they can pool their knowledge, skills, and perspectives to come up with better solutions [2]. In order to be successful, agents must be able to overcome a number of challenges including:

(a) Asymmetry: Agents may have different capabilities, knowledge and goals.

(b) Non-stationary: The environment may change over time and agents must be able to adapt to these changes. **Opportunism:** Agents may try to exploit each other in order to achieve their own goals. Despite these challenges, multi-agent collaboration can be a powerful tool for solving complex problems. For example, multi-agent systems have been used to control robots in manufacturing, to coordinate traffic flow and to play games. The reinforcement learning paradigm known as "multi-agent reinforcement learning" [3] (MARL) relates to interaction with both the environment and each other, with the aim of acquiring knowledge and improving their ability to achieve their respective objectives.

MARL is a challenging problem due to the fact that agents must learn to coordinate their efforts to accomplish their goals, while also avoiding being exploited by other agents. Communication can be a powerful tool for improving the performance of MARL agents [4]. By communicating with each other, agents can share information about the environment, their goals, and their current state. This information can be used to coordinate actions, avoid collisions, and learn more quickly.

1.1 Tools and Technologies

Multi-agent collaboration can be aided by a variety of tools and technologies, including [5]:

1.1.1 Agent development environments

These environments provide developers with the tools and resources they need to create and test multi-agent systems.

1.1.2 Communication protocols

These protocols define how agents can communicate with each other.

1.1.3 Distributed databases:

These databases store information that is shared among agents.

1.1.4 Machine learning algorithms

These algorithms can be used to train agents to learn from their interactions and improve their performance over time.

1.1.5 Ontologies

These ontologies define the terms and relationships that are used by agents to communicate with each other.

*Corresponding author: rimshakhan642@gmail.com

1.1.6 Simulation environments

These environments allow developers to test multi-agent systems in a controlled environment.

1.1.7 Middleware Platforms

These platforms provide a framework for developing and deploying multi-agent systems.

1.2 Algorithms used

There are many different algorithms that can be used for multi-agent collaboration and the choice of algorithm will depend on the specific application and requirement. Some common algorithms for multi-agent collaboration include [1-6]:

1.2.1 Reinforcement learning

This algorithm can be used to enable agents to learn from their surroundings and improve their performance over time.

1.2.2 Game theory

This mathematical framework can be used to model strategic interactions among agents.

1.2.3 Distributed optimization

This class of algorithms can be used to optimize a global objective function in a decentralized manner.

1.2.4 Consensus Algorithms

This class of algorithms can be used to enable agents to agree on a common value or decision.

1.2.5 Auctions and market-based mechanisms

This class of algorithms can be used to enable agents to trade goods or services with each other.

1.2.6 Communication protocols

This class of algorithms can be used to enable agents to exchange information and coordinate their actions. Numerous real-world situations involve the interaction of multiple agents that have an impact on the shared environment. Illustrative instances are self-directed driving, sensor networks, robotics, and game playing. A possible approach to addressing these problems is MARL, in which agents use reinforcement learning (RL) approaches to grow cooperative, competitive, or hybrid cooperative and competitive behaviors.

Partial observability is a key presumption in MARL [5, 6] since agents are usually scattered across the environment. Agents in MARL cannot access the status of the entire environment instead they are limited to using just their local observations. Since each agent not only interacts with a dynamic environment but also is impacted by the changing and adapting policies of other agents, MARL is also prone to the non-stationary problem [7]. Among agents, communication can stabilize learning by conveying valuable information such as observations, intentions, or experiences. This allows agents to acquire a more comprehensive understanding and coordinate their behaviors effectively [8, 9]. The present study is centered on investigating how communication can be harnessed to enhance RL agents in an environment, with a particular emphasis on learnable communication protocols. Unlike fixed communication protocols that are predetermined, learnable communication protocols are the ones that agents can acquire through learning, rather than being provided with them beforehand.

This approach aligns with recent research that highlights the importance of dynamic and adaptable communication in MARL, involving the acquisition of knowledge on when, how, and what to communicate. To achieve this, advanced deep reinforcement learning techniques have been employed [10, 11].

Despite several surveys, there is an urgent need for a systematic and organized technique to distinguish and classify Comm-MARL systems according to research on MARL enhanced with communication (Comm-MARL) [12, 13]. The design and deployment of MARL systems would be made easier by the creation of such a methodology. Think about the scenario when our intention is to build a new Comm-MARL system for a specific task. The system can be characterized using various aspects.

When developing a Comm-MARL system, the following aspects should be considered:

i. Learning to determine with whom to communicate
ii. Learning to identify when communication is necessary
iii. Learning to select the relevant information to communicate
iv. Learning to integrate and combine received information
v. Learning to determine the learning goals that can be achieved through communication

By addressing these aspects, a Comm-MARL system can be developed that maximizes the effectiveness of communication between agents and enhances the overall learning performance. We propose a multidimensional structure consisting of 9 dimensions. By thoroughly analyzing and comparing these dimensions, we aim to provide insight into the creation and design of MARL systems with communication components. Recent Comm-MARL systems may be mapped into this framework to help us better grasp the state of the art and identify important directions for future system designs.

In Section 2 of our survey, we summarize recent advancements in Comm-MARL systems, highlighting the need for a structural methodology. In Section 3, we proposed recent works categorized according to each dimension. Finally, in Section 4, conclusions based on the proposed dimensions are presented.

2. Literature Review

The seminal works of CommNet, DIAL, and RIAL have enabled deep RL agents to learn to communicate with partial observations in cooperative games. In CommNet, local observations are processed by a shared neural network and each agent's decisions are influenced by a mean vector of messages (hidden layers) from other agents. Similarly, DIAL

uses a shared network and allows agents to learn to selectively attend to certain aspects of their observations and the received messages. Reinforced Inter-Agent Learning (RIAL) introduces a centralized critic that estimates the joint value of actions taken by all agents, which is then used to guide communication among agents. These works have demonstrated the effectiveness of communication in enhancing the functionality of RL agents in multi-agent environments. Three key works in the field of multi-agent reinforcement learning are the CommNet, DIAL, and RIAL. CommNet allows agents to process their local observations using a shared neural network and their decision depends on observations. RIAL and DIAL, on the other hand, allow each agent to learn to exchange a binary or real value message that is appropriate for brief exchanges of information. These works have paved the way for many recent works in the field, which follow the end-to-end training paradigm of integrating the learning of communication and environment policy [14, 15].

Recent works [15, 16] have addressed the limitations of fully connected communication and have explored more efficient and effective ways for agents to communicate with each other. Some of these works have introduced communication constraints, such as limited bandwidth or range, to more closely mimic real-world communication scenarios. Additionally, some works have proposed communication structures that are learned or adaptive, rather than predefined, allowing agents to better tailor their communication to the specific task at hand.

Earlier approaches used a mechanism that involved a gate for each agent to determine if they should send their messages or not. ATOC [16] introduces a communication method where only agents in a specific observable area are involved. Within this group, a bi-LSTM algorithm combines the messages from each agent and sends them back to the members. IC3Net [17], an extension of CommNet deterministically decides whether to send messages to all or none. Moreover, IC3Net assigns individualized rewards to each agent instead of globally shared rewards, leading to more diverse behaviors in competitive or mixed environments. ETCNet [18] also employs a gate mechanism, but it regularizes the overall probability. In I2C [19], the causal effect of whether to communicate with others in peer to peer [20] manner is measured.

The gate mechanism allows communication alternative approaches to prioritize communication chances in a more explicit and global manner. For example, a certain number of agents are chosen by SchedNet [20] and assimilated to distribute messages. A shared graph is assimilated by GA-COMM [21], MAGIC [22], and FlowComm [23] to decide if and with whom agents should interact. GA-Comm utilizes an attention mechanism to construct an undirected communication graph, allowing pairs of agents to communicate with each other. On the other hand, MAGIC and FlowComm create a directed graph among agents, allowing for more fine-grained control over communication, with connected agents being able to communicate unilaterally or bilaterally.

Certain works adopt preexisting relationships to convey information and comprehend the messages' meaning. The agent-entity graph [24] establishes links between agents by using a pre-trained graph. Then, linked agents exchange each other encoding. Based on networked multi-agent systems (NMAS) where dispersed agents are connected, network communication [25, 26] is based on the sparse, predefined communication network. In this approach, agents exchange explicit messages during both training and execution in an NMAS.

To decide on the content of messages, many works make use of local information. In some cases, this includes individual observations [27-29]while in others it includes intended actions or plans [30, 31]. To prevent the loss of information, received messages are often concatenated [32-34]. In addition, agents may attach signatures to their messages to indicate their importance.

TarMAC and IMMAC use different methods to assign weights to received messages. While IMMAC employs softmax, TarMAC utilizes an attention mechanism. Similarly, GAComm decides whether to communicate and to determine the importance of agents. In addition, GAComm incorporates a graph neural network (GNN) to compile messages. However, a neural network can also learn implicitly about the importance of messages. Bi-LSTM layers are used in another method called BiCNet to link policy and value functions. Agents can exchange messages and learn from each other's memory states in a collaborative multi-agent reinforcement learning (Comm-MARL) system. However, such systems need to address practical constraints such as costly communication and stochastic environments. To minimize communication overhead and contention, SchedNet [1, 35] selects to send messages to a shared communication channel. TMC [35] disallows agents from broadcasting similar messages and stores received messages in a buffer to compensate for missing messages.

Gated-ACML [36 , 37] introduces a two-step approach that aggressively removes messages. Similar to ATOC and IC3Net, the initial phase is studying a gate mechanism to determine whether to send messages or not. The second phase involves the assumption of a centralized message coordinator by Gated-ACML, who organizes the messages and distributes them to each agent. This strategy lessens communication overhead, as each agent theoretically only needs to communicate with the coordinator.

2.1 MARL system

Two methods [37] for coping with communication constraints in ETCNet use MARL. and variable-length coding. ETCNet computes an upper limit on the likelihood that agents can communicate at each time step and optimizes policies accordingly. In contrast, variable-length coding permits agents to control the quantity of bits they send out at any one moment. While both methods are effective in

enhancing the performance of MARL agents, ETCNet is computationally more demanding than variable-length coding.

3. Proposed dimensions

We aim to provide a systematic and structured approach to design Comm-MARL. We suggest that there are nine dimensions that may be used to describe Comm-MARL systems. Many aspects and the target issues are shown in Table 1. In the following subsections, recent works in Comm-MARL have been summarized and classified based on the proposed dimensions.

Table 1: Dimensions and their targeted problems

Dimensions	Targeted problems
Communication type	Which type of agents to communicate with?
Communication policy	When and how to build communication links among agents?
Communicated messages	Which piece of information to share?
Message combination	How to combine received messages?
Inner integration	How to integrate combined messages into learning models?
Communication constraints	How to fulfill realistic requirements?
Communication learning	How to train and improve communication?
Training schemes	How to utilize collected experience from agents?
Controlled goals	What kind of behaviors are desired to emerge with communication

3.1 Communicates Type

In Comm-MARL systems, the communicate type dimension refers to the classification of agents based on whether they communicate with each other directly or not. In the literature, this dimension has been classified into different categories.

Table 2: Category of communication type

Types	Sub types	Methods
Agents in the MAS	Nearby AGENTS	DGN[38];MAG-NET-SA-GS-MG[46]; AGENT-ENTITY GRAPH[29]; LSC[45]; NEURCOMM[32];IP[33];FLOWCOMM[14]; GAXNET[44]
	Other agents	DIAL[11];RIAL[11];COMMNET[12];BICNET[36];TARMAC[20];MADDPGM[47];IC3NET[24];SCHEDNET[25];DCCMD[48];VBC[39];DIFFDISCRETE[49];12C[28];IS[34];ETCNET[27];VARIABLE LENGTH CODING[43]; TMC [40]
PROXY	====	MAGIC[13];GA-COMM[22];MS-MARL-GCM[50]; IMAC[21]; ATOC[23]; MD-MADDPG[37]; GATED-ACML[26]; HAMMER[51];

3.2 Agents in MAS

In this category, some agents may not be able to communicate with all other agents in the MAS. Therefore, two types of agents are distinguished. Type 1 agent can communicate with all other agents in the MAS and Type 2 agents can only communicate with a subset of agents in the MAS. In some MARL systems, agents can only communicate with nearby agents, which can be defined in different ways such as agents that may be observed or nearby agents.

3.2.1 Neighboring agents on a graph:

In this communication type, agents are connected to each other on a graph and they can only communicate with their neighboring agents. This can be defined in a few ways, such as:

- Observable agents: Agents that can observe each other
- Agents within a certain distance: Agents that are within a certain distance of each other
- Neighboring agents: Agents that are connected to each other on a graph

For instance, GAXNet [38] allows agents that are observable to each other to communicate. DGN [39] limits communication to the three closest neighbors of each agent. The agent-entity graph [40] measures the distance between agents and enables communication between any two agents that are close to one another. Agents within a cluster radius can choose whether to become leader agents using LSC [41].

Both the networked multi-agent systems NeurComm [42] and IP [43] employ an established graph structure among their agents. As a result, communication between agents is limited to those that are related to one another on the graph. Similar to this, MAGNet-SA-GS-MG [44] likewise limits agent communication by using a pre-trained graph.

3.2.2 Other (Learning) Agents:

In certain MARL setups, communication between agents can occur without any proximity constraints. An example is IC3Net [45], where learning agents can communicate with their opponents, even if they have fixed policies. The results of experiments show that opponents eventually learn to communicate to avoid exploitation. Another way to facilitate communication in MARL is to use a proxy agent. This agent acts as a central point for communication among other agents but has no direct impact on the environment. Its role is to coordinate and transform messages between agents

Various types of proxies can be used to facilitate communication among agents in a Comm-MARL system [44-46]. A scheduler that collects encoded data from all agents and communicates with each one individually, a message coordinator that allows agents to decide whether to communicate with each other, and a system that combines messages from agents depending on their weights. Table 2 provides an overview of recent works on communication type.

Agent 1 can communicate directly with nearby agents 3 and 4, but also with agent 2 via a central proxy. The proxy coordinates and transforms messages to allow agent 1 and agent 2 to communicate with each other, despite not being nearby agents.

3.3 Communication policy

A communication policy is a set of rules that govern how agents communicate with each other. Predefined

communication policies are fixed and do not change during learning. For example, a predefined communication policy might allow all agents to communicate with each other, or it might only allow agents to communicate with their neighbors. Learned communication policies are updated during learning. For instance, an agent might learn to communicate with other agents that have been helpful in the past, or it might learn to communicate with agents that have similar goals. There are four main categories of communication policies: [46-49, 63]

Full communication: All agents are permitted to speak with one another.

Partial structure: Agents can communicate with a subset of other agents, based on a predefined rule.

Individual control: Each agent learns its own communication policy.

Global control: A central agent learns a communication policy for all agents.

Full communication is the simplest communication policy. It is permitted for all agents to converse with one another regardless of their location or goals. This policy is easy to implement, but it can be inefficient if agents are not communicating with the agents that are most relevant to them. Partial structure is a more complex communication policy. Only a selected group of other agents are permitted to communicate based on a predefined rule. This rule can be based on the agents' location, their goals or any other relevant factor. Partial structure can improve efficiency by reducing the number of unnecessary messages.

Individual control is a more flexible communication policy. Each agent learns its own communication policy. This policy can be more efficient than partial structure because agents can learn to communicate with the agents that are most relevant to them. However, individual control can be more difficult to implement because each agent needs to learn its own policy. Global control is the most complex communication policy. A central agent learns a communication policy for all agents. This policy can be the most efficient because the central agent can take into account the communication needs of all agents. However, global control can be the most difficult to implement because the central agent needs to possess a thorough awareness of the environment and the objectives of the agents.

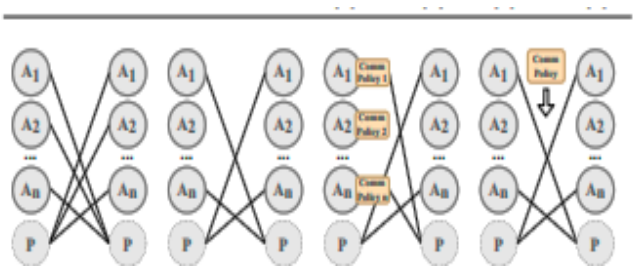

Fig. 1: **C**ommunication standards with agents: [46-49, 63]

The choice of communication policy depends on the specific application. If efficiency is the most important factor, then full communication or partial structure might be the best choice. If flexibility is the most important factor, then individual control might be the best choice. If accuracy is the main significant factor, then global control might be the best choice**.**

3.4 Communicated Messages

Once agents have established communication links, they need to decide what information to share. Partial observability means that each agent only has access to a limited view of the environment, so sharing local observations can be helpful for coordination. Agents can also share historical experiences, desired courses of action, or upcoming plans to produce more enlightening communications.

Recent research in this field varies depending on whether further information is simulated and encoded and can be classified into two categories:

3.4.1 Non-Future-Aware Communication:

In this category, agents do not consider future information when deciding what to communicate. They only share local observations, historical experiences, or intended actions.

3.4.2 Future-Aware Communication:

In this category, agents consider future information when deciding what to communicate. They may simulate future outcomes, encode future plans, or use other methods to generate more informative messages.

The choice of communication strategy depends on the specific application. If efficiency and accuracy are the most important factors, then non-future-aware communication might be the best choice.

3.5 Message Combination [47]

To process received messages, most existing Comm-MARL works typically handle them as a single entity. Message combination involves merging multiple received messages into a single message that can be used in an agent's internal model. In the presence of a proxy, agents typically receive a coordinated and combined message from the proxy, which takes care of the message combination process as discussed in the communicated messages dimension. In the absence of a proxy, agents need to individually determine how to combine multiple messages. As communicated messages capture the senders' interpretation of some messages may be more important than others depending on the situation or the learning process. For example, a message from an agent who has a lot of experience in the environment may be more valuable than a message from an agent who is new to the environment. There are a few different approaches to message combination. One approach is to simply average the values of the messages. Another approach is to use a weighted average, where the weights are determined by the senders' expertise or other factors. A third approach is to use a more complex

algorithm, such as a neural network to combine the messages. The choice of message combination approach depends on the specific application. If efficiency is a highly valued factor, then a simple approach, such as: averaging might be the best choice. If accuracy is the most important factor, then a more complex approach, such as: using a neural network might be the best choice. There are three [48-49] main approaches to message combination: concatenation, equal weighting, and unequal weighting. Their discussion is presented below:

3.5.1 Concatenation:

In this approach, the messages are simply concatenated together. This means that no preference is introduced and all messages are treated equally. Concatenation can be a good approach if the messages are relatively short and if it is important to preserve all of the information in the messages.

3.5.2 Equal Weighting:

In this approach, the messages are weighted equally. This means that each message is given the same weight when it is combined with the other messages. Equal weighting can be a good approach if the messages are all of similar quality and if it is important to keep the message combination process simple.

3.5.3 Unequal Weighting:

In this approach, the messages are weighted unequally. This means that some messages are given more weight than others. Unequal weighting can be a good approach if the messages are of different quality. The weighting of the data may be done in a variety of ways. One of the methods is messages unequally. One common method is to use an attention mechanism. Attention mechanisms assign weights to the messages based on their relevance to the current task. Another common method is to use a neural network. Neural networks can learn to weight the messages automatically, based on the data.

The choice of message combination approach depends on the specific application. If efficiency is the most important factor, then concatenation might be the best choice. If accuracy is the most important factor, then unequal weighting might be the best choice.

3.6 Inner Integration

For this, the literature generally approaches the concept of inner integration. Messages are typically seen as additional observations, which can be fed as an extra input either to a value function, a policy function, or both.

3.6.1 Policy-level:

To integrate messages into a policy model, agents can use the received messages to choose the next action. This way, agents can exploit information from other agents and act in a coordinated manner rather than independently. There are various methods for learning the policy model, such as policy gradient with REINFORCE, which gains reward in episodes and trains the model at the end of each episode, and actor-critic methods, which use a Q-function as a critic model to guide the learning of a policy network as an actor model.

3.6.2 Value-level:

Messages are considered as input to a value function, also known as an action-value function, in this category. DQN-like methods are commonly used in most of the works in this category.

3.6.3 Policy-level & Value-level

Integrating messages into both a policy and value model typically involves applying actor-critic techniques. These approaches use the messages that have been sent as additional inputs for the actor and critic models, respectively. As an alternative, the messages might be used in conjunction with nearby observations to produce fresh internal states that could then be communicated to both the actor and critic models.

The choice of the inner integration approach depends on the specific application. If efficiency is the most important factor, then policy-level integration might be the best choice. If the highest priority is accuracy, then integrating messages at the policy and value levels could be the optimal option.

3.7 Communication Constraints

To address realistic challenges such as the price of communication and noisy environments, systems Comm-MARL need to consider communication constraints. Recent work in this domain can be classified into three types:

3.7.1 Limited communication rounds:

In this type of constraint, agents are only allowed to communicate a limited number of times. This can be a realistic constraint in applications where communication is expensive such as in satellite communications.

3.7.2 Noisy communication:

In this type of constraint, messages can be corrupted or lost. This can be a realistic constraint in applications where communication is unreliable such as: in wireless communications.

3.7.3 Partial observability:

In this type of constraint, agents do not have access to all environmental information. This can be a realistic constraint in applications where it is difficult or impossible at the end of each episode, and obtain complete information about both the model and actor-critic techniques that employ a Q-function.

The choice of communication constraint depends on the specific application. If efficiency is the highly valued factor, then limited communication rounds might be the best choice. If accuracy is the most important factor, then noisy communication or partial observability might be the best choice.

3.8 Limited Bandwidth

Communication constraints refer to the limitations of communication bandwidth and capacity, which can affect the performance of Comm-MARL systems in realistic settings. Recent work [40-49, 57] in this domain can be classified into three types:

The first type assumes that because of the restricted communication bandwidth and capacity, early works try to send brief messages to cut down on communication overhead. DIAL [46] and RIAL [45] propose binary and real-value messages, respectively, to communicate between two agents and alleviate limited channel capacity. SchedNet [47] selects a subset of agents to broadcast their messages according to their importance. With reduced communication cost than SchedNet, VBC [48] and TMC [49] use specified criteria to filter out extraneous traffic. A probabilistic gate unit to block messages and a message coordinator are learned via gated ACML, which requires adjusting the gate through learning compared to handcrafted thresholds. These methods all attempt to reduce communication overhead in order to enhance Comm-MARL systems' performance in low bandwidth settings.

3.8.1 Noisy Channel:

In this categorization, ambient noise may interfere with how signals are sent between agents. The DIAL method, which works with Gaussian noise, shows how adding noise to real-valued signals may change their distribution. Contrarily, discrete attempts to back-propagate derivatives using discretized real-valued messages while addressing a noisy channel. Gradients may be obtained by using the suggested approach, which mathematically equates transmitting real-value signals to the discretized signal with additive noise [50-52].

3.8.2 Shared Medium:

This division of disagreement deals with situations where messages are transmitted through a single medium. MD-MADDPG solves this problem by allowing agents to access shared memory space sequentially to avoid contention. SchedNet selects agents who place a high priority on spreading their message, reducing the likelihood of contention.

3.8.3 Communication Learning:

Communication Learning deals with updating and adjusting a communication protocol through acquiring knowledge about a communication strategy and message. The education process can utilize defined feedback in the form of rewards, which can be enhanced in addition to learning the environment policy by a reinforcement learning process. To give richer and denser feedback, gradients can also be back-propagated from one agent to another. However, if agents learn discrete sending behaviors, this approach may be impractical because it necessitates differential messages and communication behaviors. On the basis of how communication feedback is used, recent studies in this dimension are grouped.

3.8.4 Reinforced:

In this category, the communication protocol is trained using reinforcement learning methods. RIAL and HAMMER concentrate on teaching the message's content in its entirety without considering whether to communicate. Other works consider both the learning of message content and the decision of whether to communicate. In addition, most works employ a centralized critic to provide feedback to all agents, while some works use a decentralized critic to provide feedback to individual agents.

3.8.5 Policy Gradient:

In this category, the communication policy is learned using policy gradient methods. This approach is more efficient than reinforcement learning but it requires the communication policy to be differentiable.

3.8.6 Backpropagation:

In this category, gradients are back-propagated through the communication policy. This approach is more accurate than policy gradient, but it requires the communication policy to be differentiable and the messages to be discretized.

3.9 Imitation Learning

In this category, an expert communication policy is observed and imitated by the agents. This approach is simple to implement but it requires an expert communication policy to be available. The choice of communication learning approach depends on the specific application. If efficiency is the most important factor, then reinforced learning might be the best choice. If accuracy is the most important factor, then back-propagation or imitation learning might be the best choice.

4. Training Scheme

It deals with how to leverage the accumulated experience from the agents in a Comm-MARL system including observations, actions, incentives, and messages. One approach [53] is to train each agent's model in a decentralized manner using its own experience. Another approach [53-55] is to train the agents centrally resulting in a single model to control. However, both have their drawbacks. Decentralized learning needs to handle a non -non-non-stationary environment due to agents that change and adapt. On the other hand, centralized learning faces a stationary environment while also struggling with a sizable common policy area that can be challenging to search.

A common approach [43-47, 55, 60-63] that balances the benefits of centralized and decentralized training is the CTDE technique, where agents get centralized training and decentralized execution and learn their local policies while being guided by central information. Recent works [12, 13]on training schemes can be classified based on how agents' experiences are utilized.

(a) Centralized Learning: Recent works in this area do not assume the presence of a central controller during the execution of tasks, where experiences are collected into a central unit for learning to control all agents.

(b) Decentralized Learning: Each agent in this category develops their own policy independently. This approach is simple to implement, but it can be slow to converge.

(c) Centralized-Decentralized Learning: In this category, agents first learn a centralized policy, which is then

decomposed into decentralized policies. This approach can be more efficient than decentralized learning, but it can be more difficult to implement.

(d) Federated Learning: In this category, agents learn their own policies locally and then exchange information with each other. This approach can be more efficient than centralized learning, but it can be more difficult to implement. The choice of training scheme depends on the specific application. If efficiency is the highly valued factor, then decentralized learning might be the best choice. If accuracy is the most important factor, then centralized learning or federated learning might be the best choice.

4.1 Decentralized Learning

Experiences are collected on an individual basis and agents are trained independently in this category. While this approach is straightforward to implement, it may converge slowly.

4.2 CTDE

We can further classify recent works in CTDE based on how they utilize experiences from all agents for optimization. Parameter sharing is also crucial for improving data efficiency by allowing a single set of parameters and information might be exchanged across agents as a Q-function or a policy. Agents may nevertheless behave differently since they get unique observations at each time step. These insights allow us to distinguish between the most recent researches in the following groupings [56-59].

4.3 Personalized (Policy) Parameters

Local policies in this scenario possess distinct sets of parameters and a central unit is responsible for accumulating all experiences to offer universal guidance and information, including gradients. To train the complete system, we can utilize techniques like the policy gradient actor-critic-based techniques or an algorithm (like REINFORCE).

4.4 Parameter Sharing

Typically, in this situation, DQN-like algorithms, actor-critic-based techniques, and policy gradients with REINFORCE are used. A local Q-function will learn to take into account all experiences if a DQN-like method is used or a separate global Q-function will be used to direct the learning. A shared actor (i.e., policy model) is trained to include all observation-action pairings when an actor-critic-based technique is utilized and it gets gradient instruction from a central critic [12]. Now here is the summarization of the whole discussion in a comparison table named Table 3. In Table 3 we have discussed all 9 dimensions of the communication used in MARL system and what are their further methods of implementation

4.5 Concurrent

Agents are allowed to make a backup of all experiences by observing the behavior and observations of other agents.

Compared to decentralized learning, this is different. In this case, while getting guidance including global information, each local policy maintains a unique set of parameters. Actor-critic-based methods are frequently employed in concurrent CTDE, where each agent has its central critic to guide its local policy.

Table 3: Comparative Analysis of Dimensions of Communication in Multi-Agent Reinforcement Learning

Dimension	Description	Examples
Communication type	The way in which agents communicate with each other. direct or indirect.	*__Direct communication__: Agents send and receive messages. *__Indirect communication__: Agents learn to coordinate their actions without explicitly communicating.
Communication policy	The rules that govern how agents communicate.	*__Full communication__ *__Partial structure__ *__Individual control__ *__Global Control__
Communicated messages	The information that agents share with each other.	*__Non-Future aware communication.__ *__Future aware communication.__
Message combination	The way in which agents combine the messages they receive.	*__Concatenation:__ Agents concatenate the messages they receive into a single message. *__Equal weighing:__ The messages are weighted equally. *__Unequal message weighing:__ The messages are not weighted equally.
Inner integration	The way in which agents incorporate the messages they receive into their decision-making process.	*__Policy level:__ To integrate messages into a policy model, agents can use the received messages to choose the next action. *__Value level__: Messages are considered as input to a value function. *__Policy-level & Value-level__ Integrating messages into both a policy and value model typically involves applying actor-critic techniques.
Communication constraints	The limitations on how agents can communicate.	*__Limited communication rounds__: In this type of constraint, agents are only allowed to communicate a limited number of times. * __Noisy communication:__ In this type of constraint, messages can be corrupted or lost. * __Partial observability:__ In this type of constraint, Agents do not have access to all environmental information.
Communication learning	The way in which agents learn to communicate.	*__Supervised learning:__ Agents are given a reward for sending messages that lead to good outcomes. *__Reinforcement learning__: Agents learn to communicate by trial and error.
Training schemes	The way in which agents are trained to communicate.	*__Independent training__: Agents are trained separately. *__Cooperative training:__ Agents are trained together.
Controlled goals	The goals that agents are trying to achieve through communication.	*__Coordination__: Agents are trying to coordinate their actions to achieve a common goal. *__Competition:__ Agents are trying to compete with each other to achieve a better outcome.

4.6 Controlled Goal

It is expected to achieve its aim by defining a reward configuration. The behavior correlates to different reward setups and learning may be divided into three types: cooperative, competitive, and mixed. It is worth mentioning that some studies have examined multiple scenarios to demonstrate their flexibility and scalability. Recent Research [13] in this area is divided into categories according to the behavior that is intended to emerge among learning agents with varying reward configurations.

4.7 Cooperative

In a cooperative situation, actors are compelled to interact in order to improve performance as a whole of the team. A team of agents may receive a collective reward that does not consider the contribution of each agent separately. As an alternative, agents might get regional incentives that are created to be dependent on the collective performance of their teammates, penalize collisions, or share rewards with neighbors to foster cooperation [14].

4.8 Competitive

StarCraft is a prevalent testing environment that involves multiple competitive teams. However, most studies only control one team and therefore, are not of interest to us. Based on our observations, only one study, IC3Net has examined samples having antagonistic benefits. IC3Net reveals that only when it is necessary, competing agents learn to communicate.

4.9 Mixed

In a mixed scenario, agents can exhibit either cooperative or competitive behavior, depending on the circumstances. For instance, agents may collaborate to achieve a shared objective but then compete for rewards after the objective is accomplished.

5. Conclusion

We have identified nine dimensions for analyzing and comparing various CommMARL systems, which researchers can utilize to develop their Comm-MARL system. Despite the success in this field, there are still some issues that require further examination and resolution. Most recent studies on Comm-MARL employ communication that is facilitated by the Sender-Receiver or Sender-Proxy-Receiver paradigm. This approach is helpful for learning since gradients may easily be back propagated from communicatees. Agents can, however, also ask their counterparts for specific data. Take Xuan et al. as an example. [12, 13] outline that agents can ask questions or sync their knowledge.

Secondly, as discussed, communication limitations are crucial for scenarios that necessitate low communication costs and reliable communication, necessitating further investigation and integration with practical use cases.

Thirdly, assessing the impact of a communication protocol is tough since it is hard to tell whether performance improvements are due to messages sent or environmental events. We have found two methods for learning communication in the dimension of communication learning protocol: reinforcement and differential. However, reinforcement learning requires human input to design suitable feedback for learning, while differential learning may face difficulties in determining how each agent contributes to a shared reward. Thus, it is necessary to develop more advanced and efficient methods for learning communication protocols.

Moreover, parameter sharing has become popular in recent works but it assumes homogeneous learning models. Developing Comm-MARL systems for heterogeneous agents is an area that needs further exploration. We are optimistic about the future of Comm-MARL. With the continued advancement of artificial intelligence, we can anticipate the development of more complex and sophisticated Comm-MARL systems that can tackle more challenging problems.

References

[1] C. Amato, A. Oliehoek, and C.A. T. Juan, "A Concise Introduction to Decentralized POMDPs," Springer, 2016.

[2] M.S. Zaïem, M. Etienne, and Bennequin, "Learning to communicate in multi-agent reinforcement learning," CoRR, abs/1911.05438, 2019.

[3] G. Papoudakis, F. Christianos, A. Rahman, and S.V. Albrecht, "Dealing with non-stationarity in multi-agent deep reinforcement learning," CoRR, abs/1906.04737, 2019.

[4] J.N. Foerster, G. Farquhar, T.A. fouras, N. Nardelli, and S. Whiteson, "Proceedings of the Thirty-Second AAAI Conference on Artificial Intelligence," AAAI Press, pp. 2974-2982, 2018.

[5] J.N. Foerster, Y.M. Assael, N. de Freitas, and S. Whiteson, "Learning to communicate with deep multi-agent reinforcement learning," in Advances in Neural Information Processing Systems, vol. 29, no. (NIPS), pp. 2137-2145, 2016.

[6] J. Kober, J.A. Bagnell, and J. Peters, "Reinforcement learning in robotics: A survey," Int. J. Robotics, vol. 32, no. (11), pp. 1238-1274, 2013.

[7] M. Vinyals, J.A. Rodríguez-Aguilar, and J. Cerquides, "A survey on sensor networks from a multiagent perspective," Comput. J., vol. 54, no. 3, pp. 455-470, 2011.

[8] P. Hernandez-Leal, B. Kartal, and M.E. Taylor, "A survey and critique of multiagent deep reinforcement learning," Autonomous Agents and Multi-Agent Systems, vol. 33, no. 6, pp. 750-797, 2019.

[9] P. Hernandez-Leal, B. Kartal, and M.E. Taylor, "A survey and critique of multiagent deep reinforcement learning," Autonomous Agents and Multi-Agent Systems, pp. 750-797, 2019.

[10] R. Lowe, Y. Wu, A. Tamar, J. Harb, P. Abbeel, and I. Mordatch, "Multi-agent actor-critic for mixed cooperative-competitive environments," in Advances in Neural Information Processing Systems, vol. 30, no. (NIPS), pp. 6379-6390, 2017.

[11] S. Sukhbaatar, A. Szlam, and R. Fergus, "Learning multiagent communication with backpropagation," in Advances in Neural Information Processing Systems, vol. 29, no. (NIPS), pp. 2244-2252, 2016.

[12] S. Shalev-Shwartz, S. Shammah, and A. Shashua, "Safe, multi-agent reinforcement learning for autonomous driving," CoRR, abs/1610.03295, 2016.

[13] N. Sandholm, T. Brown, and T. Tuomas, "Superhuman AI for multiplayer poker," Science, vol. 365, no. (9495), pp. 885-890, 2019.

[14] Y. Du, B. Liu, V. Moens, Z. Liu, Z. Ren, J. Wang, X. Chen, and H. Zhang, "Learning correlated communication topology in multi-agent reinforcement learning," in 20th International Conference on Autonomous Agents and Multiagent Systems (AAMAS), pp. 456-464, 2021.

[15] Y. Niu, R.R. Paleja, and M.C. Gombolay, "Multi-agent graph attention communication and teaming," in 20th International Conference on

Autonomous Agents and Multiagent Systems (AAMAS), pp. 964-973, 2021.

[16] T.T. Nguyen, N.D. Nguyen, and S. Nahavandi, "Deep reinforcement learning for multi-agent systems: A review of challenges, solutions, and applications," CoRR, abs/1812.11794, 2018.

[17] Lee, J., Lee, M, Lee J., & Choi S. (2021). Deep reinforcement learning for multiagent collaboration arXiv preprint arXiv 210209561.

[18] S. Gronauer and K. Diepold, "Multi-agent deep reinforcement learning: a survey," Artificial Intelligence, pp. 1-49, 2021.

[19] A. Oroojlooyjadid and D. Hajinezhad, "A review of cooperative multiagent deep reinforcement learning," CoRR, abs/1908.03963, 2019.

[20] A. Wong, T. Bäck, A.V. Kononova, and A. Plaat, "Multiagent deep reinforcement learning: Challenges and directions towards human-like approaches," CoRR, abs/2106.15691, 2021.

[21] A. Das, T. Gervet, J. Romoff, D. Batra, D. Parikh, M. Rabbat, and J. Pineau, "Tarmac: Targeted multi-agent communication," in Proceedings of the 36th International Conference on Machine Learning (ICML), pp. 1538-1546, 2019.

[22] R. Wang, X. He, R. Yu, W. Qiu, B. An, and Z. Rabinovich, "Learning efficient multi-agent communication: An information bottleneck approach," in Proceedings of the 37th International Conference on Machine Learning (ICML), vol. 119, pp. 9908-9918, 2020.

[23] Y. Liu, W. Wang, Y. Hu, J. Hao, X. Chen, and Y. Gao, "Multi-agent game abstraction via graph attention neural network," in The Thirty-Fourth AAAI Conference on Artificial Intelligence (AAAI), pp. 7211-7218, 2020.

[24] J. Jiang and Z. Lu, "Learning attentional communication for multiagent cooperation," in Advances in Neural Information Processing Systems 31 (NIPS), pp. 7265-7275, 2018.

[25] A. Singh, T. Jain, and S. Sukhbaatar, "Individualized controlled continuous communication model for multiagent cooperative and competitive tasks," in International Conference on Learning Representations (ICLR), 2019.

[26] D. Kim, S. Moon, D. Hostallero, W. J. Kang, T. Lee, K. Son, and Y. Yi, "Learning to schedule communication in multiagent reinforcement learning," in 7th International Conference on Learning Representations (ICLR), no. OpenReview.net, 2019.

[27] H. Mao, Z. Zhang, Z. Xiao, Z. Gong, and Y. Ni, "Learning agent communication under limited bandwidth by message pruning," in The Thirty-Fourth AAAI Conference on Artificial Intelligence, no. AAAI Press, pp. 5142-5149, 2020.

[28] G. Hu, Y. Zhu, D. Zhao, M. Zhao, and J. Hao, "Event-triggered multi-agent reinforcement learning with communication under limited-bandwidth constraint," CoRR, abs/2010.04978, 2020.

[29] Z. Ding, T. Huang, and Z. Lu, "Learning individually inferred communication for multi-agent cooperation," in Advances in Neural Information Processing Systems 33 (NeurIPS), 2020.

[30] A. Agarwal, S. Kumar, K. P. Sycara, and M. Lewis, "Learning transferable cooperative behavior in multi-agent teams," in International Foundation for Autonomous Agents and Multiagent Systems, pp. 1741-1743, 2020.

[31] K. Zhang, Z. Yang, and T. Basar, "Decentralized multi-agent reinforcement learning with networked agents," Frontiers Inf. Technol. Electron. Eng., vol. 22, no. 6, pp. 802-814, 2021.

[32] K. Zhang, Z. Yang, and T. Basar, "Multi-agent reinforcement learning: A selective overview of theories and algorithms," CoRR, abs/1911.10635, 2019.

[33] T. Chu, S. Chinchali, and S. Katti, "Multi-agent reinforcement learning for networked system control," in 8th International Conference on Learning Representations (ICLR), no. OpenReview.net, 2020.

[34] C. Qu, H. Li, C. Liu, J. Xiong, J. Zhang, W. Chu, Y. Qi, and L. Song, "Intention propagation for multi-agent reinforcement learning," CoRR, abs/2004.08883, 2020.

[35] W. Kim, J. Park, and Y. Sung, "Communication in multi-agent reinforcement learning: Intention sharing," in 9th International Conference on Learning Representations (ICLR), 2021.

[36] C. Sun, B. Wu, R. Wang, X. Hu, X. Yang, and C. Cong, "Intrinsic motivated multi-agent communication," in AAMAS '21: 20th International Conference on Autonomous Agents and Multiagent Systems, 2021.

[37] P. Peng, Q. Yuan, Y. Wen, Y. Yang, Z. Tang, H. Long, and J. Wang, "Multiagent bidirectionally-coordinated nets for learning to play starcraft combat games," CoRR, abs/1703.10069, 2017.

[38] E. Pesce and G. Montana, "Improving coordination in small-scale multi-agent deep reinforcement learning through memory-driven communication," Machine Learning, vol. 109, no. 9-10, pp. 1727-1747, 2020.

[39] J. Jiang, C. Dun, T. Huang, and Z. Lu, "Graph convolutional reinforcement learning," in 8th International Conference on Learning Representations (ICLR), no. OpenReview.net, 2020.

[40] S. Q. Zhang, Q. Zhang, and J. Lin, "Efficient communication in multi-agent reinforcement learning via variance-based control," in Advances in Neural Information Processing Systems 32 (NeurIPS), pp. 3230-3239, 2019.

[41] S. Q. Zhang, Q. Zhang, and J. Lin, "Succinct and robust multi-agent communication with temporal message control," in Advances in Neural Information Processing Systems 33 (NeurIPS), 2020.

[42] C. E. Shannon, "A mathematical theory of communication," Bell Syst. Tech. J., vol. 27, no. 3, pp. 379-423, 1948.

[43] R. L. Freeman, "Telecommunication system engineering," John Wiley & Sons, vol. 82, 2004.

[44] B. Freed, R. James, G. Sartoretti, and H. Choset, "Sparse discrete communication learning for multi-agent cooperation through backpropagation," in IEEE/RSJ International Conference on Intelligent Robots and Systems (IROS), pp. 7993-7998, 2020.

[45] W.J. Yun, B. Lim, S. Jung, Y.C. Ko, J. Park, J. Kim, and M. Bennis, "Attention-based reinforcement learning for real-time UAV semantic communication," CoRR, abs/2105.10716, 2021.

[46] J. Sheng, X. Wang, B. Jin, J. Yan, W. Li, T. H. Chang, J. Wang, and H. Zha, "Learning structured communication for multiagent reinforcement learning," CoRR, abs/2002.04235, 2020.

[47] A. Malysheva, T.T. K. Sung, C. Sohn, D. Kudenko, and A. Shpilman, "Deep multi-agent reinforcement learning with relevance graphs," CoRR, abs/1811.12557, 2018.

[48] O. Kilinc and G. Montana, "Multi-agent deep reinforcement learning with extremely noisy observations," CoRR, abs/1812.00922, 2018.

[49] W. Kim, M. Cho, and Y. Sung, "An efficient training method for multi-agent deep reinforcement learning," in The Thirty-Third AAAI Conference on Artificial Intelligence, pp. 6079-6086, 2019.

[50] B. Freed, G. Sartoretti, J. Hu, and H. Choset, "Communication learning via backpropagation in discrete channels with unknown noise," in The Thirty-Fourth AAAI Conference on Artificial Intelligence, pp. 7160-7168, 2020.

[51] X. Kong, B. Xin, F. Liu, and Y. Wang, "Revisiting the master-slave architecture in multi-agent deep reinforcement learning," CoRR, abs/1712.07305, 2017.

[52] N. Gupta, G. Srinivasaraghavan, S. K. Mohalik, and M. E. Taylor, "HAMMER: multi-level coordination of reinforcement learning agents via learned messaging," CoRR, abs/2102.00824, 2021.

[53] H. Mao, Z. Zhang, Z. Xiao, Z. Gong, and Y. Ni, "Learning agent communication under limited bandwidth by message pruning," in The Thirty-Fourth AAAI Conference on Artificial Intelligence (AAAI), AAAI Press, 2020.

[54] E. Jang, S. Gu, and B. Poole, "Categorical reparameterization with gumbel-softmax," in 5th International Conference on Learning Representations (ICLR), OpenReview.net, 2020.

[55] L. Kraemer and B. Banerjee, "Multi-agent reinforcement learning as a rehearsal for decentralized planning," Neurocomputing, vol. 190, pp. 82-94, 2016.

[56] L. Busoniu, R. Babuska, and B. De Schutter, "Multi-agent reinforcement learning: A survey," in Ninth International Conference on Control, Automation, Robotics and Vision (ICARCV), IEEE, pp. 1-6, 2006.

[57] L. Matignon, G.J. Laurent, and N. Le Fort-Piat, "Independent reinforcement learners in cooperative Markov games," Knowledge Engineering Review, vol. 27, no. 1, pp. 1-31, 2012.

[58] B. Liu, Q. Liu, P. Stone, A. Garg, Y. Zhu, and A. Anandkumar, "Coach-player multi-agent reinforcement learning for dynamic team composition," Proceedings of Machine Learning Research, vol. 144, pp. 6860-6870, 2021.

[59] P. Xuan, V.R. Lesser, and S. Zilberstein, "Communication decisions in multi-agent cooperation: model and experiments," in Proceedings of the Fifth International Conference on Autonomous Agents, 2001.

[60] V. Hakami, V. Barghi, H. Mostafavi, S. Arefinezhad, and Z. Hakami, "A resource allocation scheme for D2D communications with unknown channel state information," Peer-to-Peer Netw. Appl., vol. 15, pp. 1189-1213, 2022.

[61] Y. Du, B. Liu, V. Moens, Z. Liu, Z. Ren, J. Wang, X. Chen, and H. Zhang, "Learning correlated communication topology in multi-agent reinforcement learning," in 20th International Conference on Autonomous Agents and Multiagent Systems (AAMAS), pp. 456-464, 2021.

[62] Y. Niu, R.R. Paleja, and M.C. Gombolay, "Multi-agent graph attention communication and teaming," in 20th International Conference on Autonomous Agents and Multiagent Systems (AAMAS), pp. 964-973, 2021.

[63] D. Silver et al., "Mastering the game of Go without human knowledge," Nature, vol. 550, no. 7676, pp. 354-359, 2017.

The Nucleus ***60***, *No. 2 (2023) 185-198*

www.thenucleuspak.org.pk

The Nucleus

ISSN 0029-5698 (Print)
ISSN 2306-6539 (Online)

Machine Learning Techniques for Urdu Audio Feedback for Visual Assistance: A Systematic Literature Review

Murtaza Hanif*, Tauqir Ahmad, Muhammad Aslam, Muhammad Waseem

Computer Science, University of Engineering & Technology, Punjab, Pakistan

ABSTRACT

Visually impaired individual faces many challenges when comes to object recognition and routing inside or out. Despite the availability of numerous visual assistance systems, the majority of these system depends on English auditory feedback, which is not effective for the Pakistani population, since a vast population of Pakistanis cannot comprehend the English language. The primary object of this study is to consolidate the present research related to the use of Urdu auditory feedback for currency and Urdu text detection to assist a visually impaired individual in Pakistan. The study conducted a comprehensive search of six digital libraries, resulting in 50 relevant articles published in the past five years. Based on the results, a taxonomy of visual assistance was developed, and general recommendations and potential research directions were provided. The study utilized firm inclusion/exclusion criteria and appropriate quality assessment methods to minimize potential biases. Results indicate that while most research in this area focuses on navigation assistance through voice audio feedback in English, the majority of the Pakistani population does not understand the language rendering such systems inefficient. Future research should prioritize object localization and tracking with Urdu auditory feedback to improve navigation assistance for visually impaired individuals in Pakistan. The study concludes that addressing the language barrier is crucial in developing effective visual assistance systems for the visually impaired in Pakistan.

Keywords: *Visual Assistance, Visually Impaired, Auditory Feedback, Visually Impaired, Vision Impairment, Currency, Urdu Text, Urdu Auditory.*

1. Introduction

An individual with all-out visual deficiency or visual hindrance faces many difficulties in doing their different routine task [1]. Visually impaired people are dependent upon others for looking, moving, and other everyday tasks [1]. Worldwide 38.5 million are visually impaired including 1.12 million in Pakistan while the numbers are anticipated to grow nearly to 587.6 million, by 2050 [2]. The problem is becoming more of a concern as the number of visually handicapped people rises by millions every decade [3]. This circumstance has captured the attention of several in the search for improving the quality of life for those visually impaired [4]. Previously, human guides [5], and smart canes [6] have been the study of practitioners for navigational assistance.

Recently, machine learning algorithms have made significant contributions to the study of humans such as smile detection [7], robotic arms [8], and pose recognition [9]. Similarly, machine learning algorithms have also been used for the safe routing of the visually impaired using a convolutional neural network (CNN) [10]. To ensure the use of safe navigation deep learning-based object localization along with a range of distance-calculating sensors [11], the system contains a wearable interface made of the RGB-Depth camera that effectively instructs the visually impaired to roam [12], while understanding the surroundings [13], and recognizing the traffic signs [14]. Moreover, a deep learning approach is employed to calculate the current rotation, and speed performed by the visually impaired [15], with audio feedback in the English language [15], and alarm-based [16].

The existing review paper covers up to 2022 and mostly focuses on the detection of objects, text, and currency detection using English auditory response while paying less attention to Urdu text and Pakistani currency using Urdu auditory feedback as shown in Table 1, the following table brings comparison amid the present reviews centered on five key perceptions, navigation, object detection, Urdu text detection, currency detection, and audio feedback in the Urdu language. We included only comparisons for reviews that were published in reputable journals.

The novelty of our systematic analysis provides Urdu audio feedback for the visually challenged population integrating detection of Urdu texts [17], Urdu texts in images [18], and currency recognition [1]. Given that Urdu has been designated as the official language of the country, it occupies a central position in various domains, including government institutions, administrative offices, and educational establishments. Urdu serves as the primary medium of communication and instruction in schools and offices across the nation. Consequently, the provision of support and assistance in the Urdu language would be exceptionally appreciated and embraced on a national scale. The widespread adoption of such assistance throughout the country reflects the inherent value placed on Urdu as a means of communication and underscores the significance of catering to the needs of Urdu-speaking individuals, particularly in the visually impaired community.

This systematic literature review offers a full analysis of the problem tackled by the visually impaired while covering all 5 major perspectives discussed in Table 1. Additionally, 50 papers have been selected for further examination based on systematic reviews.

The paper is organized as follows. Section 2 debates the present survey and motivation for this systematic literature review. Section 3 provides the approach to conduct this review along with the research question and objectives. The answer to the queries has been examined in section 4. In section 5 the taxonomy of this literature review is discussed. Finally, the paper has been concluded in section 6.

*Corresponding author: murtaza.najaf92@outlook.com

Table 1: Comparison table

Ref	Focus of Study	Survey	YOP	High-Level Feature Extraction					Target Library
				Navigation	Object Detection	Urdu Text Detection	Currency Detection	Urdu Audio Feedback	
1	Analysis of Navigation Assistance for Blind and Visually Impaired People	Review Paper	2021	✓	x	x	x	x	IEEE
2	Assistive Navigation System for Visually Impaired & Blind People	Review Paper	2021	✓	✓	x	x	x	IEEE
3	A Systematic Review of Urban Navigation Systems for Visually Impaired People	Review Paper	2021	✓	x	x	x	x	MPDI
4	A Survey on Currency Identification Systems for Blind and Visually Impaired	Review Paper	2021	✓	✓	x	x	x	MPDI
5	A Comparative Review on Object Detection System for Visually Impaired	Review Paper	2021	✓	x	x	x	x	IEEE
6	Indoor Navigation Systems for Visually Impaired Persons: Mapping the Features of Existing Technologies to User Needs	Review Paper	2020	✓	✓	x	x	x	MPDI
7	Tools and Technologies for the Blind and Visually Impaired Navigation Support	Review Paper	2022	x	✓	x	x	x	Taylor & Francis
8	Insight on Electronic Travel Aids for Visually Impaired People: A Review on the Electromagnetic Technology	Review Paper	2019	x	✓	x	x	x	MPDI
9	Developing Walking Assistants for Visually Impaired People	Review Paper	2019	x	x	x	x	x	IEEE
	Current Study	SLR	2023	✓	✓	✓	✓	✓	

2. Literature Survey

Prior employed approaches used for indoor and outdoor navigation includes: E-cane, trained dogs, and sensor-based walking sticks for the navigation of visually impaired individual, which incorporates infrared and ultrasonic-based navigation, has short-range capabilities for object detection, While, laser-based navigation can hurt assuming it straightly hitting them on their eyes [19]. Moreover, an electronic transfer aid was adopted for the direct routing of the blind in unfamiliar indoor conditions with embedded high points for finding the obstacles [20]. A large number of proposed indoor and outdoor navigation systems have weaknesses related to friendliness and adaptability, personal learning, and variation time with the new framework [21]. In addition, an electronic travel aid in the vision of electromagnetic was recognized as a rising invention, because of its high degree of accessible execution concerning accuracy adaptability, and cost viability [22]. Besides that, the global positioning system (GPS) tracker can assist to localize and recognize positions, planning, and security and health services [23]. Moreover, in the translation of the environment, utilization of computer vision and artificial intelligence more specifically the deep learning methodologies help outdoor navigation for the visually impaired individual [24].

Apart from that, a framework has been involved for expansion in the field of sensors, computer vision, and smartphone-based walking generations that guarantee the portability and security of blind people. The existing review articles emphasize more on sensors and lasers utilized for object localization, as well as the use of global positioning systems (GPS) for tracing the location of visually impaired individuals. However, there is a notable bias toward discussing tools, devices, power consumption, usability, and portability, while comparatively less attention is given to addressing the comprehension of assistive challenges specific to visually impaired individuals. It is essential to prioritize research that focuses on enhancing visual understanding.

The novelty of this systematic analysis incorporates visual assistance with audio feedback, enabling visually impaired individuals to effortlessly comprehend the objects in their native language. Introducing assistance through Urdu acoustic feedback can make a significant contribution to their independence and overall well-being. By providing tailored audio guidance in a language familiar to them, the paper aims to enhance their understanding and ensure a more effective and accessible assistive experience.

3. Research Methodology

We conducted this systematic literature review to examine and assess Urdu-based audio feedback assistance systems for visually impaired persons. We applied the identical method.

We applied the identical method [25], and [26], which recognizes and evaluates the publication of an Urdu-based aid system. Directing of this systematic literature review can be partitioned into three divisions. Preparation of review, conducting and finally reporting of the review as shown in Fig.1. The methodology of recognizing the research topic based on problem statements and research gap is displayed in

Fig. 2 and the research process used to acquire and examine existing material allied to audio feedback is shown in Fig. 3.

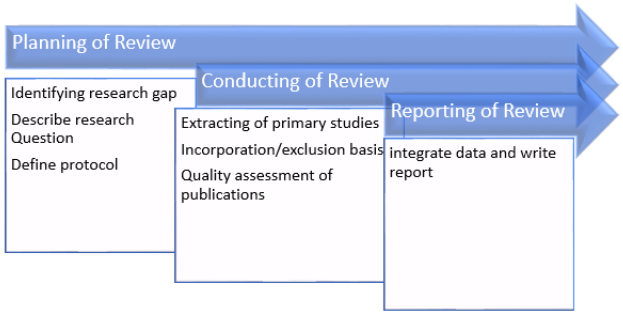

Fig. 1: Stages of study plan

3.1 Review Plan

A suitable search plan has been employed to gather all significant studies. Fig. 1 and 2 demonstrate the procedure for finding the related papers, publication mapping, and classification framework. A highly organized procedure was used in conducting this review which includes.

- Research questions and objectives
- Coordinating database searches
- Studies including/ excluding
- Inspecting related studies
- Combining result
- Concluding the review

It is crucial to express primary research questions (RQs) as mentioned in Table 2 to acquire the main objective as follows:

1. RQ 1: Aims to mention the objective to build a library of publications for the visually impaired including recognition of more efficient work for the visually challenged population in Pakistan
2. RQ 2: Focuses on comprehending the tools beneficial for the visually impaired and other applications of the navigational system.
3. RQ 3: The objective is to categorize the prior solution for indoor and outdoor navigation, which is mostly based on the sensor with audio feedback both in English and alarm.
4. RQ 4: Tries to recognize the challenges met while producing navigational assistance with auditory feedback.
5. RQ 5: The final question covers identifying the medium of instruction for the visually impaired person in Pakistan. The language is effective and easily adapted.

3.2 Review Conduct

The technique of carrying out this review has been stated in four steps, expressed below. At first, related primary studies have looked at the most used digital libraries. The selection of papers based on decided criteria has been included and excluded during the second phase. We have developed quality evaluation principles to improve the quality of our review and finally, the snowballing is executed to fetch crucial publications performing the last phase.

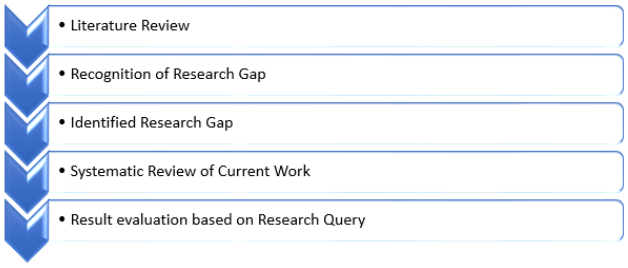

Fig. 2: Research Approach for systematic literature review

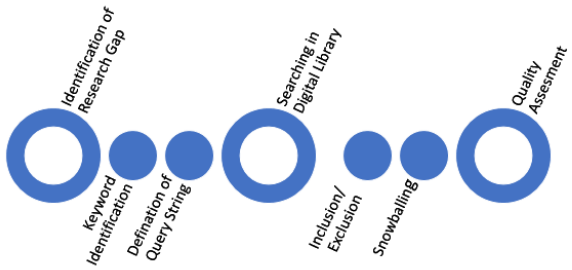

Fig. 3: Procedure to excerpt and study related to the research article

3.2.1 Research Question

The crucial step in conducting a systematic literature review is to look at the problem statement and research gap identified by the earlier studies. The research question makes it easier to formulate a research question. The collection of research questions that should be assessed for this study is shown in Table 2.

3.2.2 Search Strategy

The term searching strategy describes a series of activities necessary to carry out a systematic literature review. The procedure entails browsing relevant published research publications through digital libraries and search engines. Compose the search string after choosing the appropriate search environment. Below is the list of digital libraries that we utilized to find the research resources for automated extraction.

- ACM Digital Library Linkyhttp://dl.acm.org
- IEEE Explore http://ieeexplore.ieee.org
- Science Direct https://www.sciencedirect.com
- Springer Link https://link.springer.com/
- Google Scholar https://scholar.google.com/
- Semantic Scholar https://www.semanticscholar.org

The goal of the search is to gather specific publications in the library resources mentioned above.

Table 2: Research Queries and their objectives

RQ	Research Question	Objective and Motivation
1	Which articles are appropriate for navigational assistance? Determine the type of channel, as well as the demographic distribution?	To Recognize • High-impact papers for navigational assistance. • Selected papers from 2019- 2023
2	What are the principal purposes of navigational assistance?	To Study and understand • Real-time employment for navigational assistance i.e. Autonomous Vehicles, beneficial tools for visually impaired persons.
3	How to examine and recognize the similarities and differences between high-level extracted features in current research?	To identify and compare • Existing work for indoor and outdoor navigation, sensor-based navigation, and feedback both in English and alarm.
4	How to determine the primary concerns and challenges that navigation aid will face for Pakistani people?	To identify • Challenges encountered while developing navigational assistance with auditory feedback.
5	What are the effective and interactive communication mediums for the Pakistani population?	To Understand • To Provide Urdu auditory feedback to ease the navigation system for the visually impaired.

Table 3: Research keywords used to define our work

Term	Primary key	Secondary key	Third Key	Additional key
T1	Navigational assistance	Visually impaired	Sensors based	Voice feedback
T2	Navigational analysis	Blind	Machine learning based	Audio feedback
T3	Routing assistance	Weaken	AI-based	Auditory feedback
T4	Route guidance	Vision-impaired	Deep-learning	Acoustic feedback
T5	Navigation aid	Visually handicapped	Computer Vision	Aural feedback
T6	Travel routing	Non-sighted	Laser-based	Listening feedback

3.2.3 Define A Query String

The searching can be accomplished by capitalizing the right search string. Table 3 shows the keywords that contain the term and groups them to generate a valid string. The word "OR" is utilized to imply synonymous, while AND serves to link words together."

(Navigational assistance OR navigational analysis OR routing assistance OR route guidance OR navigation aid OR travel routing) AND (Visually impaired OR blind OR weaken OR vision-impaired OR visually handicapped OR non-sighted) AND (sensors-based OR machine learning OR AI-based OR deep-learning OR computer vision OR laser-based) AND (voice feedback OR audio feedback OR auditory feedback OR acoustic feedback OR aural feedback OR listening feedback).

List 1: Query String

We have used the primary term as a key component for research on blind assistance. Along with the primary key other keywords or additional words were chosen. Integrating the keywords, with "AND", and" OR" operators generate a final query string for search as mentioned.

The overhead mentioned query seems to be limited during the initial search process. It was found that the preceding search query was ineffective at including the article for the visually impaired. Table 4 shows the final search query employed to discover six digital libraries with custom filters by applying the keywords in ACM Journal, Science Direct, IEEE, Google Scholar, Springer Link, and Semantic Scholar.

Table 4: Searching plan for digital libraries

Digital Library	Search Query	Filter
ACM Digital Library	(Navigational assistance OR navigational analysis OR routing assistance OR route guidance OR navigation aid OR travel routing) AND (Visually impaired OR blind OR weaken OR vision-impaired OR visually handicapped OR non-sighted) AND (sensors-based OR machine learning OR AI-based OR deep-learning OR computer vision OR laser-based) AND (voice feedback OR audio feedback OR auditory feedback OR acoustic feedback OR aural feedback OR listening feedback)	Publication Date: 2019-2023 Journal and Conference paper
IEEE Explore	(Navigational assistance OR navigational analysis OR routing assistance OR route guidance OR navigation aid OR travel routing) AND (Visually impaired OR blind OR weaken OR vision-impaired OR visually handicapped OR non-sighted) AND (sensors-based OR machine learning OR AI-based OR deep-learning OR computer vision OR laser-based) AND (voice feedback OR audio feedback OR auditory feedback OR acoustic feedback OR aural feedback OR listening feedback)	2019-2023 Journal and Conference paper
Science Direct	(Navigational assistance OR navigational analysis OR routing assistance OR route guidance OR navigation aid OR travel routing) AND (Visually impaired OR blind OR weaken OR vision-impaired OR visually handicapped OR non-sighted) AND (sensors-based OR machine learning OR AI-based OR deep-learning OR computer vision OR laser-based) AND (voice feedback OR audio feedback OR auditory feedback OR acoustic feedback OR aural feedback OR listening feedback)	2019-2023 Journal and Conference paper

Springer Link	(Navigational assistance OR navigational analysis OR routing assistance OR route guidance OR navigation aid OR travel routing) AND (Visually impaired OR blind OR weaken OR vision-impaired OR visually handicapped OR non-sighted) AND (sensors-based OR machine learning OR AI-based OR deep-learning OR computer vision OR laser-based) AND (voice feedback OR audio feedback OR auditory feedback OR acoustic feedback OR aural feedback OR listening feedback)	2019-2023 Journal and Conference paper
Google Scholar	(Navigational assistance OR navigational analysis OR routing assistance OR route guidance OR navigation aid OR travel routing) AND (Visually impaired OR blind OR weaken OR vision-impaired OR visually handicapped OR non-sighted) AND (sensors-based OR machine learning OR AI-based OR deep-learning OR computer vision OR laser-based) AND (voice feedback OR audio feedback OR auditory feedback OR acoustic feedback OR aural feedback OR listening feedback)	2019-2023 Journal and Conference paper
Semantic Scholar	(Navigational assistance OR navigational analysis OR routing assistance OR route guidance OR navigation aid OR travel routing) AND (Visually impaired OR blind OR weaken OR vision-impaired OR visually handicapped OR non-sighted) AND (sensors-based OR machine learning OR AI-based OR deep-learning OR computer vision OR laser-based) AND (voice feedback OR audio feedback OR auditory feedback OR acoustic feedback OR aural feedback OR listening feedback)	2019-2023 Journal and Conference paper

Table 5: Stages and results of selected papers

	ACM	IEEE	Science Direct	Springer Link	Google Scholar	Semantic Scholar	Total Paper
QS Searching	1050	2230	890	915	3106	870	9061
Filter	450	1090	589	735	1130	385	4379
Filter (Title)	260	134	48	112	162	38	754
Filter (Abstract)	54	28	27	56	42	16	220
Filter (Introduction and Conclusion)	10	27	11	14	37	9	104
Inspection	10	20	2	8	6	4	50

3.2.4 Selection Upon Including and Excluding Norms

Inclusion norms

- The articles included must be relevant to the domain of blind assistance in auditory feedback.
- Articles with the appropriate organization of modeling, experiment approach, and assessment metrics are incorporated.
- An article with an experimental approach that utilizes the published dataset to train and validate it.
- Include the latest and most relevant research publication with a review on visual assistance in Urdu.

Exclusion Criteria

- Don't include the non-English Publications.
- Publications from unrecognized journals and unauthentic internet sources should be included.
- Don't include the paper that does not discuss visual assistance for blinds.
- Discard the papers published before 2019.

3.2.5 Selection Based on Snowballing

After conducting a quality evaluation, we performed snowballing [27] through the list of established studies to carry out publications. Those papers selected that have been passed through filtration of inclusion and exclusion criteria. The inclusion and exclusion of the publication have been finalized after scanning the abstract and additional portion of the paper. We identified a total of 50 papers for the primary study.

3.2.6 Quality Valuation

The quality valuation of the publications tracked for the addition of related papers is shown in Table 6 below. The quality evaluation score for each distinct criterion is shown in Table 7 which shows the selected publication in the range between 4 to 10.

The following are some unique quality assessment classification methodologies to consider.

- The unpublished papers are not included. Moreover, they are examined if they were published in peer-reviewed journals plus if they have any satisfactory citations.
- Is there any convincing explanation of how Urdu audio feedback is used for the visually impaired?
- Is the research goal aligned with the goal of the current research questions?
- Can the experimental techniques and findings from these investigations be repeated? Is the author able to sufficiently describe the experimental procedure such that it can be repeated using the supplied data and techniques?
- Does the published article aim to aid the visually impaired individual?

The act of conducting the quality evaluation is done by allocating proper scores to the above-mentioned criteria. The final score of all those mentioned questions is displayed in Table 8.

Table 6: Categorization for quality valuation

Ref	YOP	Journal/ Conference	Empirical	Approach	Citation	Quality valuation					Score
						a	b	c	d	e	
1	2021	Conference	Primary	Resnet 18	63	2	2	2	2	2	10
2	2021	Journal	Primary	Fuzzy logic based	35	2	2	2	1	1	8
3	2021	Conference	Primary	Haptic based cues	47	2	2	1	2	1	8
4	2019	Journal	Primary	CNN object recognition	69	2	2	2	2	0	8
5	2019	Conference	Primary	RANSAC method	31	2	1	1	0	0	4
6	2021	Journal	Primary	Sensor Based	58	2	0	0	2	2	6
10	2022	Journal	Primary	CNN object recognition	53	2	2	2	0	2	8
11	2020	Journal	Primary	YOLO V3	76	2	2	0	2	2	8
12	2021	Journal	Primary	Deep learning	49	2	2	0	0	2	6
13	2022	Conference	Primary	Raspberry Pi	29	2	2	2	0	0	6
14	2019	Conference	Primary	Open CV Raspberry Pi	81	2	1	2	0	0	5
15	2019	Journal	Primary	Deep learning	78	2	0	2	0	2	6
16	2021	Journal	Primary	Vibrating actuator	32	2	1	0	1	1	5
17	2020	Conference	Primary	Image Processing	24	2	2	1	0	0	5
18	2019	Conference	Primary	Deep learning	45	2	2	0	1	1	8
19	2021	Journal	Secondary	SLR	33	2	2	1	0	0	5
20	2021	Conference	Secondary	SLR	26	2	0	1	1	0	4
21	2021	Journal	Secondary	SLR	57	2	2	0	1	1	4
22	2020	Journal	Secondary	SLR	49	1	2	1	0	2	6
23	2020	Journal	Secondary	SLR	50	0	2	0	2	0	4
24	2019	Journal	Secondary	SLR	68	2	2	2	0	0	6
29	2019	Journal	Secondary	SLR	19	2	1	1	1	0	5
31	2023	Journal	Primary	Sensors	61	2	2	0	2	2	8
32	2021	Journal	Primary	Bluetooth, BLE	61	2	2	2	2	2	10
35	2020	Conference	Primary	IoT based sensors	54	2	0	1	0	2	5
36	2020	Journal	Primary	RFID based electronic	38	2	0	1	0	1	4
37	2019	Journal	Primary	Deep learning	61	2	2	1	0	0	5
38	2020	Journal	Primary	Deep learning	39	2	2	2	0	2	8
39	2023	Conference	Primary	Machine Learning	37	2	2	1	0	0	5
40	2021	Journal	Primary	Computer Vision	54	2	2	1	0	0	5
41	2018	Conference	Primary	Computer Vision	28	2	2	1	0	0	5
42	2020	Journal	Primary	Ultrasonic sensor,	37	2	2	0	0	2	6
43	2021	Journal	Primary	Machine Learning	64	2	2	0	2	2	8
44	2023	Journal	Primary	Computer Vision	27	1	2	0	1	0	4
45	2021	Journal	Primary	CNN	28	2	2	0	2	0	6
46	2020	Journal	Primary	Deep learning	33	2	2	0	2	0	6
47	2021	Journal	Primary	CNN- RNN	65	2	1	1	0	0	4
48	2019	Journal	Primary	Deep learning	41	2	2	1	0	0	5
49	2019	Conference	Primary	Gps tracking	19	2	2	2	1	1	8
50	2019	Conference	Primary	Gps location	30	2	2	2	1	1	8
51	2020	Conference	Primary	Voice output	43	2	2	0	2	2	8
52	2023	Journal	Primary	Voice feedback	35	2	2	2	0	2	8
53	2021	Conference	Primary	Emergency	17	2	2	0	0	2	6
54	2018	Conference	Primary	E-speak	30	2	2	2	0	2	8
55	2021	Journal	Primary	Voice	28	2	2	1	0	0	5
58	2019	Conference	Primary	Vision-based	41	2	0	1	1	0	6
59	2021	Conference	Primary	Visual positioning	27	2	2	2	2	2	10
60	2019	Journal	Primary	Tracking	64	2	2	0	1	1	6
61	2019	Conference	Primary	Navcane	31	2	2	0	1	1	6

Table 7: Quality evaluation score distribution

References	Score	Total
[1][32][59]	>8 to<= 10	3
[2][3][4][10][11][18][31][38][49][50][51][52] [54]	>6 to <=8	13
[[6][12][13][15][22][24][42][45][46] [53][58][60][61]	>5to <= 6	13
14][16][17][19][35][37] [39][40][41][48][55][57]	>4 to <= 5	12
[5][14][20][21][23][36][44]47]	>=4	8

Table 8: Article score

Publication score	Channel	Ref	No	%
Internal Conference on Emerging Technologies	Conference	[1]	4	2
Micromachines	Journal	[2]	1	0.5
28th Conference of Open Innovations Association (FRUCT)	Conference	[3]	2	1
Electronic	Journal	[4][24][47]	3	1.5
International Conference on Recent Trends in Electronics, Information, Communication & Technology (RTEICT)	Conference	[6]	1	0.5
Proceedings of the National Academy of Sciences	Journal	[10]	1	0.5
In Proceedings of the IEEE/CVF Conference on Computer Vision and Pattern Recognition	Conference	[9][12][42][48]	4	2
Sensors	Journal	[22][46]	3	1.5
Entropy	Journal	[11]	1	0.5
International Conference on Communication and Signal Processing	Conference	[13]	1	0.5
International Conference on Engineering of Modern Electric Systems	Conference	[14][54]	2	1
ACM Transactions on Accessible Computing (TACCESS)	Journal	[15]	1	0.5
Virtual Reality	Journal	[16]	1	0.5
2020 IEEE International Conference on Convergence to Digital World – Quo Vadis (ICCDW 2020)	Conference	[17]	1	0.5
International Workshop on Arabic and Derived Script Analysis and Recognition (ASAR),	Journal	[18]	1	0.5
IEEE Access	Journal	[19][20]	3	1.5
International Conference on Artificial Intelligence and Machine Vision (AIMV)	Conference	[21]	1	0.5
IETE Technical Review	Journal	[23][29][31]	5	2.5
Mechatronics	Journal	[32]	1	0.5
IEEE International Conference on Robotics and Automation	Conference	[44][55]	3	1.5
CHI Conference on Human Factors in Computing Systems	Conference	[41]	1	0.5
International Conference on Communication and Electronics Systems (ICCES)	Conference	[35]	1	0.5
Cloud Computing, Data Science & Engineering (Confluence)	Journal	[36][43]	2	1
CEUR Workshop Proc	Journal	[37]	1	0.5
International Conference on Microelectronics (ICM)	Conference	[38][52]	1	0.5
International Conference on Artificial Intelligence, Automation, and Control Technologies	Conference	[39][58]	2	1
International Conference on Trends in Electronics and Informatics (ICOEI)	Conference	[40]	1	0.5
Review of Applied Management and Social Sciences (RAMSS)	Journal	[41][56][57]	3	1.5
Applied Science	Journal	[45]	1	0.5
International Conference on Computational Intelligence in Data Science	Conference	[49][53]	2	1
Internal conference on smart structure and system(ICSSS)	Conference	[50][51][59]	3	1.5
International Journal of Advance Computer Science and Application	Journal	[60]	1	0.5
IEEE Transaction on Human-Machine System	Journal	[61]	1	0.5

3.3 Review Report

Understanding the assistive system for the blinds and formulating appropriate supervision through auditory feedback has become an emerging study these days. The present systematic literature review is executed to carry out related studies from digital libraries. These papers have undergone skimming and critical evaluation. Nonetheless, no previous research of this kind has been done that target high-level feature i.e., Urdu-based audio feedback, Urdu text detection, currency detection, and recognition using various deep learning methods. The extracted studies afterward an intensive study based on the above-listed research question.

4. Research Queries Valuation

4.1 Research Question (01) Which articles are appropriate? Determine the type of channel, as well as the demographic distribution.

In the area of navigational assistance, various approaches have been deployed. To evaluate and review the recent research we carried out a publication based on produced string with several filters for the extraction of the relevant publication. Fig. 4. demonstrates the complete number of publications filtered from the year 2019-2023. The bulk of the research articles come from IEEE with 40%. ACM also provides a significant contribution with 20% of the paper being downloaded from their digital library. Google Scholar was another valuable resource, providing 12% of the papers. Springer Link and Semantic Scholar were responsible for 16% and 8% of the research article downloads respectively. Science Direct, while providing fewer papers, still played a role, contributing 4% of the sources. Overall, with a diverse range of digital libraries, we have filtered the most relevant and effective research articles.

These publications are later evaluated through manual filtering such as reviewing the title, abstract, and other porting of the article, which is depicted in Table 5. The output of browsing based on the string with filter from 2019- 2023 is presented in Fig. 5, which includes 14 papers published in 2019, 13 papers from 2020, 8 papers released in 2021, 11 papers from 2022, and 4 papers from 2023. It is excellent to have a varied collection of papers from different years as it enables you to stay current with the latest research and concepts in your field. The collection of paper is a valuable resource.

Additionally, instead of coming from a blog or another unpublished article. We chose articles for our study from high-impact journals, conferences, and relevant review papers. For this purpose, we have collected a variety of sources of our research with 60% being from journal papers, 34% being conference papers, and 4% being reports published. The journal papers are typically peer-reviewed and considered to be more rigorous and reliable, while conference papers may provide more recent or cutting-edge research. Reports can also be valuable sources of information, particularly if they contain data or analysis that is not available elsewhere.

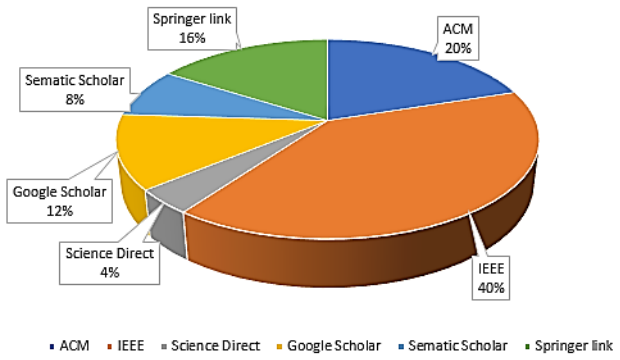

Fig. 4: Query string outcome in digital libraries

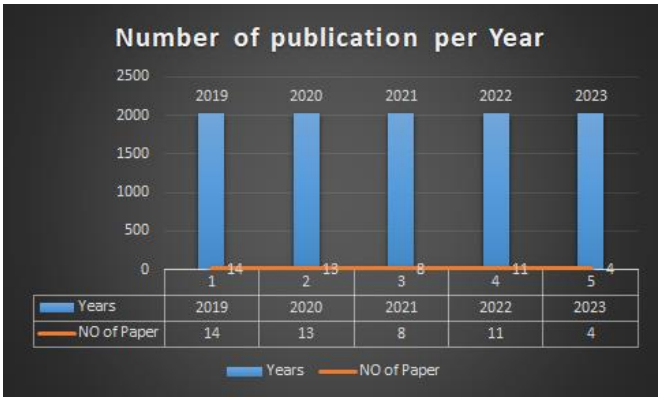

Fig. 5: Annual number of articles

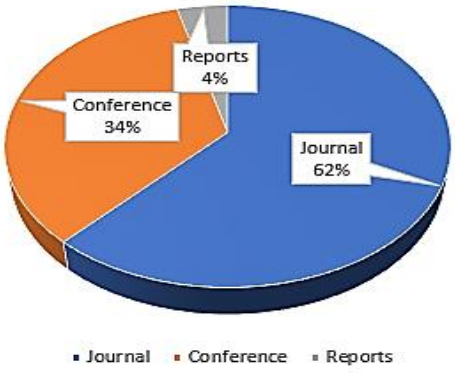

Fig. 6: Types of publications

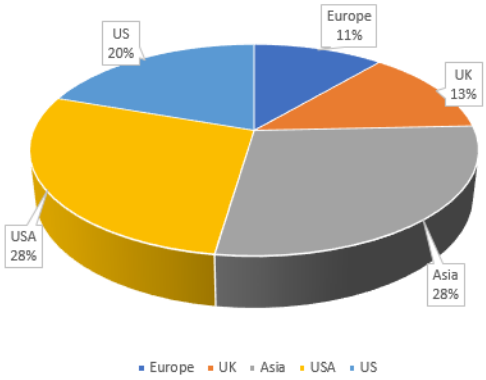

Fig. 7: Global classification of articles

Fig. 6 illustrates the comprehensive breakdown of the types of publications included in this study. The figure reveals a substantial majority, constituting 62% of the selected publications, correspond to esteemed journal papers. Conference papers, comprising 34% of the total, exhibit a notable presence in the research landscape, indicating their significance in disseminating scholarly findings. The remaining 4% encompasses other published reports, denoting a smaller yet noteworthy contribution from alternative sources of intellectual discourse. This presents a clear visual representation of the distribution of the publication types within the study. Fig. 7 illustrates the geographical distribution of the collected papers from different regions

across the world. Out of the total papers collected, 28% of them are from the United States of America, 20% are from Australia, 11% are from Europe, 13% are from the United Kingdom, and 28% are from Asia. Furthermore, Fig. 7 suggests that the paper collection is diverse and represents a broad range of perspectives and experiences from different parts of the world. It may also indicate that you have a particular interest in these regions.

Moreover, the contribution made by each journal and conference to the chosen research paper is demonstrated in Table 8 with publication scores for the papers.

4.2 Research Question (02) What is the principal purpose of navigational assistance?

Simple navigation is used to route people in unfamiliar environments, calculating the distance, route, and traffic. With the advancement of navigational assistance technology for the visually impaired person, making them independent. There are several applications including autonomous vehicles [28], currency identification [1], public transport [29], robot navigation [30], robotic dogs [31], and airport accessibility [32]. These applications aid the visually impaired in their everyday task while examining the navigational assistance. The following Table 9 displays the related application fields from the finalized published articles.

Table 9: Solution delivered by the particular publication

Study	Contribution	Approach
[16]	The video is forwarded to the caregiver to guide the user indoor and outdoor situations using haptic and audio communication.	Kinesthetic-based approach for routing guidance for moving left and right, while a single actuator for differentiating pattern.
[35]	To route through surfaces and obstacles based on IOT sensors with walking sticks.	The paradigm delivers a means to the visually impaired using various sensors to detect anomalies including obstacles, and stairs.
[36]	To provide the visually impaired the support to route in surrounding places and also access public transport.	Radio frequency identity is employed to aid the blind the accessing public transport, by buying a ticket, as well as reaching the bus stand using a global positioning system.
[34]	To evaluate the BLE navigation system for the blind at the airport and examine its effect.	The airport is equipped with Bluetooth low energy to perform user navigation and related routing exercises.
[37]	Smartphone cameras along with deep learning are used for the recognition of objects with the estimated distance from the visually impaired.	Mobile-based navigation system to aid the blind in and outdoors with audio feedback.
[38]	The system is founded for the blind to locate the object, and determine the position of the visually impaired for secure routing.	The model is trained to locate the object, wet surfaces, and the user's fall.
[41]	The sensory device with computer vision algorithm to deliver the surrounding knowledge to the visually impaired.	The basic aim is to deliver 3D information about the surroundings through hearing and sensing.
[43]	The shoes are integrated with IOT devices to traverse around using a computer vision algorithm to locate and recognize the hurdles.	An architecture to aid the blind in spinning around with shoes integrates the smart devices using a computer vision approach.
[48]	Generating three-dimensional information of a scene from video captured, which is comprehensively quickly delivered.	Depth map of the environment is calculated for the RGB images which later deliver three-dimensional information about the surroundings.
[50]	The system provides visual assistance to walk independently enabling the current location of the blind to their caretaker.	Audio routing and GPS are used for the bind. The SMS is delivered to the caregiver through a global system of mobile communication.
[39]	The platform is integrated with object localization and speech recognition based on deep learning for navigating purposes.	The system is modeled with a helmet mount camera in the front, using the web application and clouding computation.
[51]	The model easily traces the user in an unpleasant situation. The guardian gets an alert using SMS while the located object is informed using audio feedback.	The approach is conducted for observation and localization of the surrounding objects and provides the information using an audio command.
[54]	Raspberry Pi is the main source of collecting the frame of the environment and translating it into voice.	The cap aids the blind to route in the environment without anyone's assistance using the camera that captures the nearby objects.
[1]	The deep neural network is utilized to recognize the Pakistan currency for the visually impaired.	To manipulate the visual world into auditory by informing the blind about the obstacles in their way.
[52]	The approach provides a three-dimensional scene using voice output.	Travel aid system for the blind comprised of sensors for separating depth information and translating it into sound.

4.3 Research Question (03) How to examine and recognize the similarities and differences between high-level extracted features in current research?

Practitioners have made plenty of effort in the area of navigational assistance for the visually impaired ranging from sensor-based systems to advanced machine learning-based approaches, including deep learning, computer vision, and many other hybrid methodologies. These approaches assist in everyday daily tasks while aiding through sensing, locating, and identification of the object. Table 10 illustrates the classification of various methodologies for navigational assistance and the overview of related available articles is discussed below.

a) Sensors-based navigation system

The navigation system is the approach in which the object or the obstacle is detected using various types of sensors in real time. The application aid in daily life routine while locating various object through sensors mounted on walking sticks [16], an IOT-based E-cane [33], and radio frequency identification (RFID) for buying tickets and airport accessibility [32, 34].

Table 10: Prospectus outcome of the revised papers

Aspect	Basis	ref	Method	Finding
Sensor- Based	To reveal the sensor-based navigation	[16]	The vibrating sensor is utilized to instruct the visually impaired to move left and right and another single sensor is for differentiating the actuator	1) The study provides navigational assistance using various vibrating sensors for the blind to assist in the routing 2) Inform users through alerts using vibrators
	Internet of thing base smart came for navigation	[35]	IoT paradigm to deliver information through employing sensors utilized to locate anomalies	To route the blind through various surfaces and objects. The cane is to deliver the current location to the caregiver of the visually impaired individual
	Radiofrequency identification	[36]	Radiofrequency identification is used to traverse the blind to access public transport	The practice presents model gives support to the blind in accessing transport with any assistance
	Bluetooth low energy	[34]	BLE system is deployed for traversing and calculating user experience	The proposed system is found based on BLE for the navigation of the blind in the international airport
Computer Vision Based	Smartphone camera integrated with deep learning	[37]	The deep learning algorithm is generated for the recognition and various obstacles and calculating the distance	Mobile-based routing system to aid the blind in an outdoor navigation system with audio feedback
	Smart shoes	[38]	The model was developed mainly for detecting wet surfaces and placing the blind in real-time for safe and secure routing	The system enables the user to detect the wet surface and also inform their caretaker in case of a fall-down
	Raspberry pi	[40]	The system delivers walkable spaces, text identification, and text-to-speech	Wearable devices enable them to signal objects to users plus read the text
	Computer Vision	[41]	The vision model device is integrated with computer vision to deliver knowledge of the surroundings to the user	To develop a system while providing 3D information of the surroundings for travers
	Deep learning	[39]	Integrated system with OCR, speech processing, and another visionary to locate the object based on deep learning	Generated an integrated system with multiple functions for object localization and recognition
	Convolutional Neural Network	[45]	To assess the depth camera with Fast-SCNN and the depth map	To achieve walkability and guide the user with voice feedback
	Deep learning	[48]	To evaluate the novel technique to generate three-dimensional information using deep learning	To develop approaches with a depth camera that provide three-dimensional information for the blind
	Hybrid Approach	[47]	To examine the hybrid approach using CNN-RNN with decoder and encoder method	To secure a model that comprehends the distinct scene and is delivered in the form of text
Global Positioning System	Smart Eye	[49]	The device captures the location of the user, including generating a warning when objects are located on the way	Multiple devices are integrated to enable a system that directs the visually impaired with voice
	Global positioning location	[50]	The system delivers messages with their location during the hindrance. Visual voice using IOT to enable the walk	To achieve voice navigation and global positioning system tracking for the visually handicapped.
	Massage Generations	[51]	To analyze the system that can trace the user in an emergency using GPS	The system that locates the objects and provides voice output
	voice feedback	[53]	To acquire information of surroundings through voice using deep learning method object identification	The method provides an understanding of the surroundings in voice feedback

b) Object localization and identification

The process of locating the presence of an object in the video stream. Locating the various moving objects is the real-time application of the navigational system. Obstacles or objects can be localized and identified through various approaches including deep learning [35], smart shoes [36], and visual-based concurrent detection and mapping [37], Object detection and identification also convey assistive features. Such as locating various object from the continuous video stream aid the blinds to safely route in the surrounding [38], without collision using a computer vision technique [39]. The located objects in the frame can be further identified and traced by picturing depth information in the motion frame. This can be beneficial in the surveillance, traffic, and healthcare sectors.

c) Global positioning system with auditory feedback

Besides employing the different sensors [40] based on visually impaired navigation [41], machine learning approaches [42], CNN [43], deep learning [44] and hybrid methods [45] for object localization and recognition [46], while navigating in the surrounding the global positioning system [47] with the massage to their caretaker [48] is generated through voice feedback [49-50] which trace the current location of the person in an unpleasant situation [51].

4.4 Research Question (04) How to determine the primary concern and challenges that navigation aid will face for Pakistani people?

Though practitioners have done substantial research in the field of navigation for the visually impaired. Still, those approaches are shortages in covering millions of blinds in Pakistan. The developed approaches are mostly English-based [52-53]. While majority of Pakistanis do not speak or comprehend the English Language, which limits the concept of voice navigation and auditory feedback for them.

4.5 Research Question (05) What is the effective and interactive communication medium for the Pakistani population?

Urdu is a commonly spoken and comprehended language around Pakistan. The language was declared the national language [54], and is used in schooling, works, offices, and even law court [55]. For any navigational assistance, the medium of instruction in Urdu would be warmly welcomed by the people of Pakistan, especially by the visually impaired. Locating and identifying the object in the video frames [56], visual placing [57], tracking [58], and many other state-of-the-art sensor-based approaches [59-61] integrate with the language that is mostly understood to enhance the adaptability and improve the concept of autonomous navigation system for visually impaired in Pakistan.

5 Discussion and Future Direction

This part precise and debates the result relevant to the systematic literature review. The scrutiny of navigational assistance, tools, approaches, and evaluation for the development of an international standard for the visually impaired.

5.1 Taxonomic Hierarchy

The purpose of this SLR was to evaluate the existing knowledge in visual assistance by censoriously examining 50 relevant publications. To conduct this, we developed a taxonomic hierarchy of selected studies as shown in Fig. 8. Discarded the studies that have not authenticated their approaches empirically. We have explored development and challenges for the characteristics such as approaches and application of navigational assistance. However, these features are additionally distributed into many sub-levels displaying the depth of each feature and their role in the improvement of visually impaired life.

5.2 General Observations & Future Direction

Numerous opinions can be drawn from the findings of this systematic literature review (SLR), while comprehending the navigational assistance, various RQs were established to determine various approaches, resources, characteristics, and constraints. As a result, several patterns and discoveries can be noted regarding the constraints of navigational assistance. These include the subsequent observations and future directions.

5.3 Sensor Based

The goal of this systematic literature review is to examine the current research to carry out and comprehend useful information that incorporates the field of navigational assistance. Various elements of navigational assistance have been discussed by the practitioners. The features include: identifying multiple objects [32, 33], lane tracking [34], and an actuator [16] for differentiating the different patterns through alarm-based feedback.

Table 11: Finding a solution for auditory feedback.

Aspect	Basis	Ref	Method	Finding
Audio Feedback	Visionary based guide	[58]	To evaluate the architecture lies on camera the vision act and artificial cane able to locate lanes while walking	The proposed model helps in maintaining the lane while jogging or walking for the visually impaired
	Mobility solution for the blind	[59]	To find a method using the visual solution and API to identify text, images and logos	This model aims to integrate visual positioning and API for the recognition of objects
	Lidar based approach	[63]	The method uses Lidar to calculate the distance and the identified images are acknowledged using audio	To find an approach that facilitates the distance calculation and recognition of object
	currency recognition	[1]	The deep neural network is deployed to estimate the tag for the provided images and give the feedback using Urdu language	The proposed model employed deep learning for the recognition of currency and gives output in Urdu
	Urdu Text Recognition	[18]	To combine the OpenCV with OCR for Urdu text detection and the recognized text in then spoken for the blind	The developed model provides audio assistance for the blind detecting the Urdu text.
	Urdu text in images	[19]	To examine the CNN model for locating the Urdu text in the given image, and providing feedback using Urdu auditory feedback	The model aims to recognize the text in the given images while providing auditory feedback

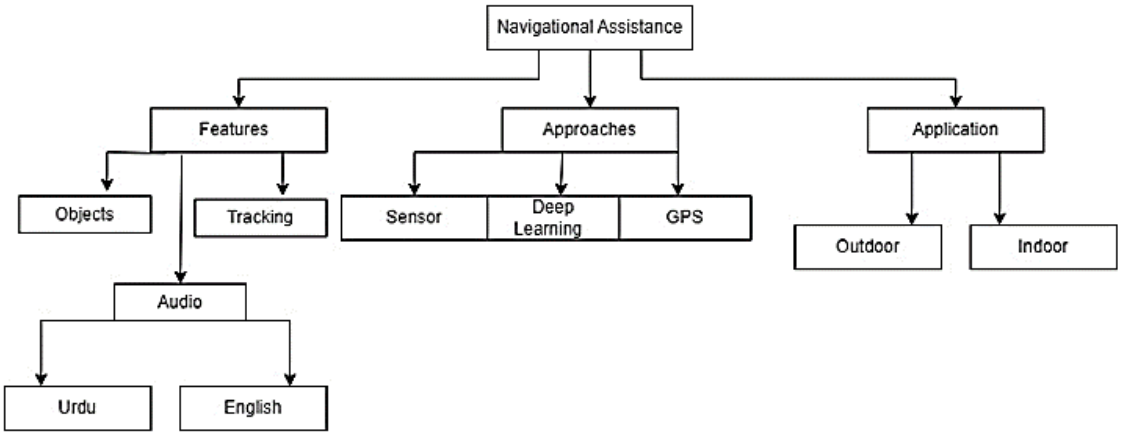

Fig. 8: Taxonomy of visually impaired

Various practitioners have put effort into the detection of objects and recognition, but still the gap exists. For the effectiveness of navigational assistance in real-time, the auditory feedback in the Urdu language for the Pakistani people is taken as a major challenge.

5.4 Deep Learning Approaches or Methods

Various practitioners recommended different methods to examine and comprehend object localization and recognition using different techniques for the routing of the blinds. Relatively, plenty of practitioners worked on different techniques of deep learning [35, 36], such as convolutional neural networks [43-46], and recurrent neural networks [45] for active calculation. The deep learning approaches provide better performance for the analysis of interest, which enhances the computational power. Reduces the training and testing time leading toward efficient object localization and identification.

5.5 Application of Visual Assistance

The massive mainstream of this literature is thought to be developed for providing the necessary assistance for a safe and independent life [47]. The practitioners at the beginning concentrated on the navigation system for the blinds, then they put effort into this developing field of navigational assistance with voice feedback [48, 49], to enhance their movability [50] and confidence in traveling freely and performing daily tasks with ease.

The visual assistance-based extraction of quality papers, location and quantitative study is needed. A maximum of 20 papers have been selected from the IEEE library and around partial of the amount is finalized from ACM as displayed in Table 5. The total number of publications concerning the years is shown in Fig. 4. It is also witnessed from Fig. 6 that a huge number of publications were recognized from journals and the second-highest publications were taken from quality conferences. The SLR included in our article is identified as a report which is about 4% of the total percentage. The regional distribution of articles is depicted in Fig. 7. Where the majority of available publications are from the USA and Asia sharing an equal number of 28%. The rest of the publications are from European countries.

The article score for the selected study is awarded related to questions shown in Table 8, it is obvious to see that the score ranges between 4-10. Overall classification results and quality valuation of finalized studies have been presented in Table 6. Additionally, we have acknowledged the sources of chosen research, the publication platform, and the overall study proportion mentioned in Table 8. About 40% of selected papers have been published in a journal named IEEE, where the ACM preceding is the second highest publication source 20%.

4. Conclusion

The existing literature on navigational assistance mainly focuses on object detection using sensors and GPS tracking to monitor the location of individuals. In addition, these sources explore the effectiveness of deep learning in object localization, as well as the adaptability and portability of such systems. However, there are limitations associated with these approaches that hinder their ability to provide comprehensive support for the visually impaired. To address this gap, we conducted a review of current research trends in visual assistance for the visually impaired, specifically in the English language. We employed a systematic approach to evaluating the impact of high-level characteristics, interpreting research findings and exploring various domains to gain a better understanding of the topic. Moreover, we aim to include additional insights that highlight the unique challenges and opportunities associated with providing navigational assistance for individuals with visual impairments. To obtain relevant publications related to visual assistance for the visually impaired, we developed a custom query string and applied it to six distinct digital libraries. The search criteria included: inclusion-exclusion guidelines and a thorough quality evaluation process that spanned from 2019 to 2023. We identified 50 articles that were considered worthy of further criticalexamination. Moreover, Urdu auditory feedback has also contributed to the visually impaired by

locating the Urdu text [17], Urdu text in images [18] and Pakistani currency recognition [1].

The limitations of a systematic literature review typically relate to search strategies, insufficient selection of data and incorrect categorization. Nevertheless, we have minimized the potential for biased selection by utilizing various search terms across multiple digital libraries in this study.

Through the use of firm inclusion/exclusion criteria and appropriate quality assessment methods, primary papers were selected based on their relevance to the research topic. The results indicate that the majority of the chosen articles were sourced from journal proceedings, with enough conference papers being selected. The majority of the research that was selected focused on exploring various approaches to the development of navigation assistance through voice audio feedback in the English language. However, the vast majority of the Pakistani population doesn't understand the English language so navigational assistance would not be so efficient. Finally, the future studies on navigational assistance, more consideration should be paid to object localization and tracking with Urdu auditory feedback for the visually impaired people in Pakistan. Mitigating the limitation of the language barrier who don't comprehend the English language since plenty of work has been done for the Urdu language including Urdu text so the navigation assistance for the visually impaired would in Urdu be a great contribution.

Acknowledgments.

We would like to express our sincere gratitude to all those who have contributed to the successful completion of this review paper.

We would like to thank our colleagues, who provided valuable feedback and suggestions throughout the research process. We are also grateful to the various experts in the field who took the time to review our work, providing us with invaluable insight and direction. This review would not have been possible without the support of our funding agencies and institutions.

References

[1] Z. Ahmed, M, Rizwan. M, Khan. S.Y, Arafat "Urdu Language-based Assistance App for the Blind and Visually Impaired People," 16th International Conference on Emerging Technologies (ICET) IEEE, pp. 1-5, 2021.

[2] Y. Bouteraa, Yassine "Design and development of a wearable assistive device integrating a fuzzy decision support system for blind and visually impaired people," Micromachines, vol. 12(9), pp. 1082, (2021).

[3] B. Chaudary, I, Paajala. L, Arhippainen. P, Pulli. "Studying the navigation assistance system for the visually impaired and blind persons and ICT use by their Caretakers," 28th Conference of Open Innovations Association (FRUCT), 2021.

[4] J. Bai. Z, Liu. Y, Lin. S, Lian. D, Liu. "Wearable travel aid for environment perception and navigation of visually impaired people," Electronics, vol. 8(6), pp.697, 2019.

[5] C. Zatout.S, Larabi. I, Mendili. S, Ablam Edoh Barnabe, "Ego-semantic labeling of a scene from a depth image for visually impaired and blind people," In Proceedings of the IEEE/CVF International Conference on Computer Vision Workshops, 2019.

[6] K.N. Kumar.R, Sathish. S, Vinayak. T.P, Pandit, "Braille assistance system for visually impaired, blind & deaf-mute people in indoor & outdoor application," 4th International Conference on Recent Trends on Electronics, Information, 2019.

[7] B. Mitra. K, Sharma. S, Acharya. Mishra. A, Guglani., "Real-time Smile Detection using Integrated ML Model," 6th International Conference on Intelligent Computing and Control Systems (ICICCS). IEEE, pp. 1374-1381, 2022.

[8] S. Wu. Q, Ze. J, Dai. N, Udipi. G.H, G Paulino. R, Zhao, "Stretchable origami robotic arm with omnidirectional bending and twisting," In Proceedings of the National Academy of Sciences, vol. e2110023118, p. 118(36), 2021.

[9] K. Li. S, Wang. X, Zhang. Y, Xu. W, Xu. Z,Tu, "Pose recognition with cascade transformers," In Proceedings of the IEEE/CVF Conference on Computer Vision and Pattern Recognition, pp. 1944-1953, 2021.

[10] F. Ashiq. M, Asif. M.B, Ahmad. S, Zafar. K, Masood, "CNN-based object recognition and tracking system to assist visually impaired people," IEEE Access, vol. 10, no. 2022, pp. 14819-14834., 2022.

[11] R.C. Joshi. S, Yadav. M, Dutta. M.C, Travieso-Gonzalez, "Efficient multi-object detection and smart navigation using artificial intelligence for visually impaired people," Entropy, vol...22(9), pp. 941, 2020.

[12] Y. Lin. K, Wang.W, Yi, Yi. S, Lian, "Deep learning based wearable assistive system for visually impaired people," In Proceedings of the IEEE/CVF International Conference on Computer Vision Workshops, 2019.

[13] C. Ananth.S, Jacob. J.D, Rosita. M.S, Muthuraman. T.A, Kumar, "Low-Cost Visual Support System for Challenged People," International Conference on Smart Technologies and Systems for Next Generation Computing (ICSTSN), pp. 1-4, 2022.

[14] L. Tepelea. I, Buciu. C, Grava. I, Gavrilut. A, Gacsadi, "A vision module for visually impaired people by using Raspberry PI platform," 15th International Conference on Engineering of Modern Electric Systems (EMES), pp. 209-212, 2019.

[15] D. Ahmetovic. S, Mascetti. C Bernareggi. J, Guerreiro. U, Oh. C, Asakawa, "Deep learning compensation of rotation errors during navigation assistance for people with visual impairments or blindness," ACM Transactions on Accessible Computing, 2019.

[16] B. Chaudary. S, Pohjolainen. S, Aziz. L, Arhippainen. P, Pulli, "Teleguidance-based remote navigation assistance for visually impaired and blind people—usability and user experience," Virtual Reality, vol. 27(1), pp. 141-158., 2023.

[17] H. Ali, "Leveraging machine learning for less developed languages," Progress on Urdu text detection, 2022.

[18] A. Chandio.M.D, Asikuzzaman. P.R, Mark. L, Mehwish, "Cursive text recognition in Natural Language Scene Images using deep learning Convolutional Recurrent Neural," IEEE Access, vol. 10, pp. 10062–10078, 2022.

[19] S. Khan.S, Nazir. U.H, Khan, "Analysis of navigation assistants for blind and visually impaired people: A systematic review," IEEE Access, vol. 9, pp. 26712-26734, 2021.

[20] D. Plikynas. A, Zvironas. A, Budrionis. M, Gudauskis, "Indoor navigation systems for visually impaired persons: Mapping the features of existing technologies to user needs," Sensors, vol. 20(3), p. 636, 2020.

[21] B. Kuriakose. Shrestha. F.E, Sandnes, "Tools and technologies for blind and visually impaired navigation support: a review," IETE Technical Review, vol. 39(1), pp. 3-18, 2022.

[22] E. Cardillo. A, Caddemi, "Insight on electronic travel aids for visually impaired people: A review on the electromagnetic technology," Electronics, vol. 8(11), p. 1281, 2019.

[23] N. Tyagi. D, Sharma. J, Singh. B, Sharma. S, Narang, "Assistive navigation system for visually impaired and blind people: a review," International Conference on Artificial Intelligence and Machine Vision (AIMV), pp. 1-5, 2021.

[24] F. El-Taher. A, Taha. J, Courtney. S, Mckeever "A systematic review of urban navigation systems for visually impaired people," Sensors, vol. 21(9), p. 3103, 2021.

[25] B. Kitchenham, "Procedures for performing systematic reviews," Keele, UK, Keele University, vol. 33, pp. 1-26, 2004.

[26] C. Okoli. K, Schabram, "A guide to conducting a systematic literature review of information systems research," 2010.

[27] Q. Zhang. H, Sun. X, Wu. H, Zhong, "Edge video analytics for public safety: A review," Proceedings of the IEEE, vol. 107(8), pp. 1675-1696, 2019.

[28] H. Jing. Y, GAO. Shahbeigi. M. Dianati, "Integrity monitoring of GNSS/INS based positioning systems for autonomous vehicles: State-of-the-art and open challenges," IEEE Transactions on Intelligent Transportation Systems., 2022.

[29] S. Martinez-Cruz. L,Morales-Hernández. G.I, Pérez-Soto. J. P, Benitez-Rangel. K. A, Camarillo-Gómez. "An outdoor navigation assistance system for visually impaired people in public transportation," IEEE Access, vol. 9, pp. 130767-130777, 2021.

[30] J.A, Dulce-Galindo. M.A, Santos. G.V, Raffo. P.N, Pena, "Distributed supervisory control for multiple robot autonomous navigation performing single-robot tasks," Mechatronics, vol. 86, p. 102848, 2022.

[31] Z. Li. N, Xu. X, Zhang. X, Peng. Y, Song. "Motion Control Method of Bionic Robot Dog Based on Vision and Navigation Information," Applied Sciences, vol. 13(6), p. 3664, 2023.

[32] J. Guerreiro. D, Ahmetovic. D, Sato. K, Kitani. C, Asakawa, "Airport accessibility and navigation assistance for people with visual impairments.," In Proceedings of the 2019 CHI Conference on Human Factors in Computing Systems, pp. 1-14, 2019.

[33] V. Kunta. C, Tuniki. U, Sairam, "Multi-functional blind stick for visually impaired people," 5th International Conference on Communication and Electronics Systems (ICCES), pp. 895-899, 2020.

[34] S. Choudhary. V, Bhatia. K.R, Ramkumar, "IoT-based navigation system for visually impaired people," 8th International Conference on Reliability, Infocom Technologies and Optimization (Trends and Future Directions) (ICRITO), p. 521, 2020.

[35] S. Shadi. S, Hadi. M.A, Nazari. W, Hardit, "Outdoor navigation for visually impaired based on deep learning," In Proc. CEUR Workshop Proc., vol. 2514, pp. 97-406, 2019.

[36] J. Chehade. G, abou haydar. A, hayek. J, boercsoek. J. J. S, olmedo, "Design and Implementation of Smart Shoes for Blind and Visually Impaired People for More Secure Movements," 32nd International Conference on Microelectronic, pp. 1–6, 2020.

[37] A. Yang. M, Beheshti. T. E, Hudson. R, Vedanthan. W, Riewpaiboon. P, Mongkolwat. J.R, Rizzo, "UNav: An Infrastructure-Independent Vision-Based Navigation System for People with Blindness and Low Vision," Sensors, vol. 8894, pp. 22(22), 2022.

[38] L. Abraham. N.S, Mathew. L, George. S.S, Sajan, "VISION-wearable speech-based feedback system for the visually impaired using computer vision," 4th International Conference on Trends in Electronics and Informatics (ICOEI), p. 48184, 2020.

[39] S. Shilaskar. M, Dhopade. J, Godle. S, Bhatlawande, "Machine Learning-Based Pavement Detection for Visually Impaired People," In Advances in Cognitive Science and Communications and Cyber-Physical Engineering (ICCCE 2022), 2023.

[40] M. R. Reenu. A, Mouni. T, Karthiga, "Audio Navigator for Visually Impaired People," 2019.

[41] S. Rao. V.M, Singh, "Computer vision and IoT based smart system for visually impaired people," 11th International Conference on Cloud Computing, Data Science & Engineering (Confluence) IEEE, pp. 552-556, 2021.

[42] A. Ghosh. S.A, Al Mahmud. T.I.R, Uday. D.M, Farid, "Assistive technology for visually impaired using tensor flow object detection in Raspberry Pi and coral USB accelerator.," IEEE Region 10 Symposium (TENSYMP), pp. 186-189, 2020.

[43] I.H, Hsieh. H.C, Cheng. H.H, Ke. H.C, Chen. J.W, Wang, "A CNN-based wearable assistive system for visually impaired people walking outdoors," Applied Sciences, vol. 11(21), p. 10026, 2021.

[44] S.S. Singh. M, Agrawal. M, Eliazer, "Collision detection and prevention for the visually impaired using computer vision and machine learning," Advances in Engineering Software, vol. 179, p. 103424, 2023.

[45] D. Pintado. V,Sanchez. E, Adarve. M, Mata. Z, Gogebakan. B, Cabuk. P, Oh, "Deep learning based shopping assistant for the visually impaired," IEEE International Conference on Consumer Electronics (ICCE) IEEE, pp. 1-6, 2019.

[46] Z. Bauer. A, Dominguez. E, Cruz. F, Gomez-Donoso. S, Orts-Escolano. M, Cazorla, "Enhancing perception for the visually impaired with deep learning techniques and low-cost wearable sensors," Pattern recognition letters, vol. 137, pp. 27-36, 2020.

[47] I.J.L. Paul. S, Sasirekha. S, Mohanavalli. C, Jayashree. P.M, Priya. K.Monika "Smart eye for visually impaired-an aid to help the blind," International Conference on Computational Intelligence, pp. 1–5, 2019.

[48] B. Nivetha, "GPS navigation with voice assistance and live tracking for visually impaired travelers," International Conference on Smart Structures and Systems (ICSSS), pp. 1-4, 2019.

[49] A. Devi. M.J, Therese. R.S, Ganesh "Smart navigation guidance system for visually challenged people," International Conference on Smart Electronics and Communication (ICOSEC), pp. 615-619, 2020.

[50] P. Skulimowski. M, Owczarek. A, Radecki. M, Bujacz. D, Rzeszotarski. P, Strumillo "Interactive sonification of U-depth images in a navigation aid for the visually impaired," Journal on Multimodal User Interfaces, vol. 13, pp. 219-230, 2019.

[51] M.I. Hussan. D, Saidulu. P.T, Anitha. A, Manikandan. P, Naresh "Object detection and recognition in real-time using deep learning for visually impaired people." IJEER 10(2), pp. 80–86, 2022.

[52] M. Joshi. A, Shukla. J, Srivastava. M, Rastogi. S, Mujumdar. H, Tripathi "DRISHTI: Visual Navigation Assistant for Visually Impaired," Journal of Physics: Conference Series. vol. 2570, no. 1, p. 012032", 2023.

[53] C. L. Lu. Z.Y, Liu. J.T, Huang. C.I, Huang. B.H, Wang. Y, Chen. P.Y, Kuo, "Assistive Navigation Using Deep Reinforcement Learning Guiding Robot With UWB/Voice Beacons and Semantic Feedbacks for Blind and Visually Impaired People," Frontiers in Robotics and AI 8, pp. 1–23, 2021.

[54] S, Jawad. B, Ali. D.M, Asad. D.M.S, Thaheem "Urdu as official language: A constitutional mandate," Review of Applied Management and Social Sciences (RAMSS), 2021.

[55] A. Raj, "The case for Urdu as Pakistan's official language," The case for Urdu as Pakistan's official language, pp. 176, 2021.

[56] L, Hou. K, Lu. X, Yang. Y, Li. J, Xue, "Gaussian representation for arbitrary-oriented object detection," Remote Sensing, pp. 15(3), 757, 2023.

[57] J. Gonçalves. S, Paiva "Inclusive mobility solution for visually impaired people using Google Cloud Vision.," IEEE International Smart Cities Conference (ISC2), pp. 1-7, 2021.

[58] O. Younis. W, Al-Nuaimy. M.H, Alomari. F, Rowe, "A hazard detection and tracking system for people with peripheral vision loss using smart glasses and augmented reality.," International Journal of Advanced Computer Science and Applications, pp. 1-9, 2019.

[59] V. V. Meshram. K, Patil. V.A, Meshram, F.C, Shu, "An astute assistive device for mobility and object recognition for visually impaired people." IEEE Transactions on Human-Machine Systems vol. 49(5), pp. 449-460, 2019.

[60] N. E. Shandu. P.A, Owolawi. T, Mapayi. K, Odeyemi, "AI-based pilot system for visually impaired people," International Conference on Artificial Intelligence, Big Data, Computing and Data Communication Systems (icABCD), pp. 1-7, 2020.

[61] P. Chitra. V, Balamurugan. M, Sumathi. N, Mathan. K, Srilatha. R, Narmadha, "Voice Navigation Based Guiding Device for Visually Impaired People." International Conference on Artificial Intelligence and Smart Systems (ICAIS), pp. 911-915, 2021.

The Nucleus ***60***, *No. 2 (2023) 199-204*

www.thenucleuspak.org.pk

The Nucleus

ISSN 0029-5698 (Print)
ISSN 2306-6539 (Online)

A Holistic Approach for Detecting Socialbots on Twitter: Integration of Diverse Features

Muhammad Owais*, Muhammad Shoaib, Muhammad Waseem

Computer Science, University of Engineering & Technology 54890, Punjab, Pakistan

ABSTRACT

The usage of social media platforms has grown, offering individuals diverse avenues for communication, expressing opinions and sharing online content. However, this surge has also given rise to the emergence of social bots, which are programmed accounts designed to imitate human behavior. Such bots possess the capability to disseminate false information, manipulate financial markets, aid terrorism, and disrupt democratic processes. To tackle this issue, various approaches have been utilized to detect social bots, including approaches based on profiles, time patterns, content analysis, behavior, and network characteristics. However, neither of the approaches effectively combines all these features to implement social bot detection comprehensively. This paper introduces an ensemble methodology that merges profile, behavioral, temporal, network, graph, and content-based attributes, culminating in a comprehensive model for discerning social bots on the Twitter platform. We utilize the Twibot-22 dataset for conducting experiments and evaluate the performance of our approach against benchmark models. The XGBoost model, with an accuracy of 0.898, exhibited superior performance compared to the benchmark models. This research contributes to the continuous endeavor focused on safeguarding the authenticity of tweet content and mitigating the risks associated with social bots on social networks.

Keywords: *Machine Learning, Social bot, XGBoost, Twitter, detection*

1. Introduction

Online social networking platforms have revolutionized communication by providing a platform for individuals to share their thoughts and personal information regarding current events [1]. A significant portion of the global population actively engages with one or more OSNs, with Twitter and Facebook being particularly popular choices. In fact, as of December 2022, Twitter boasted a staggering user base of over 368 million monthly active users worldwide, and this number is projected to continue growing in the coming years [2]. However, the widespread adoption of Twitter has also brought about an upsurge in the presence of Twitter bots, which are automated accounts designed to mimic human behavior [3]. These social bots, comprising approximately 9 to 15 percent of active Twitter accounts, serve various purposes but are often associated with malicious intentions [4]. Their activities encompass spreading false information [5], stock market manipulation [6], endorsing terrorist activity [7], disseminating explicit content [8] and even interfering in the 2016 United States presidential election [9]. Consequently, the proliferation of social bots undermines the authenticity of online trends, erodes democratic processes and poses significant harm to society.

Socialbots use contemporary techniques to imitate human qualities to hide their true identity online and avoid being detected. Therefore, it is essential to detect Twitter bots to maintain the genuineness of tweet content. In pursuit of this objective, experts utilize various methods to distinguish between human users and programmed accounts. Machine learning algorithms have quickly advanced, giving researchers the ability to detect the presence of bots and suspect sources. In the past, machine learning algorithms, specifically supervised learning, utilized various manually created characteristics to identify bots [10]. Prior studies have shown enhanced performance in social bot identification through recent advancements in machine learning methods such as profile metadata-based methods [1], graph network-based approaches [11], behavior-based techniques [12], as well as temporal modeling-based methods [3]. Nevertheless, these previous approaches have certain limitations. For instance, the profile-based technique is vulnerable to spoofing, as it can be manipulated to resemble human behavior more closely [13]. Similarly, the graph partitioning-based method primarily focuses on analyzing the network information and the behavioral patterns of programmed accounts, which makes it ineffective in detecting bots that successfully establish connections with regular users [14]. Moreover, the limitations of these techniques stem from their dependence on textual, temporal, and profiling data. On the other hand, behavioral and temporal-based research methodologies have been utilized to detect bots. Nevertheless, unlike alternative methods, these models solely detect a particular bot category based on user information [15].

Beforehand, different methods including profile metadata-based, behavioral-based, temporal-based, network-based, graph-based and content-based techniques have been separately utilized to detect social bots. However, to the best of our knowledge, none of these approaches have integrated all the mentioned features and capabilities in combination.

In our proposed approach, the model was trained on the Twibot-22 dataset. The unique aspect of this research lies in the incorporation of various features such as profile-based, behavioral-based, temporal-based, graph network-based and content-based techniques to identify social bots. When evaluating the model's performance on the Twibot-22 dataset, it exhibited superior results compared to benchmark models.

Section 2 provides an overview of the relevant research and the motivation behind detecting social bots on Twitter. Section 3 offers a sophisticated method for locating social bots on Twitter using a thorough multi-feature analysis. Transitioning to Section 4, we provide the resources and

*Corresponding author: owaiskhana635@gmail.com

techniques used in this investigation. In Section 5, we explore the results obtained from the conducted experiments, assessing the efficacy of the proposed approach. Lastly, Section 6 delivers a thorough summary of the article.

2. Related Work

Online social media platforms' programmed profiles mimic human traits to manipulate public perception or spread inaccurate information. Several machine-learning techniques have been suggested to curb the impact of social bot profiles. The profile-based framework was created to detect social bots, achieving an accuracy of 89% through the utilization of a random forest algorithm and six hybrid-selected features [16]. Similarly, the detection of a bot account through profile metadata, incorporating an extra tree classifier for feature selection and the weight of evidence encoding attained an impressive 88% accuracy with random forest [17].

Furthermore, to detect social bots, the authors [3] analyzed users' online behavior as if it were DNA sequences. They utilized the Term Frequency-Inverse Document Frequency (tf-idf) a numerical method adopted to compute entropy on segments, aiming to identify the pattern linked to bots. This approach achieved an accuracy of 94%. GANBOT [12] employed LSTM as a common interface to link the discriminator and, generator allowing for the assessment of online users' behavioral patterns. This approach demonstrated promising results on the Cresci dataset. Similar to the other bot detection methods, [18] utilized a Network graph approach to identify social botnet communities, taking into account behavior similarity and participant trust values. This strategy employed deep autoencoder technology. Additionally, the study delved into the interrelation between the social and collaborative network of the account as part of the endeavor to identify social bots.

This involved applying a semi-supervised learning algorithm that incorporated label propagation and an iterative traversal of the users' proximity graph in sequence [11].

Moreover, the adoption of content-based identification for social bots has also taken place. The researcher [19] employed CNN and LSTM in conjunction with BERT to classify tweets as either generated by programmed accounts or originating from real users. In addition, a fabricated prediction algorithm was utilized to calculate the sentiment score of each piece of content, enabling the identification of social bot accounts with a 97% accuracy rate [20].

In the study by Kosmajac et al. [21], a temporal-based approach to detect social bot accounts has been implemented. The approach utilizes statistical diversity measures to examine the variation in user behavior during a specific period. Additionally, they developed a method to identify malicious tweets by analyzing the pairwise similarity of individual retweeting behavior, focusing on temporal features [22]. While various techniques have been utilized for social bot detection, encompassing aspects such as profile analysis, timestamps, content examination, behavioral assessment, network relationships, and graph analysis, a research gap exists in the lack of emphasis, in prior studies, on integrating multiple features like metadata, content, interactions, and timing for accurate social bot identification [14]. This study uniquely addresses this gap by comprehensively incorporating all available features - profiles, content, timestamps, behavior, and network connections - to significantly advance the precision of social bot identification.

3. Proposed Methodology

Social media platforms often employ social bot detection techniques to distinguish between real human users and automated bots. The diverse functions of these bots, including spreading propaganda and overwhelming users with irrelevant content, present a challenge to preserving the integrity of tweet content. As a result, detecting social bot accounts would greatly benefit the preservation of content integrity. To address the issue of social bot detection, we have put forth an approach aimed at identifying programmed accounts. The system architecture is depicted in Figure 1.

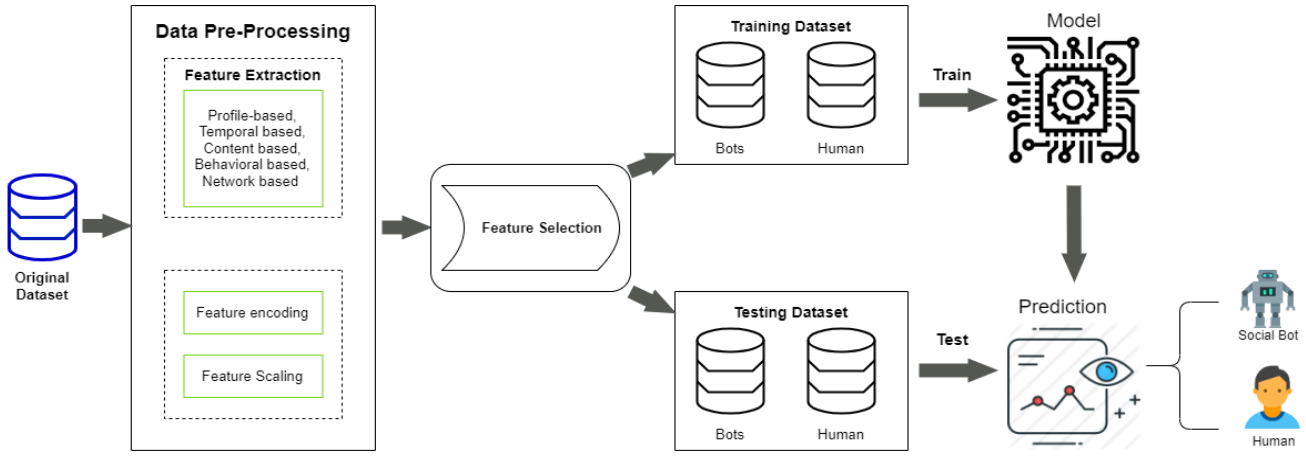

Figure 1: Architectural Framework

The model was trained and social bots were identified using a hybrid features-based method. The model was trained using a publicly accessible dataset. Before training, the features were extracted to analyze their high correlation. The closely interrelated attributes, obtained by integrating a comprehensive set of features - profiles, content, timestamps, behavior and network connections - to markedly enhance the accuracy of social bot identification, were subsequently chosen for categorical encoding and feature scaling. The chosen classifier utilized these selected features as input and the evaluation parameters were employed to assess their performance.

4. Materials and Methods

The paper's section discusses an approach for identifying social bot accounts, consisting of multiple phases outlined below.

4.1) Dataset

This research paper addressed the problem of Twitter bot localization by utilizing the publicly accessible Twibot-22 datasets [23]. The datasets consist of 1,000,000 diverse users, comprising 860,057 humans and 139,943 bots. Table 1 illustrates that the dataset contains 4 types of entities and 14 types of relations. These entities include the user, hashtag, tweet, and list and the relations encompass pin, contain, retweet, follower, post, mention, like, reply, quote, own, follow, member, discuss, and following.

Table 1: Dataset details

Twibot-22	
Human	860,057
Bot	139,943
User	1,000,000
Tweet	86,764,167
Edge	170,185,937
Entity	User, Tweet, List, Hashtag
Relation	Follower, following, post, pin, like, mention, retweet, quote, reply, own, member, follow, contain, discuss

4.2 Data Pre-processing

Data pre-processing entails the preparation of data for analysis. The initial step consists of feature encoding; wherein categorical data is transformed into machine-learning data with significant meaning. During this process, Boolean values into a binary representation, and the encoding of the account attribute is 0 for humans and programmed accounts is 1. After encoding the features, the machine learning algorithm's efficiency is improved by scaling the numeric attributes. Scaling is an important step because numeric attributes with a diverse set of values can hinder the algorithm's speed or result in convergence on a local minimum.

To enhance data training and remove biases, numerical attributes are scaled using the standard scaler. Equation (i) enables the computation of the standardized value "y" for a certain numeric feature value "x".

$$Y = \frac{x - mean}{std} \quad (1)$$

In this context, "mean" signifies the numerical attribute's average, while "std" indicates its standard deviation.

4.3 Feature Selection

Feature selection is employed to identify and select a subset of relevant features, aiming to improve the model's performance and remove unnecessary features.

Using correlation feature selection [24], a commonly employed method to discern pertinent features, we chose the features depending on how well they correlated with the target variable. Features with a high correlation were thought to be more important and preserved, while others were dropped. As a result, we obtained a list of the top 51 features with the highest correlation, shown below.

1) Profile description: Is there a description in the profile?
2) Profile Location: Is there a location specified in the profile?
3) Profile URL: Is there a URL associated with the profile?
4) Verified: Is the profile confirmed to be authentic?
5) Bot word in name: Is there a word in the username that relates to the bot?
6) Screen name containing a bot word: Is the screen name chosen from a list of words to identify the bot?
7) Bot word in description: Is the word related to the bot from a list of words present in the description?
8) Username size: How long is the username?
9) Screen name size: How long are screen names?
10) Description length: What is the size of a description?
11) Followees count: User's account follows count
12) Followers count: User's follower count
13) Follower to Followee Ratio: Followee ratio refers to the proportion of people a user follows compared to the number of people following that user on social media platforms
14) Tweets count: Total number of tweets by user
15) Listed count: User's membership in public lists
16) Username digit count: The number of digits in the username as a whole
17) Screen name numeral count: Total digits in the screen name
18) Hashtags in username: Hashtag count within the username
19) Hashtags in description: The description's hashtag count
20) URLs in description: URLs count within the description

21) Def image: Is there a default profile image associated with the account?

22) URLs: Tweets' URLs are taken into account.

23) Protected: Does the profile have protection?

24) Pinned tweet: Is there a pinned tweet on the account?

25) Counting mentions: Mentions in the description are taken into account

26) Average tweets: Daily tweet count

27) Entropy of screen names: It is the measure of how unpredictable or random a screen name's characters are.

28) Listed growth: User membership in public lists grows daily.

29) Follower' s growth: Follower growth indicates the rate at which a user's or account's follower count increases over a specific period on social media platforms.

30) Characters: Characters count within the tweets

31) Hashtags: Hashtag count within the tweets

32) Words: Tweet word count

33) Hashtags to words: Word-to-hashtag proportion

34) Mentions: The mention count in tweets

35) Numeric characters: The numeric characters count in tweets

36) URLs to words: ratio of URLs to words

37) Times like Times like refers to the number of times a tweet has been marked as liked by other users on Twitter.

38) Times retweeted: The tweet's retweet count per post

39) Links ratio: The proportion of links within a tweet

40) Ratio of distinct linkages: The proportion of unique URLs in the tweets

41) Mention ratio: The proportion of mentions within a tweet

42) Unique mention ratio: The number of distinct mentions contained within the tweets

43) Eigen centrality: A node's importance is assessed by taking into account its links to other important nodes

44) Harmonic centrality: Calculates the mean distance to every other node within a network

45) Authority: A node's expertise or trustworthiness within a network can be quantified

46) Hub score: A node's ability to connect with other important nodes is measured

47) Degree centrality: Evaluates the number of connections associated with a node

48) Eccentricity: Calculates the farthest distance to every other node in a network

49) Page Rank: A node's significance is determined by the significance of the nodes that are connected to it

50) Coreness: measures the degree of connectedness between a node and the network's most important nodes

51) Symbols: Symbols count in tweets

4.4 Training Model

The detection of Twitter bots was accomplished by utilizing various classification algorithms, each of which was closely monitored for its performance throughout the process. In this inquiry, ineffective algorithms were removed, while retaining the effective ones. The algorithms employed included Extra-Trees Classifier, AdaBoost, Decision Trees, Random Forest, and XGBoost. Table 1 demonstrates that XGBoost surpassed the other algorithms.

Using a stratified technique, we separated the dataset into training, test, and validation sets. The dataset as a whole was made up of 70% training data, 10% test sets, and 20% validation data, respectively. The XGBoost algorithm was subsequently utilized to create decision trees sequentially, with an overall of 500 trees established. Each tree had a maximum depth of 4, while the learning rate, responsible for regulating the individual tree's impact within the sequence, was set to 0.1. The objective function was specifically configured for binary logistics to optimize the classification problem. Moreover, to avoid overfitting, the incorporation of a regularization term with an alpha parameter of 10 was crucial for managing the model's complexity. This parameter effectively penalized significant coefficients within the decision trees. In general, these contributions played a vital role in establishing a strong model that possesses the ability to effectively classify binary data while minimizing the likelihood of overfitting.

4.5 Evaluation metrics

We employ established performance metrics, including Precision, F1-score, Accuracy, and Recall, to assess the model's effectiveness. Using the formula, accuracy indicates the model's percentage of correct predictions out of all of its forecasts:

$$Accuracy = \frac{TP+TN}{TP+TN+FP+FN} \quad (2)$$

The number of true negatives and true positives in the context is denoted by TN and TP, respectively, while the number of false negatives and false positives is denoted by FN and FP. Precision is the percentage of correct positive predictions among all positive predictions made by the model. The formula below can be used to determine the precision.

$$Precision = \frac{TP}{TP+FP} \quad (3)$$

The recall represents the proportion of accurate positive predictions made by the model compared to the total number of positive cases. To calculate recall, use the following formula:

$$Recall = \frac{TP}{TP+FN} \quad (4)$$

The F1-score is a calculation that merges precision and recall, determining their overall performance. The harmonic mean of recall and precision is used to derive it. A higher F1 score indicates improved recall and precision. The following formula is used to determine the F1 score.

$$F1 - score = \frac{2 * Precision * Recall}{Precision + Recall} \quad (5)$$

5. Experimental Results

The Twibot-22 training dataset was used to train the XGBoost classification model in this study and it exhibited remarkable performance. The model successfully classified 89.8% of the input data, achieving an accuracy of 0.898. The F1 score, which provides a balanced measure of precision and recall, achieved a value of 87.5%. The precision of our model stood at 87.6%, indicating a high proportion of correctly identified social bots compared to the total predicted positive cases. Additionally, the recall, or true positive rate, reached 89.9%, suggesting that the model effectively captured a significant portion of the actual positive cases in the dataset. The effectiveness of the XGBoost algorithm in social bot detection, which is crucial for preserving the integrity of social media platforms, is emphasized by these findings. A comparison of the XGBoost model's performance with those of the other models used in this investigation is shown in Table 2.

Table 2: Model performance comparison

Models	Accuracy	F1 score	Precision	Recall
Decision Tree	0.8892	0.8670	0.8701	0.8872
Extra-Trees Classifier	0.8906	0.8660	0.8722	0.8915
Random Forest	0.8921	0.8683	0.8748	0.8934
AdaBoost	0.8888	0.8648	0.8684	0.8895
XGBoost	0.8986	0.8751	0.8767	0.8997

The Gini index served as the splitting criterion in the decision tree. It selected 300 trees without any depth restrictions, yielding an accuracy of 0.8892. The Random Forest method utilized 500 trees to find the optimal split node, resulting in an accuracy of 0.8921. Similarly, the Extra Tree Classifier employed 300 trees and achieved an accuracy of 0.8906. Utilizing 1000 weak learners, a learning rate of 0.1, and using alpha as the regularization parameter, the AdaBoost model achieved an accuracy of 0.8888.

The comparison section analyzes the performance of the model and compares it to other baseline models, such as the Extra-Trees Classifier, AdaBoost, Decision Trees, Random Forest and XGBoost. We evaluated the performance of these algorithms when applied to hybrid features, including profile metadata-based, behavioral-based, temporal-based, graph network-based, and content-based features. The results demonstrate the efficiency of these particular algorithms in accurately detecting programmed accounts.

The performance comparison was conducted in terms of precision, accuracy, F1 score, and recall. XGBoost demonstrated superior performance compared to the previous classification algorithms, exhibiting impressive accuracy and making minimal errors in detecting and classifying the social bots.

6. Conclusion

To sum up, the utilization of online social networks has brought about a noteworthy revolution in people's communication methods and their ability to express personal and public viewpoints. However, the rise of social bots on websites like Twitter has become a major problem since they compromise the veracity of tweets, spread false information, and hurt both people and society as a whole. Therefore, it is crucial to identify and locate social bots on Twitter to maintain the credibility of tweet content and protect democratic principles.

Past research has utilized a range of methods, including profile-based, behavioral-based, temporal-based, graph network-based, and content-based approaches, to detect social bots; however, each of these approaches has its limitations and lacks sufficient effectiveness in accurately identifying social bots. Consequently, this study introduces a novel approach that synergistically integrates all of the mentioned attributes to definitively and accurately identify social bots.

After testing our XGBoost model on hybrid features using the Twibot-22 dataset, we discovered that it outperforms other classifiers in identifying Twitter social bots, attaining an accuracy of 89.8. This research offers an efficient solution for identifying and finding social bots on Twitter, which helps protect the authenticity of tweet content and support democracy. In conclusion, while our proposed approach holds promise for enhancing social bot detection accuracy on Twitter, there are avenues for further refinement. Future research endeavors could involve synergizing our method with additional techniques such as topic modeling, sentiment analysis, and natural language processing. Additionally, it is important to acknowledge the limitations of our current research, which primarily focused on Twitter and may require adaptation for application on other platforms.

Acknowledgment

I would like to express my sincere gratitude to all those who have contributed to the completion of this research paper. I extend my heartfelt appreciation to my supervisor for their guidance, support, and valuable insights throughout the entire process. I would also like to thank the participants who generously provided their time and cooperation for data collection. Additionally, I am grateful to my colleagues and friends for their encouragement and assistance during this endeavor. Finally, I acknowledge the funding agencies that have supported this research, enabling its realization.

References

[1] K. Hayawi, S. Mathew, N. Venugopal, M.M. Masud, and P.H. Ho, "DeeProBot: a hybrid deep neural network model for social bot detection based on user profile data," Social Network Analysis and Mining, vol. 12, pp. 43, 2022.

[2] J. León-Quismondo, "Social Sensing and Individual Brands in Sports: Lessons Learned from English-Language Reactions on Twitter to Pau Gasol's Retirement Announcement," International Journal of Environmental Research and Public Health, pp. 895, 2023.

[3] R. Gilmary, A. Venkatesan, and G. Vaiyapuri, "Detection of automated behavior on Twitter through approximate entropy and sample entropy," Personal and Ubiquitous Computing, pp. 1-15, 2021.

[4] B. Wu, L. Liu, Y. Yang, K. Zheng, and X. Wang, "Using improved conditional generative adversarial networks to detect social bots on Twitter," IEEE Access, pp. 36664-36680, 2020.

[5] M. Heidari, S. Zad, P. Hajibabaee, M. Malekzadeh, S. HekmatiAthar, O. Uzuner, and J.H. Jones, "Bert model for fake news detection based on social bot activities in the COVID-19 pandemic," IEEE 12th Annual Ubiquitous Computing, Electronics & Mobile Communication Conference (UEMCON), 2021.

[6] M. Kolomeets, O. Tushkanova, D. Levshun, and A. Chechulin, "Camouflaged bot detection using the friend list," In 2021 29th Euromicro International Conference on Parallel, Distributed and Network-Based Processing (PDP), 2021.

[7] E. Puertas, L.G. Moreno-Sandoval, F.M. Plaza-del Arco, J.A. Alvarado-Valencia, A. Pomares-Quimbaya and L. Alfonso, "Bots and gender profiling on Twitter using sociolinguistic features," CLEF (Working Notes), pp. 1-8, 2019.

[8] L. Ilias and I. Roussaki, "Detecting malicious activity in Twitter using deep learning techniques," Applied Soft Computing, pp. 107360, 2021.

[9] R. Bailurkar and N. Raul, "Detecting bots to distinguish hate speech on social media," in International Conference on Computing Communication and Networking Technologies, 2021.

[10] L. Alkulaib, L. Zhang, Y. Sun and C.T. Lu, "Twitter Bot Identification: An Anomaly Detection Approach," IEEE International Conference on Big Data (Big Data), 2022.

[11] M. Mendoza, M. Tesconi and S. Cresci, "Bots in social and interaction networks: detection and impact estimation," ACM Transactions on Information Systems (TOIS), vol. 39, pp. 1-32, 2020.

[12] S. Najari, M. Salehi and R. Farahbakhsh, "GANBOT: a GAN-based framework for social bot detection," Social Network Analysis and Mining, vol. 12, pp. 1-11, 2022.

[13] M.M. Pingili, M.J. Lakshmi, M. Divya, D. Abhishek, K. Naresh and P. Sparsha, "Detection of malicious social bots using learning automata with URL features in twitter network," IEEE Transactions on Computational Social Systems, vol. 7(4), pp. 1004-1018, 2020.

[14] Y. Wu, Y. Fang, S. Shang, J. Jin, L. Wei and H. Wang, "A novel framework for detecting social bots with deep neural networks and active learning," Knowledge-Based Systems, vol. 211, pp. 106525, 2021.

[15] M. Mazza, S. Cresci, M. Avvenuti, W. Quattrociocchi and M. Tesconi, "Rtbust: Exploiting temporal patterns for botnet detection on twitter," Proceedings of the 10th ACM conference on web science, 2019.

[16] E. Alothali, K. Hayawi and H. Alashwal, "Hybrid feature selection approach to identify optimal features of profile metadata to detect social bots in Twitter," Social Network Analysis and Mining, vol. 11, pp. 1-15, 2021.

[17] H. Shukla, N. Jagtap and B. Patil, "Enhanced Twitter bot detection using ensemble machine learning," 6th International Conference on Inventive Computation Technologies (ICICT), 2021.

[18] G. Lingam, R.R Rout, D.V. Somayajulu and S.K. Das, "Social botnet community detection: a novel approach based on behavioral similarity in twitter network using deep learning," Proceedings of the 15th ACM Asia Conference on Computer and Communications Security, 2020.

[19] S. Kumar, S. Garg, Y. Vats and A.S. Parihar, "Content based bot detection using bot language model and bert embeddings," 5th International Conference on Computer, Communication and Signal Processing (ICCCSP), 2021.

[20] C. Monica and N. Nagarathna, "Detection of fake tweets using sentiment analysis," SN Computer Science, vol. 1, pp. 1-7, 2020.

[21] D. Kosmajac and V. Keselj, "Twitter bot detection using diversity measures," Proceedings of the 3rd International Conference on Natural Language and Speech Processing, 2019.

[22] N. Vo, K. Lee, C. Cao, T. Tran and H. Choi, "Revealing and detecting malicious retweeter groups," in Proceedings of the 2017 IEEE/ACM International Conference on Advances in Social Networks Analysis and Mining, 2017.

[23] S. Feng, Z. Tan, H. Wan, N. Wang, Z. Chen, B. Zhang, Q. Zheng, W. Zhang, Z. Lei, S. Yang and X. Feng, "TwiBot-22: Towards graph-based Twitter bot detection," 2022.

[24] M.A. Hall, "Correlation-based feature selection for machine learning," The University of Waikato, 1999.

The Nucleus ***60***, *No. 2 (2023) 205-209*

www.thenucleuspak.org.pk

The Nucleus

ISSN 0029-5698 (Print)
ISSN 2306-6539 (Online)

Biosynthesis of Silver Nanoparticles Using Vinca Rosea Leaf Extract and its Biological Applications Against Human Pathogens

D. Lalasangi[1,2*], S.M. Hanagodimath[2], M.S. Jadhav[3], V.B. Tangod[4], G. Vanti[5]

[1]*Department of Physics, Government First Grade College, Dharwad, Karnataka, India*

[2]*Department of Physics, Gulbarga University, Kalaburagi, Karnataka, India*

[3]*Department of Physics, J.S.S Arts, Science and Commerce College, Gokak, Karnataka, India*

[4]*Department of Physics, Government First Grade College for Women, Dharwad, Karntaka, India*

[5]*Multi-Disciplinary Research Unit, Karnataka Institute of Medical Sciences, Hubballi, Karnataka, India*

ABSTRACT

We report green synthesis of silver nanoparticles (Ag-NPs) for biological applications against human pathogens. Vinca rosea leaf extract was used to swiftly generate silver nanoparticles which were characterized by different techniques. The structural and optical properties of the synthesized nanoparticles were measured using UV-visible spectrophotometer, X-ray diffractometer, scanning electron microscope (SEM) coupled with energy-dispersive X-ray spectroscopy (EDS), and transmission electron microscopy (TEM). The surface morphology of the nanoparticles was found to be of spherical shape with crystalline phase. Further, the antibacterial activity, anti-cancer, anti-diabetic, anti-microbial, anti-oxidant properties, anti-helminthic, anti-ulcer, hypotensive, anti-diarrheal, wound healing, and hypolipidemic activity of Vinca rosea reduced silver nanoparticles reveal that they are highly effective agents for gram-positive and gram-negative bacteria. The green silver nanoparticles have shown significant antibacterial potential against different bacterial strains.

Keywords: *Antibacterial Activity, Biosynthesis, E. coli, S. Aureus, Vinca rosea*

1. Introduction

The nanotechnology area has been a fascinating field, as lots of research work is going to be done to explore the various possible applications of nanoparticles [1, 2]. Various approaches that have been explored to synthesize nanoparticles are broadly classified into bottom-up and top-down processes. An essential component of nanotechnology research is the creation of an environmentally friendly method for creating silver nanoparticles [3, 4]. There have been reports [5-8] on the synthesis of metal nanoparticles utilizing various techniques. A novel method of synthesis involves producing metal nanoparticles from bacteria, algae, plant leaves, stems, and flowers [9-12]. The green synthesis of nanoparticles using leaf extract has been attracting the scientific community because of its environmentally benign and cost-effective nature. This method is environment-friendly, non-toxic, reliable, and low-cost, whereas the synthesized nanoparticles have various applications [13-17]. Noble metal nanoparticles like Au, Ag, and Pt as well as their composites have been synthesized for various applications like sensors, solar cells, catalysis, and biomedical [7, 18–21]. Due to their unique physiochemical properties like high surface-to-volume ratio, surface plasmon resonance in the visible region, and reactivity towards the bacterial cell wall, they can be used in enormous applications. Syntheses of different metal nanoparticles using green methods for biological applications have been reported so far [9, 22–32]. Silver nanoparticles have shown good antibacterial activities against both gram-positive and gram-negative bacteria like S. aureus and E. coli. The antibacterial activity of silver species has been well-known since ancient times because silver is not toxic to human cells.

In this article, we reveal a novel approach to synthesizing silver nanoparticles using Vinca rosea leaf extract. Leaf extract has the potential to have anti-cancer, anti-diabetic, anti-microbial, anti-oxidant properties, anti-helminthic, anti-ulcer, hypotensive, anti-diarrheal, wound healing, and hypolipidemic activities. Hence, our approach takes a new direction in the medical field by using Vinca rosea-reduced silver nanoparticles to treat deadly diseases effectively and economically as well as prevent hazardous chemicals.

2. Materials and Methods

2.1 Materials

Vinca rosea leaves collected from the botanical garden, silver nitrate ($AgNO_3$) of analytical grade purchased from Hi-media, doubly distilled water, and Whatman's filter paper No. 4. All chemicals were used without further purification.

2.2 Preparation of leaf extract

Vinca rosea plant leaf extract was prepared after washing twice with doubly distilled water, drying and chopping 30 g of Vinca rosea leaves into 30 ml of water and kept at 70^{o}C for 45 minutes until the color of the sample was changed. The formation of the extract was confirmed by a change in the dark green color of the solution-binary mixture. Whatman's filter paper No. 4 was employed to filter the obtained extract twice to remove the broth and get a pure extract. The process of Vinca rosea leaf extraction is shown in Fig. 1.

*Corresponding author: dayanandlalasangi@gmail.com

Fig. 1: Preparation of Vinca rosea leaves extract

2.3 Synthesis of silver nanoparticles

A typical reaction procedure for the formation of Ag nanoparticles was performed in aqueous medium. 0.01M of $AgNO_3$ was taken and dissolved in 5 ml of deionized water, kept for some time to form the binary mixture, and then heated to 70°C with constant stirring for 20 min.

The Vinca rosea leaf extract was added drop by drop until it showed a color change from colorless to dark yellow.

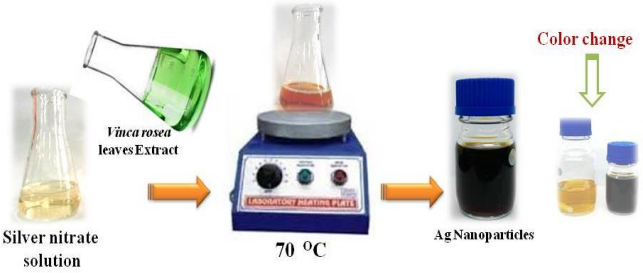

Fig. 2: Green synthesis of silver nanoparticles using Vinca rosea

A change in color confirms the formation of Ag nanoparticles, as shown in Fig. 2. Ag-NPs were centrifuged and washed several times to get an impurity-free Ag nanoparticle colloidal solution, then dried to get a dry powder the sample. The prepared Ag nanoparticles were used for further characterization to study the surface morphology and particle size of the prepared material.

2.4 In-vitro bactericidal activity

In-vitro efficacy of Ag-NPs effect on gram-positive Staphylococcus aureus and gram-negative Escherichia coli was verified utilizing the disc agar-diffusion method. The testing bacteria (1×10^6 CFU/mL in nutrient broth) were spread on nutrient agar (NA) plates. A clean sheet of sterilized paper disc (6 mm) was placed on the NA plates to observe the bacterial susceptibility to NPs. 30 and 60 µg concentrations of NPs suspension (based on the Minimum Inhibitory Concentration assay) were placed on the paper disc. As controls, 100 g of streptomycin and distilled water were used. The inhibitory zone was measured after 24 hours of 37°C incubation on the plates. The findings of the experiment which were completed in triplicate are displayed as the average size of the inhibitory zone.

2.5 Characterization techniques

UV-Vis spectra are employed to investigate the surface plasmon resonance (using Ocean OpticsHR4000 spectrophotometer). To access the crystalline nature of the prepared AgNPs, the data was collected utilizing X-ray diffractometer device (Rigaku) with radiation of Cu Kα = 1.54178 Å wavelength and angle 2θ ranging from 20° to 80°. The size and shape of the nanoparticles were observed using SEM (JEOL JSM-6360, Mira-3, Tescan, Brno, Czech Republic). The grain particle sizes of the synthesized nanoparticles were confirmed by TEM analysis.

3. Results and Discussion

Silver nanoparticle fabrication using Vinca rosea leaf extract was carried out. The produced nanoparticles have been identified based on their optical characteristics, structural analysis, morphology, and crystalline nature. Furthermore, the antibacterial activity was evaluated against gram-negative bacteria (E. coli) as well as gram-positive bacteria (S. aureus). The Phytochemicals of Vinca rosea (Fig. 3) are alkaloids like vinblastine, vincristine, vindesine, and vinorelbine, which are responsible for reducing the silver salt into silver nanoparticles.

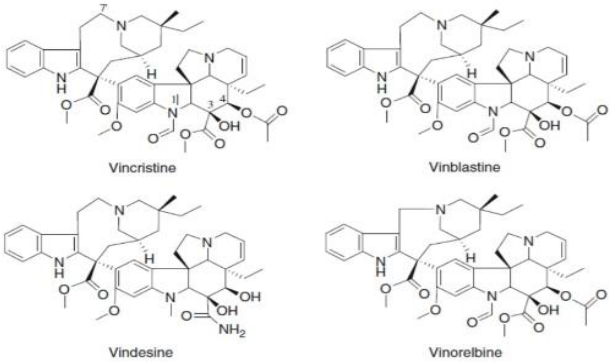

Fig. 3: Phytochemicals in Vinca rosea

3.1 Optical analysis of Ag nanoparticles

The absorption spectrum of synthesized Ag nanoparticles was recorded using UV-visible spectrophotometer. The absorption peak at 420 shows preliminary confirmation of the formation of nanoparticles (Fig. 4). It has been reported that maximum absorption occurs around 420 nm [10, 33–35], which is the characteristic of Ag nanoparticles.

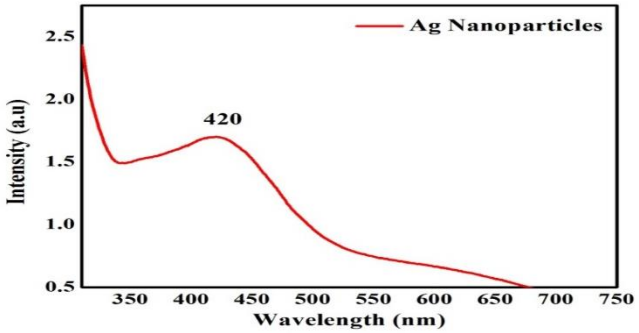

Fig. 4: UV- Visible spectrum of Ag nanoparticles.

3.2 Surface morphology and elemental analysis

The scanning electron microscope (SEM) images displayed in Fig. 5 (a, b) exhibit spherical-shaped synthesized nanoparticles with an average diameter of 30 nm. The SEM images confirm well-dispersed Ag nanoparticles within the nanometer range [10, 33–38]. Elemental examination of the synthesized Ag nanoparticles was performed using Energy Dispersive X-ray (EDX) analysis coupled with SEM. The EDX analysis shows the formation of Ag nanoparticles (Fig. 5c). The spectra show the presence of C, O, and Ag in the synthesized nanoparticles. The phytochemicals present in the extract help reduce particles to nanosize [38, 39]. These biochemicals have capping and reducer effects.

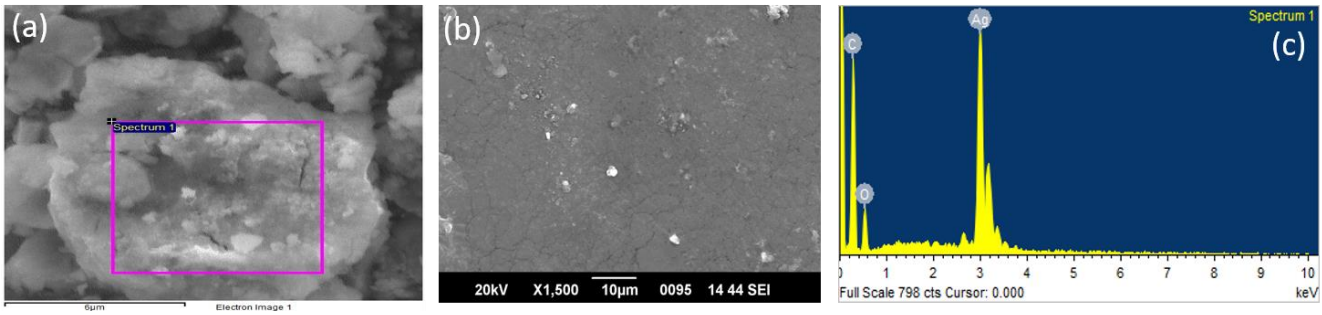

Fig. 5 (a, b): Scanning electron microscope images and (c) EDX image of synthesized Ag nanoparticles

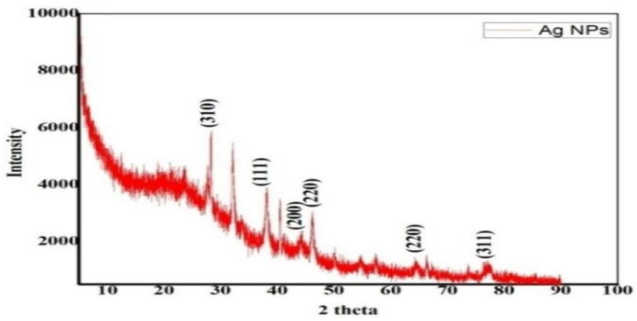

Fig. 6: X-ray diffraction patterns of Vinca rosea-produced silver nanoparticles (Ag-NPs)

3.3 XRD analysis of Ag nanoparticles

Fig. 6 shows the XRD images of AgNP's synthesized using Vinca rosea. The XRD pattern of synthesized nanoparticles reveals the FCC (Face-centered Cubic) structure of the prepared nanoparticles. In addition, all the AgNP's have a similar diffraction pattern and XRD peaks at 2θ of 28.39°, 38.08°, 44.13°, 46.15°, 64.26°, and 77.08° and could be attributed to 310, 111, 200, 220, 220 and 311 crystallographic planes of the FCC cubic silver crystals, respectively (JCPDS file no. 84-0713 and 04-0783) [12, 38, 40].

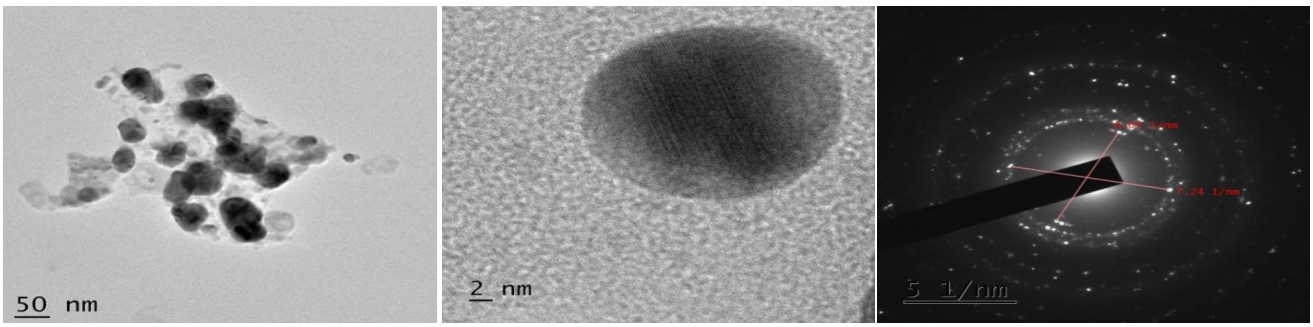

Fig. 7: (a) TEM image of Ag nanoparticles (b) A HR-TEM image of a single Ag nanoparticle (c) SAED pattern

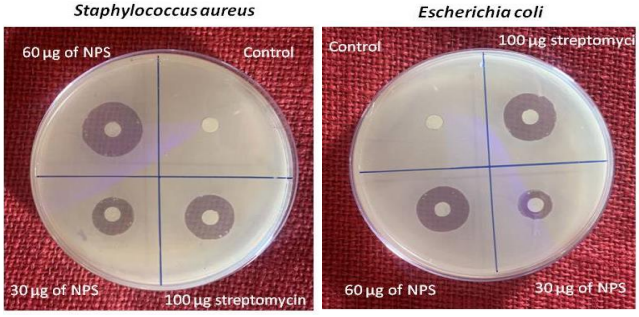

Fig. 8: Antibacterial activity of silver nanoparticles using gram-positive and gram-negative bacteria

Thus, it is evident from the XRD spectrum that the produced in this work were crystalline in nature. Due to the imperfections, it is believed that silver was the only crystalline phase present in the prepared samples. In both XRD and EDX analyses, it was confirmed that the prepared samples were silver nanoparticles.

3.4 HR-TEM analysis of Ag nanoparticles

The prepared silver nanoparticles were treated with nitrate $AgNO_3$ solution using Vinca rosea leaf extract. Fig. 7(a, b) shows the HR-TEM analysis of synthesized nanoparticles with the green synthesis method. UV-Vis absorption spectra show that the broad SPR band contains a peak at 420 nm. The existence of a peak shows that there is a wide dispersion of Ag hydrosol present. Thus, the UV-visible spectral investigation [41–43] is consistent with the existence of large distributions of particles in the HR-TEM image. The selected area electron diffraction (SAED) pattern shown in Fig. 7(c) confirms the well-crystalline structure of Ag nanoparticles [44, 45]. Additionally, the HR-TEM micrographs verified that the nanoparticles were fabricated in the 30-35 nm size range. Similar SAED patterns of silver nanoparticles have also been observed in other works [44–46].

3.5 In-vitro bactericidal activity

Different NP concentrations' *in vitro* bactericidal efficacy against S. aureus and E. coli was evaluated by the disc diffusion method. At 60 µg mL^{-1} NPs, S. aureus showed an inhibition zone of 17.8±0.8 mm, whereas 30 µg mL^{-1} NPs showed an inhibition zone of 12.5±1 mm [3, 6, 47–49]. Similarly, E. coli showed 16.2±1.1 mm and 11.4±0.8 mm at 60 and 30 µg mL^{-1} NPs, which are statistically significant compared to the control.

Moreover, positive control streptomycin shows an inhibition zone of 17.2±0.8 mm and 16.8±1.2 for S. aureus and E. coli, respectively (Fig. 8). This shows that the synthesized Ag nanoparticles play an active role with excellent activity for the gram-negative bacteria with MIC 16.8±1.2.

4. Conclusion

We have successfully synthesized silver nanoparticles via a Vinca rosea leaf extract-mediated process. The synthesized nanoparticles were capped by the phytochemicals present in the leaf extract. The UV-Vis spectrum shows the formation of Ag nanoparticles, with the surface plasmon resonance peak at 420 nm. The synthesized nanoparticles have a crystalline structure as confirmed by the XRD pattern. The analysis indicates the formation of Ag nanoparticles with an average size of 30 nm. The synthesized Ag nanoparticles have excellent free radical and antibacterial activities. From our findings, the synthesized nanoparticles show growth-inhibitory activities against both gram-positive and gram-negative pathogenic bacteria. Thus, the synthesized nanoparticles can be used in medicine as therapeutic agents due to their antimicrobial activities against the bacteria evaluated in vitro.

Acknowledgment

D.S. Lalasangi is thankful to the Principal, Government First Grade College, Dharwad, and Commissioner, Department of Collegiate and Technical Education Government of Karnataka, Bengaluru, for providing an opportunity to carry out this research work.

References

[1] S.M. Hosseini, I. Abdolhosseini Sarsari, P. Kameli, and H. Salamati, "Effect of Ag doping on structural, optical, and photocatalytic properties of ZnO nanoparticles," Journal of Alloy and Compounds, vol. 640, pp. 408–415, 2015.

[2] S. Baruah and J. Dutta, "Nanotechnology applications in pollution sensing and degradation in agriculture," Environmental Chemistry Letters, vol. 7, no. 3, pp. 191–204, 2009.

[3] R. Dobrucka and J. Długaszewska, "Biosynthesis and antibacterial activity of ZnO nanoparticles using Trifolium pratense flower extract," Saudi Journal of Biological Sciences, vol. 23, no. 4, pp. 517–523, 2016.

[4] F. Charbgoo, M. Ahmad, and M. Darroudi, "Cerium oxide nanoparticles: green synthesis and biological applications," International Journal of Nanomedicine, vol. 12, pp. 1401–1413, 2017.

[5] S. Dagher, Y. Haik, A.I. Ayesh, and N. Tit, "Synthesis and optical properties of colloidal CuO nanoparticles," Journal of Luminescence, vol. 151, pp. 149–154, 2014.

[6] G.A. Martinez-Castanon, N. Niño-Martínez, F. Martínez-Gutierrez, J. R. Martínez-Mendoza, and F. Ruiz, "Synthesis and antibacterial activity of silver nanoparticles with different sizes," Journal of Nanoparticle Research, vol. 10, no. 8, pp. 1343–1348, 2008.

[7] K.S. Lee and M.A. El-Sayed, "Gold and silver nanoparticles in sensing and imaging: Sensitivity of plasmon response to size, shape, and metal composition," Journal of Physical Chemistry B, vol. 110, no. 39, pp. 19220–19225, 2006.

[8] R.P. Shubha, J. Chatterjee, and M.S. Mustak, "Glob J Nanomed Use of Honey in Stabilization of ZnO Nanoparticles Use of Honey in Stabilization of ZnO Nanoparticles Synthesized via Hydrothermal Route and Assessment of their Antibacterial Activity and Cytotoxicity," Global Journal of Nanomedicine, vol. 2, no.2, 2017.

[9] M.S. Jadhav, S. Kulkarni, P. Raikar, D.A. Barretto, S.K. Vootla, and U.S. Raikar, "Green biosynthesis of CuO & Ag–CuO nanoparticles from Malus domestica leaf extract and evaluation of antibacterial, antioxidant and DNA cleavage activities," New Journal of Chemistry, vol. 42, no. 1, pp. 204–213, 2018.

[10] H. Huang and X. Yang, "Synthesis of polysaccharide-stabilized gold and silver nanoparticles: a green method," Carbohydrate Research, vol. 339, pp. 2627–2631, 2004.

[11] P. Raveendran, J. Fu, and S.L. Wallen, "Completely 'Green' Synthesis and Stabilization of Metal Nanoparticles," Journal of the American Chemical Society, vol. 125, no. 46, pp. 13940–13941, 2003.

[12] K. Kavitha, S Baker, D Rakshith, H U Kavitha, H C Yashwantha Rao, B P Harini, S Satish., "Plants as Green Source towards Synthesis of Nanoparticles," International Research Journal of Biological Sciences Int. Res. J. Biological Sci, vol. 2, no. 6, pp. 66–76, 2013.

[13] J.E. Hutchison, "Greener Nanoscience: A Proactive Approach to Advancing Applications and Reducing Implications of Nanotechnology," vol. 2, no. 3, pp. 395–402, 2008.

[14] N. Vigneshwaran, R.P. Nachane, R.H. Balasubramanya, and P.V. Varadarajan, "A novel one-pot 'green' synthesis of stable silver nanoparticles using soluble starch," Carbohydrate Research, vol. 341, no. 12, pp. 2012–2018, 2006.

[15] S.K. Nune, N Chanda, R Shukla, Kavita Katti, R.R. Kulkarni, S. Thilakavathy, S Mekapothula, R Kannan, Kattesh Katti "Green nanotechnology from tea: Phytochemicals in tea as building blocks for production of biocompatible gold nanoparticles," Journal of Materials Chemistry, vol. 19, no. 19, pp. 2912–2920, 2009.

[16] M. Sundrarajan and S. Gowri, "Green synthesis of titanium dioxide nanoparticles by nyctanthes arbor-tristis leaves extract," Chalcogenide Letters, vol. 8, no. 8, pp. 447–451, 2011.

[17] Y. Zheng, S. Gao, and J.Y. Ying, "Synthesis and cell-imaging applications of glutathione-capped CdTe quantum dots," Advanced Materials, vol. 19, no. 3, pp. 376–380, 2007.

[18] M. Tsuji, S. Hikino, R. Tanabe, M. Matsunaga, and Y. Sano, "Syntheses of Ag/Cu alloy and Ag/Cu alloy core Cu shell nanoparticles using a polyol method," Cryst Eng Comm, vol. 12, no. 11, p. 3900, 2010.

[19] Y. Li, J Xu, L Wang, Y Huang, J Guo, X Cao, F. Shen, Y Luo, C Sun "Aptamer-based fluorescent detection of bisphenol A using nonconjugated gold nanoparticles and CdTe quantum dots," Sensors and Actuators, B: Chemical, vol. 222, pp. 815–822, 2016.

[20] N.R. Kim, K. Shin, I. Jung, M. Shim, and H.M. Lee, "Ag-Cu Bimetallic Nanoparticles with Enhanced Resistance to Oxidation: A Combined Experimental and Theoretical Study," J. Phys. Chem. C, vol. 118, no. 45, pp. 26324–2633, 2014.

[21] Z. Wu, J Zhang, R.E. Benfield, Y Ding, D Grandjean, Z Zhang, X Ju "Structure and Chemical Transformation in Cerium Oxide Nanoparticles Coated by Surfactant Cetyltrimethylammonium Bromide (CTAB): An X-ray Absorption Spectroscopic Study," The Journal of Physical Chemistry B, vol. 106, no. 18, pp. 4569–4577, 2002.

[22] V.B. Tangod, P Raikar, BM Mastiholi, US Raikar, "Determination of extinction, absorption and scattering coefficients of gold nanoparticles," Journal of Shivaji University (Science & Technology), 41 (2), 2014-2015.

[23] V.B. Tangod, PU Raikar, BM Mastiholi, SG Kulkarni, MS Jadhav, US Raikar, "Photophysics studies of highly fluorescent ADS680HO laser dye conjugate with green silver nanoparticles," Optik, vol.127 (2) pp. 677-685, 2016.

[24] S. Dadami, V.B. Tangod, "Absorption and Fluorescence Mechanisms of Red Mega 480 Laser Dye Coupled with Silver Nanoparticles," The Nucleus, vol. 60, pp.132-136, 2023.

[25] N. Chowdareddya, Ashok R. Lamania, A.G. Pramodc, V.B. Tangod, "Nonlinear refractive index enhancement of Nd3+ ions loaded borate glasses in the near–infrared region by silver nanoparticles", Optical Materials, vol. 142, 114067, 2023.

[26] V.B. Tangod, "Quenching of Fluorescent ADS680HO molecule with Eco-Friendly Synthesized Silver Nanoparticles", The Nucleus, vol. 60, no. 1, pp. 56-59, 2023.

[27] S.R. Mannopantar, H.H. Bendigeri, V.K. Kulkarni, V.S. Patil, D.H. Manjunatha, M.N. Kalasad, "Preparation of colloidal Ag nanoparticles," Materials Today: Proceedings, vol 60, pp.1156–1159, 2022.

[28] L. Wang, C. Hu, and L. Shao, "The antimicrobial activity of nanoparticles: Present situation and prospects for the future," International Journal of Nanomedicine, vol. 12, pp. 1227–1249, 2017.

[29] Y. Hamauzu, H. Yasui, T. Inno, C. Kume, and M. Omanyuda, "Phenolic profile, antioxidant property, and anti-influenza viral activity of Chinese quince (Pseudocydonia sinensis Schneid.), quince (Cydonia oblonga Mill.), and apple (Malus domestica Mill.) fruits," Journal of Agricultural and Food Chemistry, vol. 53, no. 4, pp. 928–934, 2005.

[30] P.P.N. V. Kumar, U. Shameem, and P. Kollu, "Green Synthesis of Copper Oxide Nanoparticles Using Aloe vera Leaf Extract and Its Antibacterial Activity Against Fish Bacterial Pathogens," BioNanoscience, vol. 5, pp. 135–139, 2015.

[31] S.M. Hunagund, V.R. Desai, J. S. Kadadevarmath, D.A. Barretto, S. Vootla, and A.H. Sidarai, "RSC Advances hydrothermal route and their antibacterial activities," RSC Advances, vol. 6, pp. 97438–97444, 2016.

[32] H. Kumar and R. Rani, "Antibacterial Study of Copper Oxide Nanoparticles Synthesized by Microemulsion Technique," Recent Advances in Biomedical & Chemical Engineering and Materials Science, pp. 197–201, 2014.

[33] A.K. Mittal, A. Kaler, and U.C. Banerjee, "Free Radical Scavenging and Antioxidant Activity of Silver Nanoparticles Synthesized from Flower Extract of Rhododendron dauricum," Nano Biomedicine & Engineering, vol. 4, no. 3, pp. 118–124, 2012.

[34] V. Parashar, R. Parashar, B. Sharma, and A.C. Pandey, "Parthenium leaf extract mediated synthesis of silver nanoparticles: A novel approach towards weed utilization," Digest Journal of Nanomaterials and Biostructures, vol. 4, no. 1, pp. 45–50, 2009.

[35] J.P. Ruparelia, A. Kumar, and S.P. Duttagupta, "Strain specificity in antimicrobial activity of silver and copper nanoparticles "Acta Biomaterialia", vol. 4, No. 3, pp. 707-716, 2008.

[36] J. Huang, Q Li, D Sun, Y Lu, Y Su, Y Su, X Yang, H Wang, Y Wang, W Shao, N He "Biosynthesis of silver and gold nanoparticles by novel sundried Cinnamomum camphora leaf," Nanotechnology, vol. 18, no. 10, 2007.

[37] V.K. Sharma, R.A. Yngard, and Y. Lin, "Silver nanoparticles: Green synthesis and their antimicrobial activities," Advances in Colloid and Interface Science, vol. 145, no. 1–2, pp. 83–96, 2009.

[38] S.M. Lee, K.C. Song, and B.S. Lee, "Antibacterial activity of silver nanoparticles prepared by a chemical reduction method," Korean Journal of Chemical Engineering, vol. 27, no. 2, pp. 688–692, 2010.

[39] C. Krishnaraj, E.G. Jagan, S. Rajasekar, P. Selvakumar, P. T. Kalaichelvan, and N. Mohan, "Synthesis of silver nanoparticles using Acalypha indica leaf extracts and its antibacterial activity against water borne pathogens," Colloids and Surfaces B: Biointerfaces, vol. 76, no. 1, pp. 50–56, 2010.

[40] S. Iravani, "Green synthesis of metal nanoparticles using plants" Green Chemistry, RSC pp. 2638–2650, 2011.

[41] L. Baia and S. Simon, "UV-VIS and TEM assessment of morphological features of silver nanoparticles from phosphate glass matrices," Modern Research and Educational Topics in microscopy, pp. 576–583, 2007.

[42] G. Ren, D. Hu, Eilen.W.C. Cheng, M.A. Vargas-Reus, P. Reip, and R.P. Allaker, "Characterization of copper oxide nanoparticles for antimicrobial applications," International Journal of Antimicrobial Agents, vol. 33, no. 6, pp. 587–590, 2009.

[43] H.R. Ghorbani and R. Rashidi, "Antimicrobial activity of silver nanoparticles synthesized by reduction technique," Journal of Pure and Applied Microbiology, vol. 9, no. 2, pp. 1747–1749, 2015.

[44] S. Li, Y Shen, A Xie, X Yu, L Qiu, L Zhang, Q Zhang "Green synthesis of silver nanoparticles using Capsicum annuum L. extract," Green Chemistry, vol. 9, no. 8, pp. 852–858, 2007.

[45] Y. Hou, H. Kondoh, T. Ohta, and S. Gao, "Size-controlled synthesis of nickel nanoparticles," Applied Surface Science, vol. 241, no. 1-2 SPEC. ISS., pp. 218–222, 2005.

[46] J. Suárez-Cerda, H. Espinoza-Gómez, G. Alonso-Núñez, I. A. Rivero, Y. Gochi-Ponce, and L. Z. Flores-López, "A green synthesis of copper nanoparticles using native cyclodextrins as stabilizing agents," Journal of Saudi Chemical Society, vol. 21, issue 3, pp. 341-348 2016.

[47] P. Amornpitoksuk, S. Suwanboon, S. Sangkanu, A. Sukhoom, N. Muensit, and J. Baltrusaitis, "Synthesis, characterization, photocatalytic and antibacterial activities of Ag-doped ZnO powders modified with a diblock copolymer," Powder Technology, vol. 219, pp. 158–164, 2012.

[48] M.J. Hajipour, K. M. Fromm, A K Ashkarran, V Serpooshan, W. J. Parak, M. Mahmoudi "Antibacterial properties of nanoparticles," Trends in Biotechnology, vol. 30, no. 10, pp. 499–511, 2012.

[49] A. Saxena, R.M. Tripathi, F. Zafar, and P. Singh, "Green synthesis of silver nanoparticles using aqueous solution of Ficus benghalensis leaf extract and characterization of their antibacterial activity," Materials Letters, vol. 67, no. 1, pp. 91–94, 2012.

Information for Authors

Submission: Manuscripts [in Word (.doc, .docx, .rtf)] should be submitted by one of the authors of the manuscript through the online submission system at www.thencleuspak.org.pk after registration of corresponding author. If for some technical reason on-line submission is not possible, then write an email describing the problem along with your phone no. at editorinchief@thenucleuspak.org.pk

Terms of Submission: Each submission to The Nucleus implies that the manuscript presents the results of original scientific research and has not been published nor has been submitted for publication elsewhere. The article is written in clear and Standard English. The reported research meets all applicable ethical standards and research integrity. The submitted manuscripts is screened for plagiarism during the editorial process.

Units of Measurement: should be presented simply and concisely using System International (SI) units.

Article Structure

Subdivision - numbered sections: The article should be divided into clearly defined and numbered sections. Subsections should be numbered 1.1 (then 1.1.1, 1.1.2, ...), 1.2, etc. (the abstract is not included in section numbering). Any subsection may be given a brief heading. Each heading should appear on its own separate line.

Title: should be concise and informative. Avoid abbreviations and formulae where possible.

Author names and affiliations: Provide complete name of all the authors, their affiliation, complete postal addresses, contact numbers and e-mail addresses. Present the authors' affiliation addresses below the names. Indicate all affiliations with a lower-case superscript letter immediately after the author's name. Clearly indicate the corresponding author by superscript*. Further when manuscript is under review process, as per policy of the journal, author cannot be addeded, deleted and sequence of author can't be altered.

Keywords: Provide a maximum of 6 keywords, These keywords will be used for indexing purposes.

Introduction Section: States the objectives of the work and provides an adequate background, avoiding a detailed literature survey or a summary of the results.

Experimental Section: should contain sufficient detail to allow the work to be reproduced. Methods already published should be indicated by a reference, only relevant modifications should be described.

***Theory/calculation S**ection:* Should extend, not repeat, the background to the article already dealt with in the Introduction and lay the foundation for further work. In contrast, a Calculation section represents a practical development from a theoretical basis.

Results and Discussion: should provide the significance of the results of the work. A combined Results and Discussion section is often appropriate. Avoid extensive citations and discussion of published literature.

Conclusions: It should be presented in a short Conclusions section.

Acknowledgments: (if any) should be included at the very end of the paper before the references and may include supporting grants, presentations, and so forth.

References: We follow IEEE style for citations of references. Must be numbered consecutively and citations of references in text should be identified using numbers in square brackets (e.g., as discussed by Smith [9]; as discussed elsewhere [9, 10]). Reference to a publication:

[Ref number] Author's initials. Author's Surname, "Title of article," Title of journal abbreviated in Italics, vol. number, issue number, page numbers, Abbreviated Month Year.

[4] K.A. Nelson, R.J. Davis, D.R. Lutz, and W. Smith, "Optical generation of tunable ultrasonic waves," Journal of Applied Physics, vol. 53, no. 2, pp. 1144-1149, Feb., 2002.

For more details please see the link IEEE style for citations of different materials

Figures and Tables: Include all figures and tables in the word file of the manuscript. Figures and tables should not be submitted in separate files. If the article is accepted, authors may be asked to provide the source files of the figures. All figures should be cited in the paper in a consecutive order. In all figures, remove all unnecessary boxes, lines, marks. The resolution of all the figures must be at least 300 dpi. Tables should be cited consecutively in the text. Every table must have a descriptive title and if numerical measurements are given, the units should be included in the column heading. Vertical rules should not be used.

The Nucleus

An Open Access International Scientific Journal

ISSN : 0029-5698 (Print)
EISSN : 2306-6539 (Online)

Recognized by HEC in 'Y' Category

Call for Papers

Why Publish in The Nucleus?

- One of the Oldest Scientific Journals in Pakistan
- Regularly Published since 1964
- Published Both Electronically & in Paper Format
- Multidisciplinary
  - Natural Sciences
  - Applied Sciences
  - Engineering & Technology
  - Management Sciences
- Open Access
- Peer Reviewed*
- No Publication Charges
- High Visibility
- Electronic Submission
- Rapid On-line Publication (within three months)

Abstracted and Indexed in:

- Chemical Abstracts
- Biological Abstracts
- INIS Atom Index
- Bibliography of Agriculture (USA)
- The Institute of Electrical Engineers Publications
- Virology Abstracts (England)
- Pakistan Science Abstracts

For Further Information

Editorial Office The Nucleus
PINSTECH, 45650 Nilore
Islamabad. Pakistan
For Online
http://www.thenucleuspak.org.pk
E-mail
editorialoffice@thenucleuspak.org.pk

Why Perish when you can Publish in The Nucleus?

*Potential Reviewers are Invited to Submit their CV's Through E-mail